UNIVERSITY OF SOUTHAMPTON

FACULTY OF MEDICINE

School of Medicine

Department of Cancer Sciences

Manipulation of immunotherapy by targeting the inhibitory Fcγ receptor.

by

Emily Louisa Williams, BSc. (Hons)

Thesis for the degree of Doctor of Philosophy

June 2011

UNIVERSITY OF SOUTHAMPTON

ABSTRACT

FACULTY OF MEDICINE, SCHOOL OF MEDICINE,
DEPARTMENT OF CANCER SCIENCES

Doctor of Philosophy

Manipulation of immunotherapy by targeting the inhibitory Fcγ receptor.

Emily Louisa Williams BSc. (Hons)

The inhibitory Fc receptor for IgG, FcγRII (CD32), has been shown to modulate *in vivo* cytotoxicity against tumour targets. Usually expressed on monocytes, macrophages and B lymphocytes, CD32 deficiency enhances the efficacy of some therapeutic mAb. Unfortunately, suitable reagents capable of specifically and exclusively binding mouse CD32 have been lacking, leading to an ignorance of how CD32 might be manipulated for therapeutic benefit *in vivo*. We generated a panel of mAb which are highly specific for CD32 that do not cross-react with any other Fc receptors, allowing us to study the potential of CD32 as a therapeutic target able to alter effector cell function and concurrent immunotherapy.

In vitro analysis on murine lymphoma cell lines showed that the anti-CD32 mAb fall into two distinct categories; those which cause tyrosine phosphorylation and subsequent receptor activation (agonistic) and those which block receptor phosphorylation (antagonistic). Consequentially, these anti-CD32 mAb exert differing functions in a range of cellular and biochemical assays. Agonistic mAb trigger programmed cell death whilst antagonistic anti-CD32 mAb have relatively little effect. Interestingly, the agonistic mAb are able to block the magnitude and duration of the calcium signalling triggered by BCR engagement whilst antagonistic mAb potentiate these responses. Furthermore, these mAb were shown to trigger phagocytosis of antibody coated B-cells by murine bone marrow derived macrophages (BMDMs) and to enhance the phagocytic potential of BMDMs *in vitro.* The ability of these mAb to elicit therapeutic responses in a variety of different mouse models was however limited. Further study revealed that in wild-type mice the anti-CD32 mAb are rapidly consumed in comparison with other, similar, mAb. Together with our observation that the anti-CD32 mAb are internalised *in vitro* and *in vivo*, these data provide the rationale for the inadequate immunotherapy observed in our model systems.

Table of contents

Abstract i
Table of contents iii
List of figures ix
Lists of tables xii
Declaration of Authourship xiii
Dedication xv
Acknowledgements xvii
Abbreviations xix

CHAPTER 1 Introduction 1

1.1. Introduction. 1

1.2. Immunotherapy. 2
1.2.1. Active immunotherapeutic strategies. 3
1.2.1.1. Cancer vaccination. 3
1.2.1.2. Immunostimulatory mAb. 5
1.2.2. Passive immunotherapeutic strategies. 6

1.3. Direct targeting mAb immunotherapy. 7
1.3.1. Antibody structure. 7
1.3.2. Development of mAb technology. 9
1.3.3. Effector mechanism of therapeutic mAb. 11
1.3.3.1. Induction of ADCC. 12
1.3.3.2. Induction of CDC. 12
1.3.3.3. Signal perturbation (PCD and altered endogenous signalling). 13
1.3.3.4. Additional anti-tumour functions. 15
1.3.4. Improving therapeutic mAb efficacy. 17
1.3.4.1. mAb conjugation. 17
1.3.4.2. Maximising FcγR:Fc interactions. 18

1.4. The Fc receptor family. 19

1.5. The Fcγ Receptors. 19
1.5.1. FcγR binding affinity for IgG. 21
1.5.2. The activatory-to-inhibitory ratio and its importance in cell activation. 22
1.5.3. Structure of the FcγR. 23
1.5.4. The FcγR:Fc interaction (binding of IgG to FcγR). 25
1.5.5. Regulation of FcγR expression. 27

1.6. The activatory FcγR. 28
1.6.1. The function of activatory FcγR. 28
1.6.2. Activatory FcγR signalling. 29

1.7. B cell signalling. 32
1.7.1. BCR-induced cytosolic calcium flux. 33
1.7.2. BCR-induced activation of MAP kinase signalling pathway. 34
1.7.3. BCR-induced activation of AKT. 34
1.7.4. The important of lipid rafts in ITAM receptor signalling. 35

1.8. The inhibitory FcγR. 37
1.8.1. Expression of CD32 38
1.8.1.1. Expression of CD32 isoforms. 38
1.8.2. Inhibition of activatory FcγR signalling. 40
1.8.3. Inhibition of BCR signalling. 41
1.8.3.1. CD32 recruitment to lipid rafts after BCR co-ligation. 42
1.8.3.2. Inhibition of BCR-induced cytosolic calcium flux. 43
1.8.3.3. Decreased survival by inhibition of AKT. 43
1.8.3.4. Reduced cell proliferation by inhibition of MAP kinase pathways. 44
1.8.4. Direct B-cell apoptosis induced by CD32 activation. 46

1.9. Expression of FcγR in cancer. 48

1.10. FcγR as mediators of anti-tumour immunotherapy. 50
1.10.1. The role of FcγR in immunotherapy. 50
1.10.2. Inhibitory FcγR in immunotherapy. 50

1.11. Project aims. 52

CHAPTER 2 Materials and Methods 53

2.1. Animals. 53

2.2. Tissue culture. 53

2.3. Cell quantification. 54

2.4. B cell purification by MACS® separation. 54

2.5. Lymphoprep of whole blood. 55

2.6. Mouse genotyping by polymerase chain reaction (PCR). 55
2.6.1. Myc genotyping. 56
2.6.2. $CD32^{-/-}$ genotyping. 56
2.6.3. $\gamma\text{-chain}^{-/-}$ genotyping. 56
2.6.4. $Bim^{-/-}$ genotyping. 57

2.7. Mouse phenotyping by immunofluroscence. 57

2.8. Eμ-myc mice; tumour generation, processing and characterisation. 58

2.9. Antibodies and antibody fragments. 58
2.9.1. Generation of antibodies. 58
2.9.2. Generation of $F(ab')_2$ antibody fragments. 59

2.10. Antibody dialysis. 59

2.11. Measurement of surface antigens by immunofluorescence. 59

2.12. *In vitro* Apoptosis Assay. 60
2.12.1. AnV/PI staining of lymphoma and B cells. 60
2.12.2. AnV/PI staining of BMDMs. 61

2.13. Calcium flux assay. 61

2.14. Western blot analysis. 62

2.15. mAb immunotherapy. 63

2.16. Tumour tracking. 64

2.17. *Ex vivo* modulation assay. 64

2.18. *In vitro* Modulation assays. 64

2.19. Alexa-488 quenching Assay. 65
2.19.1. Alexa-488 labelling of mAb. 65
2.19.2. Quenching assay. 65

2.20. Adoptive transfer of CFSE labelled cells. 66
2.20.1. CFSE labelling of target and non-target splenocytes. 66
2.20.2. Adoptive transfer of target and non-target cells. 66

2.21. BMDMs phagocytosis assay. 66

2.22. ELISA to determine half life *in vivo* of anti-CD32 mAb. 67

2.23. Production of clodronate liposomes. 68

2.24. Polymerase chain reaction for murine CD32 isoforms. 68
2.24.1. RNA extraction. 69
2.24.2. cDNA production. 69
2.24.3. PCR for murine CD32 isoforms. 69

2.25. BIAcore analysis to determine affinity of anti-CD32 mAb. 69

2.26. Production of immune complexes. 70

CHAPTER 3 *In vitro* characterisation of the Eμ-myc mouse model 73

3.1. Chapter introduction. 73

3.2. Kaplein Meier survival. 75

3.3. Presentation of the primary tumour. 76
3.3.1. Physical tumour presentation. 76
3.3.2. Histological examination of tissues from tumour bearing mice. 80
3.3.2.1. Histological examination of lymphoid tissue from the C57BL/6 and Eμ-myc mice. 80
3.3.2.2. Histological examination of non-lymphoid tissue from C57BL/6 and Eμ-myc mice. 81
3.3.2.3. Histological examination of tissues from the Eμ-myc/CD32$^{-/-}$ mice. 81

3.4. Primary tumour characterisation. 86
3.4.1. Tumour phenotype. 86
3.4.2. Tumour transplantation into WT C57BL/6 mice. 89

3.5. Eμ-myc and Eμ-myc/CD32$^{-/-}$ cell line characterisation 90
3.5.1. Eμ-myc and Eμ-myc/CD32$^{-/-}$ cell line growth 90
3.5.2. Changes in IgM expression as cells adapt to culture. 91
3.5.3. Response of Eμ-myc cell-lines to etoposide or BCR stimulation 92

3.6. Chapter Discussion 97

CHAPTER 4 *In vitro* analysis of anti-CD32 mAb on lymphoma cells 103

4.1. Chapter Introduction. 103

4.2. Generation of anti-CD32 mAb. 103
4.2.1. anti-CD32 mAb binding specificity and affinity. 104
4.2.2. Identification of epitope specificity. 108
4.2.3. The anti-CD32 mAb block immune complex binding. 108

4.3. Activation of CD32. 111
4.3.1. Tyrosine phosphorylation of CD32, SHIP-1 and SHP by anti-BCR antibodies. 111
4.3.2. Tyrosine phosphorylation of CD32 by the anti-CD32 mAb. 112
4.3.3. Tyrosine phosphorylation of SHIP-1 following activation of CD32 by the anti-CD32 mAb. 113
4.3.4. Tyrosine phosphorylation of CD32 by the anti-CD32 mAb whole IgG and $F(ab')_2$ fragments. 115
4.3.5. Co-ligation of CD32 by AT130-2 and AT130-5 is in a *cis* fashion. 116

4.4. Ability of the anti-CD32 mAb to affect calcium flux. 119
4.4.1. Fc engagement by anti-idotype mAb reduces the magnitude of anti-idiotype Ca^{2+} flux. 119
4.4.2. Effect of anti-CD32 on anti-idiotype induced Ca^{2+} flux. 120
4.4.3. Effect of anti-CD32 mAb on anti-IgM induced Ca^{2+} flux. 121
4.4.4. Effect on anti-idiotype induced Ca^{2+} flux by the anti-CD32 mAb whole IgG and $F(ab)_2$ fragments. 123

4.5. Induction of programmed cell death. 124
4.5.1. Induction of programmed cell death by the anti-CD32 mAb. 125
4.5.2. Correlation between PCD and CD32 expression. 128
4.5.3. Induction of PCD by anti-CD32 mAb by whole IgG and $F(ab)_2$ fragments. 129

4.6. *In vitro* effect of anti-CD32 mAb on anti-BCR activity. 130
4.6.1. Correlation between CD32 and BCR expression. 130
4.6.2. Effects of BCR expression on CD32 induced cell death. 131
4.6.3. Additive effect of anti-IgM and anti-CD32 on PCD. 132

4.7. Chapter discussion. 135

CHAPTER 5 *In vitro* analysis of anti-CD32 mAb on B cells and macrophages 141

5.1. Chapter introduction. 141

5.2. *In vitro* effects of anti-CD32 mAb on normal B cells. 141
5.2.1. Tyrosine phosphorylation of CD32 and SHIP-1 on normal B cells. 143
5.2.2. Effect of anti-CD32 mAb on BCR-induced Ca^{2+} flux. 145
5.2.3. Induction of programmed cell death on B cells by anti-CD32 mAb. 146
5.2.4. Summary of anti-CD32 mAb activity in splenic B cell. 148

5.3. *In vitro* effect of anti-CD32 mAb in BMDMs. 148
5.3.1. Tyrosine phosphorylation of CD32 and SHIP-1 in BMDMs. 149
5.3.2. Induction of programmed cell death on BMDMs by anti-CD32 mAb. 150

5.4. The anti-CD32 mAb induce phagocytosis of opsonised B cells by BMDMs. 151
5.4.1. The anti-CD32 mAb induce phagocytosis of opsonised B cells. 151
5.4.2. The anti-CD32 mAb induce phagocytosis of opsonised B cells in a dose dependent manner. 155
5.4.3. $CD32^{-/-}$ BMDMs induce an enhanced level of phagocytosis than WT BMDMs and this is dependent on the presence of activatory FcγR. 157
5.4.4. Pre-treatment of macrophages with anti-CD32 mAb enhances phagocytic activity of WT BMDMs. 159
5.4.5. Summary of anti-CD32 activity on BMDMs. 161

5.5. Chapter discussion. 161

CHAPTER 6 Manipulation of immunotherapy by anti-CD32 mAb. 165

6.1. Chapter introduction. 165

6.2. Manipulation of Immunotherapy *in vivo.* 166
6.2.1. Anti-idiotype immunotherapy in WT and $CD32^{-/-}$ BALB/c mice. 166
6.2.2. *In vivo* efficacy of anti-CD32 mAb on anti-idiotype therapy. 167
6.2.3. Effect of anti-CD32 mAb on tumour growth. 169

6.3. *In vivo* consumption of mAb. 171
6.3.1. *In vivo* consumption of mAb in BCL_1 and A31 treated mice. 171
6.3.2. *In vivo* consumption of mAb in WT and $CD32^{-/-}$ mice. 172
6.3.3. Comparing the rate of AT130-2 consumption in WT, $CD32^{-/-}$ and γ-$chain^{-/-}$ mice 177
6.3.4. Repeated doses of AT130-5 *in vivo.* 179
6.3.5. Tissue specific consumption of mAb *in vivo***.** 179

6.4. *In vivo* antigenic modulation of CD32. 183
6.4.1. *In vivo* antigenic modulation of CD32 in the WT mouse. 183
6.4.2. Loss of surface CD32 *in vivo* is not a result of FcγR-dependent macrophage shaving. 185

6.5. *In vitro* antigenic modulation of lymphoma cell lines and WT B cells. 187

6.6. Alexa-488 quenching assays demonstrate internalisation of CD32 by agonistic anti-CD32 mAb *in vitro.* 190

6.7. CD32 modulation on non-B cells (BMDMs). 192
6.7.1. Modulation of CD32 on BMDMs *in vitro.* 192

6.8. B cells express the CD32b1 isoform and macrophages express the CD32b2 isoform. 194

6.9. The effects of anti-CD32 mAb in adoptive transfer assay. 196
6.9.1. The anti-CD32 mAb can deplete target B cells in adoptive transfer depletion assays in $CD32^{-/-}$ but not WT recipients. 196

6.10. Effect of anti-CD32 mAb consumption on CD32 expression *in vivo.* 198

6.11. Anti-CD32 mAb immunotherapy in $CD32^{-/-}$ mice inoculated with BCL_1. 201

6.12. Depletion of B cells and macrophages in the BCL_1 model of lymphoma. 203

6.13. Chapter discussion. 206

CHAPTER 7 Concluding remarks and future directions 215

APPENDICES 223

Appendix 1: Common Stock buffers 223

Appendix 2: 60 – 70 kDa band detected by Western blot associated with phosphorylation of CD32. 227

Appendix 3: Binding of anti-FcγR mAb to FcγR fusion proteins by ELISA. 229

Appendix 4: Densitomerty analysis of Figure 5.2 and Figure 5.3. 231

REFERENCES 233

List of figures

CHAPTER 1

Figure 1.1. Methods of immunotherapy.....3
Figure 1.2. The structure of IgG1.....9
Figure 1.3. Effector function of mAb therapy.....14
Figure 1.4. The FcγR family. 21
Figure 1.5. Structure of FcγRIIb and the interaction between FcγRIIIa and IgG1. 26
Figure 1.6. Schematic demonstrating confirmational change in IgG after interaction with FcγR. 27
Figure 1.7. Activatory FcγR signalling. 32
Figure 1.8. B-cell signalling. 35
Figure 1.9. Schematic to show the co-ligation of the BCR and CD32 by immune complex engagement. 42
Figure 1.10. SHIP-1 mediated inhibition of BCR activity after CD32 co-ligation.....45

CHAPTER 3

Figure 3.1. Kaplan Meier curve of Eμ-myc and Eμ-myc/CD32$^{-/-}$ mice. 76
Figure 3.2. Size and location of commonly occurring tumours in Eμ-myc mice. 77
Figure 3.3. Comparison of spleen weight and lymph node size between Eμ-myc and Eμ-myc/CD32$^{-/-}$ mice. 80
Figure 3.4. Altered histology in the lymphoid organs of Eμ-myc mice. 82
Figure 3.5. Tumour infiltration of peripheral tissues in the Eμ-myc mouse. 83
Figure 3.6 Altered histology in the lymphoid organs of Eμ-myc/CD32$^{-/-}$ mice. 85
Figure 3.7. Immunophenotyping of Eμ-myc primary lymphoma cells. 87
Figure 3.8. Immunophenotyping of Eμ-myc/CD32$^{-/-}$ primary lymphoma cells. 87
Figure 3.9. Changes in IgM expression of Eμ#6 primary lymphoma cell lines adapting to culture. 94
Figure 3.10. Changes in IgM expression of Eμ#7 primary lymphoma cell lines adapting to culture. 94
Figure 3.11. Response to anti-BCR and etoposide treatment. 95

CHAPTER 4

Figure 4.1, Binding profiles of anti-CD32 mAb against WT, CD32$^{-/-}$ and CD16$^{-/-}$ splenocytes. 106
Figure 4.2. FITC-conjugated anti-CD32 mAb labelling of Eμ myc cell lines. 106
Figure 4.3. BIAcore analysis of anti-CD32 mAb. 107
Figure 4.4. Cross-blocking by the anti-CD32 mAb. 110
Figure 4.5. Anti-CD32 mAb block immune complex binding. 111
Figure 4.6. Tyrosine phosphorylation of CD32, SHIP-1 and pSHP by anti-IgM antibodies. 112
Figure 4.7. Tyrosine phosphorylation of CD32 by anti-CD32 mAb. 114
Figure 4.8. Tyrosine phosphorylation of CD32 and SHIP-1 by anti-CD32 mAb. 114
Figure 4.9. Tyrosine phosphorylation of SHIP-1 by AT130-2 and anti-IgM. 115
Figure 4.10. Effect of whole IgG or F(ab')$_2$ fragment CD32 mAb on tyrosine phosphorylation of CD32. 116
Figure 4.11. Schematic demonstrating the *cis* and *trans* engagement of CD32 by anti-CD32 mAb on CD32 expressing cells. 118

Figure 4.12. Tyrosine phosphorylation of CD32 is cis-acting rather than trans-acting. ... 118
Figure 4.13. Engagement of CD32 by the Fc domain of anti-idiotype mAb reduces the magnitude of anti-idiotype Ca^{2+} signalling. ... 120
Figure 4.14. The effect on anti-idiotype induced calcium flux by pre-incubation with CD32 mAb. ... 122
Figure 4.15. The effect on anti-IgM, Fcμ induced calcium flux by pre-incubation with CD32 mAb. ... 123
Figure 4.16. Effect on BCR-induced Ca^{2+} flux by IgG and $F(ab')_2$ fragment CD32 mAb. ... 124
Figure 4.17. Induction of programmed cell death by anti-CD32 mAb. ... 127
Figure 4.18. Programmed cell death induced by AT130-2 (anti-CD32 mAb) on the Eμ-myc and Eμ-myc/$CD32^{-/-}$ cell lines. ... 127
Figure 4.19. Correlation between CD32 expression and programmed cell death. ... 129
Figure 4.20. Effect of whole IgG and $F(ab')_2$ fragment on CD32 induced PCD. ... 130
Figure 4.21. Correlation between BCR and CD32 expression on Eμ-myc LCLs. ... 131
Figure 4.22. Comparison of relative cell death of IgM positive and IgM negative Eμ-myc LCL. ... 132
Figure 4.23. Additive effect of anti-CD32 mAb and anti-BCR stimulation on PCD. ... 134
Figure 4.24. Proposed binding of agonistic and antagonistic anti-CD32 mAb. ... 140

CHAPTER 5

Figure 5.1. Purification of splenic B cells and their expression of CD32. ... 142
Figure 5.2.Tyrosine phosphorylation of CD32 in C57BL/6 splenic B cells. ... 144
Figure 5.3. Tyrosine phosphorylation of CD32 in BALB/c splenic B cells. ... 144
Figure 5.4. Tyrosine phosphorylation of CD32 and SHIP-1 in C57BL/6 and BALB/c splenic B cells. ... 145
Figure 5.5. The effect of anti-CD32 mAb on BCR-induced calcium flux in normal splenic B cells. ... 146
Figure 5.6. Induction of programmed cell death by the anti-CD32 mAb in normal splenic B cells and comparison with lymphoma cell lines. ... 147
Figure 5.7. BMDM differentiation during adaption to culture ... 149
Figure 5.8. Expression of CD32 on C57BL/6 and BALB/c BMDMs. ... 149
Figure 5.9. Tyrosine phosphorylation of CD32 and SHIP-1 on BMDMs. ... 150
Figure 5.10. Induction of PCD by the anti-CD32 mAb on BMDMs. ... 151
Figure 5.11. Schematic of the phagocytosis assay. ... 153
Figure 5.12. The anti-CD32 mAb are able to induce phagocytosis of opsonised B cells. 154
Figure 5.13. Induction of phagocytosis is dependent on mAb binding. ... 156
Figure 5.14. Phagocytosis is dependent on expression of activatory FcγR and is enhanced in $CD32^{-/-}$ BMDMs. ... 158
Figure 5.15. Treatment of BMDMs with anti-CD32 mAb leads to augmented phagocytosis. ... 160

CHAPTER 6

Figure 6.1. Anti-idiotype BCL_1 immunotherapy shows improved efficacy in $CD32^{-/-}$ mice compared with WT mice. ... 167
Figure 6.2. Effect of anti-CD32 mAb alone and in conjunction with anti-idiotype therapy of BCL_1 tumour. ... 168
Figure 6.3. BCL_1 tumour tracking assay. ... 170
Figure 6.4. A31 tumour tracking assay. ... 171

Figure 6.5. Antibody serum levels in WT mice after inoculation with BCL_1 and treatment with mAb.....174
Figure 6.6. Schematic for anti-CD32 mAb detection in murine serum by ELISA.....175
Figure 6.7. Serum levels of AT130-2 in BALB/c mice inoculated with 2 x 10^7 BCL_1.....176
Figure 6.8. Serum mAb levels of AT130-2 in WT, $CD32^{-/-}$ and γ-$chain^{-/-}$ mice and rit m2a in WT, CD20 Tg and CD20 Tg/γ-$chain^{-/-}$ mice. 178
Figure 6.9. Serum mAb levels of AT130-5 in WT mice injected with multiple 0.5 mg doses of anti-CD32 mAb. 181
Figure 6.10. Serum mAb levels of AT130-2 in WT, B cell and macrophage depleted mice. 182
Figure 6.11. *In vivo* antigenic modulation of CD32 in WT mice. 184
Figure 6.12. *In vivo* antigenic modulation of CD32 on B cells from WT and γ $chain^{-/-}$ mice after treatment with anti-CD32 mAb. 186
Figure 6.13. *In vitro* modulation of CD32 on WT B cells. 188
Figure 6.14. *In vitro* modulation of CD32 on lymphoma cell lines. 189
Figure 6.15. The agonistic and antagonistic anti-CD32 mAb show divergent CD32 modulation on πBCL_1 cell *in vitro*. 190
Figure 6.16. Alexa-488 quenching of C57BL/6 CD20 Tg B cells by anti-CD20 and CD32 mAb. 191
Figure 6.17. Fluorescence microscopy of C57BL/6 CD20 Tg B cells stained with anti-CD20 and CD32 mAb. 192
Figure 6.18. *In vitro* modulation of CD32 on BMDMs. 194
Figure 6.19. Expresssion of CD32 isoforms in normal murine B cells, macrophages and lymphoma cells. 195
Figure 6.20. Depletion of target cells by anti-CD32 mAb in WT and $CD32^{-/-}$ recipients. 197
Figure 6.21. Target cells depletion by the anti-CD20 mAb is greater than that by the anti-CD32mAb. 198
Figure 6.22. Antigenic modulation on target cells in adoptive transfer experiments in WT and $CD32^{-/-}$ mice. 200
Figure 6.23. Increasing the dose of AT130-2 does not increase deletion of target cells in adoptive transfer experiments in WT or $CD32^{-/-}$ mice. 201
Figure 6.24. Anti-CD32 mAb improve survival alone and in combination with anti-idiotype therapy in $CD32^{-/-}$ mice. 203
Figure 6.25. The effects of B cell and macrophage depletion on anti-CD32 mAb therapy in combination with anti-idiotype therapy. 206

Lists of tables

CHAPTER 1

Table 1.1. List of approved anti-cancer mAb and their clinical application. 11
Table 1.2. Summary of the expression of FcγR in mice and humans and preferential binding to IgG subclasses. 23
Table 1.3. The outcome of activatory FcγR engagement on different cell types. 29

CHAPTER 2

Table 2.1. Table 2.1: Summary of antibodies. 71
Table 2.2. Antibodies for Western Blotting 72

CHAPTER 3

Table 3.1. Criteria used to determine lymph node size in Eμ-myc and Eμ-myc/CD32$^{-/-}$ mice 78
Table 3.2. Weight of spleen and size of lymph nodes in Eμ-myc mice. 78
Table 3.3. Weight of spleen and size of lymph nodes in Eμ-myc/CD32$^{-/-}$ mice. 79
Table 3.4. Tumour infiltration in the Eμ-myc mouse. 84
Table 3.5. Summary of Eμ-myc primary phenotypes 88
Table 3.6. Summary of Eμ-myc/CD32$^{-/-}$ primary lymphoma phenotypes 89
Table 3.7. Tumour transplantability of primary tumours from Eμ-myc and Eμ-myc/CD32$^{-/-}$ mice 90
Table 3.8. *In vitro* and *in vivo* growth of the Eμ-myc/CD32$^{-/-}$ primary lymphomas. 91
Table 3.9. Percentage responsiveness of the Eμ-myc and Eμ-myc/CD32$^{-/-}$ population to DNA damge and BCR stimulation. 93
Table 3.10. Summary of Eμ-myc lymphoma cell line characteristics. 96
Table 3.11. Summary of Eμ-myc/CD32$^{-/-}$ lymphoma cell line characteristics 97

CHAPTER 4

Table 4.1. Isotype and affinity of the anti-CD32 mAb. 108
Table 4.2. Induction of programmed cell death on cell lines from Eμ-myc and Eμ-myc/CD32$^{-/-}$ mice. 128
Table 4.3. Summary of anti-CD32 mAb activity on lymphoma cells *in vitro*. 140

CHAPTER 5

Table 5.1. Summary of anti-CD32 mAb properties in normal splenic B cells from C57BL/6 mice 148
Table 5.2. Summary of anti-CD32 mAb properties in normal splenic B cells from BALB/c mice 148
Table 5.3. Summary of anti-CD32 mAb properties on BALB/c BMDMs. 161

Declaration of Authourship

I, **Emily Williams** declare that the thesis entitled:

Manipulation of immunotherapy by targeting the inhibitory FcγR.

and the work presented in the thesis are both my own, and have been generated by me as the result of my own original research. I confirm that:

- this work was done wholly or mainly while in candidature for a research degree at this University;
- where any part of this thesis has previously been submitted for a degree or any other qualification at this University or any other institution, this has been clearly stated;
- where I have consulted the published work of others, this is always clearly attributed;
- where I have quoted from the work of others, the source is always given. With the exception of such quotations, this thesis is entirely my own work;
- I have acknowledged all main sources of help;
- where the thesis is based on work done by myself jointly with others, I have made clear exactly what was done by others and what I have contributed myself;
- none of this work has been published before submission.

Signed: ……..

Date:…….

Dedication

This thesis is dedicated in memory of my mother, Susan Angela Williams, whose encouragement, love and belief resulted in my pursuit of this degree.

Acknowledgements

Firstly I would like to thank my PhD supervisors, Professor Martin Glennie and Professor Mark Cragg. Particular thanks go to Mark who, in my opinion, has gone above and beyond in helping with the execution and preparation of this thesis and has had untiring patience with my sometimes rather interesting brand of explanations. Thank you for your support, encouragement and guidance over the last few years - although I am grateful that you will no longer be returning my work covered in red pen and suggestions – who would ever have thought that the word "good" accompanied by two ticks would bring such elation?

Secondly and most importantly, I would like to thank (although such a small word does not do justice to my gratitude) Mrs Christine Penfold, who spent many hours preparing the anti-CD32 mAb – thank you for making me a priority and for supporting my antibody habits. Thanks also to Miss Alison Tutt who initially raised these mAb and was always on hand to answer any questions I might have and to Dr Claude Chan for his production of AT128 m2a. Thank you also to Ruth and Ann for their invaluable advice.

Thanks go to Tenovus Cardiff and the Leukaemia Research Fund for funding this project.

Huge thanks are also required for the insightful conversations of Dr Stephen Beers, although not always scientific! Your availability to answer questions and participate in discussions about my experiments helped me gain a deeper understanding of the subject area, experimental procedures and science in general. Thank you for the confidence.

Special recognition to the girls of the Tenovus BRF, in particular Mel and Vicki. Thank you for accommodating my "complicated" experiments. Thank you also to Kerry for her outstanding help with some of the animal work in this thesis – thank you for never saying no to my requests.

I would also like to extend my appreciation to ALL members of Tenovus (past and present), those who have provided the essential tea-time cakes, an ear to bend or a helpful word. To Claire, Charlie and Franky – thank you for listening regardless of the subject.

On a more personal note I would like to thank my family. Thank you to my parents for their lifelong encouragement and love, to Chetna for her unwavering friendship and to Lee for making the whole process just that little bit easier – I couldn't have done it without you.

Abbreviations

A/I:	Activatory-to-inhibitory
ADCC:	Antibody-dependent cell-mediated cytotoxicity
Ag:	Antigen
anti-id:	Anti-idiotype
AnV:	AnnexinV
APC:	Allophycocyanin (flurochrome)
APC:	Antigen presenting cells
Asn (N):	Asparagine
BCL_1:	B cell lymphoma-1 (tumour)
Bcl-2:	B cell lymphoma-2 (protein)
BCR:	B cell receptor
BL:	Burkitt's lymphoma
BLNK:	B cell linker protein
BMDMs:	Bone marrow dervived macrophages
bp:	Base pairs
BSA:	Bovine serum albumin
Btk:	Burton's tyrosine kinase
C:	Constant
CAR:	Chimeric antigen receptors
CD:	Cluster of differentiation
CD40L:	CD40 ligand
CDC:	Complement dependent cytotoxicity
Cdc42:	Cell division control protein 42 homolog
CDRs:	Complementarity determining regions
CFSE:	Carboxyfluorescein succinimidyl ester
CHOP:	Cyclophosphamide, hydroxydaunorubicin (doxorubicin), oncovin (vincristine
CIA:	Collagen-induced arthritis
CLL:	Chronic lymphocytic leukaemia
CO_2:	Carabon dioxide
COS-1:	Chinese hamster ovary-1 (cells)
CTLA-4	Cytotoxic T-Lymphocyte Antigen 4
CTLs:	Cytotoxic T lymphomcyte
D1:	Domain 1
D2:	Domain 2
D3:	Domain 3
DAG:	Diacylglycerol
DC:	Dendritic cell
DLBL:	Diffuse large B cell lymphoma
DMEM:	Dulbecco's Modified Eagle Medium
DMSO:	Dimethyl sulfoxide
DNA:	Deoxyribonucleic acid
Dok-1:	Adaptor protein p62dok
EBV:	Epstein-Barr virus

ECACC:	European Collection of Animal Cell Cultures
EDTA:	Ethylenediaminetetraacetic acid
ELISA:	Enzyme-linked immunosorbent assay
Erb-2:	Epidermal growth factor receptor type-2 (HER-2/neu)
ERK:	Extracellular signal-regulated kinase
Eμ:	Immunoglobulin heavy chain enhance
FcR:	Fc receptor
FcRn:	Neonatal Fc receptor (Brambles receptor)
FCS:	(Heat inactivated) Foetal Calf Serum
FcαR:	Fc alpha receptor
FcγR:	Fc gamma receptor
FcγRI:	CD64 (humans/mice)
FcγRII:	CD32 (mouse)
FcγRIIa:	CD32a (humans)
FcγRIIb:	CD32b (humans)
FcγRIII:	CD16 (mouse)
FcγRIIIa:	CD16 (humans)
FcεR:	Fc epsiolin receptor
FDCs	Follicular dendritic cells
FITC:	Fluorescein isothiocyanate
FL:	Follicular lymphoma
FL1-H:	Fluorescence channel 1
FL2-H:	Fluorescence channel 2
FL4-H:	Fluorescence channel 4
FSC-H:	Forward scatter
GC:	Germinal centre
GPI:	Glyco-Phosphatidyl Inositol
gαm:	Goat anti-mouse
H&E:	Hematoxylin and eosin
H:	heavy
h:	human
HI:	high
His (H)	Histine
HLA:	Human leukocyte antigen
HPLC:	High-performance liquid chromatography
HPV:	Human papilloma virus
hr:	Hour
HRP:	Horse radish peroxidise
i.p.:	Intraperitoneal
i.v.:	Intravenous
IC:	Immune complex
IFL:	Irinotecan, 5-fluorouracil, and leucovorin
IFN-α:	Interferon alpha
IFN-β:	Interferon beta
IFNγ:	Interferon gamma
Ig:	Immunoglobulin
IgG:	Immunoglobulin G class

Ig_h:	Immunoglobulin heavy chain
IgSF:	Immunoglobulin superfamily
Ig-α:	CD79a
Ig-β:	CD79b
IL-10:	Interleukin 10
IL-4:	Interleukin 4
Ile (I):	Isoleucine
ILN:	Inguinal lymph node
IP_3:	Inositol triphosphate
IP_3R:	Inositol triphosphate receptor
Irr:	Irrelevant
ITAM:	Immunoreceptor tyrosine-based activation motif
ITIM:	Immunoreceptor tyrosine-based inhibition motif
JNK:	c-jun N- terminal kinase
kDa:	Daulton (atomic mass unit)
L:	Light
LCL:	Lymphoma cell lines
Leu (L):	Leucine
LN:	Lymph node
LO:	Low
m :	Murine
mAb:	Monoclonal antibody
MAC:	Membrane attack complex
MAPK:	Mitogen-activated protein kinase
MB-lectin:	Mannan binding lectin
M-CSF:	Macrophage colony stimulating factor
MFI:	Mean fluorescence intensity
MgCl2:	Magnesium chloride
MHC:	Major histocompatibility complex
min:	Minute
MM:	Multiple myeloma
MMAE:	Monomethyl auristatin E
MOPS:	3-(N-morpholino)propanesulfonic acid
MRC:	Medical research council
MΦ:	Macrophage
NaCl:	Sodium chloride
NHL:	Non-Hodgkin's lymphoma
NK cell:	Natural killer cell
NQ:	Non quenched
NT :	Non-target (in the context of CFSE experiments)
NT:	Not tested
OPD:	o-Phenylenediamine tablet
OVA	Ovalbumin
Pac-1:	MAP kinase phosphatase
PBMCs	Peripheral blood mononuclear cells
PCD:	Programmed cell death
pCD32:	Phosphorylated CD32

PCR:	Polymerase Chain Reaction
PDVF:	Polyvinylidene fluoride
PE:	Phycoerythrin
PerCP:	Peridinin-chlorophyll-protein complex
PH:	Pleckstrin homology
PI:	Propidium iodide
PI3K:	Phosphoinositide-3 kinase
PIP_2:	Phoshatidylinositol-(3,4)-biphosphate
PIP_3:	Phoshatidylinositol-(3,4,5)-triphosphate
PKB:	Protein kinase B
PKC:	Protein kinase C
PLCγ:	Phospholipase C gamma
PMN:	Polymorphonuclear leukocytes (neutrophils)
Pro (P)	Proline
PSC:	Phosphatidylecholine
pSHIP:	Phosphorylated homology domain 2-containing inositol 5-phosphatases
pSHP:	Phosphorylated Src homology domain 2-containing tyrosine phophatases
PTEN:	3'inositol phosphatase
Q:	Quenched
R^2:	Coefficient of determination; correlation coefficient
Rit:	Rituximab (after molecular manipulation)
Ritux:	Rituximab
ROS:	Reactive oxygen species
RPMI:	Roswell Park Memorial Institute (medium)
Rαm:	Rabbit anti-mouse
SD:	Standard deviation
sec:	Second
SEM:	Standard error of mean
SH2:	Src homology 2
Shc:	Src homology 2 domain-containing (protein)
SHIP:	Src homology domain 2-containing inositol 5-phosphatases
SHP:	Src homology domain 2-containing tyrosine phophatases
SLE:	Systemic lupus erythematosus
SLP-76:	Leukoctye-specific phosphoprotein of 76 kDa
SNT:	Supernatant
Src:	Sarcoma (protein)
SSC-H:	Side scatter
T:	Target
TAA:	Tumour associated antigen
TBM:	Tingible body macrophages
TBS-T:	Tris buffer saline with tween-20
T-DM1:	Trastuzumab-DM1
TE:	trypsin-EDTA
TE8:	Tris-EDTA buffer at pH 8.0
Tg:	Transgenic
TGF-β:	Transforming growth factor beta
TI:	Tumour infiltration

TNFα:	Tumour necrosis factor alpha
Tosit:	Tositusimab
v/v:	Volume per volume
Val (V)	Valine
V:	Variable
VEGF:	Vascular endothelial growth factor
VEGFR:	Vascular endothelial growth factor receptor
w/v:	Weight per volume
wk:	Weak
WT:	Wild-type
x g:	Times gravity
α-chain:	Alpha chain
γ-chain:	Gamma chain

CHAPTER 1 Introduction

1.1. Introduction.

Enhanced medical treatment for infectious diseases in the Western world is supporting an ever increasing aging population. As a result, occurrence of diseases often associated with an aging population, such as cancer, are becoming more prevalent. Cancer has quickly become the second leading cause of mortality in the UK; affecting almost 300,000 people each year[1]. As a result, medical science is continually searching for improved therapeutics for the treatment for cancer and although surgery, chemotherapy and radiotherapy have been successful, they have limitations in preventing tumour recurrence/metastases and often have severe side-effects.

One of the key criteria of an ideal therapeutic is specificity – an entity capable of binding to its target (such as a tumour associated antigen (TAA)) without cross-reactivity for other molecules (for example those on host tissues). These properties would help prevent deleterious side-effects and is central to the concept of targeted therapy which was first postulated by Paul Ehrlich over 100 years ago and lead to the notion of the "magic bullet". Although the magic bullet was originally proposed as a chemical entity, it was really only with the discovery of antibodies with their exquisite target specificity in the early 1900's that this dream began to be realised[2]. More specifically, the development of monoclonal antibody (mAb) technology by Köhler and Milstein in the 1970s reinvigorated the "magic bullet" concept and has since lead to mAb being successfully applied to the treatment of a plethora of diseases, from autoimmunity to cancer. In the latter, the aim of mAb treatment is to induce cell clearance or deletion by specifically targeting antigens preferentially expressed by tumour cells. Over the last 3 - 4 decades, we have developed a good knowledge of the mechanisms employed by mAb to delete tumour cells, increasing their success and leading to the situation today where we currently have 10 different mAb approved for the treatment of cancer (Table 1).

Perhaps the best example of a type of cancer that has benefitted from the introduction of therapeutic mAb is B cell lymphoma and more specifically, non-Hodgkin's lymphoma (NHL). This particular form of cancer originates from lymphocytes and can be characterised by transformed lymphoma cells accumulating in lymphoid organs, often with detrimental effects, such as reduction in the number and quality of other immune cells. Lymphoma is the 6th most common cancer in the UK, accounting for 10,000 new cases

annually with 85% being of B-cell origin[3]. Lymphoma, like many other cancers, occurs as a result of genetic mutations that alter normal cellular control and thus leads to uncontrolled expansion of cells, which will eventually saturate the normal lymphocyte compartment [4]. In 2005, of those diagnosed with lymphoma just under half (4,451 people) died within 5 years of presentation, as a result of the disease, thus identifying a substantial need for improved treatment[5]. Historically, lymphoma has been treated using chemotherapy and radiotherapy. However, as mentioned, these therapies have considerable side effects, such as pain, nausea and hair loss. Recent advancements in lymphoma treatment have both improved tumour clearance and reduced side effects. For example, the clinical introduction of the anti-CD20 mAb, rituximab, has significantly improved disease survival (Reviewed in [3]). Despite these advances, there is still considerable scope for the enhancement of lymphoma immunotherapy.

This thesis is concerned with the improvement of mAb therapy and although we will outline current immunotherapeutic strategies, our discussions will focus on therapeutic mAb. In particular, we will be discussing the role of the Fc gamma receptors (FcγR) in the induction of anti-tumour responses by mAb, focusing on evidence that points towards the inhibitory FcγR, FcγRIIb (CD32b) in humans and FcγRII (CD32) in mice as an immunotherapeutic target for the treatment of cancer.

1.2. Immunotherapy.

Immunotherapy can be defined as the treatment of disease by inducing, enhancing or suppressing the immune system and is a promising means of cancer therapy as it has the potential to provide specific tumour targeting without negative side effects. In the case of cancer, immunotherapy attempts to utilise the patient's own immune system to reject, destroy and clear tumour cells and in some cases provide long term immunity against tumour regrowth.

There are currently two main categories of cancer immunotherapeutic agents employed in the clinic to target malignant cells. The first are the active immunotherapies, where the patient's own immune system is hijacked to stimulate an immune response against tumour cells. Commonly this is achieved by the administration of vaccine strategies or the application of immunostimulatory mAb. The second is passive immunotherapy, which involves the administration of immune components not generated in the patient to directly target tumour cells, such as cytokines and direct targeting mAb, or adoptively transferred

immune cells, for example T cells or natural killer (NK) cells. Examples of immunotherapeutic strategies are shown in Figure 1.1.

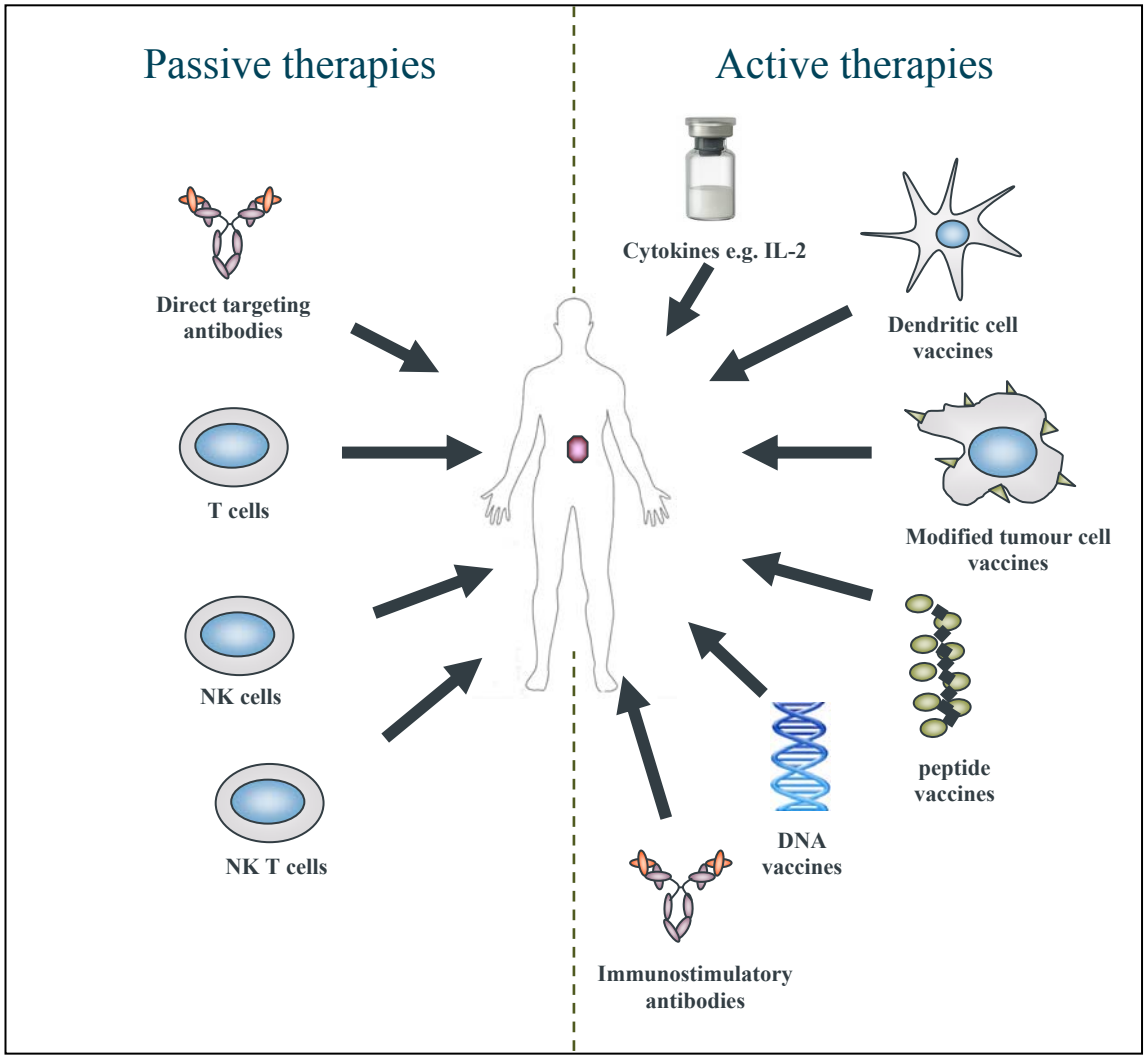

Figure 1.1. Methods of immunotherapy.
Immunotherapy can be broadly sub divided into passive and active immunotherapies. The passive immunotherapies (left) involve the transfer of aspects of the immune system not raised in the patient that are directed against a specific tumour associated antigen, whilst the active immunotherapies (right) involve reagents that will stimulate the patient's own immune system to generate an anti-tumour response. Reproduced with kind permission from Dr Juliet Gray.

1.2.1. Active immunotherapeutic strategies.

1.2.1.1. Cancer vaccination.

Cancer vaccination commonly involves the immunisation of patient's with antigenic peptides derived from the tumour, in the hope of stimulating an immune reaction directed specifically against the tumour cells[6]. There are several different ways in which this is achieved, including the use of peptide loaded dendritic cells (DC), modified tumour cells, isolated TAA and DNA vaccines (Reviewed in [7]). For example, animal studies have demonstrated that activated DC loaded with synthetic peptide[8], tumour lysates[9], tumour RNA[10] or dying tumour cells[11] have been able to produce tumour specific immunity in a

variety of animal studies. However, these reagents have demonstrated limited efficacy in clinical trials in humans and require concurrent vaccine optimization and regulatory T cell reduction[12,13]. In addition, tumour vaccines are limited currently in many cancer types by our knowledge of tumour antigens, thus limiting targets for vaccination. Recently however, fusions of DC and tumour cells have been used and shown to produce more potent anti-tumour immunity, possibly as the use of whole tumour cells expands the range of TAA presented by the DC to T cells. However, even these DC/tumour cell fusions have shown limited efficacy in phase I/II clinical trials (Reviewed in [14]). Alongside this, the use of autologous cells means that these vaccines have to be individually produced and this leads to increased cost, commonly associated with other forms of cancer vaccination and other cell based therapies, which will be discussed in section 1.2.2.

Despite these various drawbacks, a plethora of therapeutic cancer vaccines are currently being developed for the treatment of a variety cancers, including, breast[15], lung[16], and prostate[17] cancers. These vaccines have been shown to be safe, with few clinical side-effects, but with limited clinical response. More recently investigations have administered additional therapeutics, such as electroporation, alongside the cancer vaccine to increase efficacy, although this is associated with increased side effects[18]. It has also been suggested that cancer vaccines will be of most use where the tumour burden is low, in a minimal residual disease context[19], such as after surgery or chemotherapy.

An alternative approach to targeting the tumour antigens specifically involves vaccination against agents that have a strong causative link to cancer development and as such can be described as prophylactic cancer therapies. For example human papilloma virus (HPV) infection has been linked to the development of cervical cancer. Patients are vaccinated against certain serotypes of HPV (HPV-16 and HPV-18) prior to infection with the virus as a way to prevent cervical cancer development (Reviewed in [20]). There are two HPV vaccines currently licensed for use, Gardasil (Mereck & company) and Cervarix (GlaxoSmithKline). The latter had 96.9 % efficacy at preventing HPV infections versus placebo over 4.5 years ($p < 0.0001$). This was associated with a 98 % efficacy in the reduction of cervical cancer versus placebo, with only one case of cervical cancer being recorded out of 5305 participants (Reviewed in [21]). Cervarix was approved in September 2007 by the European Union for a national vaccination programme for pre-teenage girls aged 12–13 and teenage girls aged 17–18 with a hope of reducing cervical cancer cases in the future. However, although this approach is very cost effective and vaccination being efficacious, very few cancers have such strong links to viral pathogen.

1.2.1.2. Immunostimulatory mAb.

An alternative means of stimulating an anti-tumour immune response therefore, is the use of immunostimulatory mAb. The immunostimulatory mAb aim to stimulate the patient's endogenous immune response by directly stimulating key cell surface receptors on immune cells. These types of mAb often act as surrogate ligands, providing co-stimulation to T cells to augment ineffectual anti-tumour responses and can elicit a broad immune response against the tumour. Immunostimulatory mAb achieve this by one of three main mechanisms; by providing agonistic signalling to co-stimulatory molecules on T cells, by decreasing inhibitory signalling on T cells that suppresses the immune response, or by increasing DC licensing to increase antigen (Ag) presentation by these cells[22]. The structure of mAb and the development of mAb technology that has lead to the evolution of these reagents will be discussed in detail in section 1.3.

Molecules on T cells that have been identified as targets for co-stimulation include, CD28, OX40 and 4-1BB that are expressed at various points of T cell activation. Co-ligation of these molecules with their respective ligands, expressed by antigen presenting cells (APC) CD80/CD86, OX40L and 4-IBBL, respectively, induces and enhances T cell activation. The use of agonistic mAb directed towards co-stimulatory molecules expressed by T cells has been demonstrated to augment T cell proliferation and survival (Reviewed in [22]). Recent work in this laboratory has demonstrated the generation of CD8+ T cell dependent anti-tumour immunity after combination treatment with various immunostimulatory mAb *in vivo* in pre-clinical mouse models[23,24]. However, there is limited clinical trials data in humans concerning the role of the immunostimulatory mAb in human disease.

In contrast, other molecules exist that antagonise T cell activation, such as anti-CTLA-4 (Cytotoxic T-Lymphocyte Antigen 4). In a recent phase III clinical trial a human anti-CTLA-4 mAb, ipilimumab, was shown to increase the survival of patients with metastatic melanoma (median survival improved from of 6.4 month to 10.1 months after treatment, p 0.003)[25]. Unfortunately, although this trail observed improvements in patient survival, it was demonstrated that treatment with ipilimumab resulted in an increase in immune-related adverse effects in 10 – 15 % of patient's compared with only 3 % of the control population. Therefore use of these mAb in the future would require the establishment of a fine balance between anti-tumour efficacy and increased autoimmunity against the host.

The development of adverse immune-related side-effects, such as the development of autoimmunity, is a key area of concern with this class of reagents. An example of such a

severe side-effect was demonstrated in the 2006 trial of TGN1412, an anti-CD28 mAb. This infamous phase I clinical trial resulted in the admission and prolonged stay in the intensive care unit in Northwick Park, of the six healthy individuals undergoing the trial due to multiorgan faliure[26]. It was thought that the adverse effects that resulted due to the anti-CD28 mAb were due to the initiation of a cytokine storm.

An alternative to mAb targeted against molecules expressed by T cell, is the use of agonistic mAb against molecules expressed on DCs, that can be used drive the activation and maturation of DCs. This results in the increased expression of co-stimulation molecules, as described above, leading to increased T cell activation and thus, further augmentation of the anti-tumour immune response. An example of such a target on DCs is CD40. Anti-CD40 mAb mimics the activity of CD40 ligand (CD40L) that is expressed by activated T cells. Pre-clinical investigations into the use of anti-CD40 mAb by this laboratory[27] and by others[28,29,30] have shown promising efficacy in animal models of B cell malignancies. More recently, humanised anti-CD40 mAb have been evaluated in phase I clinical trials in patients with relapsed multiple myeloma (MM)[31], NHL[32] and chronic lymphocytic leukaemia (CLL)[33] and have demonstrated favourable safety and some anti-tumour activity. For example, treatment with dacetuzumab (anti-CD40; SGN-40) resulted in stable disease in 20 % of MM patients (8/44)[31], and 42 % of CLL patients (5/12)[33]. Objective responses (one complete and five partial) were observed in six (out of 50) patients after treatment with dacetuzumab for NHL[32]. These trials reported no severe adverse events and those mild and moderate adverse events reported included cytokine release, fatigue, headaches, anorexia and conjunctivitis. Despite these reports, some of the largest advances in mAb immunotherapy in recent years have been through the application of direct targeting mAb, which will be discussed below.

1.2.2. Passive immunotherapeutic strategies.

There are two main branches of passive immunotherapy, direct targeting mAb that have been raised against specific TAA, which bind to the tumour cells and instigate a plethora of effector mechanisms (discussed in detail in section 1.3.3) and the adoptive transfer of immune cells. The latter commonly involves the use of tumour reactive T or NK cells. There are two approaches typically taken with regards to adoptive transfer of tumour reactive T cells. Tumour specific cells can be isolated from the peripheral blood of human leukocyte antigen (HLA)-matched donors or be derived from autologous T-cells and expanded *in vitro*. These cells are then adoptively transferred into patients, in order to target an adaptive immune response against the tumour cells[34].

There has been some clinical success using adoptively transferred cytotoxic T lymphocytes (CTLs), from an appropriately HLA-matched donor. Donor cells are selected *in vitro* due to their ability to lyse the patient's leukaemia cells and inhibit the proliferation of progenitor cells. Infusion of these cells into the patient leads to suppression of disease progression, demonstrated by eradication of CML cells *in vivo*[35,36]. Adoptive transfer of CTLs generated *in vitro* and not from donation has been shown to have clinical efficacy, where the generated CTLs lines show anti-tumour activity in the patient resulting in disease stability or even regression[37,38]. However these therapies often require the patient to undergo lymphodepletion prior to T-cell transfer, which has associated side-effects[39]. In addition, generation of tumour specific T cells is a lengthy and expensive process and transplanted cells may have limited *in vivo* longevity[40]. There are however several advantages to the use of T cell adoptive transfer therapies, including specific targeting of the anti-tumour response and the potential development of immunological memory against specific tumour antigens [34], although this is more likely however the use of vaccination strategies.

Although all these approaches have shown potential in pre-clinical and some clinical studies, to date, they have had limited clinical impact. In contrast, the direct targeting mAb have had a much greater impact on the clinic in the treatment of many malignancies. This thesis is concerned with augmenting the efficacy of direct targeting mAb. Next, we will discuss the structure of mAb, the development of mAb technology, the interactions with effector systems that allow anti-tumour activity and how these interactions could be manipulated to enhance therapeutic outcome, focusing of Fc to FcγR interactions.

1.3. Direct targeting mAb immunotherapy.

1.3.1. Antibody structure.

The structure and endogenous function of antibodies make them ideally suited as a therapeutic approach that mimics Ehrlich's "magic bullet". mAb are immunoglobulins (Ig) of which there are five Ig classes in mice and humans (IgA, IgD IgE, IgG, IgM). In general, the Ig are comprised of four separate polypeptide chains, two identical light chains ($_L$) and two identical heavy chains ($_H$), held together by both inter-chain disulfide bonds and by non-covalent interactions. Both the $_H$ and $_L$ chain can be further divided into the constant (C) and the variable (V) domains, which are comprised of several structural Ig domains. The number of Ig domains varies between Ig classes, for example, the most commonly used therapeutic Ig, IgG, contains one V and one C domain within the $_L$ chain,

whilst the $_H$ chain contains one V and three C domains, wheras IgE and IgM contain four C domains within their $_H$ chain[2].

The Ig molecule can also be divided into two functional domains which provide their specificity (Fab region) or effector functions (Fc region) (Figure 1.2). The specificity of mAb derives from the complementarity determining regions or CDRs within the V domains of the Fab regions, which possess a unique sequence and resultant binding specificity. In contrast the Fc region is composed of constant domains which are invariant for Ig of each subclass and provide the interaction with key immune effector systems such as complement and effector cells. Therapeutic mAb can employ several different mechanisms to elicit their therapeutic effects. These include Fc-dependent functions such as antibody-dependent cell-mediated cytotoxicity (ADCC), and complement-dependent cytotoxicity (CDC), as well as Fc-independent functions such as the induction of direct cell signalling that can elicit programmed cell death (PCD). Alternatively, mAb can block key pro-survival signalling in the tumour cells, by Fab regions (Figure 1.3).

There are four IgG subclasses in humans (IgG1, IgG2, IgG3 and IgG4) and these vary in their capacity to initiate host defences. Both IgGl and IgG3 can mediate ADCC and also bind complement, whereas IgG2 and IgG4 are relatively deficient in these functions, though IgG2 does have some ability to bind complement[41,42,43]. As IgG3 is also more susceptible to enzymatic cleavage than IgG1 which would limit it's half-live *in vivo*[44,45,43,46] , the most common therapeutic mAb isotype is IgG1, as it is able to initiate both ADCC and CDC, key effector systems in anti-tumour clearance by mAb[47]. It is thought that the differences in biological function between subclasses is due to differences in the amino acid composition and structure of the hinge region, where the more "flexible" hinge region of IgG1 and extended hinge region of IgG3 allow these molecules to interact more readily with effector systems, whereas the more rigid hinge region of IgG2 and IgG4 restricts such interactions [43,48]. In mice, the IgG subclasses vary slightly, (mice have IgG1, IgG2a, IgG2b and IgG3), however IgG2a and IgG2b have been demonstrated to be the most efficient IgG subclasses at engaging complement and inducing ADCC[48,49], so these isotypes are commonly used in murine therapeutic models.

The anti-tumour mechanisms induced by therapeutic mAb will be discussed in turn in section 1.3.3. Prior to this the development of mAb technology will be discussed.

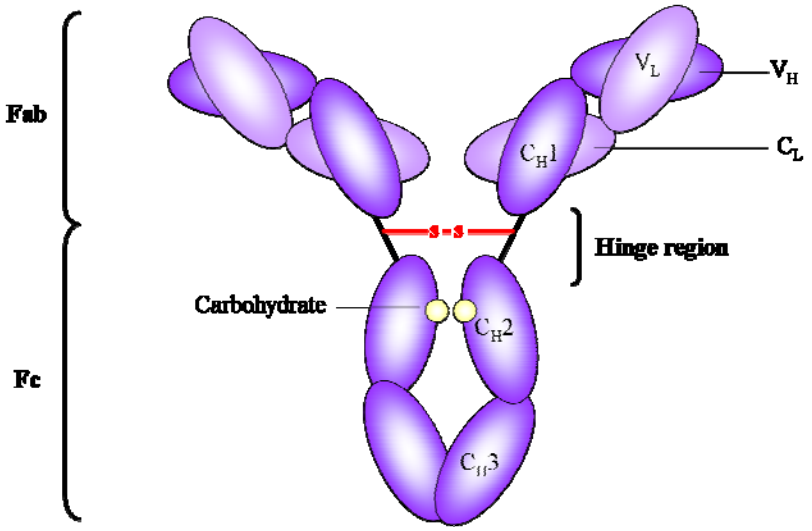

Figure 1.2. The structure of IgG1.
The general structure of an Ig is comprised of four separate peptide chain. They are comprised of two identical light chains ($_L$) and two identical heavy chains ($_H$). These chains are held together by both inter-chain disulfide bonds and by non-covalent interactions. Both the heavy and light chain can be divided into two regions, the constant region (C) and the variable region (V). In addition, the whole IgG molecule can be divided into two main functional domains, the Fab regions, which contain identical antigen binding sites for interaction with antigens and the Fc region, which engages and interacts with effector cell systems via Fc receptors and complement. Ig also contains a hinge region which provides flexibility for the molecule, which is essential for interactions with antigens. In the case of IgG1, carbohydrates are attached to the C_H2 domain. These carbohydrates aid the interaction of IgG1 with antigen and effector cells.

1.3.2. Development of mAb technology.

The first mAb were produced from the fusion between murine myeloma cells and splenocytes from mice previously immunised with a specific foreign substance (the antigen). These so-called hybridoma cells undergo selection and single cell cloning to ensure that they produce a single antibody specificity directed to a unique region of the immunised substance, known as the epitope[50]. Although a success in terms of proof of principle, therapeutically these early mAb were disappointing in terms of the magnitude of the clinical effects induced. One of the main issues confounding their use was the fact that these murine mAb elicited human anti-mouse antibody responses, or HAMA, which resulted in their rapid clearance from the circulation. For this reason and with the advent of molecular biology, subsequent years saw a concerted effort to make mAb less immunogenic.

In 1986 Jones *et al*, working under Greg Winter at the Medical Research Council (MRC) facilities in Cambridge were successful in producing chimeric murine mAb with human Fc domains[51]. These mAb retained the binding specificity of the original mAb, but with the benefits of reduced immunogenicity, longer half-life and more efficient engagement of human effector systems[52]. Moreover, in 1988, in what is considered a seminal paper in the

field, Reichmann *et al*, again working at the MRC, first introduced the concept of humanisation of murine mAb, where the specific CDRs of the murine mAb was grafted onto a human framework[42]. Later, in the early 1990s the same group produced a fully human anti-TNFα (anti-tumour necrosis factor-alpha) mAb using phage display technology[53,54]. Phage display technology by-passes the need for animal immunisation (and therefore issues of self-tolerance i.e. raising antibodies against antigens that already exist in the host) by using bacteria to express randomly generated human antibody chains that are then selected through their specific binding properties *in vitro* [54,55].

Others have also employed humanisation techniques to more fully humanise rodent mAb such as CDR grafting[56] and alternatively, immunisation of genetically modified mouse strains carrying human Ig genes to produce similar fully humanised reagents[57]. Irrespective of the technique employed, the key features of such antibodies are that mAb can be raised and targeted against targets expressed by tumour cells which have very little immunogenicity in patients. Moreover, molecular biology now allows the further manipulation of these mAb to enhance interaction with specific effector systems (discussed below), leading to the generation of so-called second and third generation mAb.

As a result of these advances in techniques for mAb generation and the introduction of these mAb into the clinic improved disease survival and increased the time to progression of various malignancies has been observed. As a result, mAb immunotherapy probably reflects the largest advance in the treatment of lymphoproliferative disorders, including lymphoma, in last 30 years. This is largely due to the clinical introduction of rituximab, a chimeric mAb that targets the B cell marker CD20. The combined use of rituximab with chemotherapy regimens (such as CHOP; cyclophosphamide, hydroxydaunorubicin (doxorubicin), oncovin (vincristine), prednisolone) for the treatment of diseases such as follicular lymphoma (FL)[58] and diffuse large B-cell lymphoma (DLBL)[59,60] has substantially increased the survival of these patients in comparison to chemotherapy alone. For example, between 1991 and 1997 mortality due to diagnosis with NHL was increasing by 1.6 % annually. With the clinical introduction of rituximab in 1997, mortality from NHL has decreased by 2.8 % annually[61]. In terms of patient survival, there was a 42 % increase in the survival of patients treated with rituximab combined with CHOP in comparison to CHOP alone[62]. In addition, rituximab is now being investigated as maintenance therapy for patients with end-stage, relapsed or refractory disease[63]. Moreover, rituximab is currently undergoing clinical trials in autoimmune disorders, such

as rheumatoid arthritis and with promising results [64,65]. Table 1.1 lists examples of other mAb that are currently being used in the treatment of cancer.

Table 1.1. List of approved anti-cancer mAb and their clinical application.

mAb name	Trade name	Type	Target	Effective in the treatment of:	Year approved:
rituximab	Rituxan®	Chimeric	CD20	non-Hodgkin lymphoma[66]	1997
trastuzumab	Herceptin®	Humanised	HER2/neu	breast cancer[67]	1998
gemtuzumab ozogamicin*	Mylotarg®	Humanised	CD33	acute myelogenous leukaemia (AML)[68]	2000
alemtuzumab	Campath®	Humanised	CD52	chronic lymphocytic leukaemia (CLL)[69]	2001
ibritumomab tiuxetan*	Zevalin®	Murine (IgG1)	CD20	non-Hodgkin lymphoma[70]	2002
tositumomab*	Bexxar®	Murine (IgG2a)	CD20	non-Hodgkin lymphoma [71]	2003
cetuximab	Erbitux®	Chimeric (IgG1)	EGFR	colorectal cancer[72] head & neck cancers[73]	2004 2006
bevacizumab	Avastin®	Humanised	VEGF-A	colorectal cancer[74] non-small cell lung cancer[75] breast cancer[76] glioblastoma[77] kidney cancer[78]	2004 2006 2008 2009 2009
panitumumab	Vectibix®	Fully human (IgG2)	EGFR	colorectal cancer[79]	2006
ofatumumab	Arzerra®	Fully human	CD20	chronic lymphocytic leukaemia (CLL)[80]	2009

Table 1.1 shows the mAb currently approved by the FDA for use in cancer treatment along with their structures, target specificity and disease indications. *indicates mAb that are conjugated to toxins or radioisotopes.

1.3.3. Effector mechanism of therapeutic mAb.

As mentioned previously, the direct targeting mAb recruit and employ a range of different effector systems in order to generate an anti-tumour response *in vivo* (Figure 1.3). In some cases, mAb can induce several different effector systems. Currently, a central focus in the field of mAb immunotherapy is delineating which are the key effector mechanisms

employed by direct targeting therapeutic mAb We discuss in more detail below the effector mechanisms employed by the direct targeting mAb.

1.3.3.1. Induction of ADCC.

ADCC is initiated when activatory FcγR, expressed by effector cells such as macrophages and NK cells, engage with the Fc portion of mAb bound to the target cell and results in the release of reactive oxygen species (ROS), cytotoxic granules and/or phagocytosis[81]. There are a variety of activatory FcγR in mice and humans, most of which require the associated gamma (γ) chain for surface expression and activity. For example, NK cells engage with tumour bound antibody via the activatory FcγRIIIa (CD16) to induce ADCC through the release of cytotoxic agents such as ROS, perforin and granzymes[82]. In addition, NK cells can release other cytokines that can directly inhibit cell proliferation, e.g. interferon-gamma (IFNγ)[52]. In contrast, macrophages elicit ADCC through phagocytosis (also known as antibody-dependent cell-mediated phagocytosis) and physical engulfment of the target cell. In mouse models, it has been shown that ADCC is essential for anti-tumour functions of mAb as γ-chain$^{-/-}$ mice, which lack surface expression of activatory FcγR, show abrogated tumour clearance[83]. Many mAb such as rituximab, but also trastuzumab (Herceptin) an anti-HER2/neu mAb[84] and alemtuzumab (Campath), an anti-CD52 mAb[85], used in the treatment of breast cancer and CLL respectively, are able to mediate ADCC at least *in vitro*. The FcγR will be discussed in greater detail in sections 1.5.

1.3.3.2. Induction of CDC.

Induction of CDC involves the mobilisation of complement cascades. The complement system is comprised of three pathways; the classical, mannan-binding lectin (MB-lectin) and the alternative pathways, which are activated by C1q, mannan-binding lectin and the spontaneous cleavage of C3, respectively. The result of all of these pathways is the production of C3 convertase. With regards to mAb mediated CDC, this is initiated when sufficient numbers of appropriately located Fc regions (of mAb) are bound by C1q, initiating the classical complement pathway. As a result, a cascade is triggered that involves the cleavage of intermediate components of the complement system, resulting in cell lysis through the assembly within the cell membrane of the membrane attack complex (MAC)[47]. Activation of the C1 complex results in the cleavage of C2 and C4, the products of which (C2b and C4b) form the C3 convertase complex. This is turn cleaves C3 to yield C3a and C3b, the latter of which associates with C3 convertase to form C5 convertase. This shift in enzymatic activity, results in the cleavage of C5 to C5a and C5b, the latter of

which associates with the cell surface and initiates the assembly of the MAC, by the binding of first C6, then C7, followed by C8 and finally the recruitment of several C9 molecules to complete the MAC and instigate cell lysis (reviewed in [86]).

In addition to the induction of cell lysis, a number of complement by-products are generated that have the potential to enhance mAb therapy. For example, the C3b fragments produced as a result of C3 cleavage by C3 convertase, leads to opsonisation, activation and enhanced phagocytic and cytotoxic activity[87]. Furthermore, several other products of the complement cascade such as C3a and C5a are potent chemotactic and inflammatory agents that could readily enhance the cytotoxicity of effector cells, thereby providing a link between the two different Fc-dependent effector functions.

1.3.3.3. Signal perturbation (PCD and altered endogenous signalling).

In addition to the Fc-dependent effector functions of mAb, binding to the target antigen through the Fab regions can also have anti-tumour effects by manipulating intracellular signalling. These occur mainly through triggering intracellular signalling in the target cell resulting in growth inhibition or PCD or by blocking the normal pro-tumour function of a targeted cell surface receptor. Examples of the former include anti-idiotype mAb, which bind to the unique regions of the B cell receptor expressed by lymphoma cells to elicit apoptosis, probably by mimicking antigen responses by immature B cells (reviewed in [88]). Examples of the latter include trastuzumab and panitumumab. Trastuzumab (Herceptin®), is perhaps the most well publicised therapeutic mAb that acts in this way. It targets the human epidermal growth factor receptor type-2 (ErbB-2), generally referred to as ‘‘HER-2/neu” that becomes over-expressed in approximately 25-30% of breast cancers[89,90]. HER2/neu is a known proto-oncogene and its expression correlates with disease progression and severity[91,92]. By blocking HER2/neu signalling, trastuzumab has been show to disrupt downstream proliferation and survival pathways, to inhibit cell cycle progression and to have anti-angiogenic effects[93]. For the treatment of HER2/neu positive metastatic breast cancer, trastuzumab, when combined with a docetaxel chemotherapy regimes, significantly enhanced the overall response rate (61% vs. 34%; P = 0.0002), overall survival (median, 31.2 vs. 22.7 months; P = 0.0325), and time to disease progression (median, 11.7 vs. 6.1 months; P = 0.0001) compared with chemotherapy alone[94,95]. Currently, trastuzumab is used for late and end-stage disease and is generally well-tolerated although is associated with some toxicity and cardiovascular events, similar to bevacizumab (see below)[96]. Other mAb with a similar mode of action include panitumumab. Panitumumab targets EGFR which is overexpressed in many human

cancers, including those of the colon and rectum and also serves to block signalling leading to growth, survival, motility and proliferation. Although blocking signalling appears the main function of these mAb, they can also induce ADCC of antibody bound tumour cells[97], further promoting their anti-tumour effects.

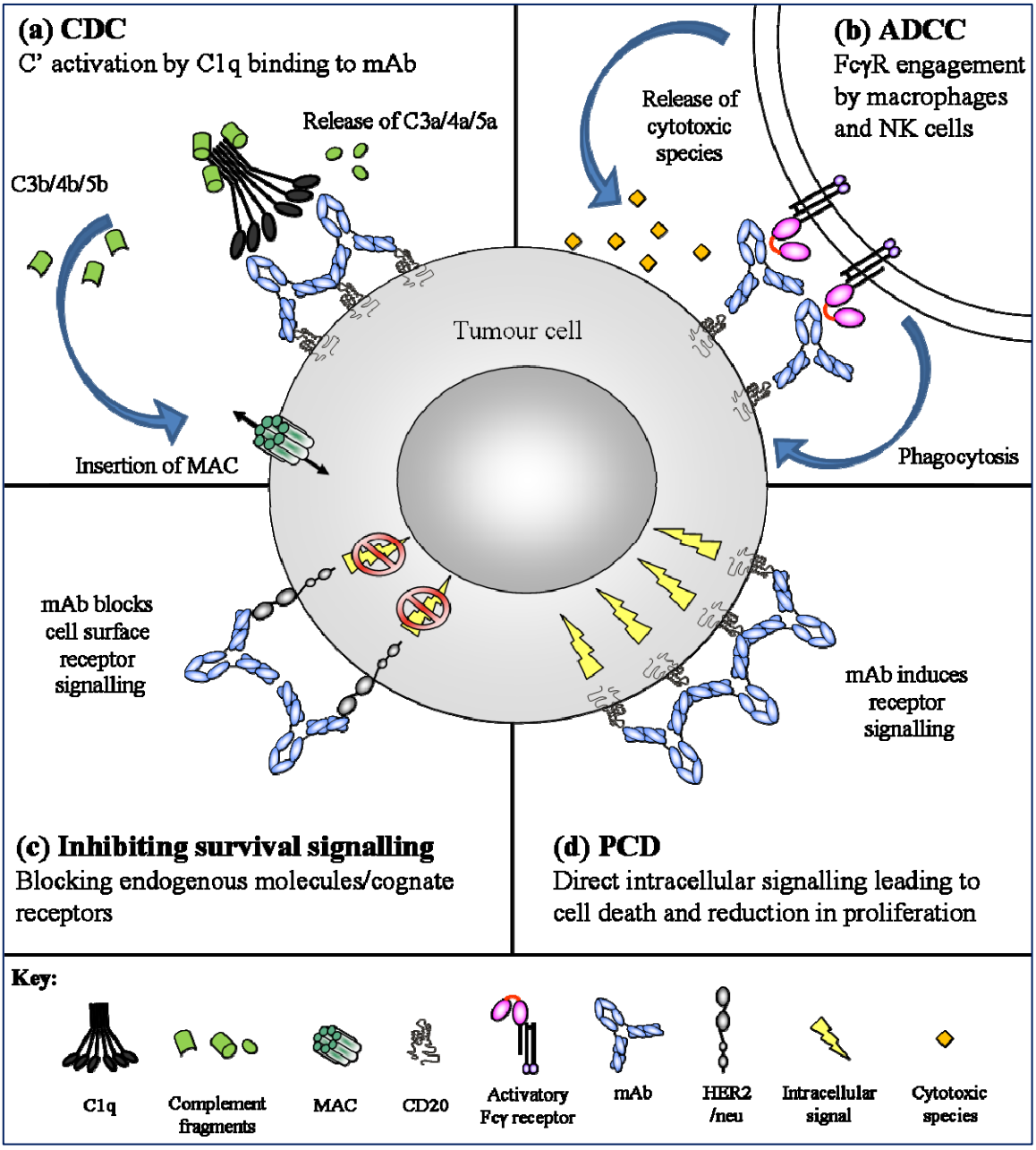

Figure 1.3. Effector function of mAb therapy.
Therapeutic mAb employ a variety of mechanisms to induce tumour cell clearance. These include (a) Complement mediated cytotoxicity (CDC) through initiation of the classical complement cascade; (b) Antibody-dependent cell-mediated cytotoxicity (ADCC) through engagement of FcγR-expressing effector cells; (c) inhibition of endogenous survival signalling arising from cell surface receptors; (d) induction of programmed cell death (PCD) by direct signalling. In addition to the mechanisms depicted, therapeutic mAb can also be employed to elicit anti-tumour effects by interacting directly with the immune system (so-called immunostimulatory mAb) or block interactions between the tumour and the microenvironment. The prime example of the latter is bevacizumab, which blocks tumour secreted VEGF from binding to host epithelial VEGFR thereby preventing neoangiogenesis

1.3.3.4. Additional anti-tumour functions.

In addition to those detailed above, mAb may also employ a variety of other mechanisms to prevent tumour growth. These include, the promotion of anti-tumour T cell responses, by the use of immunomodulatory mAb (briefly discussed in section 1.2.1.2), and the cross presentation of TAA. In this latter case, engagement of FcγR can indirectly initiate cell-mediated immune responses to tumour cells by triggering phagocytosis and ADCC, leading to antigen processing and peptide presentation[98] in a process known as cross presentation[99]. Ag presentation in the context of major histocompatibility complex (MHC) class I induces CTL activation and direct lysis of tumour cell, whereas Ag presentation in the context of MHC class II can lead to activation of T_H cells, which provide CD40 help to B-cells, initiating production of endogenous anti-tumour mAb[99].

Other additional mechanisms employed by mAb is to block critical host to tumour interactions. An example of a therapeutic mAb that functions in this way is bevacizumab (Avastin™), an antibody directed against vascular endothelial growth factor (VEGF). Bevacizumab has been used mainly in the treatment of colo-rectal cancer, but has also been implicated for use in the treatment of other solid neoplasms, such as metastatic breast cancer[76], melanoma[100] and renal cell carcinoma[78]. VEGF binds to its cognate receptor expressed on host endothelial cells (VEGFR) and encourages angiogenesis within the tumour microenvironment, a process known as tumour neovascularisation[101]. This formation of new blood vessels is a critical step in the growth and progression of solid tumours[102]. It has been shown that VEGF becomes overexpressed in certain tumours, therefore by targeting VEGF bevacizumab blocks the interaction with VEGFR and as such prevents endothelial cell proliferation and new blood vessel formation. Essentially this 'starves' the tumour cells, restricts their growth and by reducing their survival signalling makes them more susceptible to death[103]. Combination treatment of bevacizumab with chemotherapy has clear clinical efficacy[74]. For example, Bevacizumab, when given with the chemotherapy agents irinotecan, 5-fluorouracil, and leucovorin, termed the "IFL" regimen, was shown to increase the response rate (44.8% compared to 34.8%, $p = 0.004$), progression-free survival (10.6 months vs. 6.2 months, $p < 0.001$) and overall survival (20.3 months vs. 15.6 months, $p < 0.001$) in a phase III randomised trial for the treatment of colorectal cancer in comparison to IFL treatment alone[74]. Other studies have shown similar enhanced treatment efficacy in metastatic breast cancer[104] and non-small-cell lung cancer[105]. To date, bevacizumab is not a curative regime and is commonly prescribed in late-stage colorectal disease to extend patient survival, but is associated with haemostatic and cardiac problems[106]. It is also most commonly used when other, more traditional

forms of therapy have failed or when patients present with relapsed disease, due to the described side effects[107]. In addition, the use of bevacizumab as a maintenance regime has been shown to be effective and more recently in a phase II clinical trial bevacizumab showed efficacy in the treatment of carcinoma of unknown primary site, a disease that is particularly hard to treat [108].

It is important to remember that the effector mechanisms employed by therapeutic mAb are not mutually exclusive. For example, although the exact mechanism for the anti-tumour action of rituximab is still the subject of much debate, it has been shown to engage ADCC, CDC and PCD, but it is still uncertain which of these are critical *in vivo* and whether the critical mechanism is the same for each disease (reviewed in [109]). Rituximab targets CD20, a molecule which is expressed on the surface of normal and malignant B cells after the pro-B cell stage, but which is absent from plasma cells and haematopoietic stem cells. This expression pattern is important for the success of rituximab as it allows for the repopulation of B cells after therapy and allows continued antibody production by existing plasma cells. Furthermore, even mAb targeting the same receptor have been shown to work in different ways. For example, rituximab and tositumomab both target CD20 and yet appear to rely on different effector systems[110].

Rituximab triggers both ADCC and CDC strongly, whereas tositumomab appears to work through induction of ADCC and PCD with the absence of CDC (reviewed in [111]). Interestingly, the ability to induce CDC seems to be dependent on the redistribution of the target Ag into lipid raft regions of the plasma membrane[112]. For example, tositumomab does not induce relocation of CD20 into lipid rafts and as a result has been shown not to bind complement or induce CDC efficiently. The importance of complement in rituximab mediated anti-tumour effector function has been demonstrated in xenograft models of lymphoma, where reduced rituximab therapy was observed in complement depleted or deficient mice[110,113,114]. However, in other syngeneic models[115] no effect of complement deficiency was observed and an enhancement of efficacy has been seen in other models[47], implying that complement activation is a hindrance to rituximab function. For this reason, current thinking is divided as to the importance of CDC in the efficacy of rituximab in humans. It has also been proposed that mAb binding of CD20 can directly transmit intracellular signals that lead to PCD (reviewed in [111,116]), although the evidence for this (at least with rituximab) on primary tumour samples is not strong. In contrast, good evidence exists that ADCC plays an important role. In addition to the pre-clinical mouse studies detailed earlier which highlight the absolute requirement for activatory FcγR in rituximab

therapy[83], studies in humans demonstrate that patients who possess polymorphisms in the binding domain of their FcγR, specifically FcγRIIIa, which display higher affinity interactions with rituximab demonstrate increased treatment efficacy[117,118] (discussed later in section 1.10.1). For these reasons, it is currently anticipated that ADCC is the predominant effector mechanism employed by rituximab in humans, at least in FL.

1.3.4. Improving therapeutic mAb efficacy.

Despite all that is know about the abovementioned mAb, it should be noted that the direct targeting mAb are rarely used alone. Most commonly, these immunotherapeutic are employed alongside chemotherapy such as CHOP, which is administered alongside rituximab (section 1.3.2). Part of the reason for the success of therapeutic mAb is that they have limited side effects, allowing their combination with chemotherapy to increase treatment efficacy without significantly increasing negative side effects experienced by patients. Although these therapeutic mAb have made a profound impact on clinical treatment in certain instances and cancer treatment with mAb has come a long way in terms of technology and application in the clinic, they are still some way short of the "magic bullet" effect proposed by Ehrlich. The next goal in the field is therefore to improve upon these so-called naked mAb and to design mAb with augmented anti-tumour activities.

1.3.4.1. mAb conjugation.

One way in which to improve mAb efficacy is to link the mAb to toxins or radioconjugates. Three of the currently FDA approved mAb have taken this approach; gemtuzumab ozogamicin (Mylotarg®) is an anti-CD33 mAb linked to the cytotoxic calicheamicin ozogamicin for the treatment of acute myelogenous leukaemia[68], ibritumomab tiuxetan (Zevalin®) and tositumomab (Bexxar®) both of which are anti-CD20 mAb for the treatment of non-Hodgkin lymphoma[70,71]. Although efficacious, these treatments, in particular the radioconjugates, are more difficult to use clinically and are typically reserved for use in specialist centres for patients with otherwise refractive disease. More recent advancements in this field include the anti-CD30 mAb, SGN-35, which is conjugated to anti-tubulin destabilizing toxin monomethyl auristatin E (MMAE) and has been demonstrated to be well tolerated and induced objective responses in a majority of patients (discussed in [119]). Alongside this, there has been recent phase I[120] and phase II[121] clinical success following the use of trastuzumab-DM1 (T-DM1), a mAb-conjugate that combines the biologic activity of trastuzumab with an anti-microtubule

agent. DM1, belongs to a family of drugs know as maytansinoids, that are derivatives of the anti-mitotic drug maytansine. These drugs bind to microtubules, such as tubulin, inhibiting the assembly of these microtubules as a result this abrogates mitosis and cell growth[122]. The anti-microtubule reagents have shown anti-tumour efficacy and are undergoing clinical development[123]. Specifically, anti-microtubule agents have shown efficacy when combined with trastuzumab treatment of HER2/neu positive breast cancer in pre-clinical and clinical studies[124,125,126]. Further to this, direct conjugation of trastuzumab to DM1 was shown to increase the efficacy of trastuzumab in xenograft models of HER2/neu positive breast cancer[127]. As aforementioned, trastuzumab has been shown to be effective in the treatment of HER2/neu positive breast cancer, however many patient's still succumb to their disease, thus these reagents may bridge the gap in treatment of metastatic breast cancer.

1.3.4.2. Maximising FcγR:Fc interactions.

An alternative approach to those described above has been to use molecular biology and mAb engineering to maximise interactions with the mAb effector systems, particularly those governed by FcγR. There are currently two main methods for enhancing beneficial FcγR:Fc interactions leading to augmented ADCC; artificially modifying amino acids in the Fc region of antibodies using random or rational design[128-130] or removal of fucose from Fc-linked oligosaccharides[131-136]. This technology is yet to be perfected; however an example of a so called glyco-engineered mAb that is currently undergoing phase II/III clinical trials is GA101. GA101 has been developed by Roche in association with Genentech and Glycart and is thought to be a Type II anti-CD20 mAb[137]. In comparison to the unmodified parent mAb, GA101 induces much more potent ADCC and so it will be interesting to observe whether it performs better than rituximab in patients[138]. By contrast, an unmodified fully human anti-CD20 mAb, ofatumumab (Arzerra®), was just recently approved for the treatment of CLL[80]. Although unmodified, this mAb has a far higher affinity for CD20 and far higher CDC activity than rituximab, potentially due to unique binding site, and so it will be interesting to see how it performs compared to both rituximab and the glyco-modified GA101.

Despite all of these advances, central to the activity of therapeutic mAb are the interactions between mAb and FcγR. To fully appreciate these effects we next discuss the FcγR family in detail.

1.4. The Fc receptor family.

The Fc receptors (FcR) are a group of type I surface glycoproteins that are the mediators of antibody-triggered effector functions and play a role in modulating the immune response. There are specific FcR for each Ig subclass, IgE is specifically engaged by FcεRI and FcεRII (CD23), IgG is engaged by the FcγR (reviewed in [139]) and IgA is engaged by FcαRI (CD89) and also by Fcα/μR which is specific for both IgA and IgM[140]. In contrast, the neonatal FcR (FcRn) is a unique FcR and non-classical MHC class I protein, that has been shown to be involved in transcytosis, the transport of maternal Ig across the placenta and also Ig from colostrum across the infant gut[141]. FcRn is also involved in the recycling of IgG, rescuing it from intracellular degradation and therefore extremely important in extending Ig half-life[142]. With regards to immunotherapy however the FcγR, expressed predominately by cells of the haemopoietic system, hold the most interest, as almost all therapeutic mAb are of the IgG class as mentioned earlier (section 1.3.1).

1.5. The Fcγ Receptors.

There are four classes of FcγR which have been identified in mice; FcγRI (CD64), FcγRII (CD32), FcγRIII (CD16) and the more recently discovered FcγRIV[143]. They can be broadly classified into two functional groups; the activatory FcγR (FcγRI, III and IV), that contain immunoreceptor tyrosine-based activation motif (ITAM) within their signalling domains and the inhibitory FcγR, (FcγRII) that contains immunoreceptor tyrosine-based inhibition motif (ITIM) within its cytoplasmic domain. In humans, the expression profile of FcγR is slightly different and although the functional group classification is identical, additional isoforms of FcγR have been noted in humans, i.e. isoforms of FcγRI (FcγRIa, FcγRIb & FcγRIc) and FcγRII, (FcγRIIa and FcγRIIc) do not exist in mice, whilst FcγRIV does not seem to be expressed in humans[143]. It has however been reported that FcγRIIIa, expressed in humans is likely to be homologous to the FcγRIV in mice[144], whilst human FcγRIIa is most similar to mouse FcγRIII[145] (Figure 1.4). In humans the inhibitory FcγR has the nomenclature of FcγRIIb (CD32b) to distinguish it from FcγRIIa and FcγRIIc, whereas in mouse it is referred to simply as FcγRII (CD32).

The FcγR are widely expressed throughout the haematopoietic system[146], although there is little evidence of their constitutive expression on T lymphocyte populations[147,148,149]. Cells of the innate immune system, such as mast cells, neutrophils and macrophages, co-express both inhibitory and activatory FcγR and the relative levels of expression of the activatory FcγR also varies between cell types[150]. For example, in mice, monocytes and macrophages

express all of the FcγR, whereas in contrast, neutrophils predominately express CD32, FcγRIII and FcγRIV (Table 1.2). In contrast, other cell types, such as B and NK cells only express one type of FcγR. B cells in mice and humans only express the inhibitory FcγR, whereas mouse NK cells only express FcγRIII (CD16). In addition to expression on haematopoietic cells FcγR expression on other cell types, such as follicular dendritic cells (FDC), endothelial cells, microglial cells, neural crest cells, osteoclasts and mesangial cells has also been demonstrated, although, with the exception of FDCs, the roles of the FcγR on these cell types has not been rigorously tested[143 151].

The differential expression of the FcγR is also thought to provide a mechanism for "fine-tuning" the response of particular cell types to IgG engagement, where the balance of activatory and inhibitory engagement regulates cell activation and effector cell function by setting cellular activation thresholds (discussed below). This regulation of cell activation is essential, as, for example, it has been shown that when there is deficiency in the expression of the inhibitory FcγR, there is heightened inflammatory response[152] and increased DC maturation[153] in response to immune complex (IC) and an almost completely abrogated response to IC in cases where there is a deficiency in activatory FcγR[153,154]. Alongside this, $CD32^{-/-}$ mice have been demonstrated to have increased antibody responses, cytokine production and macrophage activation[154]. Therefore, this indicates that the balance between activatory and inhibitory FcγR determines the magnitude of the immune response.

Interestingly, there are several reports of alternative ligands for the FcγR, including complement-reactive protein (CRP)[155], oxidised low density lipoprotein[156] and complement receptor 3 or MAC-1[157]. CRP is a produced during the acute phase response to infection, inflammation, and trauma and binds to FcγRI and FcγRII on the surface of cells during the inflammatory response, but this is inhibited by prior exposure to IgG[158]. However, in the inflammatory environment binding of CRP to cells, such as macrophages and neutrophils may enhance tumourcidal activity, by promoting complement binding and oxidative metabolism[159,160], thus influencing and augmenting the anti-tumour response mediated through effector cells. In addition, early literature suggests that alternative ligands for FcγR may be expressed on thymic and bone-marrow derived stromal cells during embryonic development and engagement by FcγR expressing thymic pro-T cell with these ligands these result in a skewing of the T cell population, with similar interactions occurring with pro-B cells[161,162].

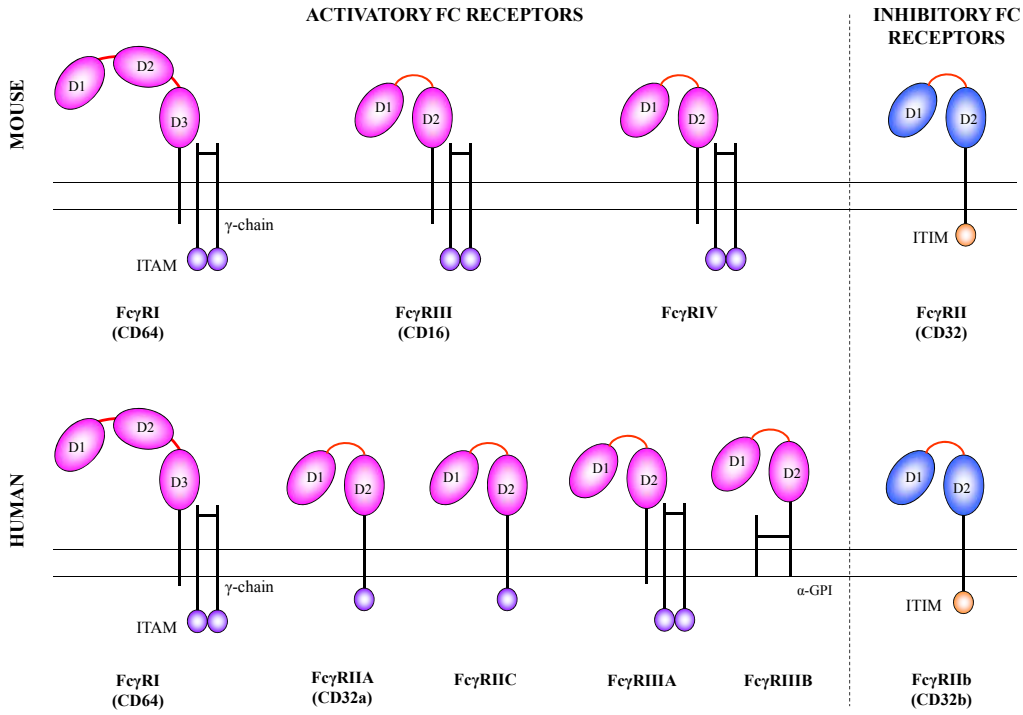

Figure 1.4. The FcγR family.
The FcγR show strong family structural homology and in general consist of two extracellular domains (D1 and D2) connected by a hinge region (bent at 50-55˚) to a transmembrane domain. FcγRI contains a third extracellular domain (D3), which has been suggested to enhance Fc interactions. The activatory FcγR are commonly associated with a common γ-chain that contains the signalling ITAM residues. In humans however some FcγR lack the γ-chain and contain ITAM within a cytoplasmic tail. In contrast, the inhibitory FcγR, FcγRII is a single chain molecule which contains an ITIM signalling residue, (Review in [143]). Fc engagement most often occurs in the context of immune complex, again with the exception of FcγRI which can engage monomeric IgG. It has been demonstrated that the interaction between Fc and FcγR occurs at domain 2 (D2) of the FcγR receptors, which bind the C_H2 domains of IgG[163].

1.5.1. FcγR binding affinity for IgG.

As well as being classified by function, i.e. whether an FcγR is activatory or inhibitory, the FcγR are also classed by their affinity for IgG. All FcγR, with the exception of FcγRI, are medium to low affinity receptors (10^{-6} M) and as such, in most cases, require the formation of IC in order to interact with the Fc domain of IgG. However, studies have shown that monomeric IgG in plasma and in intravenous Ig preparations does have sufficient affinity to bind to FcγRII and FcγRIII[164]. FcγRI, in contrast, is high affinity so will tend to bind monomeric IgG and as a result has a propensity to be saturated *in vivo*, where circulating IgG is readily available. The higher affinity of FcγRI is thought to be conferred through the additional extracellular Ig-like domain[165], demonstrating that the structure of the FcγR is also important to their activity. An example of the differing FcγR affinity is shown through mouse IgG2a which binds to FcγRI with high affinity (10^8 to 10^9 M^{-1}), with medium affinity to FcγRIV (10^7 M^{-1}) and with low affinity to FcγRIII (10^6 M^{-1})[166].

Interestingly, as monomeric IgG is present in serum and has been shown to displace IC binding[164], it is therefore possible that the low and medium affinity FcγR are in part bound

by IgG *in vivo*. The above affinity data does not take this into account, being that these data are obtained under non-physiological conditions using surface plasma resonance techniques (see Material and Methods 2.25) and as such, the binding of therapeutic mAb to FcγR *in vivo* may differ in the presence of plasma IgG.

The FcγR also display specific binding profiles for IgG subclasses. For example, CD32 and FcγRIII in mice will bind to IgG1, IgG2a and IgG2b, whereas FcγRIV will only bind to IgG2a and IgG2b[145]. Alongside this, the FcγR display variable affinities to the given IgG isotype that they bind. Table 1.2 summarises the preferential binding of human and mouse FcγR to IgG subclasses.

As the expression profile of FcγR on different cells varies (Table 1.2), the magnitude of a cellular response is often determined by the number of activatory FcγR engaged compared with the number of inhibitory FcγR engaged, or the activatory/inhibitory FcγR ratio, described below (section 1.5.2), but as indicated above, this is also influenced by the IgG isotype produced during the immune response.

1.5.2. The activatory-to-inhibitory ratio and its importance in cell activation.

Predominantly, the threshold for FcγR-dependent cell activation is controlled through the balance between activatory and inhibitory FcγR engagement, described as the activatory-to-inhibitory (A/I) ratio. This A/I ratio has been shown to be important for antibody-mediated activation of immune cells[166]. For example, it has been shown that in mice, murine IgG2a binds with a higher affinity to activatory FcγRI than to CD32[139]. This means that when an IgG2a containing IC engages with a cell expressing both FcγRI and CD32, the IC will preferentially bind to the activatory FcγR and as such the cell will receive a stronger magnitude of activatory signal compared to inhibitory signal and thus the cell will be activated; giving the IgG2a antibody a high A/I ratio. In contrast, murine IgG1 antibodies have a higher affinity for CD32 than for FcγRI[139], therefore the predominant signal upon IgG1 containing IC engagement will be inhibitory, thus reducing cell activation, giving IgG1 a low A/I ratio[166]. This has been suggested as the reason why IgG2a (and IgG2b) mAb are considered more potent recruiters of effector function in mAb immunotherapy[145]

.

Table 1.2. Summary of the expression of FcγR in mice and humans and preferential binding to IgG subclasses.

MOUSE		Activatory FcγR			Inhibitory FcγR
		FcγRI (CD64)	**FcγRIII (CD16)**	**FcγRIV**	**FcγRII (CD32)**
Affinity		High	Low/medium		Low
Affinity for IgG (Ka, M^{-1})		$10^7 - 10^8$	10^6		9×10^5
Murine IgG subtype specificity[144]		2a = 2b >> 1 = 3	2b > 2a > 1 >>3	2a & 2b only	1 = 2b >> 2a = 3
Murine expression[143]	Mono/mac	+	+	+	+
	Neutrophils		+	+	
	NK cells		+		
	DC	+	+		
	B cells				+

HUMAN		Activatory FcγR					Inhibitory FcγR
		FcγRI	**FcγRIIa**	**FcγRIIc**	**FcγRIIIa**	**FcγRIIIb**	**FcγRIIb**
Affinity		High	Low/medium				Low/medium
Affinity for IgG (Ka, M^{-1})		10^7	10^6				10^6
Human IgG subtype specificity[167]		1 = 3 > 4	1 > 3 > 2 > 4	1 = 3 =4 >> 2	3 >> 1 >> 4 > 2	1 > 3	1 = 3 =4 >> 2
Human expression[150]	Mono/mac	+	+		+		+
	Neutrophils	+/-	+			+	
	NK cells			+	+		
	DC	+	+		+		+
	B cells						+

Mono/mac; monocytes and macrophages, DC ; dendritic cells. Adapted from [143,144,150] & [167].

1.5.3. Structure of the FcγR.

As mentioned previously, the FcγR are type I glycoproteins that belong to the Ig superfamily (IgSF) of proteins, which, by definition means that they contain at least one Ig-like extracellular domain. The ectodomains of the FcγR contain either two or three globular Ig-like domains comprised of approximately 100 amino acids, which, in general consist of several anti-parallel β-strands, linked by a β-loop arranged in two layers maintained by a disulphide bridge[168]. These extracellular domains are connected by linker

regions consisting of nine amino acids, referred to as the hinge region. This hinge region is bent at an acute interdomain angle (between 50 – 55°) and allows accessibility to the IgG binding residues of the FcγR (discussed below, section 1.5.4). The Ig-like domains are denoted D1 (N' terminus), D2 and D3 (membrane proximal/C' terminus) on FcγRI and D1 (N' terminus) and D2 (membrane proximal) on the remaining FcγR (Figure 1.5a). The membrane proximal domain is attached to a transmembrane domain of approximately 20 amino acids that is helical in structure[169], followed by a C-terminal intracytoplasmic tail, referred to as the α-chain. The only known exception to this structure is FcγRIIIb which is anchored into the cytoplasmic membrane by a covalent linked Glyco-Phosphatidyl Inositol (GPI) moiety that lacks direct signalling residues, but has been shown to "hijack" other intracellular signalling pathways, such as that mediated by completment receptor 3 (CR3)[170]. The association of FcγRIIIb with lipid raft domains has been shown to be essential to it's activity[171] and will discussed in section 1.7.4.

The intracellular domains of the FcγR contain signalling residues which confer the function of the receptor. In the mouse, the activatory FcγR associate with the common γ-chain that contains the 26 amino acid intrinsic signalling domain ITAM, phosphorylation of which leads to activation of cellular responses. The ITAM consists of two 13 amino acid segments that contain two repeating Y-x-x-L domains, where x can be any amino acid. It has been demonstrated that the number and position of these residues is important to the initiation of FcγR signalling (reviewed in [172]). For example transfection of truncated FcγRIIa, which lack these ITAM residues, into COS-1 cells ablated FcγR mediated phagocytosis in comparison to WT FcγRIIa[173].

The intracellular domains of the human FcγR are however more heterogeneous. Similar to murine activatory FcγR, human FcγRI and FcγRIIIa associate with the common γ-chain, which contains the ITAM signalling residue. In fact, the association of the α-chains of FcγRI and FcγRIIIa with the FcR γ-chain is required for cell surface expression of these receptors[174]. It is important to note that depending on the cell type, these adaptor proteins can differ. For example human FcγRIIIa can be associated with the ITAM-containing CD3 ζ-chain in NK cells, but often associates with the common γ-chain in monocytes and macrophages[139]. In contrast to FcγRI and FcγRIIIa, the intracellular α-chain of the FcγRII isoforms FcγRIIa and FcγRIIc, contain the ITAM signal-transducing domain and therefore do not require association with the common γ-chain. In both human and mice, the inhibitory FcγR are single chain transmembrane molecules, which can be distinguished

from the activatory FcγR as they contain a 13 amino acid ITIM within the α-chain and diminish cellular responses upon co-ligation with activatory FcγR[150,175].

1.5.4. The FcγR:Fc interaction (binding of IgG to FcγR).

It was initially thought that IgG interacted with two FcγR either via an interface region on both heavy chains of the IgG between C_H2 and C_H3[176,177] or by dimerisation of the FcγR via D2 interactions and binding to the Fc in an asymmetrical manner[178]. However, more recently, primarily as a result of crystallisation studies, it has been established that IgG and FcγR bind with a 1:1 stoichiometry[179]. To date, only the crystal structures of the interaction between IgG1 and FcγRIIIa have been resolved[179 180] (Figure 1.5c), however, as a result of the close homology between the FcγR, it has been suggested that the binding of Fc to FcγR can be extrapolated (Figure 1.5b)[181]. These studies demonstrated that FcγR interact with IgG via residues within the D2 domain proximal to the hinge region of the receptor and via residues in the hinge region itself. These residues recognise the hinge region of the IgG, proximal to the C_H2 domain of both Ig heavy chains. Binding between these two regions results in a conformational change in the IgG molecule, where the IgG molecule obtaining a horseshoe like structure[182] (Figure 1.6). This allows interactions between sugar moieties attached to asparagine 297 (N297) on the IgG with specific residues on the FcγR, whilst also allowing engagement via CDR regions to specific antigen on the cell surface[183,184]. Alongside this, although specific for the interatction between FcγRIIIa and IgG1, contact occurs in the region between leucine 234 (L234) and proline 238 (P238) within the lower hinge region of IgG1[185] to the hinge loops between D1 and D2 and at the BC, C'E and FG loops of the β-strand of D2[182] (Figure 1.5c). The conformational change in the IgG molecule seems to prevent the binding of a second FcγR and this is in opposition to the earlier models of FcγR:Fc interactions[182], although it should be noted that the 1:1 stoichiometry model is also supported by earlier binding studies[183,186]. To add further complexity, it has been established that the residues of the FcγR to which IgG bind depends on the receptor and the IgG isotype. For example, mutational studies have demonstrated that in humans IgG1 and IgG2 bind to diverse regions of the D2 domain of FcγRIIa and it is thought that these variation in FcγR:Fc interactions between IgG isotypes confers the different affinities of IgG to the different FcγR[178].

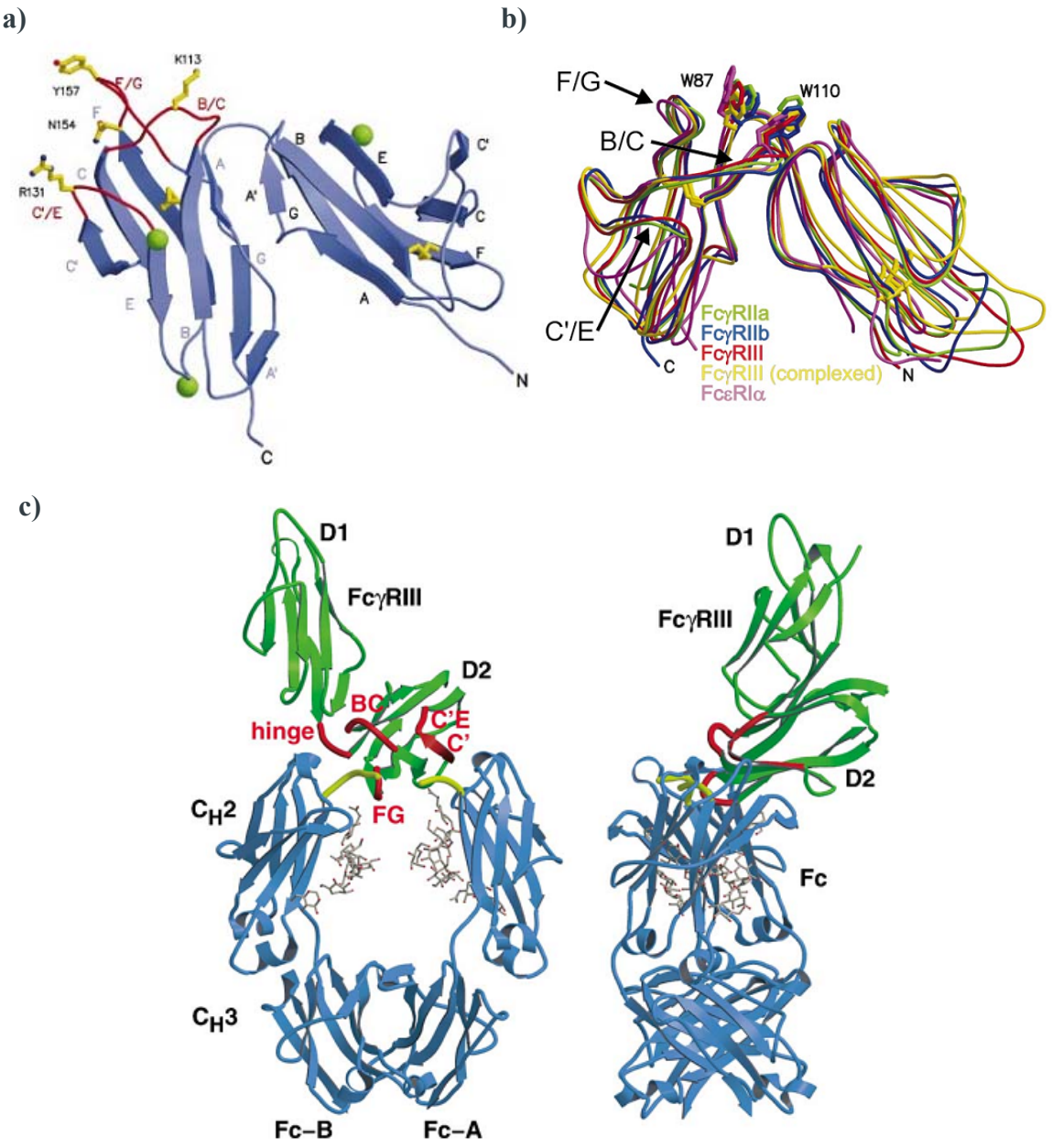

Figure 1.5. Structure of FcγRIIb and the interaction between FcγRIIIa and IgG1.
(a) Stereo ribbon representation of the soluble human FcγRIIb structure, demonstrates the loops supposed to be important for IgG binding (red) with ball and stick representations of residues within the binding site and sites of potential N-glycosylation (green balls). The N- and C-terminal are labelled, with the β-strands numbered consecutively. Adapted from [176]. (b) The structure of the FcγR superimpose upon each other. Adapted from [181]. (c) The interaction between FcγRIIIa and IgG1, showing D1 and D2 (green) and binding regions (red) of FcγRIIIa (green) and C_H2 and C_H3 (blue) and lower hinge region (yellow) of IgG1. Carbohydrate moieties attached to the conserved glycosylation site (N297) are shown in grey. Left hand figure is the front view of the complex, whilst right had figure is the side view of the complex rotated approximately 90◦. The Fc region of the IgG1 binds at L234 to P238 of the lower hinge region[185] to the hinge loops between D1 and D2 and at the BC, C'E and FG loops of the β-strand of D2[182]. Adapted from [182].

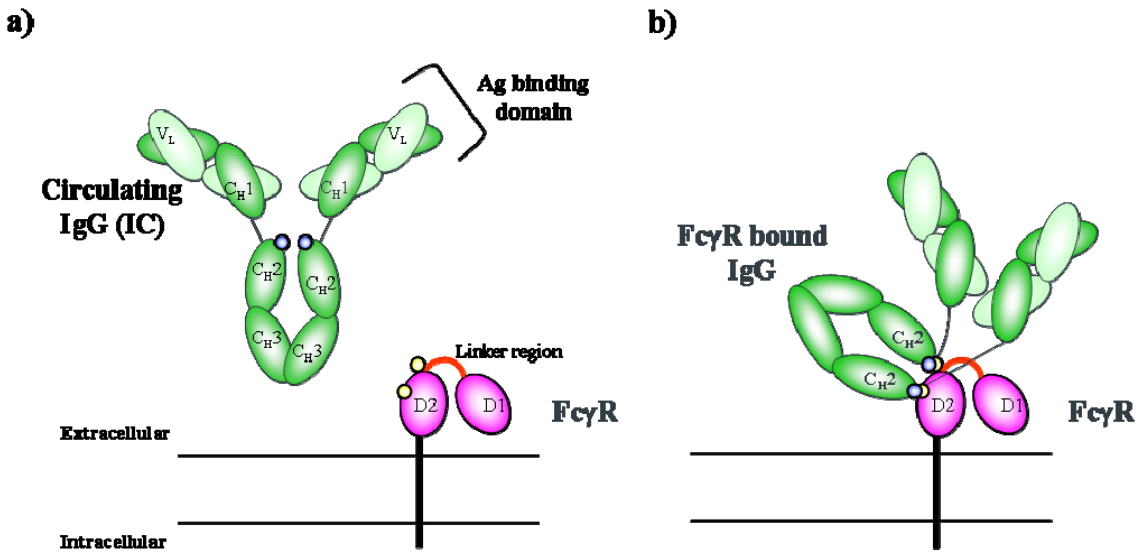

Figure 1.6. Schematic demonstrating confirmational change in IgG after interaction with FcγR. The interaction of IgG and FcγR occurs between both C_H2 domains of the IgG molecule via carbohydrate moieties attached at asparagine 297 of both C_H2 chains (blue circles) with residues in the D2 domain and with two residues (at asparagine 162) of the linker or hinge region connecting D1 and D2 (yellow circles). The interdomain angle of the FcγR increases and the IgG bends into a horse-shoe like structure, with the Fab regions point outwards from the cells, enabling the IgG to continue binding via antigen binding domains[179].

1.5.5. Regulation of FcγR expression.

The expression of the FcγR is controlled by a multitude of factors, including, environment, cell activation status and cytokine production. Inflammatory mediators, such as LPS or IFN-γ up regulate the expression of the activatory FcγR on both human[187] and mouse[144,188] monocytes and also on human mast cells[189] *in vitro*. In addition, studies have shown that IFN-α and -β in mice, but not in humans also increases FcγR expression[187,190]. Conversely, IFN-γ reduces CD32 expression, as does C5a, which was also shown to increase activatory FcγRIII expression *in vitro*[191]. This suggests that within a pro-inflammatory environment FcγR expressing cells are likely to be directed towards an activatory phenotype.

In contrast, other cytokines, such as IL-4, IL-10 and transforming growth factor-β (TGF-β) produced by T_H2 cells, suppress activatory FcγR expression on innate immune effector cells and increase CD32b expression. Tridandapani *et al* (2003) demonstrated that treatment of human myeloid cells with TGF-β resulted in a down-regulation of the activatory FcγR and associated decrease in FcγR-dependent effector function, i.e. phagocytosis[192]. Alongside this, it has been established that monocytes and polymorphonuclear leukocytes (PMN) treated with IL-4 up-regulate CD32b but suppress expression of FcγRIIa[193], as well as other activatory FcγR[144,194]. These studies also confirmed that IFN-γ treatment abrogated CD32 expression, but enhanced activatory FcγR expression. However, IL-4 has differential effects of CD32 expression depending upon the

cell type. For example, Rudge *et al* (2002) demonstrated that whilst IL-4 upregulated CD32 on myeloid cells, this cytokine down regulated the receptor on activated B cells[195]. It was also established that similar to the effects of IL-4, IL-10 treatment also upregulated CD32b on myeloid cells[196].

Alongside this, it is important to note that whilst different cytokine profiles alter FcγR expression, they also induce class switching. For example, IL-4, which up-regulates CD32 on myeloid cells and down-regulates CD32 on activated B cells preferentially induces class switching of B cells to IgG1 and IgE, whereas TGF-β induces switching to IgG2b and IgA[197,198]. Alternatively, T_H1 cytokines such as IFN-γ result in an up regulation of the activatory FcγR and also induce class switching to IgG2a, 2b, and 3[199]. This class switching of different IgG subclasses that are associated with different affinities for FcγR provides a further level of fine-tuning of the immune response to Ig.

We next go on to discuss activatory FcγR and BCR signalling, with the aim of later discussing how both these signalling pathways are manipulated after co-ligation with the inhibitory FcγR.

1.6. The activatory FcγR.

1.6.1. The function of activatory FcγR.

Activatory FcγR engagement results in the initiation of a variety of cellular responses, which include cell degranulation and cytokine production by neutrophils and mast cells, phagocytosis of mAb bound material by neutrophils and macrophages and killing of IgG-sensitized target cells by ADCC, as previously described (section 1.3.3) by macrophages and NK cells (reviewed in [139]). Seemingly, the nature of the response depends on the cell type and FcγR engaged. For example, Alongside these, activatory FcγR engagement results in cytoskeletal changes and expression of cell surface proteins associated with cellular activation, such as up-regulation of co-stimulatory molecules (discussed in section 1.2.1.2)[200]. Table 1.3 summarises the different functions of FcγR engagement on different cell types.

The importance of the activatory FcγR function has been demonstrated where genetic knockout of activatory FcγR expression. In addition, deletion of all activatory FcγR in γ-chain-deficient mice, have been demonstrated to have significant defects in antibody-dependent effector cell responses such as phagocytosis, ADCC and inflammatory

responses, but are protected from the pathological consequences of IgG-containing immune complexes[201,202,203]. However, the loss of a single FcγR showed less dramatic loss of function in response to IgG2a and IgG2b, but notably FcγRIII$^{-/-}$, results in ablation of IC mediated inflammatory responses, clearance of IgG-opsonised cells and reduced ADCC *in vivo* in response to IgG1[204,205,206].

Table 1.3. The outcome of activatory FcγR engagement on different cell types.

Cell Type	Outcome of activatory FcγR engagement
Mast cells & basophils	▪ Release of vasoactive substances ▪ Release of chemoattractants
Neutrophils	▪ Release of chemoattractants ▪ Release of cytotoxic substances ▪ Phagocytosis ▪ Oxidative burst
Monocytes & Macrophages	▪ Oxidative burst ▪ Cytotoxicity (ADCC) ▪ Release of pro-inflammatory mediators ▪ Phagocytosis
Dendritic cell	▪ Antigen presentation to T & B cells ▪ Regulation of peripheral tolerance through modulated cell activation (involve inhibitory FcγR).

The outcome of activation after FcγR engagement varies depending on the cell type expressing FcγR and the particular FcγR engaged. This table summarises the outcome of FcγR engagement on different cell types, adapted from Nimmerjahn & Ravetch (2008)[143].

1.6.2. Activatory FcγR signalling.

The responses of cells after FcγR engagement occur as a result of specific intracellular signalling cascades, largely transduced through ITAM domains within the cytoplasmic tails of the receptors (discussed in section 1.5.3). The location of the ITAM varies depending on the FcγR, but principally engagement of the activatory FcγR initiates clustering of the receptors, allowing trans-phosphorylation of protein kinases which are loosely associated with the ITAM domain, such as the Src-family (sarcoma-family) tyrosine kinase, which have been shown to be associated with resting FcγR[207,208]. Again,

depending on the cell type, the exact Src-protein that becomes activated through autophosphorylation varies. For example, in monocytes Hck and Lyn are associated with FcγR1[209], whereas only Hck is associated with FcγRIIa[210] and in neutrophils FcγRIIa is associated with Fgr[211].

The Src-proteins induce phosphorylation of two residues within the ITAM, which results in the recruitment of other kinases to the bi-phosphorylated ITAM, such as Syk, leading to phosphorylation of these proteins, increasing kinase activity and downstream signalling that commonly results in cell activation[212,213]. This recruitment and phosphorylation of Syk has been shown to be essential to the FcγR signal, where co-transfection (into Chinese hamster ovary-1 (COS-1) cells) of FcγR and γ-chain resulted in abrogated phagocytosis in comparison to transfectants containing FcγR, γ-chain and Syk[214]. Further to this, $Syk^{-/-}$ macrophages demonstrated abrogated IgG-mediated phacocytosis[215,216] and $Syk^{-/-}$ neutrophils showed impaired production of ROS in response to IgG-opsonised particles in comparison an intact response to controls[215]. Neutrophils also demonstrated impaired phagocytosis after treatment with Syk inhibitors[217]. Alongside this, it has been shown that the initiation of ADCC by NK cells, via FcγRIIIa engagement, is reliant of Syk[218].

The events that occur downstream of Syk phosphorylation to induce phagocytosis, ADCC or cytokine release have not yet been well defined and can differ between cell type and the FcγR engaged[219]. Signalling molecules though to be involved with the dissemination of FcγR signals include, protein kinase C (PKC), extracellular signal-regulated kinase (ERK), GTPases such as members of the Rho family and phospholipase Cγ (PLCγ)1 and PLCγ2, which in turn activate phosphoinositide-3 kinase (PI3K) (reviewed in [220]). Figure 1.7 summarises, in general, activatory FcγR signalling.

PI3K converts membrane associated phoshatidylinositol-(3,4)-biphosphate (PIP_2) to phoshatidylinositol-(3,4,5)-triphosphate (PIP_3). This results in enzymatic cleavage of PIP_2, releasing inositol triphosphate (IP_3) and diacylglycerol (DAG). IP_3 relocates to the endoplasmic reticulum of the cell, where it binds to IP_3 receptors (IP_3R) and initiates the release of intracellular calcium (Ca^{2+}), which has been demonstrated to be important for granule release by NK cells[221,222]. Alongside this, PI3K activation has been demonstrated to be important for the induction of phagocytosis in macrophages and neutrophils[223,224]. In addition, it has been shown that another molecule, the Src-homology 2 (SH2) domain-containing leukocyte-specific phosphoprotein of 76 kDa (SLP-76) is essential for the release of intracellular Ca^{2+} flux and ROS in neutrophils, where $SLP\text{-}76^{-/-}$ cells fail to

propagate FcγR-dependent signalling or production of ROS[225]. Crosslinking of the FcγR also activates the mitogen-activated protein kinase (MAPK) signalling pathways, including ERK1/2, p38 MAPK, and c-Jun N-terminal kinase (JNK)[226,210]. ERK in particular has been shown to become activated after Syk phosphorylation[227] and pharmacological inhibition of ERK has been shown to abolish phagocytosis in macrophages and neutrophils, but not monocytes[223,228,229]. In addition, the GTPase family of molecules, including Rho, Rac and Cdc42 have also been shown to be essential to the induction of phagocytosis[230]. These proteins are involved in the reorganisation of actin, where absence of these proteins in transfectants containing the FcγR, attenuates phagocytosis[231,232,233] (Figure 1.7).

Similar to activatory FcγR signalling, the initiation of BCR signalling also utilises ITAM residues. Having discussed ITAM-dependent signalling in the context of FcγR we next go on to discuss this with regards to BCR signalling.

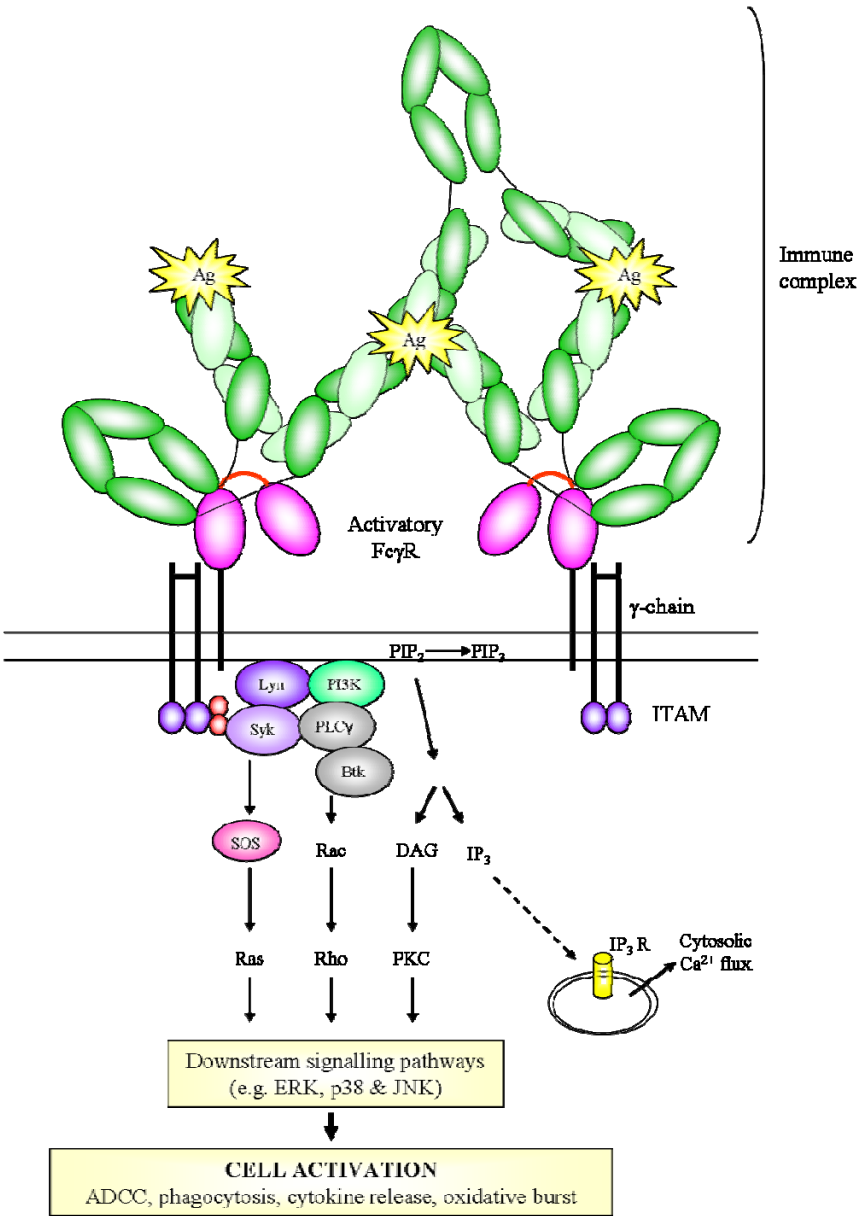

Figure 1.7. Activatory FcγR signalling.
In general, engagement and aggregation of the activatory FcγR by antigen (Ag) containing IC, results in the bi-phosphorylation (red balls) of the ITAM residues within the associated γ-chain of the FcγR by Src-kinases, such as Lyn. This results in the recruitment and phosphorylation of Syk, leading to the recruitment and activation of a plethora of downstream signalling molecules detailed above. The outcome of these signalling cascades is cell activation, resulting in ADCC, phagocytosis, cytokine release and oxidative burst.

1.7. B cell signalling.

It is through BCR engagement that antigen specific humoral responses are mounted. The BCR is a multiprotein structure that consists of membrane bound immunoglobulin (mIg) which non-covalently associates with a di-sulphide linked, signal transduction heterodimer consisting of Ig-α (CD79a) and Ig-β (CD79b), that contain ITAM within their cytoplasmic tails[234]. As a result of antigen binding to the BCR, ITAMs of Igα and Igβ[235] become phosphorylated by Src-family kinases, such as Lyn, leading in turn to recruitment of Syk, an essential protein for BCR signalling[234,236,237]. The outcome of B-cell signalling events is

the activation of secondary messengers such as DAG and IP_3 and increase in intracellular Ca^{2+} flux; this leads to activation of transcription factors such as NF-κB and other intracellular signalling, such as the MAPK pathway[238,239] (discussed below). This in turn leads to cellular proliferation, differentiation and antibody secretion and in some cases cell anergy. BCR signalling is summarised in Figure 1.8.

1.7.1. BCR-induced cytosolic calcium flux.

Syk recruitment leads to subsequent recruitment of B-cell linker protein (BLNK), which in turn recruits Burton's tyrosine kinase (Btk). BLNK targets this newly formed complex to the inner leaflet of the cell membrane[240] where Btk recruits and activates PLCγ through phosphorylation. Alongside this, a co-receptor of the BCR, CD19, targets PI3K to the BCR complex upon tyrosine phosphorylation of CD19 cytoplasmic domains by Lyn[241]. CD19 is part of a co-receptor complex (CD21-CD19-CD81) that contains phosphorylation sites in its cytoplasmic tail which lead to the recruitment and activation of a variety of BCR signalling molecules[242]. For example, CD19 plays a crucial role in stabilising and amplifying BCR signals by further recruiting and activating PI3K and Btk and as a result enhances PLCγ activation and aspects of the MAP kinase cascade[243,244]. The activated form of PI3K is also targeted towards the inner membrane leaflet, where it converts membrane associated PIP_2 to PIP_3. Btk and PLCγ both associate with the membrane by binding to PIP_3 via N terminal pleckstrin homology (PH) domains.

The collection of these molecules (BLNK, Btk, PLCγ and PI3K) forms the BCR signalsome[244], within which all molecules are co-dependent on each other for maximal activation. Without this recruitment of PI3K, e.g. in $P13K^{-/-}$ cells, Btk cannot sustain its recruitment and membrane targeting of PLCγ[243]. Similarly, deficiency in BLNK, Syk or Btk leads to defective PLCγ signalling. The singular loss, by genetic deletion, of Lyn, Syk or Btk seems to lead to defective but still functional BCR signalling, however if more than one of the signalsome molecules are absent, i.e. a combination of deficiencies such as $Btk^{-/-}$ $PLC\gamma^{-/-}$ can cause a severe loss of function[245]. There is however evidence that some of the BCR-signalling molecules can function independently of the BCR signalsome. For example, PLCγ induced Ca^{2+} release can occur independently of Btk recruitment in $Btk^{-/-}$ mice and is commonly reduced but not ablated in the absence of BLNK ($BLNK^{-/-}$)[246], suggesting PLCγ can induce Ca^{2+} independently of its recruitment to the signalsome.

As with activatory FcγR signalling, the result of this series of recruitments is the enzymatic cleavage of membrane associated PIP_2 to IP_3 and DAG by PLCγ, leading to the release of

intracellular Ca^{2+}. An increase in intracellular Ca^{2+} results in activation of downstream signalling molecules such as some protein kinase B (PKB) isoforms, JNK and MAPK, which cause an increase in cell proliferation[243,247]. DAG plays a different role in B-cell activation besides induction of Ca^{2+} release. DAG remains membrane bound, where it recruits and activates NF-κB and MAP-kinase pathways via activation of PKC and Raf-1, with eventual transcription of pro-survival molecules such as B cell lymphoma-2 (Bcl-2) and A1.

1.7.2. BCR-induced activation of MAP kinase signalling pathway.

Besides DAG production, the Ras-MAPK signalling pathway is primarily activated by the recruitment of a complex formed by the association of Grb2 and the constitutively bound SOS to tyrosine phosphorylated Src homology 2 domain-containing (Shc) or the similarly phosphorylated BLNK after BCR ligation[248,249]. This in turn leads to the activation of $p21^{ras}$ (Ras), which associates with the serine/theroine kinase Raf-1, causing the phosphorylation of MEK1/2 and sequentially MAPK[249,250]. The outcome of this pathway of activation is the phosphorylation of kinases such as JNK, ERK1/2 and p38 MAPK, which in turn activate transcription factors such as c-jun, c-fos and c-myc; leading eventually to entry into cell cycle, increased survival and proliferation[238].

1.7.3. BCR-induced activation of AKT.

PI3K mobilisation to the BCR-signalsome enhances the recruitment of PKB (or AKT) by binding of AKT to the PH domain of PIP_3 at the plasma membrane. Here, AKT acts to increase cell survival by inhibiting pro-apoptotic molecules such as caspase-9 [251] and BAD[252]. It has also been suggested that alongside sequestering BAD, AKT binds to BAX and as a result prevents it's translocation to the nucleus [253] and thus prevents the induction of permeablisation of the outer mitochondrial membrane and subsequent damage and release of apoptotic factors. In addition, AKT also promotes cell survival by dephosphorylating I-κB, leading to the release and translocation of NF-κB and ultimately transcription of molecules involved in cellular proliferations, such as c-myc [254].

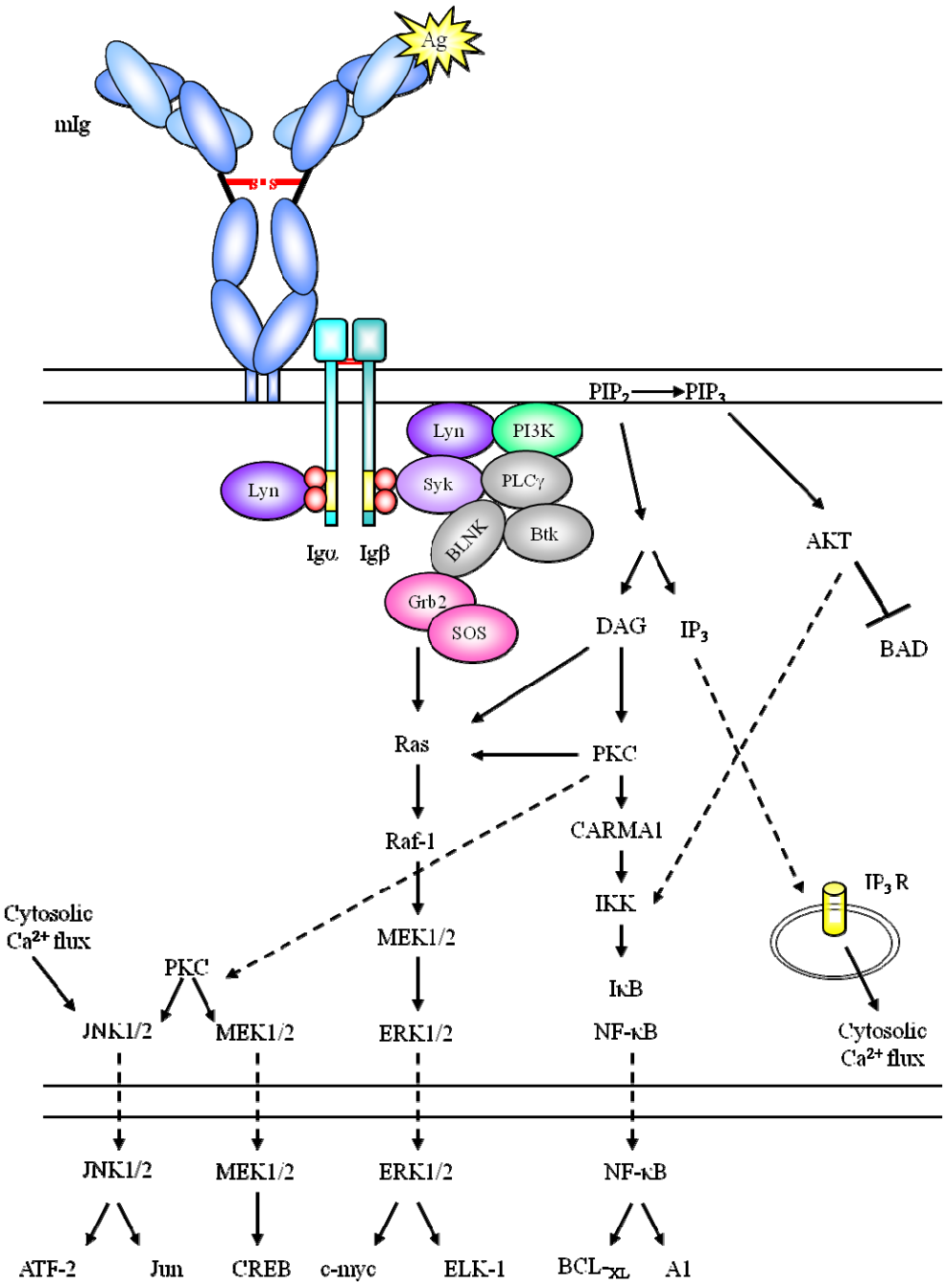

Figure 1.8. B-cell signalling.
Engagement of antigen (Ag) with the BCR (membrane bound Ig, mIg) leads to the recruitment of a set of signalling molecules, collectively known as the BCR signalsome. These molecules initiated a range of signalling pathways which result in the transcription of a range of proteins that promote entry into the cell cycle, increased cell survival and enhanced proliferation. The co-receptor complex CD19:CD21:CD81, that is located at the cell surface within the plasma membrane, is not shown here, but serves to reduce the threshold for BCR signalling, prolong BCR association with lipid rafts[255] and accordingly augments the strength and duration of BCR signalling[256].

1.7.4. The important of lipid rafts in ITAM receptor signalling.

Several ITAM containing immunoreceptors, including the FcγR and the BCR, have been shown to become incorporated within lipid rafts after engagement. It is thought that lipid rafts, which are regions within the plasma membrane that are rich in sphingolipid and cholesterol microdomains[256], allow the initiation of signalling cascades by providing a

platform for the recruitment and clustering of adaptor and signaling proteins, leading to the generation of appropriate intracellular signals.

Recruitment to lipid rafts has been shown to enhance receptor signalling in T-cells[257,258] and it seems that lipid raft domains are essential for the transduction of BCR and FcγR signalling cascades. It has been shown that whilst BCR signalling can occur independently of lipid rafts, in mature B-cells there is a strong correlation between BCR association with lipid rafts and an increase in both the strength and duration of activatory signalling through the BCR[242]. In the resting cell the BCR seems to be excluded from these lipid raft domains, but upon engagement with antigen the BCR is rapidly recruited to the lipid raft domains[259]. These clusters of BCRs within the cell membrane and their association with lipid rafts have been referred to as microclusters[260], which allow localisation of components of the BCR signalling cascade, in particular elements of the BCR signalsome, within the intracellular region of the microclusters[261]. It is this clustering of the BCR and signalling components that is thought to promote enhanced BCR signalling[262]. For example, it has been demonstrated that this association between the BCR and lipid rafts enhances ITAM phosphorylation and Syk recruitment and thus augments BCR signalling[263,264].

It has been demonstrated that relocation of the BCR and BCR-associated molecules occurs in part due to rearrangement of the cytoskeleton, in particular through actin rearrangement[265]. This process is dependent on Vav; a molecule which has previously been shown to be essential to BCR signalling. Primarily, Vav causes actin cytoskeleton rearrangement by activation of the Rho-family of GTPases, which can alter intracellular structures by hydrolysing components of the cytoskeleton. As a result, it has been suggested that Vav can promote movement of the BCR and its cognate receptors (see section 1.5.4.2.1.) into lipid rafts[265]. It has been established that other components of the signalsome, such as Btk and PLCγ are essential for BCR signalling. By demonstrating that these molecules are also essential for microcluster formation, this strongly suggests microcluster formation in lipid rafts to be an essential part of BCR signalling[266]. This is with the exception of PI3K, where deficiency in this molecule did not abrogate microcluster formation, but has been shown to be essential for effective BCR signalling[234,266].

Similar to BCR-induced lipid raft domain clustering of BCR signalling molecules, comparable processes have been demonstrated to occur with regards to FcγR signalling.

For example, cross-linking of FcγRIIa by antibodies leads to the activation and recruitment of FcγRIIa and the Src-kinase, Lyn within lipid raft domains[267,268]. In contrast, disruption of lipid rafts resulted in reduced FcγRIIa activation and Lyn recruitment[269,270], highlighting the importance of lipid rafts, in FcγRIIa signalling at least. It would also appear that lipid raft domains are essential to FcγRIIIb GPI-mediated signalling, where disruption of lipid raft domains abrogated signalling[271].

Co-ligation of either the activatory FcγR or BCR with the inhibitory FcγR has been identified as an important means of regulating cellular responses. Next we discuss the importance of CD32 expression and the means through which CD32 signals to regulate these responses.

1.8. The inhibitory FcγR.

CD32 engagement modulates cell activation by counteracting ITAM-mediated signalling. This occurs both on cells where it is the only FcγR expressed (B cells) or where it is co-expressed with activatory FcγR (effector cells), where it provides a counterbalance to cell activation.

The importance of this counterbalance of inhibitory signalling to activatory FcγR and BCR signalling has been demonstrated in several *in vivo* studies, where disruption of inhibitory FcγR expression leads to augmented IC mediated inflammation and innate immune cell activation[154,272,273], i.e. enhanced ADCC and clearance of IgG-opsonised cells *in vivo* and augmented type I, II, and III hyper-sensitivity reactions[274,152]. The consequence of these augmented immune responses is often pathogenic and can lead to the development of autoimmune-like phenotypes in these knockout animals. Mice deficient in CD32 have been shown to have a greater incidence of inducible autoimmune disorders such as collagen-induced arthritis (CIA)[275] and Systemic lupus erythematosus (SLE) (the latter predominately on the C57BL/6 genetic background)[276] and show increased levels of circulating IgG and activated plasma cells[277-279], potentially due to a lack of CD32-induced apoptosis[272]. It has been shown, that susceptibility to autoimmunity is a function of CD32 deficiency on B-cells. Through targeted cell-specific deletion, it has been shown that mice lacking CD32 on macrophages did not demonstrate an autoimmune phenotype, whilst mice lacking CD32 on B cells did display an autoimmune phenotype[277]. In contrast however, mice lacking CD32 have been shown to have increased resistance to bacterial infections[280] and also reduced susceptibility to malaria[281], suggesting that in certain situations CD32 deficiency may be advantageous.

In humans, CD32b polymorphisms and a reduction in CD32b levels have also been shown to be linked to autoimmunity, in particular a single polymorphism (threonine for isoleucine substitution at position 232, T232I) in the transmembrane domain of CD32b has been linked to development of SLE[282,283,284,285]. This polymorphism in CD32b has increased prevalence in geographical areas associated with malaria infection and murine studies in CD32$^{-/-}$ mice have shown increased disease clearance and reduced disease severity in models of malaria[281,286,287], again suggesting, that in certain circumstances CD32 deficiency may provide a selective advantage to infectious disease.

1.8.1. Expression of CD32

CD32 is expressed thoughout the haemopoietic system (see Table 1.2) and expression has also been demonstrated on non-haemopoietic tissues, such as sinusoidal lining cells in the liver[288], dermal microvascular endothelial cells[289] and placental villus endothelium[290]. The role of CD32 expression on these tissues is not entirely clear, but on placenta villus endothelium is it thought to transport IgG from the maternal system to the foetus as well as a scavenge receptor for IC, possibly in conjunction with FcRn[291].

1.8.1.1. Expression of CD32 isoforms.

The inhibitory FcγR exists in a variety of isoforms. Analysis of the CD32b gene structure indicates that CD32b1 (FcγRIIb1) and CD32b2 (FcγRIIb2) arise by differential mRNA splicing of a 141-bp exon (exon 8)[292] and the resultant protein product differs by a 47-amino acid insertion within the cytoplasmic tail of the CD32b1 isoform in mice[146]. In humans, the difference between the two isoforms is the insertion of a 19 amino acid sequence in the cytoplasmic tail of human CD32b1 up-stream of the ITIM domain[293,294] (Figure 1.9). These isoforms result from the translation of two alternative splice variants for CD32b encoded on chromosome 1 in both humans (1q23.3) and mice. In humans, this gene segment also contains the DNA sequence encoding for the greater that 95 % homologous FcγRIIa[146]. The extracellular and transmembrane regions of the two CD32b isoforms are 100% homologous[293]. In addition, human CD32b1 and CD32b2 share greater that 60 % homology with their murine counterparts[293].

The two isoforms show very specific patterns of expression. CD32b1 is predominantly expressed by B-cells and CD32b2 is mainly expressed by monocytes and macrophages[196,295,296]. CD32b2 expression on myeloid cells causes signal inhibition by attenuating activatory FcγR signals, whilst in contrast, CD32b1 expression by B cells

causes an abrogation of BCR signalling[297]. It is thought that these two isoforms have different functional properties due to differing endocytic capacities of the two splice variants. CD32b2 is able to undergo rapid receptor endocytosis upon ligation, whilst CD32b1 has been reported to lack this property[294]. A cytoskeleton-binding site, located within the cytoplasmic tail of CD32b1 lends itself towards different interactions with cytoplasmic and membrane proteins involved in signal transduction, limits phagocytosis[146]. Specifically, the amino acid insertion in CD32b1 inhibits phagocytosis by preventing accumulation in clathrin coated pits[298,299], whereas CD32b2 contains a region within its cytoplasmic domain essential for accumulation in clathrin coated pits. As a result, CD32b2-dependent phagocytosis ensures effective ligand internalisation and delivery to lysosomes[298].

The distinct structural diversity of CD32b isoforms expression confers functional diversity of cell inhibition through CD32b engagement on different cell types. Tartour *et al* (1993) discussed the potential of increased antigenic processing due to enhanced endocytosis by CD32b2 engagement[300], whereas, a study by Minskoff *et al* (1998) proposed that the inability of CD32b1 on the surface of B cells to undergo endocytosis prevented intracellular processing of Ag and as such inhibition of productive T cell responses through decreased presentation via MHC class II[301].

A third isoform of CD32b has also been reported, CD32b1' which has been demonstrated to have a truncated cytoplasmic tail in comparison to CD32b1, but extended in comparison to CD32b2. Studies by Latour *et al* (1996) demonstrated that CD32b1' functioned similarly to CD32b1 in terms of inducing surface molecule capping, but not inducing endocytosis or phagocytosis, but in contrast to CD32b1, CD32b1' was expressed by cells of both myeloid and lymphoid lineage[302]. In addition, a soluble version of CD32b, CD32b3 has also been described. Secreted exclusively by myeloid cells this isoform has yet to be definitively characterised in terms of function, but has been shown to lack the transmembrane domain of the CD32b isoforms and the intracellular domain of CD32b1[300], confirming that this is a secreted version of CD32b.

Below we consider how these different isoforms of CD32 effect signalling through other FcγR and the also the BCR.

1.8.2. Inhibition of activatory FcγR signalling.

Co-aggregation of CD32 with activatory FcγR results in the phosphorylation of the ITIM residues located within the cytoplasmic tail of CD32, likely through the activatory FcγR-associated Src kinases[303,304]. This phosphorylated ITIM provides docking sites for SH2-containing tyrosine phophatases such as SHP-1 and also SH2 domain-containing inositol 5-phosphatases, such as SHIP-1[305,306]. These molecules dephosphorylate tyrosines on target molecules, including receptors and effector molecules, such as Syk, resulting in perturbed early signalling events and downstream signals and temporary arrest of cell activation, including abrogation of phagocytosis[307,308].

Increases in SHP-1 activation after FcγR co-aggregation has been shown to decrease phagocytosis by inhibition of Syk, PI3K and Rac[309]. Similarly, over expression of SHIP-1 in macrophages leads to decreased phagocytosis in comparison to cells expressing inactive SHIP-1. It was also shown that macrophages derived from $SHIP^{-/-}$ were more efficient at phagocytosis than cells derived from WT littermate[308]. SHIP-1 has been shown to hydrolise PIP_3 (to PIP_2) and prevent membrane localisation of signalling molecules such as PLCγ[310], both of which have been demonstrated to be involved in activatory FcγR signalling (section 1.6.2). Alongside this, transfection of CD32a, CD32 and SHP-1 into COS-1 cells demonstrated attenuated phagocytosis compared with CD32a/SHP-1 transfectants, indicating that CD32 co-ligation is required for adequate inhibitory signalling. Here, the reduced activation in CD32a/CD32/SHP-1 transfectants corresponded with an increase in SHP-1 phosphorylation and decrease in CD32a phosphorylation and Syk activation.[311]. Similar results were also observed with transfectants containing SHIP-1 rather than SHP-1[311]. These studies demonstrate that inhibition of activatory FcγR signalling occurs through processes involving the recruitment of SHP-1 and SHIP-1, through interaction with CD32, which results in attenuation of downstream signalling cascades associated with activatory FcγR signalling.

Much like activatory FcγR signalling on effector cells, inhibitory FcγR signalling on these cells has not yet been fully characterised. As CD32 is the only FcγR expressed by B cells, signalling cascades occurring as a result of CD32 engagement have been more clearly defined on this cell type and will be discussed in further detail below.

1.8.3. Inhibition of BCR signalling.

Despite CD32 signalling on B cells having been more thoroughly investigated and established than on FcγR expressing cells, the mechanisms by which CD32 inhibits B cell signalling are still not entirely clear, but here we examine biochemical and genetic data that try to allude to these mechanisms of inhibition. As mentioned, alone, antigen will engage the BCR and thus activate B-cell signalling. However, if the antigen is pre-coated with antibody as part of an IC, then the Fc region of the associated antibody can bind to CD32 and bring it into proximity with the BCR. The associates CD32 then inhibits B-cell activation, primarily through cascades induced by ITIM-dependent tyrosine phosphorylation of SHIP-1[312,313], much like inhibition of activatory FcγR signalling. Principally, CD32 co-ligation on B-cells leads to a reduction in cytosolic Ca^{2+} leading to a reduction in cell proliferation and survival and induction of cell anergy[314].

Similar to CD32 signalling on effector cells, the initial event of CD32 signalling on B cells is tyrosine phosphorylation of the cytosolic ITIM residues by the BCR associated Src kinase, Lyn[315]. This is principally achieved when CD32 is pulled into close contact with the BCR, where it can associate with Lyn and become phosphorylated[150] (Figure 1.9). This phosphorylation leads to the recruitment of SHIP-1 and the initiation of three distinct, but mutually interacting, SHIP-dependent pathways that result in a potent inhibition of cytosolic Ca^{2+} release, a decrease in the activity of the serine-theronine kinase AKT and an inhibition of MAPK kinase signalling[314]. SHIP-1 phosphorylation is a pivotal step in CD32 activation, where deficiency in SHIP-1 abrogates CD32 signalling in B cells[316,238]. Alongside this it has been demonstrated that phosphorylation of SHIP-1 by Lyn and the targeting of this molecule to the inner B cell membrane is essential for the induction of SHIP-1 dependent events[317], demonstrating the essential nature of both the Lyn and SHIP-1 in the initiation of CD32 signalling in B cells.

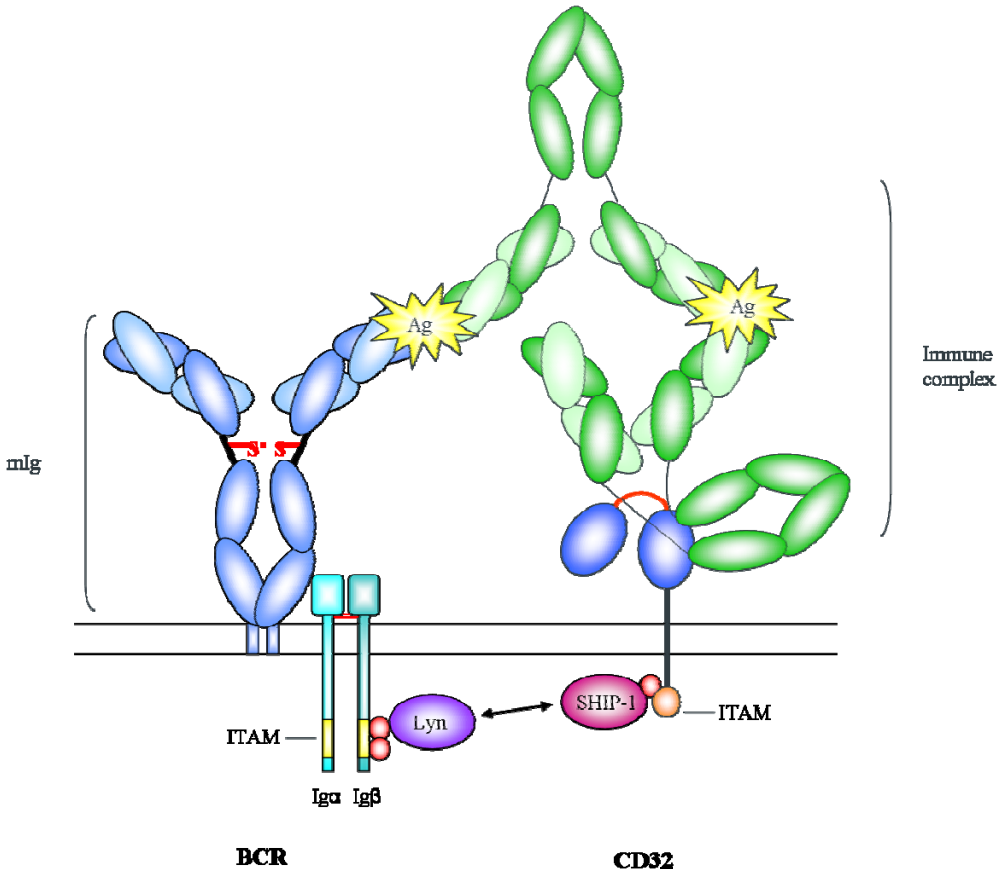

Figure 1.9. Schematic to show the co-ligation of the BCR and CD32 by immune complex engagement. Engagement of antigen (Ag) containing IC with the BCR (membrane bound Ig; mIg) can lead to the co-engagement of CD32. This co-ligation brings the ITIM-containing cytoplasmic domain of CD32 into contact with activated components of the BCR signalling cascade, such as Lyn, which phosphorylates the ITIM residues (red ball), consequently and can activate and phosphorylates SHIP-1, which initiates SHIP-1 dependent downstream signalling cascades[315]. Similar occurs when CD32 is co-ligated with activatory FcγR brings the ITIM domain of CD32 into contact with activated components of the activatory FcγR signalling cascade, leading to the phosphorylation of the ITIM and recruitment of SHP-1 and SHIP-1[305,306].

1.8.3.1. CD32 recruitment to lipid rafts after BCR co-ligation.

There are opposing opinions as to whether CD32 is resident within lipid rafts under normal physiological conditions. However, the consensus is that there is a rapid increase in mobilisation of CD32 into lipid rafts upon BCR and CD32 co-ligation, where CD32 becomes phosphorylated[264,318]. How recruitment of CD32 into lipid raft domains hampers BCR signalling is not entirely clear, however one suggested mechanism is that receptor co-ligation impedes BCR association with the lipid raft domains, an essential step in the initiation of BCR signalling[264,319]. This suggests that inhibition of BCR signalling occurs independently of CD32 signalling. However, other evidence suggests that CD32 recruitment to the lipid raft induces signalling events resulting in the inhibition of BCR signalling. It was shown that if the localisation of CD32 to lipid rafts after co-ligation with the BCR was prevented then ITIM and SHIP-1 phosphorylation decreased and this correlated with reduced inhibition of BCR signalling[320], suggesting that CD32 location to

lipid rafts and the phosphorylation of the ITIM and SHIP-1 are both essential to the inhibition of BCR signalling.

Moreover, SHIP-1$^{-/-}$ mice show abrogation of BCR inhibitory regulation by CD32[321] and an increase in PIP_3, Ca^{2+} flux[322] and MAPK activation after BCR ligation[313]. SHIP-1, is not usually found within lipid rafts under normal physiological conditions, but is recruited following the co-ligation of the BCR and CD32, where SHIP-1 is exclusively associated with CD32[318]. It is thought that within the lipid raft pSHIP-1 may dephosphorylate PIP_3 and as such result in membrane dissociation of other components of the BCR signalling complex, such as Btk, hereby causing inactivation of PLCγ[318].

Regardless of the mechanism by which CD32 recruitment to the lipid raft inhibits BCR signalling, evidence suggests that CD32 recruitment is essential for effective inhibition. Perhaps the best evidence come from the fact that a single point mutation in the transmembrane domain of CD32 (mentioned above), which is observed with higher frequency in patients with SLE, abrogates its ability to relocate into lipid rafts and removes negative modulation of BCR signalling[260,285,320].

The inhibition of BCR signalling after co-ligation of CD32 occurs as a result of key downstream signalling pathways, which are discussed in turn below.

1.8.3.2. Inhibition of BCR-induced cytosolic calcium flux.

The most clearly understood mechanism of CD32 inhibitory effects on BCR activation is abrogation of BCR-induced cytosolic Ca^{2+} release[323]. Tyrosine phosphorylation of SHIP-1 results in the hydrolisation of PIP_3 and membrane dissociation and inactivation of Btk, Vav and PLCγ; resulting in potent inhibition of BCR-induced Ca^{2+} influx[150,324,325] and inevitably reduction in Ca^{2+} dependent processes, such as activation of PKC (aforementioned in section 1.7.1)[314] (Figure 1.10a).

1.8.3.3. Decreased survival by inhibition of AKT.

A second pathway of BCR signalling regulated by CD32 is AKT activation. AKT has been reported to protect cells from apoptosis and thus seems to increase cell survival. It has been reported that AKT activity can be regulated by PIP_2 and PIP_3, but is wholly dependent on PI3K activity[326]. It was demonstrated that AKT activation was decreased after co-ligation of the BCR and CD32 compared with BCR aggregation alone and that

these changes were dependent on SHIP-1 phosphorylation and recruitment[326,327]. There is additional evidence that suggests that CD32 activation recruits 3'inositol phosphatase (PTEN), which is an antagonist molecule of PI3K and consequentially will reduced AKT activation[328]. These facts demonstrate that CD32 activation after BCR co-ligation can lead to a reduction in AKT activation and as a result a decline in cell survival (Figure 1.10b).

1.8.3.4. Reduced cell proliferation by inhibition of MAP kinase pathways.

BCR ligation leads to the activation of the MAPK signalling pathway via Shc activation [248]. Shc can also interact with tyrosine phosphorylated SHIP-1. It is thought that the interaction of Shc with pSHIP-1 leads to perturbed association of the Grb2/SOS complex and as a result, there is an observed reduction in Ras/MAPK activity[329]. Together with this, it has been shown that Grb2 preferentially binds to pSHIP-1 and other SH2 domain containing molecules associated with activated ITIM after BCR-CD32 co-ligation[330] and upon this binding Grb2 becomes dephosphorylated and is rendered inactive[331] (Figure 1.10b).

In addition, co-ligation of the BCR with CD32 results in attenuation of the Ras-MAPK pathway by the binding and activation of the adaptor protein p62^{dok} (Dok-1) by SHIP-1, leading to the inactivation of the Ras and MAP kinases, with resulting reduction in B-cell proliferation[332]. Dok-1 acts by promoting the activity of GTPase activating protein (Ras-GAP), which converts active Ras (RasGTP) to an inactive form (RasGDP)[248]. Alongside this, there seems to be an increase in ERK and MAP kinase phosphatase (Pac-1) upon BCR and CD32 co-ligation. Pac-1 dephosphorylates ERK and other members of the MAPK signalling cascade and in this way hampers on-going ERK activity[328] and as such leads to arrest of cell cycle progression and cell proliferation.

Taken together these observations of CD32 activity on B-cells all suggest that CD32 modulation of BCR signalling can lead to cell anergy by abrogating Ca^{2+} flux and subsequent Ca^{2+} dependent signalling processes, by inhibiting cell survival and by perturbing cell proliferation. Alongside these, aggregation of CD32 in the absence of BCR co-ligation has been shown to directly induce apoptosis of subsets of B cells (see discussed).

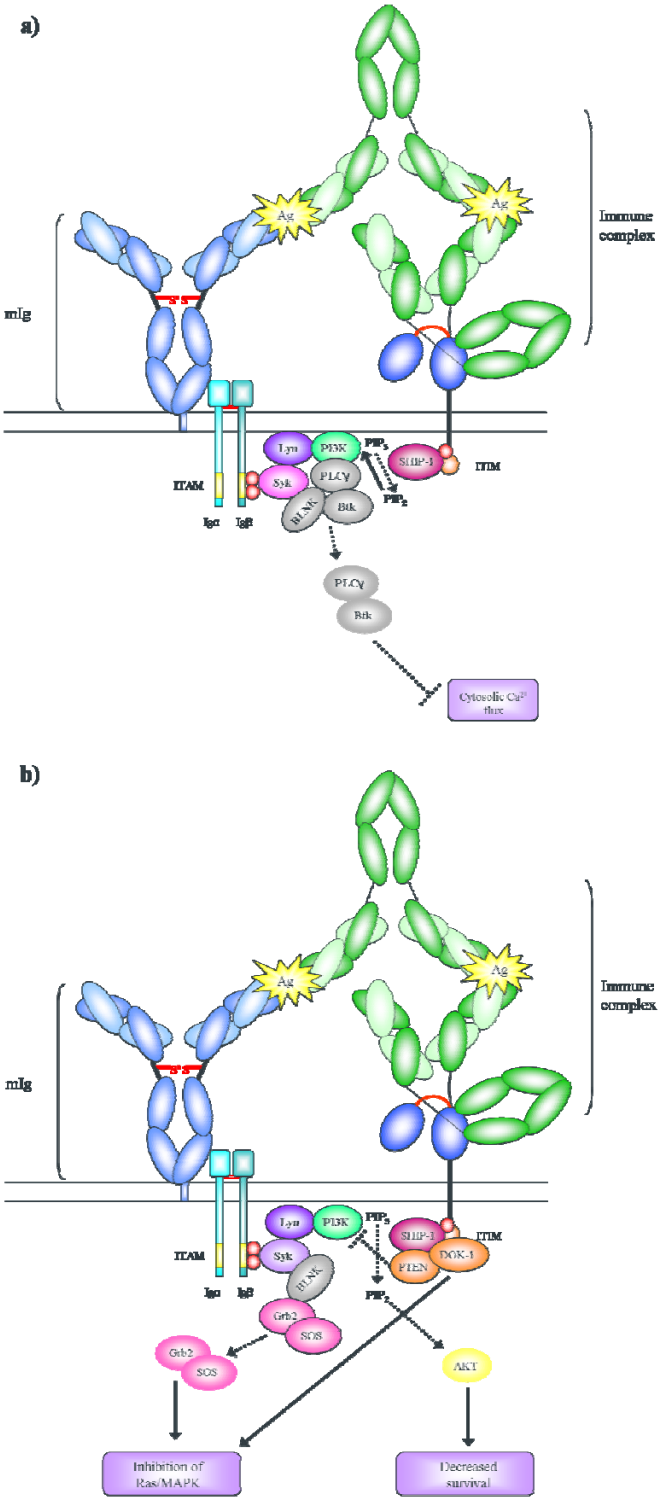

Figure 1.10. SHIP-1 mediated inhibition of BCR activity after CD32 co-ligation.
CD32 co-ligation with the BCR (membrane bound Ig; mIg) after engagement with antigen (Ag) containing IC leads to the activation of SHIP-1 by ITIM phosphorylation. This result in the hydrolisation of PIP_3 to PIP_2 and the membrane dissociation of Btk and PLCγ, consequentially, these BCR-signalling molecules can no longer causes intracellular calcium flux, and as such, calcium dependent processes such a protein kinase B activation are inhibited (a). Alongside this, PIP_3 to PIP_2 hydrolisation leads to the membrane dissociation of Akt, which will no longer suppress BAD and thus lead to apoptosis (b). SHIP-1 phosphorylation also leads to the recruitment of PTEN, which inhibits PI3K activity and thus PIP2 can no longer be converted to PIP3 and recruit BCR signalling molecules. Alongside PTEN recruitment, SHIP-1 recruits Dok-1, which cause phosphorylation and degradation of ERK and thereby inhibits the Ras/MAPK cascade. In addition, SHIP-1 can interfere with the association of Grb/SOS with BLNK (and Shc) and thereby reducing their ability to activate the Ras/MAPK pathways (b).

1.8.4. Direct B-cell apoptosis induced by CD32 activation.

A fourth distinct CD32 signalling pathway occurs that is independent of BCR co-ligation, ITIM phosphorylation and SHIP recruitment[333]. It has been shown that CD32 aggregation at the cell surface can induce direct apoptosis. The pro-apoptotic signalling observed is dependent on an intact transmembrane domain and also on Btk and JNK recruitment, where direct apoptosis induced by CD32 aggregation is abrogated in DT40 cells deficient in Btk and JNK in comparison to WT counterparts[334]. It has also been suggested that this process has some reliance on the phosphorylation and activation of c-Abl family kinase, again in an ITIM/SHIP-1 independent manner[333]. The role of c-Abl under normal physiological conditions in B-cells is not well understood. Despite this it has been shown that c-Abl dysregulation is common in some forms of cancer[335], but may have some role in apoptotic control.

In addition, the apoptotic response to CD32 cross linking seems to be in part dependent on members of the Bcl-2 family, in particular Bim, where plasma cells from $Bim^{-/-}$ mice showed abrogated CD32-induced apoptosis[272]. The apoptosis observed after CD32 coaggregation therefore, is similar to that induced in response to cell stress, via the intrinsic cell death pathway[336,337,338]. Alongside this, there seems to be an increase in mitochondrial membrane depolarization, cytochrome *c* release and activation of caspases 3 and 9 after CD32 aggregation, all of which are effectors of the intrinsic cell death pathway[333], supporting the notion that CD32 aggregation leads to apoptosis. Surprisingly, BCR- CD32 co-ligation and the activation of SHIP-1 has been shown to overcome the apoptotic signalling induced by CD32 aggregation, presumably by leading to the membrane dissociation of Btk[334] and also by the dephosphorylation of c-Abl[333].

The physiological reason for such a process of apoptosis on B cells has been suggested to be important for maintaining peripheral tolerance, particularly in cells that have undergone somatic hypermutation or down-regulated their BCR, i.e. on germinal centre (GC) B cells and plasma cells, respectively[314]. During the process of affinity maturation, B-cells will come into contact with follicular dendritic cells (FDCs) in the GC that capture Ag in the context of IC. B-cells which bind via their BCR with high affinity to Ag displayed by FDC will survive and proceed to maturation, whilst B-cells that interact with low affinity will undergo apoptosis. The Fc portions of the IC will also bind to CD32 on the B cells, either in the presence or absence of BCR engagement. It is thought that the aggregation of CD32 by IC on these germinal centre B-cells in the absence of BCR co-ligation can lead to direct apoptotic signalling[334]. This consequently suggests a mechanism that may

differentially select cells based on their affinity for Ag. Theoretically, high affinity antibodies that bind to both the BCR and CD32 will show reduced CD32 -induced apoptosis and favour survival, whereas low affinity antibodies will bind only via Fc to CD32, leading to CD32 aggregation and induction of apoptosis. However, survival of cells that have both BCR and CD32 signals is contradictory to the previously described mechanisms of CD32 activity, where co-ligation of the BCR and CD32 of circulating B cells leads primarily to modulated cell activation (see section 1.8.3). This perhaps implies that there is a threshold level at which the balance between BCR and co-signalling of CD32 may lead instead to cell survival rather than cell anergy.

Similarly, plasma cells, which have lost their BCR but continue to express CD32, also display apoptosis on CD32 crosslinking, thus providing a mechanism to control plasma cell persistence, where $CD32^{-/-}$ mice showed an increase in the persistence of plasma cells compared to WT counterparts[272]. However, in this study, crosslinking of CD32 induced approximately 2 to 5 % greater apoptosis than the control, which considering background apoptosis was approximately 5 to 10 % this increase was very slight. Alongside this, Ashman *et al* (1996) demonstrated similar induction of apoptosis after CD32 crosslinking in splenic B cells, that could be rescued by blockage (by mAb) or reduced expression (by IL-4) of CD32[339].

The importance of these processes may be evident in animal models of CD32 deficiency [340]. For example, plasma cells from autoimmune prone mice that demonstrate an SLE-like phenotype, have an increase in the number and the persistence of bone marrow plasma cells and also an increase in serum IgG levels. Alongside this, these plasma cells do not undergo CD32-dependent apoptosis[272]. In addition, GC B cells from WT mice have been shown to up-regulate CD32, but in contrast, this is not observed on GC B cells from autoimmune prone mice[341]. It is therefore thought that CD32 expression on plasma cells is essential for control of cell numbers within lymphoid compartments and protection from autoimmune disorders.

There is a further subset of B cells which has also shown susceptibility to CD32-dependent apoptosis. Pre-B cells within the bone marrow do not express the BCR at the cell surface, but do express high levels of CD32[342] and showed CD32-dependent apoptosis and decreased cell viability upon cross-linking[343]. However, unlike apoptosis induced in GC B cells, this process seemed to correlate with SHIP-1 phosphorylation and was reduced in

pre-B cells from SHIP$^{-/-}$ mice, suggesting that CD32 signalling for apoptosis may vary at different stages of B cell development.

It has been proposed, that this mechanism could be utilised to induce apoptosis in CD32-expressing tumour cells. In support of this, it was demonstrated that cross-linking (using mAb) of CD32 on myeloma cells can induce significant apoptosis in comparison to similar myeloma cells that lack CD32[272]. In addition to expression on malignant counterparts of lymphoid cells, CD32, and the activatory FcγR, have also been reported in a variety of other malignant contexts, discussed below.

1.9. Expression of FcγR in cancer.

It has been shown that there is abnormal expression of the FcγR on several lymphoid and non-lymphoid tumours[344]. Early observations in human and mouse tumours demonstrated that tumour cells can absorb sheep red blood cells (SRBC)[345] and form rosettes in their presence[346], methods that are commonly used to determine FcγR expression by cells. In addition, FcγR expression has also been shown to be increased on peripheral blood mononuclear cells (PBMCs) in patients with cancer, particularly those with breast cancer. The increase in FcγR expression on PBMCs correlated both with an increase in tumour mass and decrease in survival in patients with metastatic disease[347,348]. It was therefore thought that perhaps the FcγR expressing cells in the tumour mass were tumour infiltrating lymphocytes or inflammatory cells[349]. However, a study by Ran *et al* (1984) confirmed that both infiltrating cells and the tumour cells themselves expressed FcγR[350].

The reason for this abnormal expression of FcγR on tumour cells has not yet been determined, however it has more recently been demonstrated that it is specifically the abnormal expression of inhibitory FcγR by tumour cells that infers enhanced tumourigenicity in certain tumours[351,352,353]. Alongside this, 3T3 cells transfected with CD32b1 were more tumourgenic that CD32b1 negative cells. These authors also observed that if the tumour comprised of CD32 negative and CD32 positive cells, then the CD32 positive tumour cells would dominate the tumour cell population over the CD32 negative cells *in vivo*[352]. This suggests that CD32 expression provides a selective advantage for tumour cell growth. However, contrary to this, it was shown that tumours of long latency, i.e. those which took longer to establish in the mice, showed increased expression of CD32[351,354], implying that CD32 expression may be gained by tumour cells during the pathogenic process.

Analysis of a panel of primary tumours and metastases from those tumours using immunohistochemistry has demonstrated that etopic CD32 expression is observed in a variety of other cancers. In melanoma for example, CD32 has been shown to be overexpressed on metastatic tumour cells in 34 % of cases, with a lower percentage of ovary, brain and colon tumours (14 %, 5 % & 4 %, respectively) also demonstrating abnormal CD32 expression in comparison with normal tissue[355]. Alongside this, B cell tumours have also been shown to overexpress CD32 in comparison with normal B cells, as determined by immunohistochemistry. Similar to the example of metastatic melanoma, in some cases, an increase in CD32 expression on the B cell tumours has been linked to tumour transformation and disease progression[356]. Interestingly, Cassard *et al* (2008) also observed that CD32b expression correlated with tumour progression, in particular noting an increased percentage of CD32 expressing tumour cells at various sites of metastasis, confirming observations observed above that tumours of longer latency express CD32, suggesting that expression is gained during disease progression. It was discovered that the highest percentage of CD32b expressing cell could be found within the liver, followed by lymph nodes, lung and skin[355]. In addition, examination of tumour biopsy from both primary and metastatic sites from a single patient during disease development, consistently demonstrated absence of CD32b in the primary tumour, but expression of CD32b in the liver and lymph nodes. Taken together, these studies propose that not only does CD32 expression confer a selective advantage for tumour cell growth, but that this is likely to contribute to disease progression and prognosis.

The how and why of CD32 upregulation on non-lymphoid tumours has not yet been established, but it has been suggested that environmental factors may play a part, either in response to IgG (within IC) or as a result of interactions with the tumour microenvironment[357,358]. The latter is supported by evidence showing that CD32 expression was lost during *in vitro* culture, but restored after treatment with IFN-γ[348]. This is in contrast to what is seen under normal physiological conditions (see section 1.5.5) and could suggested alter FcγR biology within the tumour environment. In terms of tumour escape, it has been suggested that CD32 might interfere with the anti-tumour responses and as a result, protect the tumour cells from the deletion via the immune system[359,360]. Specifically, it has been postulated that CD32 might function by sequestering the Fc portion of mAb and as such limit FcγR-dependent effector functions[344,355], thereby allowing the tumour cells to evade the immune system and acquire metastatic potential. This also has further implications for mAb immunotherapy (discussed below).

1.10. FcγR as mediators of anti-tumour immunotherapy.

1.10.1. The role of FcγR in immunotherapy.

Several studies have demonstrated that the anti-tumour mechanism of many therapeutic mAb rely on FcγR engagement. Murine studies of TA99 (anti-melanoma mAb)[361,362,363] rituximab[364] and transtuzumab[83] have demonstrated that activatory FcγR are required for effective anti-tumour responses. Absence of the FcγR through genetic knockout or by blocking FcγR with specific mAb results in reduced tumour cell clearance and subsequently reduced survival.

Strikingly, human clinical trials examining mAb directed against cell surface tumour Ag have reported divergent responses correlating with polymorphisms in FcγR. For example, FL patients with a homozygous polymorphism in the binding domain of FcγRIIIa (158 valine/valine or V/V) confers higher affinity for IgG1 and more effective induction of ADCC[365,366]. Patients with this polymorphism or a polymorphism in FcγRIIa (131 histidine/histidine or H/H) responded significantly better to rituximab treatment in terms of increased survival time and reduced time to relapse[117,118]. Similar results have also been reported in breast cancer patients, where the 158 V/V polymorphism in FcγRIIIa significantly correlated with favourable objective response rate and disease free survival after treatment with trastuzumab. Here, the 131 H/H polymorphism in FcγRIIa showed a trend toward increased objective response rate and disease free survival, again likely mediated through enhanced ADCC[367].

In contrast, whilst the activatory FcγR have the potential to enhance anti-tumour mAb efficacy, it has been demonstrated that engagement with the inhibitory FcγR can attenuate immunotherapy, by limiting activatory signals in effector cells[368]. When there is a deficiency in CD32 on effector cells an increase in ADCC can be observed[369].

1.10.2. Inhibitory FcγR in immunotherapy.

It has been demonstrated that CD32 deficiency can improve cancer immunotherapy. The seminal paper that describes this was published by Clynes *et al* (2000). In a xenograft model of breast cancer, optimal doses of 4D5 and trastuzumab showed complete inhibition of tumour growth in $CD32^{-/-}$ mice compared with WT controls[83]. In addition, antibody treatment of B16 melanoma (using TA99 mAb) in $CD32^{-/-}$ mice completely abrogated tumour growth compared with WT controls and $CD32^{-/-}$ mice without antibody treatment, suggesting that a deficiency in CD32 expression leads to enhanced anti-tumour mAb

therapy. This was also the case in a separate human xenograft model, where an anti-E-cadherin mAb showed enhanced therapy of human colon carcinoma in $CD32^{-/-}$ mice compared with WT controls[369]. It is presumed that many of these direct targeting therapies rely on the recruitment of ADCC effector function and that CD32 expression results in sequestering of the Fc of therapeutic mAb and therefore mAb can no longer recruit effector functions. These data suggest that targeting of CD32 could lead to manipulation of the anti-tumour response and as a consequence improve mAb immunotherapy.

In addition, incubation of human dendritic cells with a CD32b blocking antibody was sufficient to induce DC maturation by immune complexes, demonstrated by the upregulation of costimulatory molecules[370]. Alongside DC maturation, the enhanced generation and activation of tumour specific T cells and enhanced immune responses were obsevered[312,371]. This suggests that blocking might be a strategy for generation of stronger, targeted anti-tumour responses by DC, either by mAb but also in combination with cancer vaccines.

It has also been proposed that developing therapeutic mAb that has reduced interaction with CD32 would improve immunotherapy, by enhancing the A/I ratio. There has been some success in this area, principally by engineering the Fc portion of a human IgG1 to interact with greater affinity to FcγRIIIa and with a lower affinity to CD32b and consequently enhance activatory FcγR signalling and antibody driven ADCC[129,372]

One of the problems in generating specific anti-CD32b mAb is that human activatory FcγR, FcγRIIa shares greater than 95 % homology in the extracellular region of the receptor (discussed in section 1.5). However, recently as anti-CD32b mAb capable of specifically binding CD32b has been developed and has demonstrated to be efficient at blocking endogenous IC binding and attenuating CD32 activity and enhancing the activity of activatory FcγR *in vitro*[373]. Further to this, these human CD32b mAb have been used in xenograft models of lymphoma, where the anti-CD32b mAb (2B6) was able to induced direct cell death, resulting in growth inhibition and increased survival[374]. This study also demonstrated that the anti-CD32b was able to direct ADCC towards human B-cell lymphomas *in vitro* and required intact Fc for its function *in vivo*[374].

1.11. Project aims.

In light of the evidence that suggests manipulation of CD32 can improve immunotherapy we intend to study how this could be achieved. Recently, a panel of mAb which are highly specific for CD32 was generated, allowing me to study the prospective use of anti-CD32 mAb in immunotherapy of lymphoma.

The aims of this project are outlined below.

1) Generate primary lymphomas and associated cell lines, both expressing and lacking CD32, from the Eμ-myc murine model of NHL (see Chapter 3),

2) Assess the ability of a panel of anti-CD32 mAb to regulate the intracellular signals delivered by the BCR and determine their effects on apoptosis *in vitro* (see Chapter 4),

3) Determine the effect of the anti-CD32 mAb on normal CD32 expressing cell types *in vitro* (see Chapter 5),

4) Assess the ability of the anti-CD32 mAb to manipulate mAb immunotherapy in our murine models of lymphoma (see Chapter 6).

CHAPTER 2 Materials and Methods

2.1. Animals.

Eμ-myc mice were supplied by Adrian Ochensberins (Bern, Switzerland) and were maintained on the C57BL/6 in-bred mouse strain originally obtained from Charles River Laboratories (Margate, Kent) and maintained in house. The Eμ-myc mice underwent additional breeding with $CD32^{-/-}$ C57BL/6 mice originally supplied by Dr. Sjef Verbeek (Leiden, Netherlands). CD20 transgenic (Tg) C57BL/6 mice were supplied by Prof. Mark Shlomchick (Yale, USA). Both the $CD32^{-/-}$ and CD20 Tg mice were backcrossed onto the BALB/c background, originally supplied by Harlem UK Limited (Margate, Kent) and maintained in house, for up to ten generations by Dr. Stephen Beers (University of Southampton). Human CD32 Tg mice were created in the S129 strain ES cells and back-crossed onto BALB/c and C57BL/6 backgrounds. The DNA constructs were designed by Dr. Claude Chan (University of Southampton) microinjected by Drs. Neil Smyth and Bhav Sheth (University of Southampton). CBA/H mice, used for the A31 sygeneic lymphoma model, were supplied by Harlan UK Limited (Blackthorn, Oxon, UK). All mice were maintained in local animal house facilities in accordance with Home office regulations.

2.2. Tissue culture.

The human B cell lymphoma cell lines Raji and Daudi (European Collection of Animal Cell Cultures (ECACC) Porton Down, UK) were cultured in RPMI-1640 (GIBCO Invitrogen, Paisley, UK) enriched with 10 % heat inactivated Foetal Calf Serum (FCS) (Lonza), 2 mM glutamine and 1 mM pyruvate (Invitrogen, Paisley, UK). The murine B cell lymphoma cells πBCL_1 were maintained by routine *in vivo* passage in BALB/c mice and cultured for up to 30 days in RPMI-1640, enriched as described above with the addition of penicillin and streptomycin (100 μg/ml each) (Invitrogen, Paisley, UK) and 50 μM 2-Mercaptoethanol (2-ME) (Sigma-Aldrich, Dorset, UK). Cells were cultured at 37 °C, 5 % carbon dioxide (CO_2) in tissue culture flasks.

Eμ-myc cell lines were generated in house, through this thesis, from primary lymphomas excised from the Eμ-myc mice. The Eμ-myc lymphoma cell lines (LCLs) were cultured in DMEM (Dulbecco's Modified Eagle Medium) (GIBCO Invitrogen, Paisley, UK) enriched with 10 % FCS, penicillin and streptomycin (100 μg/ml each), 2 mM glutamine and 1mM

pyruvate (Invitrogen, Paisley, UK), 50 μM 2-ME and 100 μM Asparagine (Sigma-Aldrich, Dorset, UK). Cells were cultured at 37 °C, 10 % CO_2 in six well plates. B cells isolated from murine spleens or from human whole blood were also cultured in enriched DMEM in the same way.

Murine bone marrow derived macrophages (BMDMs) were isolated from the bone marrow of the femur and tibia of mice and cultured in RPMI-1640 (GIBCO Invitrogen, Paisley, UK) enriched with 10 % FCS, 2 mM glutamine and 1 mM pyruvate, penicillin and streptomycin (each at 100 μg/ml) and 20 % L929 cell conditioned medium (see below). Cells were cultured at 37 °C, 5 % CO_2 in 6-well plates, seeded at 5 x 10^6 cells / well.

Cells were cultured for seven to 14 days prior to use. BMDMs were removed from plates by first washing with 2 ml PBS prior to 10 - 15 min incubation with 3 ml warmed trypsin-EDTA (TE) (Lonza, Switzerland) at 37 ˚C, 5 % CO_2. A Pasteur pipette was then used to forcibly remove the BMDMs from the plate surface and cells centrifuged at 450 x g for 5 min, before being resuspended in complete RPMI for use.

Murine L929 cells were cultured in RPMI-1640 (GIBCO Invitrogen, Paisley, UK) enriched with 10 % FCS, 2 mM glutamine and 1 mM pyruvate, penicillin and streptomycin (each at 100 μg/ml). Cells were cultured at 37 °C, 5 % CO_2 in tissue culture flasks. Supernatant (SNT) was collected once cells had reach full confluence, filter sterilised using a Millex 0.22μM PES membrane filter (Fisher Scientific, UK) and stored at -20 °C. The supernatant from L929 cells contains murine macrophage colony stimulating factor (M-CSF).

2.3. Cell quantification.

Cell concentrations were determined using a Coulter particle counter Z1 according to the manufacturers' instruction (Coulter Electronics, Bedfordshire).

2.4. B cell purification by MACS® separation.

B cells were isolated from murine spleens by negative selection as per the manufacturer's instructions; B cell isolation Kit (Miltenyi Biotec, CA. Order No. 130-090-862). Briefly, cells were incubated for 10 min at 4 ˚C with the Biotin antibody cocktail (antibodies against CD43, CD4, Ter-119), then for 15 min with an anti-biotin mAb. Cells were washed with 0.5 % BSA/PBS (w/v) buffer for 10 min at 450 x g. Cells were resuspended

in 3 ml 0.5 % BSA/PBS buffer and separated by magnetic separation using an LS column (Miltenyi Biotec, CA) using magnetic-activated cell sorting (MACS®).

2.5. Lymphoprep of whole blood.

20 ml of heparinised whole blood from healthy human volunteers was diluted 1:1 with PBS and layered over an equal volume of Lymphoprep solution (Axis-Sheild PoC AS, Oslo, Norway) and spun at 1800 x g for 5 min with no braking. Using Pasteur pipettes, the lymphocyte layer (between the lymphoprep and phosphate buffered saline (PBS) layers) was removed and washed with 50 ml PBS, centrifuging at 450 x g for 5 min with centrifuge braking. The cell pellet was then resuspended in 5 ml PBS.

2.6. Mouse genotyping by polymerase chain reaction (PCR).

DNA from tail or ear sections of six to ten week old mice was isolated following digestion of tissue in 0.25 ml DNA Isolation Buffer (50 mM Tris pH 8.9, 12.5 mM magnesium chloride ($MgCl_2$), 0.5 % Tween-20) and 12.5 µl Proteinase K (20 mg/ml) (Sigma-Aldrich, Dorset, UK) at 55 ˚C for at least 16 hr with agitation. The samples were then centrifuged for 10 min at 15,700 x g. 200 µl of SNT was transferred into a fresh eppendorf, an equal amount of isopropanol added and samples were centrifuged for 3 min at 15,700 x g. The SNT was removed and an equal volume of 70 % ethanol was added to the samples before a further centrifugation for 2 min at 15,700 x g. The remaining SNT was completely removed before resuspension of the pellet in 0.2 M TE8 buffer (see Appendix 1) and left at room temperature for 5 min before being placed on ice or stored at -20 ˚C prior to use.

Genomic DNA was assessed by PCR. The PCR master mix for each sample contained 1 µl 5’ primer (forward primer) and 1 µl 3’ primer (reverse primer) both at 100 ng/ml, 16 µl sterile deionised water (dH_2O), 5 µl 5X Green GoTaq buffer (Reaction buffer is at pH 8.5, and contains 7.5 mM $MgCl_2$) (Promega Ltd, Southampton, UK), 0.5 µl GoTag DNA polymerase (pH 8.5, contains 7.5 mM $MgCl_2$) (Promega Ltd, Southampton, UK), 0.5 µl dNTPs (2 mM) (Promega Ltd, Southampton, UK) and 1 µl of purified DNA (from above). PCR was performed in a PTC-100 Programmable thermal controller (MJ Research, Waltham, USA) according to the specific protocol for the gene sequence of interest (see below). A 0.7 to 2 % agarose gel was prepared (w/v with 1X TAE buffer (see Appendix 1), 1:20,000 dilution GelRed Nucleic acid stain (Cambridge BioScience, Cambridge, UK)) and the samples were analyses by gel electrophoresis. The results were obtained by

exposing the agarose gel to UV light using the GelDoc system from Bio-Rad, UK. All primers were sourced from Invitrogen, UK.

2.6.1. Myc genotyping.

5' Myc primer (myc-1): CAGCTGGCGTAATAGCGAAGAG
3' Myc primer (myc-2): CTGTGACTGGTGAGTACTCAACC

The myc PCR program was as follows: Step 1) 94 ˚C for 4 min; 2) 94 ˚C for 40 sec; 3) 55 ˚C for 30 sec; 4) 72 ˚C for 60 sec, 5) Repeat steps 2 to 4 30 cycles; 6) 72 ˚C for 5 min. The resulting PCR fragment is 900 base pairs (bp) long.

2.6.2. $CD32^{-/-}$ genotyping.

Two separate PCR reactions per DNA sample were run alongside each other; to detect the CD32 WT product (using 5' EC1 and 3' EC1) and detect the $CD32^{-/-}$ fragment (using the 3' EC1 and Neo). These reactions gave PCR products at 161bp and 232bp, respectively.

5'EC1: 5' AAA CTC GAC CCC CCG TGG ATC 3'
3'EC1: 5' TTG ACT GTG GCC TTA AAC GTG TAG 3'
Neo: 5' CTC GTG CTT TAC GGT ATC GCC 3'

The PCR program to detect $CD32^{-/-}$ was as follows: Step 1) 95 ˚C for 5 min; 2) 95 ˚C for 1 min; 3) 62 ˚C for 1 min; 4) 72 ˚C for 2 min, 5) Repeat steps 2 to 4 30 cycles; 6) 70 ˚C for 5 min.

2.6.3. γ-$chain^{-/-}$ genotyping.

Two separate PCR reactions per DNA sample were run alongside each other; to detect the γ-chain product (using 5' γ-sense and 5' γ-antisense) and the γ-$chain^{-/-}$ product (using the 5' Neo-sense and 5' γ-antisense). These reactions gave PCR products at 220 bp and 260 bp, respectively.

γ-Sense: 5' ACC CTA CTC TAC TGT CGA CTC AAG 3'
γ-Antisense: 5' TCA CGG CTG GCT ATA GCT GCC TT 3'
Neo-Sense: 5' CTC GTG CTT TAC GGT ATC GCC 3'

The PCR program to detect γ-chain$^{-/-}$ was as follows: Step 1) 95 ˚C for 5 min; 2) 95 ˚C for 1 min; 3) 62 ˚C for 1 min; 4) 72 ˚C for 2 min, 5) Repeat steps 2 to 4 30 cycles; 6) 70 ˚C for 5 min.

2.6.4. Bim$^{-/-}$ genotyping.

A single PCR per DNA sample was run, using two 3' primers. The Bim product was detected using PB20 5' (0.5 µl/ reaction) and PB335a 3' (0.5 µl/ reaction). The Bim$^{-/-}$ product was detected using PB20 5' (0.5 µl/ reaction) and PB65 3' (0.5 µl/ reaction). These reactions gave products of 400 bp and 540 bp, respectively.

PB20: 5' CAT TCT CGT AAG TCC GAG TCT 3'
PB335a: 5' GTG CTA ACT GAA ACC AGA TTA G 3'
PB65: 5' CTC AGT CCA TTC ATC AAC AG 3'

The PCR program to detect Bim$^{-/-}$ was as follows: Step 1) 95 ˚C for 10 min; 2) 94 ˚C for 30 sec; 3) 58 ˚C for 30 sec; 4) 72 ˚C for 45 sec, 5) Repeat steps 2 to 4 35 cycles; 6) 72 ˚C for 10 min.

2.7. Mouse phenotyping by immunofluroscence.

Into an eppendorf that contained approximately 10 µl of Heparin, 20 µl of murine blood was obtained by tail bleeding. 20 µl of a master mix containing 15 µl FACS buffer (see Appendix 1), 2.5 µl with fluorescein isothiocyanate (FITC)-conjugated mAb for CD20 (rituximab) or CD32 (AT130-2) and 2.5 µl Phycoerythrin (PE)-conjugated CD19 was added to 20 µl of heparinised whole blood. This was incubated at 4 ˚C for 10 min in the dark before the addition of 500 µl of red blood cell lysis buffer (diluted 1:10 in dH_2O) (AbD Serotec, Oxford, UK) then centrifuged at 450 x g for 5 min. The SNT was removed and samples washed with 3 ml PBS-BSA-Azide buffer (see Appendix 1) before further centrifugation at 450 x g for 5 min. SNT was removed for a second time, cells were resuspended in 200 µl complete DMEM and samples were assessed by flow cytometry using a FACScan (BD Biosciences-Immunocytometry Systems, CA). Routinely, 7500 cell events from the lymphocyte gate were collected, as identified by the forward scatter (FSC-H) and side scatter (SSC-H) threshold parameters. Samples were analysed using CellQuest Pro Software (BD Biosciences-Immunocytometry Systems, CA). Percentage of CD20 or CD32 positive cells (FL-1) versus CD19 positive cells (FL-2) was assessed, where a positive result gave mean fluorescence intensity (MFI) greater than 10^{1} for antigen of interest.

2.8. Eμ-myc mice; tumour generation, processing and characterisation.

Eμ-myc mice develop spontaneous Burkitt-like lymphomas, as previously described Harris *et al* (1988)[375]. The mice presented with a variety of symptoms, most commonly hunching with laboured breath. In addition, the mice became withdrawn, unkempt and agitated. In some instances the mice presented with visible lumps corresponding to tumours in the location of cervical, axillary and brachial lymph nodes. Upon pre-determined criteria mice were culled and the size and location of the lymph nodes (LN) were noted. The spleen, inguinal lymph nodes (ILN), thymus and other obvious tumour masses (including additional LN) were excised into enriched DMEM. Cell suspensions of the tumour bearing tissues such as the spleen, ILN and thymus were produced by passing tissue through a 100 μm cell strainer (BD Biosciences, Oxford, UK). The cell suspensions were immunophenotyped using direct flow cytometry analysis (see Materials and Methods section 2.11), frozen for later use in Eμ-myc freeze media (90 % FCS with 10 % dimethyl sulfoxide (DMSO; Sigma-Aldrich, Dorset, UK) and cultured at 37 ˚C, 10 % CO_2 in order to develop a primary tumour cell line. The Eμ-myc tumours and cell lines were denoted Eμ#1 to 20, the Eμ-myc/CD32$^{-/-}$ were donated Eμ32#1 to 16 and the Eμ-myc/CD20 Tg tumours and cell lines were donated Eμ20#1 to 17. In addition, 1 x 10^5 tumour cells were re-passaged intravenously (i.v.) into C57BL/6 mice to assess tumour transplantability.

Other organs including the left kidney, the left lobe of the liver, the heart, lungs and sternum were harvested into 10% formalin (Sigma-Aldrich, Dorset, UK), as were small pieces of the spleen, thymus and LN. These were paraffin imbedded and stained with hematoxylin and eosin (H&E) to examine tumour infiltration and the aforementioned tingible body macrophages (TBM, “starry sky” macrophages) quintessential of Burkitt’s lymphoma presentation in humans.

2.9. Antibodies and antibody fragments.

2.9.1. Generation of antibodies.

Details of all antibodies used are shown in Table 2.1. In-house mAb were generated by Ms. Alison Tutt, Mrs. Christine Penfold and Dr. Claude Chan (University of Southampton). The generation of the anti-CD32 mAb will be described in detail in Chapter 4.

2.9.2. Generation of F(ab')$_2$ antibody fragments.

F(ab')$_2$ fragments were prepared by pepsin digestion using the methods of Lamoyi and Nisonoff (1963) with minor modifications as detailed by Elliot *et al* (1987)[376]. For digestion of monoclonal rat IgG, the sample was first concentrated to approximately 10 mg/ml, dialysed in 0.2 M TE8 and adjusted to pH 4.2 by the addition of 2 M sodium acetate. Pepsin (Sigma chemicals, Poole, Dorset) was dissolved to 10 mg/ml in 0.07 M sodium acetate containing 0.05M sodium chloride (NaCl) to pH 4.0. The sample was then digested at 37 °C with 0.1 mg/ml pepsin (1% w/v). At one hour intervals, samples (50µl) were removed and analysed by High-performance liquid chromatography (HPLC) (Zorbax GF250 column; Dupont) to monitor the generation of F(ab')$_2$. The digestion was halted by addition of 1M Tris to pH 8.0, when either less than 10% of the sample remained as IgG or when the F(ab')$_2$ peak was no longer increasing. For the digestion of the murine anti-CD32 mAb the pH of the reaction mix was reduced to pH 4.0 by the addition of 2 M sodium acetate, as the digestion of these murine antibodies at pH 4.2 was ineffective.

Digestions usually required 4 - 8 hours to achieve completion. Digestion products were then separated on 0.2 M TE8.0 equilibrated Ultrogel ACA44 (Pharmacia). All products were dialysed into PBS prior to use.

2.10. Antibody dialysis.

Dialysis was performed in order to replace the buffer of a mAb. This was commonly performed in order to substitute the 0.2M TE8 storage buffer with non-toxic PBS buffer for *in vitro* and *in vivo* experimentation. Buffer replacement was achieved using Slide-a-lyser dialysis cassettes (Fisher Scientific Ltd, UK). mAb was injected into the cassette using a needle and syringe and the cassette placed in the buffer of choice at a 1:100 dilution, i.e. 1 ml mAb in cassette dialysed into 100 ml of buffer. The buffer was replaced twice, leaving at least 1 hr at room temperature between each buffer change. The mAb was removed from the dialysis cassette using a needle and syringe, quantified on the Nanodrop ND-1000 (Fisher Scientific Ltd, UK) and passed through a 0.22 µM filter prior to use.

2.11. Measurement of surface antigens by immunofluorescence.

Two very similar methods were employed to measure surface antigens; direct immunofluorescence was used to assess surface antigen expression and indirect immunofluorescence was used to detect modulation of surface receptors.

Cells at 1 x 10^6 cells/ml were incubated at 4 °C for 30 min with FITC-conjugated (for the direct method) or unlabelled (for the indirect method) mAb of choice (10 µg/ml final concentration). Cells were then washed once (direct) or twice (indirect) in PBS-BSA-Azide (PBS, 1 % Bovine Serum Albumin fraction V (BSA; Wilfred Smith Ltd, Middlesex), 20 mM NaN_3) and resuspended at approximately 1 x 10^6 cells/ml. For indirect immunofluorescence, cells were further incubated for 15 min at 4 °C with either a FITC-conjugated or a PE-conjugated secondary antibody directed to the first mAb and washed once in PBS-BSA-Azide before resuspension to 1 x 10^6 cells/ml and subsequent analysis. Routinely PE-conjugated anti-mouse Fc F(ab')$_2$ fragment (Stratech Scientific Ltd, Newmarket Suffolk, England) antibody was used. In addition, B cells isolated from murine or human samples were incubated for 15 min at room temperature with either Allophycocyanin (APC)-conjugated (in-house) or PE-conjugated mouse CD19 (Stratech, UK), or FITC-conjugated human CD19 (in house) and washed once with PBS-BSA-Azide prior to analysis.

Analysis was performed on either the FACScan™ or FACSCalibur™ flow cytometers (BD Biosciences-Immunocytometry Systems,CA). Routinely, 7500 live cell events were collected, as identified by the FSC-H and SSC-H threshold parameters. FITC was excited at 488 nm with emission intensity being recorded in the 515-545 nm wavelength region. PE was excited at 495 and 545/566 nm with emission intensity being recorded in the 565-585 nm wavelength region. APC was excited at 650nm with emission intensity being recorded at 660nm wavelength. Samples were analysed using CellQuest Pro Software™ (BD Biosciences-Immunocytometry Systems,CA). Fluorescence intensities were assessed in comparison to negative control samples and expressed as histograms of fluorescence intensity versus cell number.

2.12. *In vitro* Apoptosis Assay.

2.12.1. AnV/PI staining of lymphoma and B cells.

200 µl of cells at 1 x 10^6 cells / ml were incubated with 12.5 µg/ml of each antibody of interest in 96 well plates (flat bottom) at 37 ºC for 24 hr. Cells were examined under the microscope for homotypic adhesion and harvested into FACS tubes containing 10 µl of AnV/PI stock; this contains 2.5 mM AnV 100 µg/ml PI of each reagent in 10X binding buffer (see Appendix 1). AnnexinV (AnV) was produced and FITC labelled in house, propidium iodide (PI) was reconstituted in dH_2O and sourced from Sigma Aldrich (UK). Cells were incubated for 15 min at room temperature in the dark. AnV/PI allows the

identification of dead (AnV^+/PI^-) and dying/apoptotic cells (AnV^+/PI^+) as AnV binds phosphatidylserine which is only displayed at the cell surface during apoptosis whilst PI only leaches into dying cells which have lost their cell membrane integrity. The percentage of AnV/PI positive cells was assessed by flow cytometry on the FACScan™ and FACSCalibur™ flow cytometers. Cells undergoing apoptosis were identified by FL1-H versus FL2-H using the appropriate compensation.

2.12.2. AnV/PI staining of BMDMs.

200 µl of cells in enriched RPMI (including 20 % L929 enriched medium) at 1 x 10^6 cells/ml in a 48-well plate were incubated with anti-CD32 at a final concentration of 10 µg/ml at 37 ˚C, 5 % CO_2 for 24 hrs. Cells were washed with room temperature PBS-BSA-Azide buffer and then 200 µl enriched RPMI was added. 10 µl AnV/PI (see above) was added directly to cells for 15 min at room temperature. Cells were removed from the plate as described in Materials and Method section 2.2 and analysed by flow cytometry as described above.

Percentage relative cell death was calculated as:

$$\% \text{ relative cell death} = \frac{(\% T - \% NT)}{(100 - \% NT)} \times 100$$

Where, % NT was the % AnV/PI positive cell without treatment and % T was the % AnV/PI positive cell after treatment.

2.13. Calcium flux assay.

1 x 10^7 cells were centrifuged for 5 min at 450 x g at room temperature and washed twice in serum free media, either RPMI or DMEM, as appropriate. 2 µl Fluro-3-AM dye (2.25 mg/ml Fluro-3-AM, in DMSO and 10 % pluronic F127) (Sigma-Aldrich, Dorset, UK) was added to the resuspended cells. 500 µl of serum free media was then added slowly to the cells. The cells were then incubated for 30 min at 37 ºC in the dark. The cells were washed twice in serum free media, resuspended in 5 ml 5% (w/v) BSA/media and divided into 250 µl aliquots. These were left to rest in the dark prior to analysis.

Live cell events were collected, as identified by the FSC-H and SSC-H threshold parameters. In general, each 250 µl sample was assessed by flow cytometry on the

FACScan™ for 15 sec before the addition of 250 µl of 5 % BSA/media (NT sample) or the appropriate antibody (in 5% BSA media) at 5 µg/ml final concentration for anti-IgM and anti-idiotype antibodies and 50 µg/ml for the anti-CD32 mAbs and assessed for a further 2 min 45 sec.

To determine the effect of the anti-CD32 mAb on BCR-induced calcium flux, the anti-CD32 mAb was added directly to the cell aliquots at final concentration of 50 µg/ml and incubated in the dark for 12 min at room temperature, then 3 min at 37 ºC, before being assessed by flow cytometry as described above. Analysis was performed using FlowJo Software™ (BD Biosciences-Immunocytometry Systems,CA).

2.14. Western blot analysis.

1 x 10^6 cells in a volume of 1 ml were treated with antibodies of interest at a concentration of 10 µg/ml. Duration of incubation varied, but most commonly cells were incubated at 37 ˚C with the anti-CD32 mAb for 2 min and then with or without anti-IgM or anti-idiotype for a further 5 min, unless otherwise stated.

After incubation, 1 ml volume was harvested into a 1.5 ml eppendorf on ice. These were centrifuged at 500 x g for 5 min at 4 °C, washed once with 800 µl PBS and resuspended in 25 µl Onyx lysis buffer (see Appendix 1). The samples were incubated at 4 °C for 30 min before being spun at 15,700 x g for 15 min at 4 °C. Samples were stored at -20 ºC until needed and quantified by Bradford assay before use.

Between 15 to 25 µg of protein along with reduced loading buffer (see Appendix 1) were heated to 100 ºC for 5 mi. After spinning (1 min at 15,700 x g) the samples were loaded into precast gels (Invitrogen NuPAGE 10% Bis Tris Gel) and proteins separated by SDS-Page at 100 V for approximately 1 hr in MOPS buffer (see Appendix 1) using the Surelock® system (Invitrogen, Paisley, UK) and per the manufacturer's instructions. Using the XCell II™ blot module (Invitrogen, Paisley, UK), the proteins were then transferred onto activated polyvinylidene fluoride (PDVF) membranes (Millipore, UK) according to the manufacturer's instructions, at 30 V for 90 min in 1X transfer buffer (from 20X stock; Invitrogen, UK).

Membranes were blocked in 5 % (w/v) dried milk reconstituted in TRIS buffered Saline containing 0.05% Tween-20 (v/v) (TBS-T; see Appendix 1) solution for 1 hr at room temperature. The membranes were washed twice in TBS-T and then incubated with the

primary antibody in TBS-T and 0.05 % (w/v) azide solution for 1 hr at room temperature or overnight at 4 ºC. Table 2.2 summarises the primary antibodies used.

The membranes were washed three times (5 min each wash) in TBS-T and incubated for 1 hr at room temperature with the relevant horse radish peroxidise (HRP) conjugated secondary antibody (GE Healthcare, Buckinghamshire, England)(see Table 2.2) in TBS-T.

The membranes were washed three times (5 min each wash) and then incubated with ECL reagent (1:1) (Thermo scientific SuperSignal West Pico Chemiluminscent substrate) for 5 min at room temperature. Under darkroom conditions, chemiluminescence films (Hyperfilm, GE Healthcare, UK) were exposed to the membranes and developed on the Xograph Compact X4 film processor (Xograph Healthcare Ltd, UK) to detect the proteins of interests.

Membranes were processed in this way up to four times, including incubation with a loading control, such as β-actin. It is important to mention that the nature and sizes of the primary antibodies used required a particular blotting order. The mAb used gave clean, single bands of different molecular sizes negating the need to strip the membranes in-between blotting for the different proteins of interest. pCD32 was blotted for first as it gave a weak band, followed by pSHIP and pSHP and then the loading control, either β-actin or α-tubulin.

2.15. mAb immunotherapy.

1 x 10^4 fresh murine syngeneic B cell lymphoma, either BCL_1 or A31 tumour was injected i.v. into female 8-12 week old BALB/c or CBA/H mice, respectively (day 0). Each mouse (4 mice / group) received a 500 μg dose (i.v.) of either an isotype control (WR17) or anti-CD32 mAb (AT130-2 or AT128 m2a) on day 3. On day 4 mice received a 125 μg (i.v) dose of anti-idiotype mAb (Mc106A5 or Mc39/16 for the BCL_1 or A31 tumours, respectively), the same mice received the 125 μg dose of anti-idiotype or isotype control by intraperitoneal (i.p.) injection on days 5, 6 and 7. Mice were monitored for signs of sickness as outlined by Home office regulations, in particular signs of enlarged spleens and then culled appropriately. Survival was assessed by Kaplein Myer curve analysis.

2.16. Tumour tracking.

2 x 10^7 fresh BCL_1 or A31 tumour was injected i.v. into cohorts of female 8 - 12 week old BALB/c or CBA/H mice respectively (day 0). A dose of 500 µg mAb was administered i.v. four days after tumour inoculation. On days 2, 4, 6 and 8, two mice per group were sacrificed and spleens removed. Cell suspensions from these spleens were stained according to direct FACS protocols (see Materials and Methods 2.10) with FITC-conjugated anti-idiotype and PE-conjugated CD19 to determine the percentage of anti-idiotype positive cells within the mice.

2.17. *Ex vivo* modulation assay.

In order to determine surface bound mAb and antigen expression *in vivo* of mice treated with mAb two approaches were taken. To determine surface bound mAb levels, splenic cell suspensions were incubated with PE-conjugated anti-mouse Fc according to indirect immunofluroscence protocol (Material and Methods 2.17). To determine antigen expression after treatment with mAb, splenic cell suspensions were incubated for 30 min at 4 ˚C in the presence of excess mAb (10 µl at 100µg/ml), washed twice with PBS-BSA-azide buffer and then incubated with PE-conjugated anti-mouse Fc according to indirect immunofluroscence protocol as above. Maximal expression of antigen was determined by incubating splenocytes from WR17 in the same way. Prior to analysis by flow cytometry, samples were incubated with 10 µg/ml APC-conjugated CD19.

2.18. *In vitro* Modulation assays.

200 µl of 1 x 10^6 /ml cells were incubated with 10 µg/ml mAb for 0, 2, 6 and 24 hr in 96-well plates for lymphoma and B cells, or in 48-well plates for BMDMs. Cells were stained in tubes suitable for flow cytometry according to indirect immunofluorescence protocols (Materials and Methods 2.11). Prior to analysis, cells were incubated for 15 min at room temperature with APC-conjugated murine CD19 for lymphoma and B cells or APC-conjugated F480 (BD Biosciences, UK) for BMDMs and washed once with PBS-BSA-Azide buffer. BMDMs were removed from the plates as previously described (Materials and Methods 2.2).

Percentage of total CD32 expression (at 0 hr), as determined by FL-2 MFI, was calculated for each time point by:

$$\% \text{ CD32 expression} = \frac{(\text{sample MFI} - \text{background MFI})}{(0 \text{ hr MFI} - \text{background MFI})} \times 100$$

2.19. Alexa-488 quenching Assay.

2.19.1. Alexa-488 labelling of mAb.

1 mg of mAb at 2 mg/ml (0.5 ml volume) was labelled using the Zenon® Alexa Fluro® 488 Rabbit IgG labelling kit (Invitrogen, SKU# Z-25302) per the manufacturer's instructions. Briefly, 1 mg mAb at 2 mg/ml was dialysed into 0.1M sodium carbonate buffer at pH 9.0 (see Appendix 1). Alexa-488 dye (Invirtogen, UK) was resuspending in DMSO and added at a dilution of 1:20 dye to mAb and then incubated for 1 hr at room temperature with constant stiring. This was then fractionated using a Sephadex G-25 Superfine column (GE Healthcare, UK), collecting the separated mAb fraction. The labelled mAb was then dialysed into PBS, quantified on the Nanodrop ND-100 and passed through a 0.22 μM filter prior to use.

2.19.2. Quenching assay.

200 μl of cells at 1 x 10^6 cells/ml were incubated at 37 °C, 5 % CO_2 for 2, 6 or 24 hrs with 5 μg/ml final concentration of Alexa-488 labelled mAb in a 96-well flat bottomed plate. Cells were harvested and washed (twice) with 3 ml PBS-BSA-Azide and resuspended in 300 μl enriched DMEM. 100 μl of cells was left untreated (unquenched; NQ) and 100 μl of cells were added to 2.5 μl anti-Alexa-488 mAb (Invitrogen, Paisley, UK) (Quenched; Q). Cells were incubated at 4 °C for 30 min. The final 100 μl of washed cells were examined by light and fluorescence microscopy. Analysis of NQ and Q samples was performed on FACS Calibur™ flow cytometer. Results were expressed as a percentage of fluorescence of the NQ samples:

$$\% \text{ Quenching} = \frac{((\text{NQ} - \text{background}) - (\text{Q} - \text{background}))}{(\text{NQ} - \text{background})} \times 100$$

Where, NQ was the MFI of non-quenched samples and Q was the MFI of quenched (+ anti-Alexa-488 mAb) and background is the MFI of the non-treated sample.

2.20. Adoptive transfer of CFSE labelled cells.

2.20.1. CFSE labelling of target and non-target splenocytes.

2 x 10^7 splenocytes/ml from WT (target cells; T) and $CD32^{-/-}$ (non-target; NT) BALB/c mice were stained with 5 µM and 0.5 µM carboxyfluorescein succinimidyl ester (CFSE) respectively for 10 min at room temperature. FCS of the same volume was then added for 1 min to quench further labelling. Cells were washed twice with PBS (450 x g for 5 min).

2.20.2. Adoptive transfer of target and non-target cells.

Cells in PBS were injected i.v. into BALB/c mice on day -1 at a 1:1 NT:T ratio. WT and $CD32^{-/-}$ BALB/c mice (three mice per group) were injected i.v. with either 100 µg of an isotype control (WR17) or anti-CD32 mAb (AT130-2 or AT128 m2a) on day 0. Mice were culled on day 1 and splenocytes were stained with APC-conjugated CD19 for 15 min at room temperature. Analysis was performed on the FACSCalibur™ flow cytometer. Routinely, the lymphocyte population was identified by the FSC-H and SSC-H threshold parameters and 5000 CD19 positive events were collected.

The ratio of T to NT was calculated as:

T:NT = %T / % NT

This was normalised for each experiment as:

Normalised T: NT = T:NT / (average of WR17 treated T:NT)

2.21. BMDMs phagocytosis assay.

100 µl of BMDMs at 5 x 10^5 cells/ml (5 x 10^4 cells/well) were left to adhere to the bottom of 96-well plates at 37 °C, 5 % CO_2 for 2 hr. During this time, B cells from the spleens of CD20 Tg mice were isolated by MACS® (See Materials and Methods 2.4) and CFSE stained at 5 µM (See Materials and Methods 2.20.1). The isolated B cells were incubated with or without anti-CD20 and anti-CD32 mAb at 10 µg/ml for 20 min at room temperature and then washed twice with PBS (450 x g, 5 min). 100 µl of B cells at 2.5 x 10^6 cells/ml (2.5 x 10^5 cells/well) were added in triplicate to the adhered BMDMs and incubated at 37 °C, 5 % CO_2 for 1 hour. Cells were washed twice and resuspended in 200 µl PBS-BSA-Azide buffer and incubated for 15 min with 10 µl (1:10 dilution with dH_2O) of APC-conjugated F480. Cells were washed once with PBS-BSA-Azide buffer and left in

200µl cold (4 °C) PBS-BSA-Azide buffer and incubated for 15 min at 4 °C. Cells were scrapped with the tip of a pipette, transferred into FACS tubes and analysed on the FACSCanto™. Routinely, the macrophage population was identified by the FSC-H and SSC-H threshold parameters and 5000 APC-F480 (FL-4) and CFSE (FL-1) double positive events were collected. Percentage phagocytosis was calculated as below:

$$\% \text{ Phagocytosis} = (\% \text{ F480}^{+}\text{CFSE}^{+}) - (\% \text{ F480}^{+}\text{CFSE}^{-} + \% \text{ F480}^{+}\text{CFSE}^{+}) \times 100$$

2.22. ELISA to determine half life *in vivo* of anti-CD32 mAb.

All incubations were at 37 °C unless otherwise stated. A 96-well immunomaxisorb plates (Fisher, UK) was coated with 100 µl / well of OX68 $F(ab')_2$ at 5 µg/ml in ELISA coating buffer (15 mM Na_2CO_3, 28.5 mM NaHCO3 at pH 9.6) and incubated for 1 hr at 37 °C, then at 4 °C overnight. Coating solution was discarded and replaced with 100 µg/ml CD32-CD4 fusion protein (designed by Dr. Stephen Beers produced by Dr. Claude Chan, University of Southampton) diluted 1:2 with 1% BSA/PBS and incubated for at least 1 hr. During this time samples and standards were prepared accordingly. Standard dilution of the mAb of choice commenced at 100 ng/ml and a standard curve produced through doubling dilution. Sample dilutions started at 1:100 from neat serum and serially diluted 1:10 down the ELISA plate.

After 1 hr the ELISA plate was washed (three times) with PBS/Tween (see Appendix 1) using the SkanWasher300 (Cox Scientific, Northants, United Kingdom). The plate was blanked in wells A1 and B1 with 1% PBS/BSA and 100 µl of the standard curve dilutions and each sample was dispensed into the appropriate well and incubated for 90 min. The ELISA plate was then washed (five times) with PBS/Tween using the SkanWasher300. 100 µl / well goat anti-mouse FcγR-HRP (Sigma-Aldrich, Dorset, UK) diluted 1:10000 in 1% BSA/PBA was dispensed into all wells and incubated for a further 90 min. The ELISA substrate was prepared by dissolving an o-Phenylenediamine tablet (OPD, 200 µM / tablet) (Sigma-Aldrich, St Louis, USA) in 24.7 ml ELISA citrate (19.2 g/L citrate acid) in the dark for 15 min, then 25.3 ml ELISA phosphate (28.4 g/L Na_2HPO_4) and 50 ml distilled water was added and stored in the dark until use. Just before use 40 µl 30 % H_2O_2 was added to the substrate.

The ELISA plate was then washed again (five times) with PBS/Tween using the SkanWasher300. Excess buffer was removed and 100 µl/well substrate was dispensed into all wells and incubated in the dark, at room temperature for 30 min. In order to stop the

colourmetric reaction 50 µl of 2.5 M H_2SO_4 was added to each well. The ELISA results were then read at an absorbance of 495 nm on the Dynatach MR400 plate reader and serum concentration of mAb was calculated against the standard curve.

2.23. Production of clodronate liposomes.

Clodronate liposomes can be used to deplete phogocytic cells, in particular macrophages *in vivo*[377] and are prepared as follows. Glassware was used for all steps of clodronate liposomes production, due to the corrosive properties of the chloroform solution. Cholesterol (Sigma-Aldrich, Dorset, UK) was dissolved in chloroform to prepare a 0.8 mg/ml cholesterol solution. To this an equimolar amount of a 100 mg/ml phosphatidylecholine (PSC) stock solution (PSC (Sigma-Aldrich P3556 Lα PSC Type XVI-E. 99% TLC) dissolved in choloform) was added. The chloroform phase was removed by gently blowing Nitrogen into the tube for approximately 90 min or until all the solvent had completely dispersed to leave a thin white layer of PSC.

The phospholipid film was dispersed by gentle rotation of the tube for approximately 10 min in either 10 ml filter sterilised PBS or 10 ml 0.25 mg/ml chlodronate solution (Cl_2MBP (Sigma-Aldrich D-4434 Dichloromethylenediphosphonic acid) dissolved in dH_2O). Samples were then submerged in a water bath sonicator for 3 min.

Samples were centrifuges at 10,000 x g for 15 min at 4 °C in an ultracentrifuge. The clodronate-liposomes formed a milky band at the top of the clear solution, whilst the PBS-liposomes formed a pellet at the bottom of the tube. The non-encapsulated clodronate and PBS were removed using a Pasteur pipette. The clodronate and PBS liposomes were resuspended in 20 ml PBS and washed four times using ultracentrifugation at 25,000 x g for 30 min at 4 °C.

Liposomes were resuspended in 4 -5 ml filter sterilised PBS and stored under nitrogen in a parafilm sealed tube at 4 °C for up to two weeks, or at -20 °C for up to a month. For *in vivo* depletion of splenic macrophages inject mice i.v. with 200 µl liposome 48 hr apart. Depletion occurred within 24 hr and lasted up to seven days, as established by previous investigations by Dr. Stephen Beers (University of Southampton).

2.24. Polymerase chain reaction for murine CD32 isoforms.

To assess the expression of CD32 isoforms in murine tissues RNA was extracted from cells, converted to cDNA and run using standard PCR protocols.

2.24.1. RNA extraction.

RNA was extracted from the cells using a PureLink™ Micro-to-Midi Total RNA Purification System (Invitrogen) according to the manufacturer's instructions. RNA was quantified by spectrophotometry on a Nanodrop ND-1000. RNA was stored at -80 ºC for a maximum of 18 hr prior to conversion to cDNA.

2.24.2. cDNA production.

Equimolar amounts of RNA were converted to cDNA using Superscript II First-strand synthesis system for RT- PCR (Invitrogen) per the manufacturer's instructions.

2.24.3. PCR for murine CD32 isoforms.

5' mCD32 and 3' mCD32 primers were designed by Dr. Claude Chan (Tenovus, University of Southampton) and provided by Invitrogen Ltd, UK. The PCR reaction gave products at 335bp for mCD32-1 and 194bp for mCD32-2.

5' (705) - CCC AAG TCC AGC AGG TCT TTA CCA GTA TTG

3' (869/1010) - TGC TTG AGA AGT GAG TAG GTG ATC GTA TTC

The PCR program to detect murine CD32 isoforms is as follows: Step 1) 95 ˚C for 5 min; 2) 95 ˚C for 1 min; 3) 56 ˚C for 1 min; 4) 72 ˚C for 2 min, 5) Repeat steps 2 to 4 30 cycles; 6) 70 ˚C for 5 min.

2.25. BIAcore analysis to determine affinity of anti-CD32 mAb.

A BIAcore T100 analyser (GE Healthcare, Buckinghamshire, England) was used to determine mAb affinities for CD32. 10 µg/ml of purified IgG or $F(ab')_2$ fragment anti-CD32 mAb in 10 mM sodium acetate pH 5.5 was immobilised to 1000 response units (RU) were immobilised to a CM5 sensorchip (GE Healthcare, Buckinghamshire, England), using the Amine coupling kit from BIAcore (GE Healthcare, Buckinghamshire, England; BR-1000-50). Briefly, mAb was covalently bound to the carboxymethylated dextran matrix on the sensor chip (CM5, Biacore) by amine coupling using the amine coupling kit (Biacore) at a flow rate of 5 µl/minute. This involves coupling a carboxy group in the dextran matrix to an amine group on the fusion protein. The surface of the chip was exposed to a 1:1 ratio of N-hydroxysuccinimide (NHS) and 1-ethyl-3 (3-dimethylaminopropyl)-carbodiimide (EDC) coupling solutions for 6 minutes. This

converts the carboxymethyl groups to ester groups that react easily with amines. 4-1BB-Fc diluted to 25μg/ml in 10 mM sodium acetate buffer (pH 4.5) was immobilised on the sensor chip for 6 minutes and then ethanolamine.HCl (Biacore) was run over the surface of the chip for 6 minutes to block all the uncoupled ester groups. The surface was then rinsed with 0.1 M glycine.HCl buffer (pH 2.5) for 3 minutes to remove any non-specifically bound proteins. In order to test mAb kinetics the CD32 fusion protein (R & D Systems, UK) at various concentrations (80 – 4.5 nM) in 1 x HBS-EP+ buffer (GE Healthcare, Buckinghamshire, England, BR-1006-69) at 30 μl/min for 600 sec association and then 300 sec for dissociation.

2.26. Production of immune complexes.

2 mg/ml rabbit anti-ovalbumin (rabαOVA; Nordic Immunological Laboratories, Tilburgi, The Netherlans) and 100 μg/ml FITC-conjugated ovalbumin (OVA-FITC; Sigma-Aldrich, UK and fluoresceinated in-house) were incubated at equal volumes for 15 min at 25 °C.

Table 2.1. Table 2.1: Summary of antibodies.

Clone	Specificity	Isotype	Source/Ref
Mc106A5	BCL_1 idiotype	Rat IgG2a	Tenovus
Mc39/12	μ-specific	Rat IgG2a	Tenovus
Mc39/16	A31 idiotype	Rat IgG2a	Tenovus
Goat Anti-mouse IgM	μ-specific	-	Stratech, UK
$F(ab')_2$ Goat Anti-mouse IgM	μ-specific	-	Stratech, UK
Rabbit Anti-mouse IgM	μ-specific	-	Stratech, UK
AT130-2	FcγRIIb	Mouse IgG2a	Tenovus
AT130-5	FcγRIIb	Mouse IgG1	Tenovus
AT128	FcγRIIb	Mouse IgG1	Tenovus
2.4G2	FcγRIIb/ FcγRIII	Rat IgG	ATCC
AT128 m2a	FcγRIIb	Mouse IgG2a	Tenovus
Rituximab	CD20	Human IgG1	Tenovus
Rit m2a	CD20	Mouse IgG2a	Tenovus
Rit γ1	CD20	Mouse IgG1	Tenovus
B1	CD20	Human IgG2a	Tim Illidge, University of Manchester
OX68	CD4	Rat IgG	Tenovus
ID3	CD19		Tenovus
KT3	CD3	Rat IgG2a	Tenovus
1.19	IgD	Rat IgG1	Tenovus
Fluor (FITC) $F(ab')_2$ Goat Anti-Mouse IgG	IgG	-	Stratech, UK
RFB9	CD19	Human IgG	Tenovus
WR17	CD37	Mouse IgG2a	Tenovus
LOB.74	CD40	Human IgG1	Tenovus

Table 2.2. Antibodies for Western Blotting

Primary Antibody	Source	Working dilution	Molecular weight (kDa)	Secondary HRP-conjugated antibody
β-actin	Sigma Aldrich	1:10000	42	Mouse
pCD32	Cell signalling technology	1:200	40	Rabbit
pSHIP	Cell signalling technology	1:500	145	Rabbit
pSHP	Cell signalling technology	1:500	68	Rabbit
α-Tubulin	Santa cruz biotechnology Inc.	1:1000	55	Mouse

CHAPTER 3 *In vitro* characterisation of the Eμ-myc mouse model

3.1. Chapter introduction.

Dysregulation of the proto-oncogene c-myc is a key step in the development of a variety of tumours[375,378]. Commonly, translocation of c-myc into the locus of other genes can lead to changes in cell proliferation, differentiation and cell cycle control. For example, when the c-myc gene is coupled to the regulatory sequence of mouse mammary tumour virus, incidence of mammary carcinomas increases [375]. Harris *et al* (1988) presented a transgenic mouse model that further developed this principle with regards to lymphoma. They fused human c-myc to the murine immunoglobulin heavy chain enhancer (Eμ) isolated from mouse plasmacytoma[379] and injected the resultant DNA construct into F2 embryos of (C57BL/6 x SJL/J) mice [375,378].

Myc was subsequentially expressed exclusively in B-lymphoid cells and chiefly in the bone marrow, spleen and lymph nodes of these mice[375,380] and would drove proliferation of B-cells and specifically the development of lymphoma[381]. As a result, more than 95% of the transgenic mice develop B-lineage tumours within a 6 to 10 months of birth; be these pre-B-cell, B-cell lymphomas or a heterogeneous population[378,381]. The transgenic Eμ-myc model, although not identical to human Burkitt's lymphoma (BL), mimics its phenotype and clinical presentation and as such provides a good murine model of the disease; where the translocation of c-myc into the immunoglobulin heavy chain (Igh) enhancer (Eμ) locus has been shown to be the predominant factor in disease development. Although the development of other forms of BL are associated with Epstein-Barr virus (EBV) infection and immune deficiency, such as that caused by HIV infection or treatment with immune suppressive treatment regimes, the sporadic form of BL has been show to occur as a result of chromosomal translocations into the c-myc gene (8q24) in humans[382]. The mouse translocation t(12;15) results in a similar murine disease to the common variant human translocation t(8;14)(q24;32)[383]. Remarkably, histological examination of H&E stained secondary lymph tissue from Eμ-myc mice also showed the same tingible body macrophages (TBM) commonly associated with human BL[384]. This characteristic appearance is referred to as "starry sky" macrophages, on account of the light areas corresponding to macrophages within the sheet of lymphoma cells.

Besides the Eμ-myc model mimicking human BL, it was also shown that whilst the over expression of c-myc in these transgenic mice caused a marked increase in pre-B-cells and a reduction in B-cells, there was little impairment in immune responses [375,380,385]. Interestingly, the pre-B-cells under the regulation of the c-myc transgene seem to be in a pre-malignant state, and the expansion of cells appears to be benign. However, some of these cells will become malignant as uncontrolled proliferation can lead to a potential gain of additional genetic changes which are required for progression to full malignancy; including those of N-ras, C-ras and p53[385-387]. Importantly, the nature of this model allows the serial sampling of blood which can be utilised as an analytical tool to identify the progression of the circulating B-cells to malignancy and examine the mutations gained[380,386].

In recent years variations of the earlier Eμ-myc model have been developed[387]. Studies have used the Eμ-myc mouse model and its variants to focus on the role of molecules such as p53 and apoptotic mediators such as Bcl-2 and Bim in haemopoietic oncogenesis and apoptosis. Bcl-2 has been shown to promote cell survival but not proliferation[388]. Mice transgenic for both Bcl-2 under the control of the Eμ enhancer and Eμ-myc demonstrated high numbers of B-cells that rapidly develop B-lymphomas as tumour cells are not effectively removed by apoptosis [388-390]. Pro-apoptotic molecules (such as Bim, Puma and Noxa) have, in a similar way, been shown to participate in effective removal and maintenance of lymphoid cells; with dysregulation leading to a pro-tumourgenic state (reviewed in [391]).

Regardless of its close parallel to human BL, we wished to employ the Eμ-myc mouse model to examine the effects of a range of therapeutic antibodies and particular cell signalling molecules on apoptosis, and mAb therapy. The Eμ-myc model has several advantages over alternative models. Firstly, we are able to generate primary lymphomas and LCL from the Eμ-myc mice that are fully syngeneic and in contrast to heavily re-passaged tumour models and highly adapted cell lines have less additional oncogenic mutations and reduced retroviral burdens. Both of these factors can alter the phenotype of the tumour cells and as such their response to certain anti-cancer drugs. Such changes, particularly infection with retrovirus, can increase immunogenicity and will therefore also affect response to therapy, i.e. tumour clearance may occur as a result of immune stimulation rather than as a result of therapeutic intervention. The Eμ-myc model also has several advantages over xenograft models of human disease. Primarily, these xenograft models require immuno-compromised animals and as such, they do not mimic the complex

relationship between the tumour and the tumour microenvironment. Nude and SCID mice, for example, lack components of the adaptive immune system, but still have some elements of the innate immune systems. Therefore, the human cancer cells are still likely to be immunogenic within these mice and the mechanism of anti-tumour activity may be as a result of immune rejection rather than a specially generated responses. Hence, the primary tumours and associated primary tumour cell lines that we generate will contain similar characteristics to tumours occurring in the human population and consequently, therapy in these primary lymphoma models may better reflect the potential clinical effect of our reagents.

In addition, as the Eμ-myc model is genetically tractable, it also permits the generation of tumours that lack CD32 and allows the investigation of the importance of the CD32 molecule in tumour development and how it could be utilised for therapeutic benefit. This was achieved by crossing $CD32^{-/-}$ mice with the Eμ-myc mice of the same genetic background (C57BL/6). Here we describe the presentation and characteristics of both the Eμ-myc lymphomas and the Eμ-myc/$CD32^{-/-}$ lymphomas.

3.2. Kaplein Meier survival.

Cohorts of mice were crossed to WT or $CD32^{-/-}$ C57BL/6 backgrounds in the presence of the Eμ-myc transgene and monitored for signs of tumour. When sick, mice were culled in accordance to the protocol outlined in Materials and Methods section 2.8 and presence of tumour confirmed by autopsy. It was shown that mice develop spontaneous lymphoma from six weeks to six months of age as demonstrated by the generated Kaplan Meier curve (Figure 3.1), which demonstrates the rate of tumour incidence within the population of C57BL/6 WT mice, the Eμ-myc mice and the Eμ-myc/$CD32^{-/-}$ mice within this facility. Statistically, both the Eμ-myc and Eμ-myc/$CD32^{-/-}$ have a lower survival incidence than the congenic C57BL/6 WT population ($p<0.001$ and $p<0.002$ respectively, by Mantel-Cox statistical testing). However, there is no significant difference between the incidence of survival between the two transgenic populations ($p = 0.1807$ by Mantel-Cox statistical testing), suggesting that Eμ-myc mice which lack CD32 are no more or less susceptible to developing spontaneous lymphomas compared with those that express CD32. However, we did observe a small trend towards slower rate of incidence of tumour presentation on the $CD32^{-/-}$ background, which supports current literature that CD32 confers poor prognosis and increased metastatic disease[359,392,353,360]. This was also reflected when examining the disease presentation between the Eμ-myc and Eμ-myc/$CD32^{-/-}$ mice, i.e.

presence in metastasis as measure by tumour infiltration in histological sections, discussed in detail in sections 3.3.2 and 3.3.3.

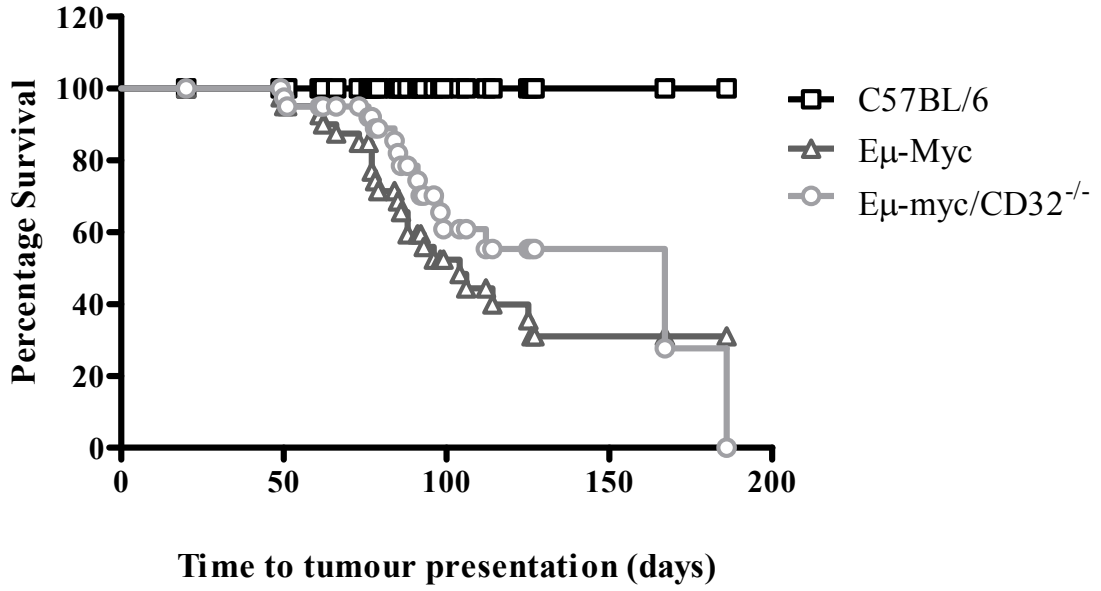

Figure 3.1. Kaplan Meier curve of Eμ-myc and Eμ-myc/CD32$^{-/-}$ mice.
Cohorts of mice were crossed to WT or CD32$^{-/-}$ C57BL/6 backgrounds in the presence of the Eμ-myc transgene and monitored for signs of tumour and when sick in accordance to the protocol outlined in Materials and Methods section 2.8 mice were culled. Days to tumour was a measure of the incidence, from birth, of spontaneous tumour development in the Eμ-myc (△) and Eμ-myc/CD32$^{-/-}$ (○) mouse populations at this laboratory in comparison with congenic C57BL/6 mice (□). Both the Eμ-myc and Eμ-myc/CD32$^{-/-}$ have a lower survival incidence than the congenic C57BL/6 WT population ($p < 0.0001$ and $p < 0.0002$, respectively). However, there was no significant difference between the incidence of survival between the two transgenic populations ($p = 0.1807$), there was nonetheless, a trend towards a slower rate of tumour incidence in the Eμ-myc/CD32$^{-/-}$ mice.

3.3. Presentation of the primary tumour.

3.3.1. Physical tumour presentation.

Eμ-myc mice developed tumours with a variety of symptoms, as previously described (Materials and Methods section 2.8). On disease manifestation the mice were culled and the size and location of the LN were noted. The size of an individual LN size was assessed on a scale of 0 - 5, where zero indicated no or normal LN and five indicated a very large LN. See Table 3.1 for detailed characterisation of LN size. These findings are in agreement with those by Harris *et al* 1988. Figure 3.2 shows a dissected Eμ-myc mouse and the location and size of commonly observed tumour masses of the LN. The weight of the spleen was also recorded. Table 3.2 and 3.3 show spleen weight and lymph node score for the Eμ-myc and Eμ-myc/CD32$^{-/-}$ tumours, correspondingly. It was observed that the Eμ-myc and Eμ-myc/CD32$^{-/-}$ tumours presented in the same locations and that there was no significant difference between the two strains of mice in terms of spleen weight,

brachial/axillary LN and cervical LN score ($p = 0.8681$, $p = 0.5277$ and $p = 0.0972$, respectively by Student's t-test). However there was a significant difference in inguinal LN score ($p < 0.01$, by Student's t-test) between the two mouse strains, where the Eμ-myc/CD32$^{-/-}$ mice presented with smaller inguinal LN in comparison with the Eμ-myc mice. Figure 3.3 compares the spleen weight and LN size between the Eμ-myc and Eμ-myc/CD32$^{-/-}$ mouse strains. The spleen weight of a WT C57BL/6 ranges between 0.080 g and 0.120 g (unpublished observations, Dr Ann White, University of Southampton), whilst the spleen weight of the Eμ-myc mouse however ranges between 0.395 g and 1.132 g and the for the Eμ-myc/CD32$^{-/-}$ mice the range was 0.189 g to 1.050 g. This demonstrates that, despite there being no significant difference between the spleen weights of the two Eμ-myc strains, the spleens of these mice are enlarged in comparison to healthy WT congeneic animals.

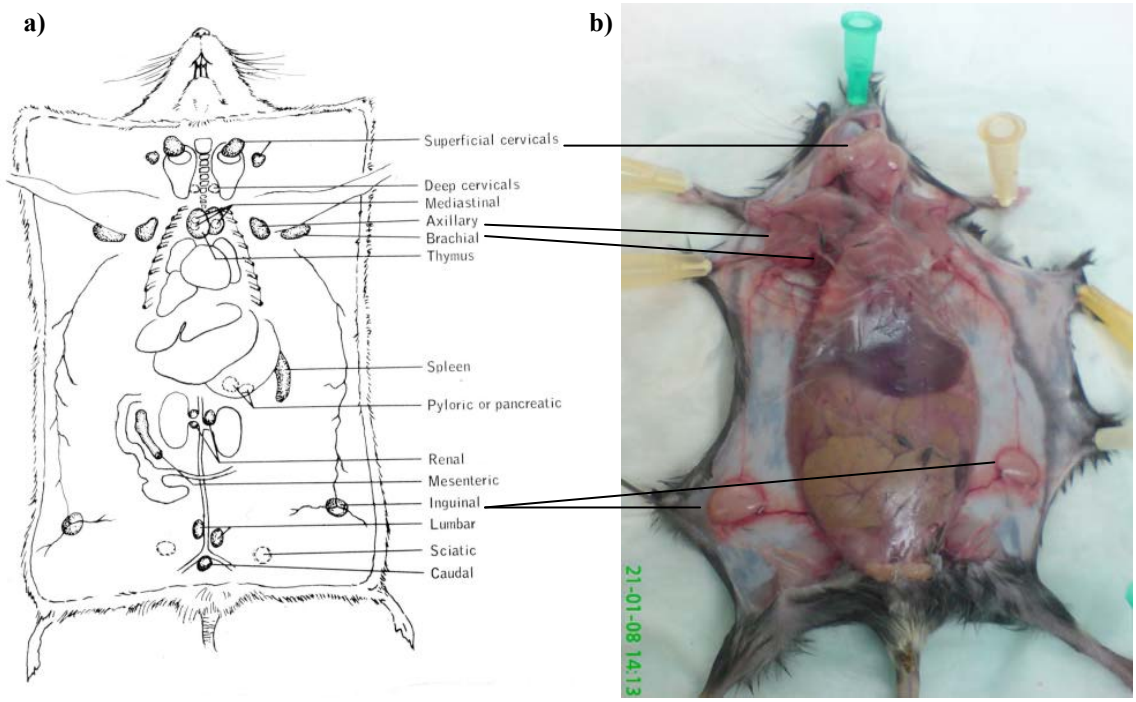

Figure 3.2. Size and location of commonly occurring tumours in Eμ-myc mice.
(a) Scheme reporting localization of the lymphatic system (see: www.informatics.jax.org/greenbook/images/13-4.jpg) (b) Midline dissection of an Eμ-myc mouse showing enlarged cervical (indicated top), axillary and brachial (indicated middle) and inguinal lymph nodes (indicated bottom). This mouse also had an enlarged spleen and thymus (not pictured). The inguinal LNs of a WT C57BL/6 mouse are less than 1mm in diameter. In the Eμ-myc mouse these can become enlarged to up to 10mm in diameter.

Table 3.1. Criteria used to determine lymph node size in Eμ-myc and Eμ-myc/CD32$^{-/-}$ mice.

Score	Size	Description
0	Normal	LN not visible or <1mm
1	Small	1 – 2 mm
2	Small-medium	3 – 5 mm
3	Medium	5 – 8 mm
4	Large	8 - 10 mm
5	Very large	> 10 mm

Table 3.2. Weight of spleen and size of lymph nodes in Eμ-myc mice.

Lymphoma	Spleen weight (g)	Inguinal LN	Brachial/ Axillary LN	Cervical LN	Thymus
Eμ#1	ND*	ND*	ND*	ND*	ND*
Eμ#2	0.54	0	0	0	0
Eμ#3	0.426	3	3	4	3
Eμ#4	0.400	4	3	2	2
Eμ#5	0.520	3	3	4	2
Eμ#6	0.580	5	4	4	5
Eμ#7	0.580	4	2	4	4
Eμ#8	0.954	3	3	4	5
Eμ#9	0.526	3	3	3	0
Eμ#10	1.152	2	3	4	0
Eμ#11	0.677	3	1	4	0
Eμ#12	0.613	3	0	4	4
Eμ#13	0.653	4	0	3	5
Eμ#14	1.307	5	4	4	0
Eμ#15	1.033	4	2	2	4
Eμ#16	0.175	1	1	0	0
Eμ#17	0.395	3	4	4	0
Eμ#18	0.565	5	5	5	0
Eμ#19	0.858	3	3	3	0
Eμ#20	0.466	1	0	0	2

The spleens of Eμ-myc mice were weighed upon dissection, whilst LN size was categorised according to scale described in Table 3.1. Statistics relating to differences in spleen weight and LN size between Eμ-myc and Eμ-myc/CD32$^{-/-}$ mice are shown in Figure 3.3. *ND: Not determined as mouse died before signs of tumour were observed.

Table 3.3. Weight of spleen and size of lymph nodes in Eμ-myc/CD32$^{-/-}$ mice.

Lymphoma	Spleen weight (g)	Inguinal LN	Brachial/ Axillary LN	Cervical LN	Thymus
Eμ32#1	0.556	2	2	2	1
Eμ32#2	0.280	1	2	2	2
Eμ32#3	0.189	2	2	ND*	ND*
Eμ32#4	ND*	4	3	4	4
Eμ32#5	ND*	ND*	ND*	ND*	ND*
Eμ32#6	0.702	3	3	2	2
Eμ32#7	1.081	3	3	4	3
Eμ32#8	0.341	1	1	5	3
Eμ32#9	0.700	1	3	1	4
Eμ32#10	0.533	3	4	3	3
Eμ32#11	0.533	2	2	2	1
Eμ32#12	0.488	4	4	4	5
Eμ32#13	0.667	3	1	1	5
Eμ32#14	0.229	1	2	2	5
Eμ32#15	2.103	0	0	0	0
Eμ32#16	1.05	0	0	1	0

As in table 3.2., the spleens of Eμ-myc/CD32$^{-/-}$ mice were weighed upon dissection, whilst LN size was categorised according to scale described in Table 3.1. Statistics relating to differences in spleen weight and LN size between Eμ-myc and Eμ-myc/CD32$^{-/-}$ mice are shown in Figure 3.3. *ND: Not determined

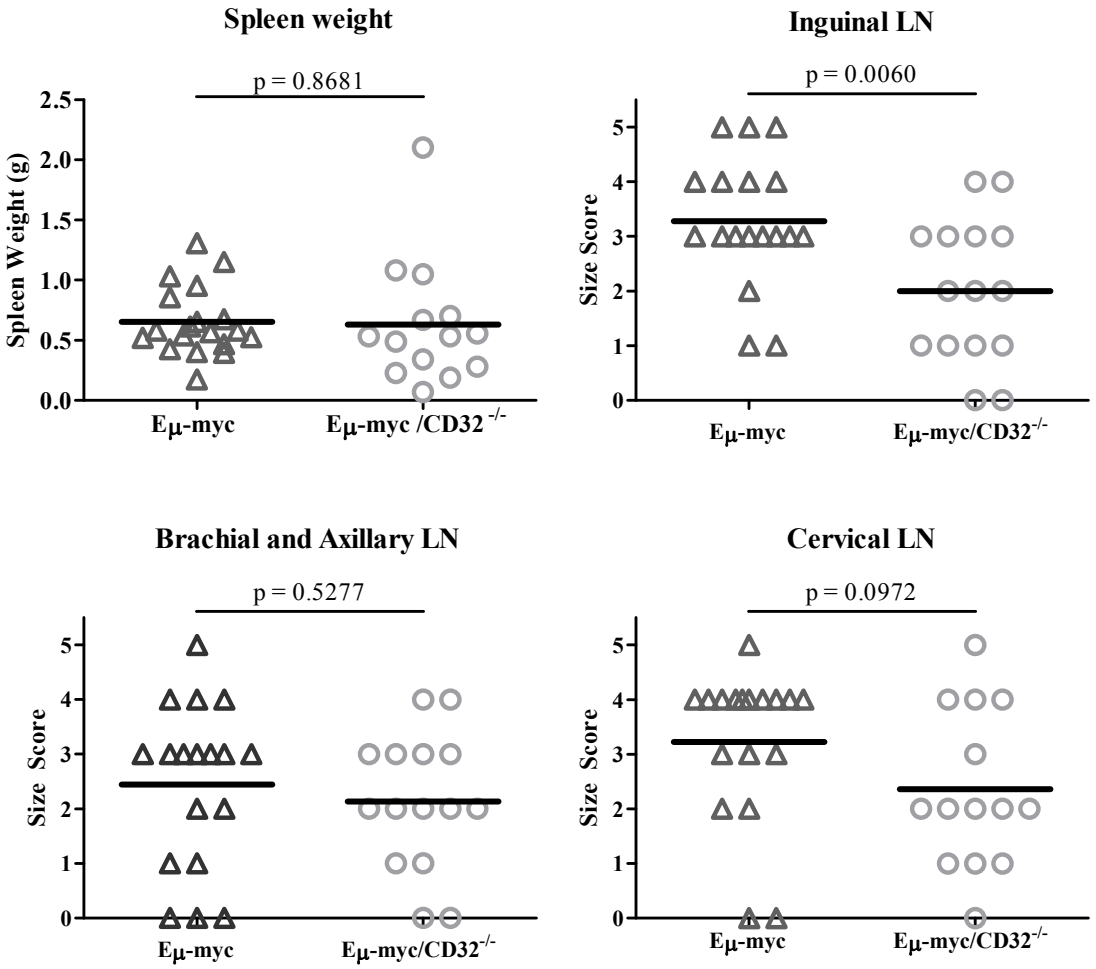

Figure 3.3. Comparison of spleen weight and lymph node size between Eμ-myc and Eμ-myc/CD32$^{-/-}$ mice.
The spleens from Eμ-myc and Eμ-myc/CD32$^{-/-}$ mice were excised and weighed, whilst the LN from the same mice were sized according to Table 3.1 upon dissection. There was no significant difference between the two strains of mice in terms of spleen weight, brachial/axillary and cervical lymph node score (by Student's t-test). However there is a significant difference in inguinal LN score ($p < 0.01$, by Student's t-test) alluding to smaller ILN in the Eμ-myc/CD32$^{-/-}$ mouse.

3.3.2. Histological examination of tissues from tumour bearing mice.

3.3.2.1. Histological examination of lymphoid tissue from the C57BL/6 and Eμ-myc mice.

Hematoxylin stains nucleic acids a deep blue-purple colour, whilst eosin stains other elements of tissues pink in a non-specific manner; meaning the nucleus of the cell stains blue, whilst the cytoplasm and extracellular matrix of cells stain to varying degrees of pink. The H&E staining of normal splenic tissue shows dense staining of the white pulp (lymphoid cells) around central arteries, with the less densely stained red pulp surrounding these. This architecture is evident in the spleen of the WT mouse (Figure 3.4b), but not in the spleen from the Eμ-myc mouse (Figure 3.4e), where tumour cells have replace normal

tissue architecture. Alongside this, in other lymphoid tissue from the Eμ-myc mice there is complete obliteration of normal tissue architecture, i.e. in the thymus and inguinal LN (Figure 3.4d & f) in comparison to corresponding tissues from the WT mouse (Figure 3.4a & c). In all of the lymphoid tissues of the Eμ-myc mouse, "starry sky" macrophages can be observed, similar to that observed in human Burkitt's lymphoma[384] Interestingly, at the same X 10 magnification the structure of the LN of the C57BL/6 mouse can be seen in its entirety, whereas only a section of the Eμ-myc LN can be observed. This demonstrates that there is expansion of the tissue on account of the tumour infiltration.

3.3.2.2. Histological examination of non-lymphoid tissue from C57BL/6 and Eμ-myc mice.

Next we went on to assess the level of tumour infiltration (TI) into other organs of the mouse. In highly vascular tissues, such as the kidney and liver TI was common (Figure 3.5i & j). Table 3.4 summarises the sites of tumour infiltration in the Eμ-myc mice. TI in other tissues such as the heart and lungs was apparent in some cases, but was less common (Figure 3.5e, f & g and Table 3.4). In the peripheral tissues of the Eμ-myc mice the normal tissue architecture was predominately intact, suggesting, as expected, that the lymphoma cells track to and accumulate predominately in the lymphoid organs[393,394].

3.3.2.3. Histological examination of tissues from the Eμ-myc/CD32$^{-/-}$ mice.

As with the Eμ-myc mice, tissues were taken from the Eμ-myc/CD32$^{-/-}$ mice and processed for H&E staining. Similar to the Eμ-myc tissue histology of the lymph node, spleen and thymus there was evidence of tingible body macrophages, but these tissues still retained normal architecture (Figure 3.6). It was also observed that the TI in the peripheral tissues of the Eμ-myc/CD32$^{-/-}$ mouse was less pronounced and at a lower level than in the Eμ-myc mouse, although this was not formally quantified due to histology only being performed on six Eμ myc/CD32$^{-/-}$ mice.

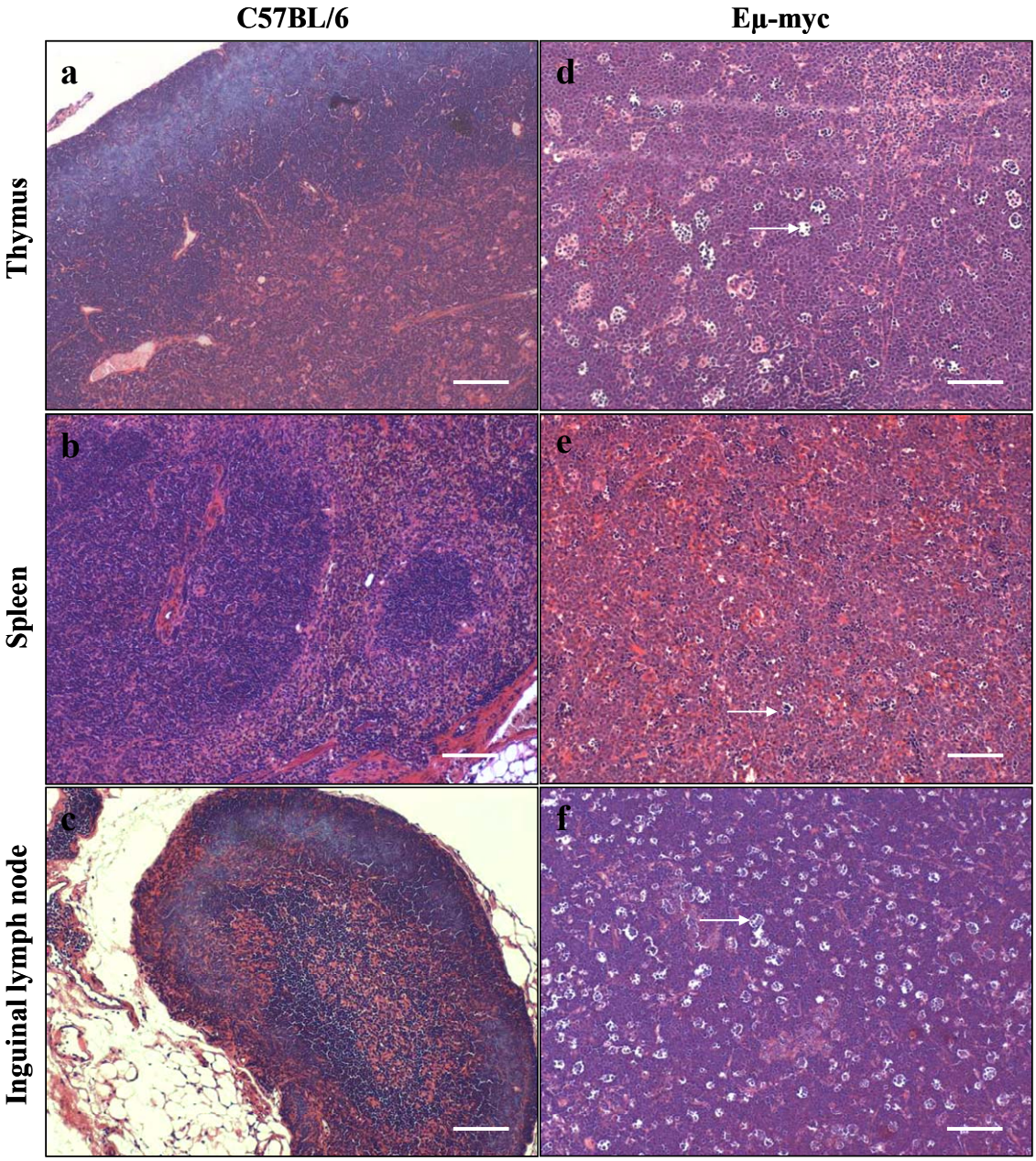

Figure 3.4. Altered histology in the lymphoid organs of Eμ-myc mice.
At dissection, tissues of the Eμ-myc mice were harvested into formalin. The tissues were paraffin imbedded and stained with H&E to examine tumour infiltration and the aforementioned TBM, quintessentially associated with BL in humans. Compared with WT C57BL/6 tissue (left hand panels) the Eμ-myc tissue shows a loss of normal architecture (right hand panels) and an increase in the physical size of the tissue (all tissue examined under X 10 magnification). In addition, the tissue from the Eμ-myc mice shows "starry sky" or TBM (arrows). These are macrophages that contain fragments of apoptotic tumour cells and appear as cleared areas in the layers of identical tumour cells. The histology shown here is similar to that observed in human BL[384]. Scale bar equivalent to 100μm.

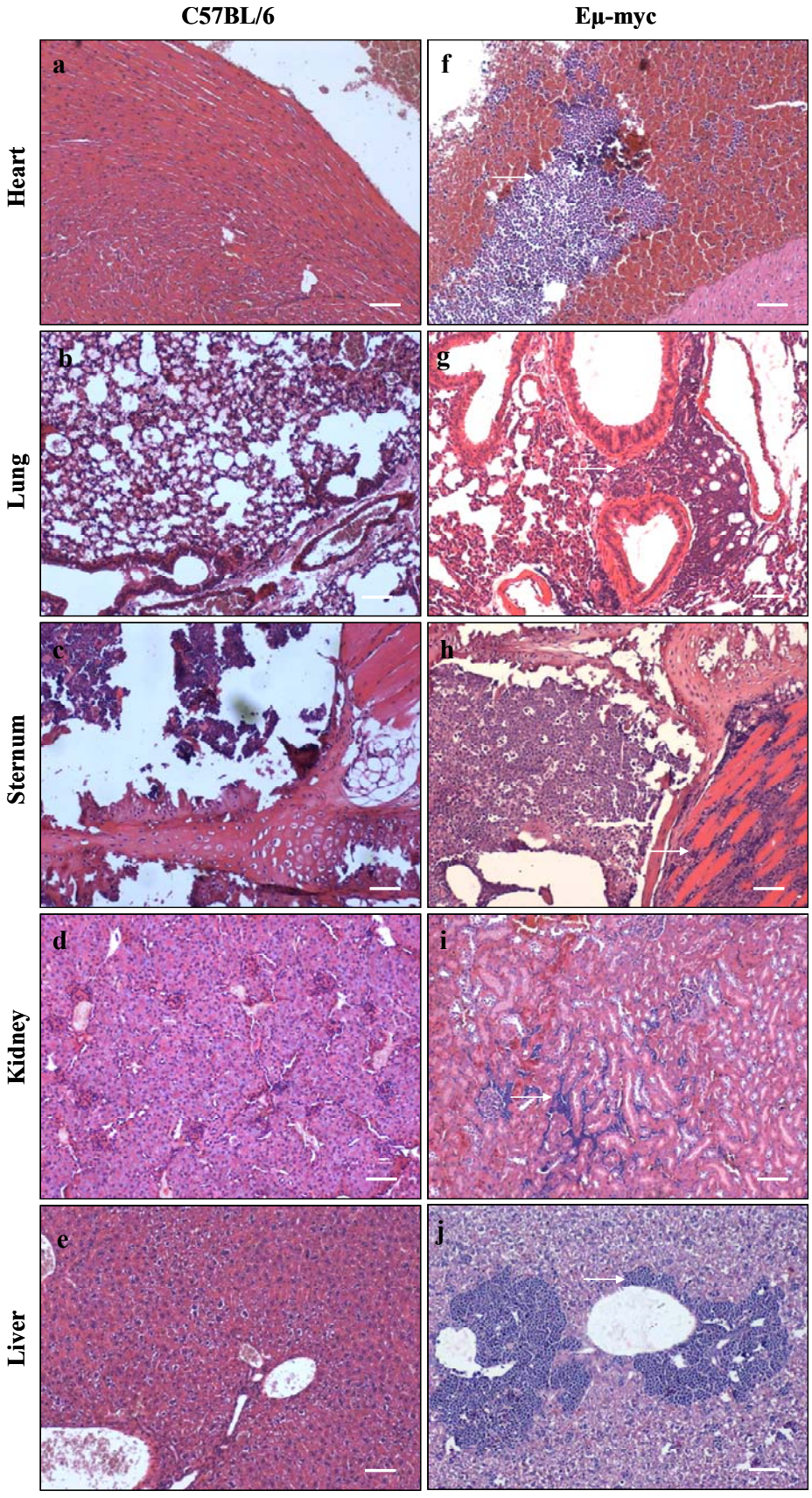

Figure 3.5. Tumour infiltration of peripheral tissues in the Eμ-myc mouse.
As previous, at dissection, tissues of the Eμ-myc mice were harvested into formalin. The tissues were paraffin imbedded and stained with H&E to examine tumour infiltration and the aforementioned TBM, quintessentially associated with BL in humans. Comparison of H&E stained tissue sections in a WT C57BL/6 mouse (left hand panel) with Eμ-myc mouse after tumour presentation (right hand panels). Areas of tumour infiltration are stained blue, as indicated by arrow. Scale bar equivalent to 100μm.

Table 3.4. Tumour infiltration in the Eμ-myc mouse.

Lymphoma	Thymus	Spleen	LN	Heart	Kidney	Lungs	Sternum	Liver
Eμ#1	ND*							
Eμ#2	ND*							
Eμ#3	TBM	Y	TBM	Y	Y	N	N	Y
Eμ#4	TBM	Y	-	N	N	N	Y	Y
Eμ#5	TBM	Y	TBM	N	N	N	Y	Y
Eμ#6	TBM	Y	-	N	Y	Y	Y	Y
Eμ#7	TBM	Y	-	N	Y	N	N	Y
Eμ#8	TBM	TBM	TBM	N	Y	Y	Y	Y
Eμ#9	-	TBM	TBM	N	Y	Y	Y	Y
Eμ#10	-	TBM	TBM	Y	Y	N	Y	Y
Eμ#11	-	N	-	N	Y	N	Y	Y
Eμ#12	TBM	Y	-	Y	Y	Y	Y	Y
Eμ#13	ND*							
Eμ#14	ND*							
Eμ#15	TBM	TBM	TBM	Y	Y	Y	Y	Y
Eμ#16	ND*							
Eμ#17	ND*							
Eμ#18	ND*							
Eμ#19	ND*							
Eμ#20	ND*							

Table indicates both the presence of TBM in lymphoid tissues and the occurrence of tumour infiltration in the non-lymphoid tissues in the Eμ-myc mice. Key: *ND: No data; -: no tissue sample taken; TBM: tingible body macrophages; Y: yes to tumour infiltration; N: no tumour infiltration.

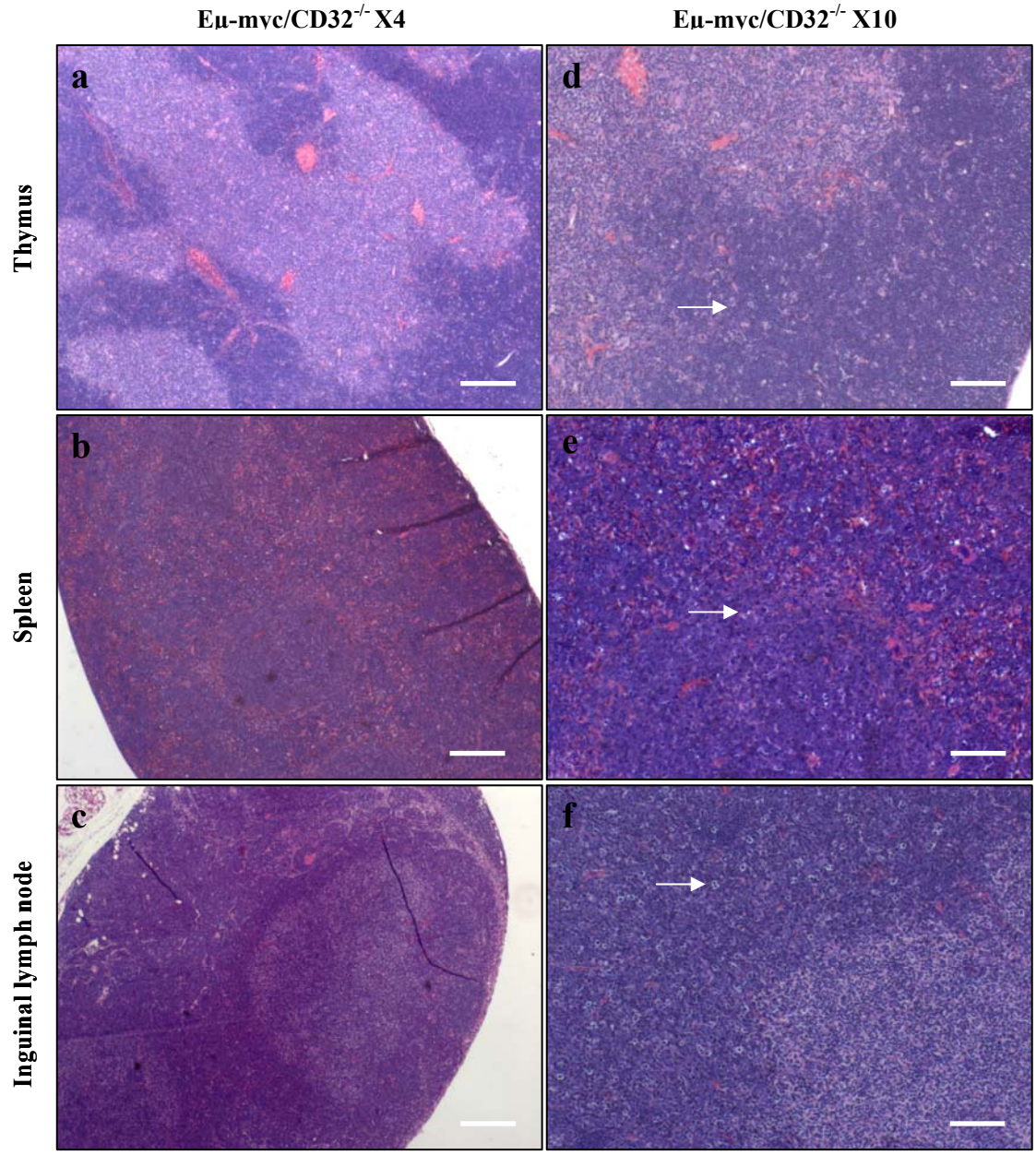

Figure 3.6 Altered histology in the lymphoid organs of Eμ-myc/CD32$^{-/-}$ mice.
As previous, at dissection, tissues of the C57BL/6 and Eμ-myc/CD32$^{-/-}$ mice were harvested into formalin. The tissues were paraffin imbedded and stained with H&E to examine tumour infiltration and the aforementioned TBM, quintessentially associated with Burkitt's lymphoma in humans. Compared with WT C57BL/6 tissue (Figure 3.4) the Eμ-myc/CD32$^{-/-}$ tissue shows retention of normal architecture but an increase in the physical size of the tissue at X 10 magnification. Alongside this, the lymphoid tissue from the Eμ-myc/ CD32$^{-/-}$ mice shows "starry sky" or tingible body macrophages (arrows). Scale bar equivalent to 10μm at X4 magnification and 100μm at X100 magnification.

3.4. Primary tumour characterisation.

3.4.1. Tumour phenotype.

The spleen, ILN, thymus and other obvious tumour bearing organs (including additional LN) were harvested into complete media. Cell suspensions of the spleen, ILN and thymus were produced. These were then immunophenotyped using flow cytometry. Tumour cells were incubated with PE-conjugated anti-CD19 (ID3) and either FITC-conjugated anti-CD3 (KT3), anti-IgM (Mc39/12), anti-IgD (1.19) or anti-IgG (Figure 3.7 and Table 3.5 – Eμ-myc mice). The Eμ-myc/ $CD32^{-/-}$ were also phenotyped for CD32 using a FITC-conjugated anti-CD32 (AT130-2) (Figure 3.8 and Table 3.6) and analysed by flow cytometry to confirm the absence of CD32 expression.

Overall, 55% of the Eμ-myc primary tumours expressed IgM. Of the 20 Eμ-myc primary tumours harvested, seven were IgM positive, whilst three showed a mixed population and one additional cell line showed weak IgM expression. In contrast 77.8% of the Eμ-myc/$CD32^{-/-}$ primary tumours expressed IgM. Seven of the nine Eμ-myc/$CD32^{-/-}$ tumours were IgM positive, although three of these tumours showed weak IgM expression. In addition, five out of the nine (55.6%) Eμ-myc/$CD32^{-/-}$ tumours were IgG positive, whilst only five of the 20 (25%) Eμ-myc tumours were IgG positive and only one of the nine (11.1%) Eμ-myc/$CD32^{-/-}$ tumours were IgD positive, whilst five of the 20 (25%) Eμ-myc tumours were IgD positive. These data imply that the Eμ-myc/$CD32^{-/-}$ tumours are generally derived from mature/class switched B cell clones in comparison to the Eμ-myc tumours which were derived from a greater proportion of immature B cell clones.

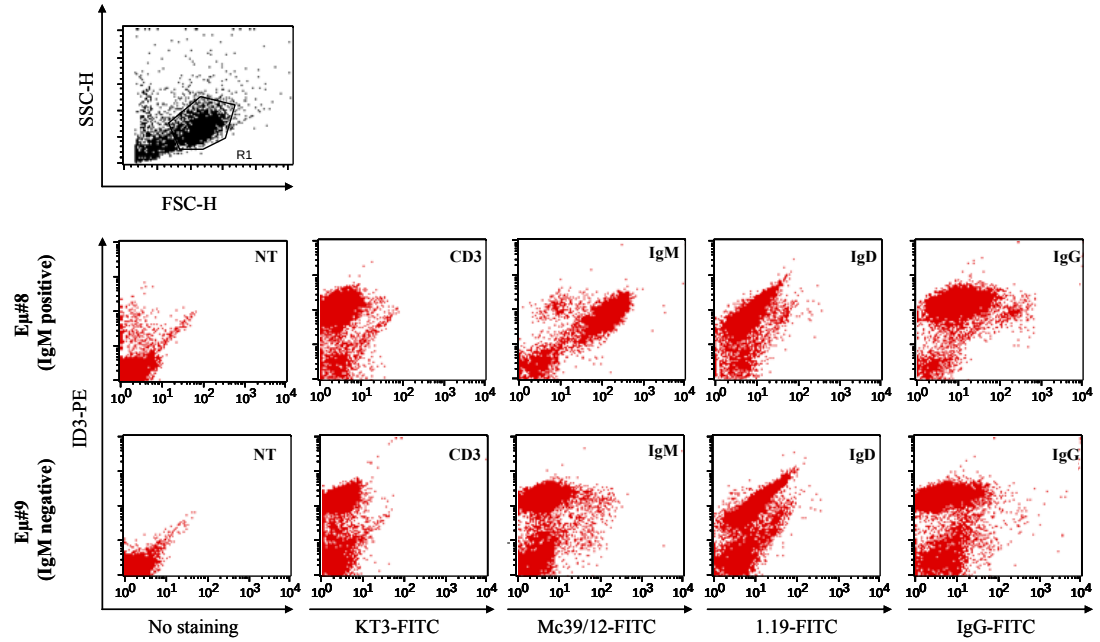

Figure 3.7. Immunophenotyping of Eμ-myc primary lymphoma cells.
Cells from the spleen of Eμ-myc mice were incubated with 5 μg/ml PE-CD19 (1D3) and 10 μg/ml FITC conjugated CD3, Mc39/12 (IgM), 1.19 (IgD) or IgG antibodies for 30 min at 4˚C and analysed by flow cytometry. 7,500 live lymphocyte events (R1), as identified by FSC-H and SSC-H were collected. The phenotype of cells within the R1 gate was expressed as PE-CD19 (FL2-H) versus FITC-antibody (FL1-H). Fluorescence of the CD19 population (FL-2) that was greater that the control (NT) were considered positive for the particular antigen. Eμ#8 (top panels) was characterised as an IgM positive tumour, whereas Eμ#9 (bottom panels) was characterised as an IgM negative primary tumour.

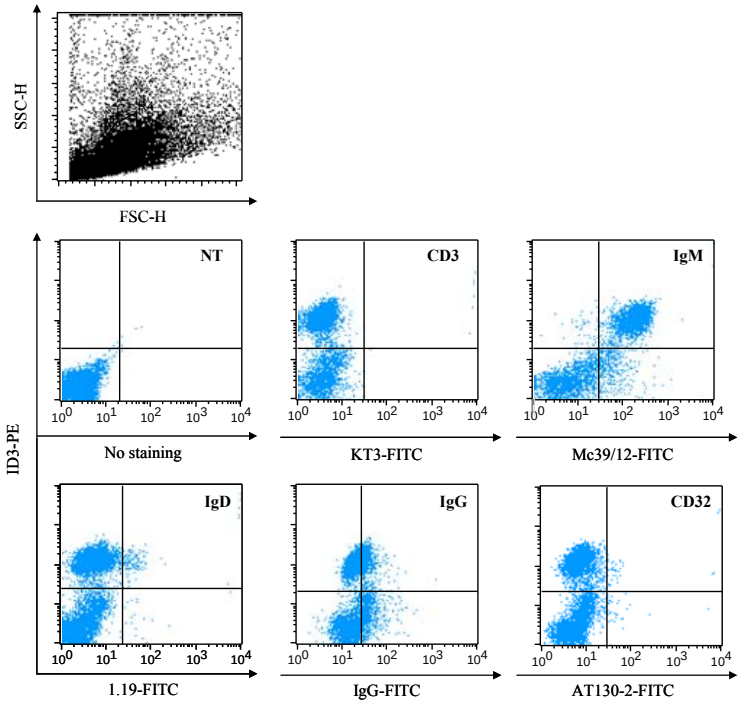

Figure 3.8. Immunophenotyping of Eμ-myc/CD32$^{-/-}$ primary lymphoma cells.
Cells from the spleen of Eμ-myc/CD32$^{-/-}$ mice were incubated with 5 μg/ml CD19-PE and 10 μg/ml FITC conjugated KT3 (CD3), Mc39/12 (IgM), 1.19 (IgD), IgG or CD32 (AT130-2) antibodies for 30 min at 4˚C and analysed by flow cytometry. 7,500 lymphocyte events (R1), as identified by FSC-H and SSC-H were collected. The phenotype of these cells was expressed as PE-CD19 (FL2-H) versus FITC-conjugated mAb. Fluorescence of the CD19 population that was greater that the control (NT) was considers positive for the particular antigen. These flow cytometry show the phenotype of Eμ32#4; an IgM positive, CD32 negative tumour.

Table 3.5. Summary of Eμ-myc primary phenotypes

1° lymphoma	CD3	CD19	IgM	IgD	IgG
Eμ#1			ND*		
Eμ#2	-	-	wk	wk	wk
Eμ#3	-	+	-	-	+
Eμ#4	-	+	+	-	wk
Eμ#5	-	+	-	-	+
Eμ#6	-	+	+	-	+
Eμ#7	-	+	mixed	-	-
Eμ#8	-	+	++	wk	-
Eμ#9	-	+	-	-	-
Eμ#10	-	+	-	-	mixed
Eμ#11	-	+	+	wk	-
Eμ#12	-	+	mixed	-	-
Eμ#13	-	+	-	-	-
Eμ#14	-	+	-	-	-
Eμ#15	-	wk	+	-	-
Eμ#16	-	+	+	+	-
Eμ#17	-	+	-	-	-
Eμ#18	-	+	-	-	-
Eμ#19	-	+	-	-	-
Eμ#20	-	+	+	+	-

Cells from the spleen, ILN and thymus of Eμ-myc mice were stained with PE-CD19 and a variety of FITC-conjugated antibodies and analysed by flow cytometry. Results for each tissue were equivalent. *ND: not determined; -: negative for Ag expression; +: positive for Ag expression; wk: weak expression.

Table 3.6. Summary of Eμ-myc/CD32$^{-/-}$ primary lymphoma phenotypes

1° lymphoma	CD3	CD19	IgM	IgD	IgG	CD32
Eμ32#1	-	+	wk	-	-	-
Eμ32#2	-	+	+	wk	+	-
Eμ32#3	-	+	+	-	-	-
Eμ32#4	-	+	+	-	-	-
Eμ32#5	-	+	-	-	-	-
Eμ32#6	-	+	-	-	+	-
Eμ32#7	-	+	+	-	+	-
Eμ32#8	-	+	wk	-	+	-
Eμ32#9	-	-	wk	-	-	-
Eμ32#10	ND*					
Eμ32#11	ND*					
Eμ32#12	ND*					
Eμ32#13	ND*					
Eμ32#14	ND*					
Eμ32#15	ND*					
Eμ32#16	ND*					

Cells from the spleen, ILN and thymus of Eμ-myc/CD32$^{-/}$ mice were stain and analysed by FACS using direct immunofluorescence with PE-CD19 and the above relevant FITC conjugated antibody. *ND: not determined; -: negative for Ag expression; +: positive for Ag expression; wk: weak expression.

3.4.2. Tumour transplantation into WT C57BL/6 mice.

A key feature of a tumour is its ability to infiltrate and establish itself *in vivo* in a congenic recipient mouse. Therefore, 1 x 10^6 primary tumour cells were injected i.v. into WT C57BL/6 mice to establish if the tumours were transplantable. The cells taken from the mice after tumour transplantation were denoted T1 tumours. It was shown that in 93.3% of cases the Eμ-myc lymphomas were transplantable, taking a mean period of 21 days to present where the range is 15 to 28 days (Table 3.7). This is with the exception of Eμ#1, where the mouse died prior to tumour development and Eμ#2 which failed to grow in the WT mice. The Eμ#2 tumour cells were CD19 negative and the physical presentation upon dissection was not in keeping with other tumour observations. Based on this we assume that the mouse did not die due to tumour development. In contrast, the Eμ-myc/CD32$^{-/-}$ tumours did not transplant as successfully. The tumours that did not transplant were still likely to be tumours as they initially presented with enlarged spleen, lymph nodes and on

one case with an enlarged thymus. As such, 37.5 % (3 of 9) of the tumours transplanted failed to grow in the WT recipients. However, of the tumours that did transplant on average these presented in 26 days, with a range of 16 to 46 days (Table 3.7).

Table 3.7. Tumour transplantability of primary tumours from Eμ-myc and Eμ-myc/CD32$^{-/-}$ mice.

1˚ Lymphoma (Eμ-myc)	Days to T1 presentation
Eμ#1	ND*
Eμ#2	NG**
Eμ#3	21
Eμ#4	20
Eμ#5	28
Eμ#6	21
Eμ#7	20
Eμ#8	19
Eμ#9	15
Eμ#10	19
Eμ#11	21
Eμ#12	19
Eμ#13	25
Eμ#14	16
Eμ#15	24
Eμ#16	13
Eμ#17	ND*
Eμ#18	ND*
Eμ#19	ND*
Eμ#20	ND*

1˚ Lymphoma (Eμ-myc/CD32$^{-/-}$)	Days to T1 presentation
Eμ32#1	NG**
Eμ32#2	36
Eμ32#3	46
Eμ32#4	21
Eμ32#5	16
Eμ32#6	17
Eμ32#7	18
Eμ32#8	NG**
Eμ32#9	NG**
Eμ32#10	ND*
Eμ32#11	ND*
Eμ32#12	ND*
Eμ32#13	ND*
Eμ32#14	ND*
Eμ32#15	ND*
Eμ32#16	ND*

$1x10^6$ primary lymphoma cells were injected intravenously into WT C57BL/6 mice and the time to T1 tumour presentation was noted. On average the Eμ-myc tumours presented within 21 days, whilst the Eμ-myc/CD32$^{-/-}$ tumours presented within 26 days. This difference is not significant, $p = 0.1357$(by Student's t-test). When comparing the percentage of tumours that were not transplantable, only 6.7 % of the Eμ-myc tumour did not transplant, compared with 33.3 % of the Eμ-myc/CD32$^{-/-}$ that were not transplantable. *ND: not determined (tumour not passaged); **NG: did not *in vivo* growth.

3.5. Eμ-myc and Eμ-myc/CD32$^{-/-}$ cell line characterisation

3.5.1. Eμ-myc and Eμ-myc/CD32$^{-/-}$ cell line growth

Cells taken from the primary tumour suspensions were cultured at 37 ˚C, 10 % CO_2 in order to grow a primary tumour cell line. This process was highly successful for the Eμ-myc lymphomas where 88.9 % (16 out of 18) primary lymphomas were established as

lymphoma cell lines. This excludes Eμ#1 and Eμ#2 that were not transplantable so considered not to be tumours populations. This process appeared to be less successful for the Eμ-myc/CD32$^{-/-}$ lymphomas, where only 66.7 % (seven of the nine) of the primary lymphomas were established as primary cell lines *in vitro*. Eμ32#2 and Eμ32#9 did not grow in culture, but Eμ32#2 was transplantable into C57BL/6 mice. Of the tumours that grew as cell lines, only five were transplantable in WT C57BL/6 mice and as such formally confirmed to be tumours (Eμ32# 3, 4, 5, 6, 7). In contrast, Eμ32#1 and Eμ32#8 did not grow *in vivo*, but were established as primary cell lines. There is a caveat here however, in that contamination of the C57BL/6 genetic background in the Eμ-myc/CD32$^{-/-}$ mice could lead to tumour rejection after cells were transplanted to C57BL/6 mice, rather than the inability of the tumour cells to grow *in vivo*. Table 3.8 is a summary of the *in vitro* and *in vivo* growth of the Eμ-myc/CD32$^{-/-}$ tumours. However, despite the data presented here that suggests a difference in the behaviour of CD32 postive and CD32 negative tumours, due to the limited number of Eμ-myc/CD32$^{-/-}$ tumours analysed in comparison to the Eμ-myc tumours it is difficult to show statistical significant between the two mouse strains, therefore we suggest that growth was similar between tumours from both mouse strains.

Table 3.8. *In vitro* and *in vivo* growth of the Eμ-myc/CD32$^{-/-}$ primary lymphomas.

Eμ-myc/CD32 $^{-/-}$ tumour	***In vitro* growth (cell line)**	***In vivo* growth (transplantable)**
Eμ32#1	G*	NG**
Eμ32#2	NG**	G*
Eμ32#3	G*	G*
Eμ32#4	G*	G*
Eμ32#5	G*	G*
Eμ32#6	G*	G*
Eμ32#7	G*	G*
Eμ32#8	G*	NG**
Eμ32#9	NG**	NG**

In vitro growth refers to ability of primary tumour to become established as a cell line. In vivo growth refers to transplantability and growth of tumour in WT C57BL/6 mice. *G: growth; **NG: no growth.

3.5.2. Changes in IgM expression as cells adapt to culture.

In some instances we observed a change in cell immunophenotype, particularly with regards to IgM expression during extensive culture *in vitro*. An example of this is Eμ#6,

where the primary tumour showed a mixed IgM population (Figure 3.9a), but over a period of several weeks not only did the percentage of IgM positive cells increase, but the MFI relating to IgM also increased. This suggested that the IgM positive cells were expressing higher levels of IgM (Figure 3.9b). However when the IgM positive and IgM negative populations of Eμ#6 were sorted by flow cytometry it could be demonstrated that the IgM negative sort gained an IgM positive phenotype over time (Figure 3.9c). This is true of a second cell line Eμ#7, which also started as an IgM mixed primary lymphoma (Figure 3.10a) which over a period of several weeks became almost entirely IgM positive (Figure 3.10b). The cell line generated from Eμ#7 was also sorted using the same gates as the Eμ#6 IgM negative population, but within two weeks of sorting the cells had reverted to the pre-sort phenotype (Figure 3.10c), suggesting either that the cells are undergoing maturation *in vitro*, or that IgM expression provided an selective advantage for *in vitro* growth. However, these experiments do not indicated whether the IgM positive populations predominate due to increased proliferation or selective pressure.

3.5.3. Response of Eμ-myc cell-lines to etoposide or BCR stimulation

If cell line growth was successful, the response to the DNA damaging drug etoposide and anti-BCR mAb was analysed. These analyses were performed with the intention of using the cells at a later date to assess the role of the Bcl-2 family of proteins in BCR and chemotherapy induced apoptosis. Cytotoxic drugs, such as etoposide induce DNA damage that, alongside inducing apoptosis, can lead to a reduction in cell proliferation through the induction of tumour suppressor molecules such as p53. Where there is a lack of response to DNA damage, i.e. low levels of cell death after etoposide treatment, this can, in many cases, be indicative of p53 mutation[395].

To test for induction of cell death in response to etoposide and BCR stimulation, cells were incubated with etoposide at 0.04, 0.2 or 1 μM in 200 μl for 6 hr or with anti-IgM polyclonal goat anti-mouse μ chain specific antibody (gαm) at 0.5, 2.5 or 12.5 μg/ml for 24 hr. Cells were then incubated with AnV/PI before being analysed by flow cytometry. Cells that responded to etoposide treatment, i.e. there was an increase in cell death at 6 hr were considered to be able to respond to DNA damage (typical plot shown in Figure 3.11c – Eμ#3 T1). Cells that did not respond to DNA damage at 6 hr were considered to be resistant to DNA damage, likely due to p53 mutation (typical plot shown in Figure 3.11c – Eμ#4). Cells that showed increased PCD (greater that 20 % relative cell death) at 24 hr were considered responsive to anti-BCR induced cell death (typical plot shown in Figure 3.11d – Eμ#4), whilst cells that did not show increased PCD at 24 hr were considered

unresponsive to anti-BCR stimulation (typical plot shown in Figure 3.11d – Eμ#3 T1). The cell death observed in both response to etoposide or anti-BCR was dose dependent, with increasing dose of either reagent causing increased cell death.

This analysis established the proportion of tumours which were responsive to DNA damage by etoposide and responsive to anti-BCR treatment. Of the 13 established Eμ-myc cell lines tested, seven (53.8 %) were responsive to DNA damage and eight were responsive to anti-BCR stimulation (53.3 %) (Table 3.10). The same analysis was performed on the Eμ-myc/CD32$^{-/-}$ cell lines. Of the six established cell lines tested, three (50 %) were unresponsive to DNA damage and only one cell line (20 %) was responsive to anti-BCR stimulation (Table 3.11). It was surprising that the Eμ-myc/CD32$^{-/-}$ cell lines did not respond to anti-IgM stimulation as the majority of the primary lymphomas expressed IgM and IgM expression in the Eμ-myc cell lines indicated response to anti-IgM stimulation (Tables 3.10 & 3.11). It is important to note that established cell lines, such as the murine πBCL$_1$ or human Raji cells tend to have around 5 – 10 % background cell death. The Eμ-myc cell lines in contrast have a high level of background cell death and this is reflected in the results being calculated as difference to control or background death, calculated by % relative cell death = ((% T - % NT) / (100 - % NT))*100. where, % NT: % AnV/PI positive cell without treatment, and % T: % AnV/PI positive cell after treatment. Table 3.9 summarises the percentage responsiveness of both the Eμ-myc and the Eμ-myc/CD32$^{-/-}$ cell lines to DNA damage and BCR stimulation.

Table 3.9. Percentage responsiveness of the Eμ-myc and Eμ-myc/CD32$^{-/-}$ population to DNA damge and BCR stimulation.

Response to	Eμ-myc (% response)	Eμ-myc/CD32$^{-/-}$ (% response)
DNA damage	53.8	50
BCR stimulation	53.3	20

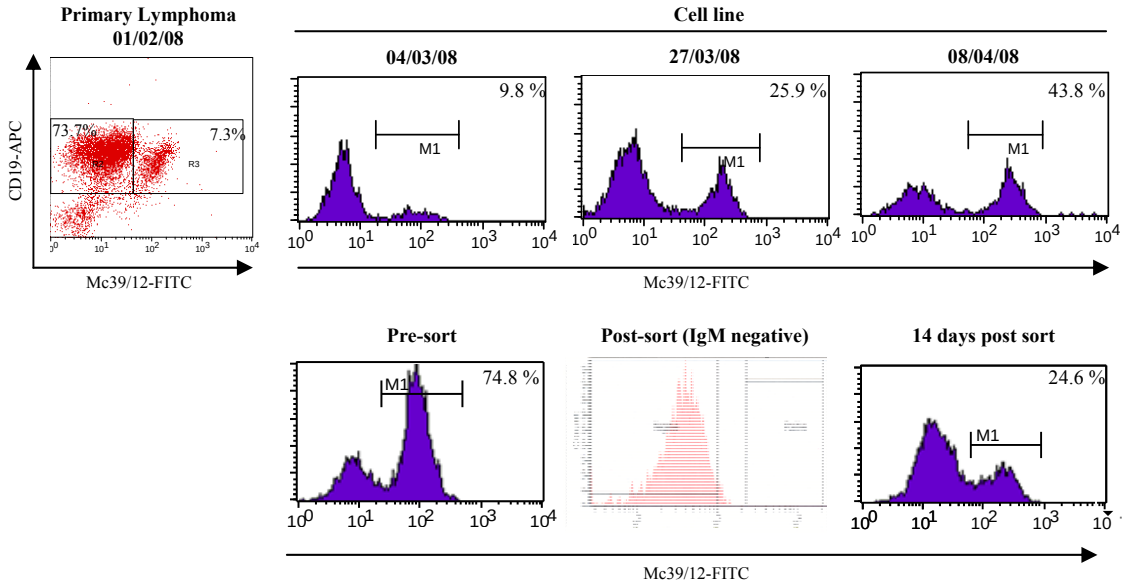

Figure 3.9. Changes in IgM expression of Eμ#6 primary lymphoma cell lines adapting to culture.
As the Eμ-myc primary tumours adapted to cell culture the phenotype of the cells was monitored over time by flow cytometry (Material and Methods 2.11). It was observed that IgM expression, as shown my staining with Mc39/12-FITC (IgM), of Eμ#6 primary lymphoma was heterogeneous, with IgM positive cells becoming the dominant phenotype as the cells adapted to culture (top panels). When the IgM negative population was sorted by flow cytometry and cultured a proportion of these cells gained an IgM positive phenotype (bottom panels).

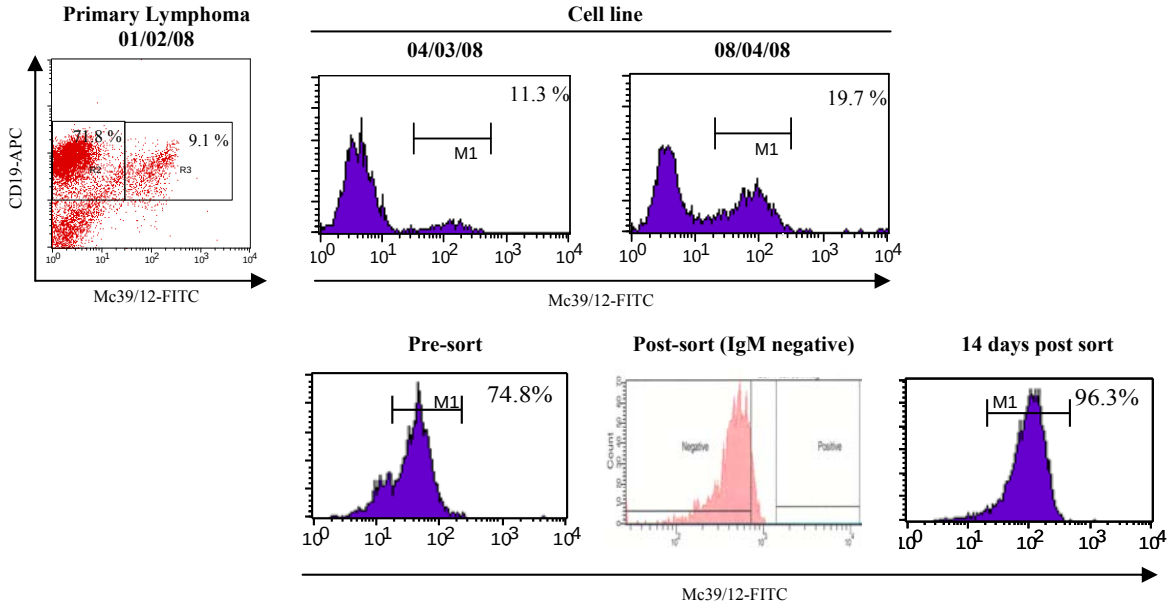

Figure 3.10. Changes in IgM expression of Eμ#7 primary lymphoma cell lines adapting to culture.
As the Eμ-myc primary tumours adapted to cell culture the phenotype of the cells was monitored over time by flow cytometry (Material and Methods 2.11). It was observed that IgM expression, as shown my staining with Mc39/12-FITC (IgM), of Eμ#7 primary lymphoma was again heterogeneous, with the percentage of IgM positive cells increasing as the cells adapted to culture (top panels). When the IgM negative population was sorted by flow cytometry and cultured as above, these cells reverted to an IgM positive phenotype (bottom panels). In fact even more of the cells are IgM positive that in the pre-sort population.

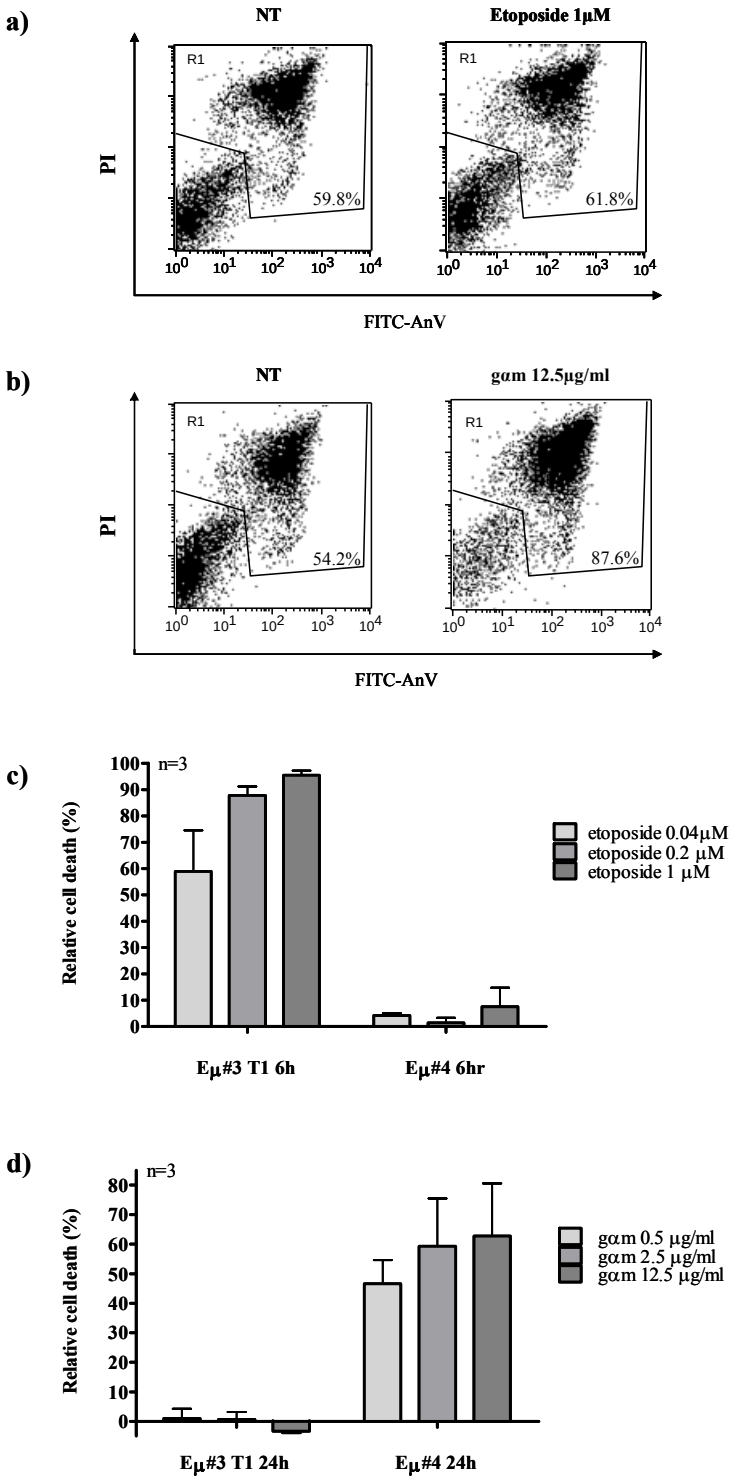

Figure 3.11. Response to anti-BCR and etoposide treatment.
Cells were treated for 6 hr and 24 hr with the DNA damaging drug etoposide at 0.04, 0.2 or 4 µM or with anti-IgM polyclonal goat anti-mouse µ chain specific antibody at 0.5, 2.5 or 12.5 µg/ml. Percentage relative cell death was calculated as detailed above, where % death refers to the percentage of cells that were AnV/PI positive compared to control (R1). This analysis shows the response to DNA damage (6 hr) (a - Eµ#4, left, NT; right, 1 µM etoposide treatment at 6 hr) and response to BCR stimulation (24 hr) (b - Eµ#4, left, NT; right, 12.5 µg/ml gαm at 24 hr). The representative Eµ-myc cell lines show response to DNA damage/etoposide at 6 hr by induction of PCD (Eµ#3 T1) and an unresponsive cell line (Eµ#4) (c). Response to anti-IgM at 24 hr indicates an IgM responsive cell line (Eµ#4), whilst a lack of cell death at 24 hr indicates an IgM unresponsive cell line (Eµ#3 T1) (d). Error expressed as standard error of mean (SEM), where n = 3 for each LCL.

Table 3.10. Summary of Eμ-myc lymphoma cell line characteristics.

Cell Line	IgM expression	% PCD by anti-IgM (whole IgG)	PCD by etoposide@6 hr	CD32 expression
Eμ#1		ND*		
Eμ#2		ND*		
Eμ#3	-	10.89	Y	n/a
Eμ#4	+	7.89	N	30.96
Eμ#5		ND*		
Eμ#6	mixed	32.54	N	45.49
Eμ#7	+	13.87	Y	49.63
Eμ#8	+	45.92	N	39.05
Eμ#9	-	4.64	Y	39.29
Eμ#10	+	ND*	N	36.81
Eμ#11	+	41.65	N	67.91
Eμ#12	-	-1.89	Y	30.14
Eμ#13	+	71.27	Y	60.58
Eμ#14	-	3.03	Y	48.75
Eμ#15	+	61.14	N	28.47
Eμ#16	+	74.90	Y	27.62
Eμ#17		ND*		
Eμ#18	-	17.39	ND*	14.25
Eμ#19	+	42.38	ND*	28.12
Eμ#20	ND*	59.86	ND*	ND*

IgM surface expression was determined by flow cytometry using direct immunofluorescence as outlined in Material and Methods section 2.11. The % PCD by anti-IgM was the relative cell death of the particular cell line after 24 hr incubation with at 12.5 μg/ml anti-BCR (polyclonal goat anti-mouse (gαm)). PCD by etoposide was determined as an increase in relative cell death in response to stimulation with 1 μM etoposide for 6 hr in comparison to the control; this established if the cell line was responsive to DNA damage, denoted Y (yes) or N (no). *ND: no data due to cell lines not growing in culture or experiments not being completed. These data represent results from three experimental repeats.

Table 3.11. Summary of Eμ-myc/CD32$^{-/-}$ lymphoma cell line characteristics.

Cell Line	IgM expression (MFI)	% PCD by IgM (IgG)	% PCD by IgM (F(ab')$_2$)	PCD by etoposide@6h
Eμ32#1	10.81	14.44	8.06	Y
Eμ32#2		ND*		
Eμ32#3	222.67	55.38	-22.14	Y
Eμ32#4	23.11	-2.00	-3.50	N
Eμ32#5	17.88	-20.07	-20.87	N
Eμ32#6	8.74	-3.39	-3.74	N
Eμ32#7	90.91	-8.72	-7.43	N
Eμ32#8	8.71	-12.60	-13.70	N
Eμ32#9		ND*		

IgM surface expression was determined by flow cytometry using direct immunofluorescence as outlined in Material and Methods section 2.11. The % PCD by anti-IgM was the relative cell death of the particular cell line after 24 hr incubation with at 12.5 μg/ml anti-BCR (polyclonal goat anti-mouse (gαm)) either whole IgG or F(ab')$_2$ fragment. PCD by etoposide was determined as an increase in relative cell death in response to stimulation with 1 μM etoposide for 6 hr in comparison to the control; this established if the cell line was responsive to DNA damage, denoted Y (yes) or N (no). *ND; no data due to cell lines not growing in culture or experiments not being completed. These data represent results from three experimental repeats.

3.6. Chapter Discussion

Here, we generated a range of primary lymphomas using the Eμ-myc mouse model. Our observations of tumour presentation in the Eμ-myc primary tumours are consistent with previously published reports[375]. Alongside generating primary tumours from WT Eμ-myc mice we have also produced a range of IgM positive and IgM negative cell lines that will be of use in characterising *in vitro* biochemical events in subsequent chapters. In addition, we also generated primary lymphomas and associated cell lines which lack CD32 which can be used to assess the importance of this molecule in normal B cell and lymphoma biology.

It seemed that CD32 expression has no significant effect on the survival rate with regards to lymphoma development in the Eμ-myc mice. Nevertheless, there is a trend towards a slower rate of tumour presentation in the Eμ-myc/CD32$^{-/-}$ (Figure 3.1), supporting previous reports that CD32 expression increased tumourigenicity[353,344]. On the other hand, it was interesting that the Eμ-myc/CD32$^{-/-}$ mice were not further protected from tumour development, since CD32 expression is thought to lend itself towards increased tumourgenecity, surely a CD32$^{-/-}$ tumour would be less aggressive, take longer to develop and thus the mice survive longer before tumour development. Alongside this, CD32$^{-/-}$

mice that lack the inhibitory FcγR will potentially have a more potent activatory FcγR-dependent anti-tumour response (see introduction section 1.3.3), implying that the Eμ-myc/CD32$^{-/-}$ mice are more likely to have heightened defenses against tumour cells and again it would be expected that Eμ-myc mice lacking CD32 would have increased survival in comparison to their WT counterparts. In our hands however this does not seem to be the case, implying that CD32 expression by both tumour and endogenous tissues had limited effect of tumour cell growth, despite reports to the contrary[353,344]. The notion that CD32 expression increases tumourigenicity was however supported by the reduced transplantabilty of the CD32$^{-/-}$ primary lymphoma cells in comparison with the CD32 positive, or WT tumours (Table 3.7). However, it is equally likely that the Eμ-myc/CD32$^{-/-}$ tumours were rejected upon transplantation due to the initiation of an immune response towards the genetically mis-matched tumour cells; i.e. the Eμ-myc/CD32$^{-/-}$ tumours were raised in mice with a mixed C57BL/6 and C57BL/KA background, but tumours were transferred into C57BL/6 mice.

Alongside the observed trend towards slower tumour development in the Eμ-myc/CD32$^{-/-}$, tumour presentation differed between the Eμ-myc and Eμ-myc/CD32$^{-/-}$ mice. As aforementioned, tumour cells accumulated in lymphoid organs, such as the spleen and LN (Figure 3.2). In the Eμ-myc and Eμ-myc/CD32$^{-/-}$ mice this accumulation of tumour cells, as determined by examination of the size and weight of several lymphoid organs, was comparable, with the exception of ILN (Figure 3.3, Table 3.2 & 3.3). This suggests that the pathogenesis of lymphoma in both the Eμ-myc and Eμ-myc/CD32$^{-/-}$ mice was similar. In contrast however, histological examination of the lymphoid organs suggested a less aggressive disease in the Eμ-myc/CD32$^{-/-}$ mice in comparison with the Eμ-myc mice, as demonstrated by complete obliteration of normal lymphoid architecture in the tissues of the Eμ-myc but not the Eμ-myc/CD32$^{-/-}$ mouse (Figure 3.4 & 3.6). This suggests that although lack of CD32 expression did not seem to influence mouse survival, it did seem to alter disease presentation.

In addition, although it was not formally quantified in the Eμ-myc/CD32$^{-/-}$ due to reasons previously described, there seemed to be less tumour infiltration in non-lymphoid tissues in the Eμ-myc/CD32$^{-/-}$ mice in comparison to the Eμ-myc mice (Figure 3.5 and Table 3.4), suggesting that CD32 positive tumours were more aggressive and as a result more likely to become metastatic. This is supported by reports in the literature that demonstrate CD32 expression on metastatic cells from solid tumours, such as melanoma [344,347,348] and suggests this may also hold true for lymphoma cells. In addition CD32 expression has been

demonstrated to be increased on both haematological and non-haematological tumour cells in comparison to normal cells of the same origin[350,356,396]. It can therefore be postulated that due to its high expression on a range of tumour types and on progressive, metastasised disease that CD32 would make a good therapeutic target.

The observation that the CD32$^{-/-}$ tumours did not transplant as well as the Eμ-myc tumours was initially unsurprising as it has been reported that CD32 expression can enhance tumourgenicity[344,353]. This suggests that without CD32 expression these tumours are likely be less tumourgenic and as such will not establish themselves *in vivo* as efficiently. However, it was later discovered that the C57BL/6 genetic background of the Eμ-myc/CD32$^{-/-}$ had been contaminated with the C57BL/Ka genetic background and therefore was more likely the reason for tumour rejection of the Eμ32 tumours upon transplantation. As a result of contamination of the genetic background of the Eμ-myc/CD32$^{-/-}$ mice, it was decided not to continue with the in-depth characterisation of the Eμ-myc/CD32$^{-/-}$ tumours as was performed with the Eμ-myc tumours. However, Kaplein Meier survival and primary tumour presentation of the Eμ-myc/CD32$^{-/-}$ mice and tumours, respectively, was still assessed. It was later decided, that it would be fortuitous to perform retrospective phenotyping of the Eμ-myc/CD32$^{-/-}$ in order to determine maturation status of the CD32 deficient B cell tumours and transplantability studies to determine how CD32 deficiency would affect tumour aggression. Unfortunately however, this could not be performed as samples were lost through freezer malfunction.

During the development of this panel of primary lymphomas and their associated established cell lines we identified differences between the tumours from the two different mouse strains (WT and CD32-/- Eμ-myc mice). Most striking was the difference in immunoglobulin (Ig) expression at the cell surface (Table 3.5 & 3.6, Eμ-myc and Eμ-myc/CD32$^{-/-}$, respectively). In general, the CD32$^{-/-}$ tumours showed a greater incidence of surface Ig (sIg) expression. It has been reported that the tumours arising from the WT Eμ-myc transgenic mice are a mixture of pre-B cells, immature and mature B cells [375] and we observed an approximate 50:50 split of sIg positive and negative tumours in our cohort. However, more of the CD32$^{-/-}$ tumours express IgM at the cell surface, as well as IgD and IgG. This suggests that the tumours arising in the CD32$^{-/-}$ mice may have a more mature, even class switched phenotype compared to the CD32 expressing tumours. It is interesting that our population of CD32$^{-/-}$ Eμ-myc tumours have a tendency to have a more mature phenotype as it has been previously reported that the c-myc transgene in this model drives proliferation rather than maturation of cells[380].

However, as CD32 expression may be a contributing factor in apoptotic control of clonal B-cell populations [272], a lack of CD32 may allow a greater proportion of mature B cells to survive *in vivo,* thereby providing a larger pool of cells available for accumulating additional oncogenic mutations. This idea is supported by data shown in this chapter that illustrates that the Eμ-myc/CD32$^{-/-}$ tumours are less susceptible to anti-BCR (IgG) induced apoptosis than the Eμ-myc tumours (Table 3.8 & 3.9, Eμ-myc and Eμ-myc/CD32$^{-/-}$, respectively). Interestingly, the IgM positive CD32$^{-/-}$ tumours did not frequently respond to anti-IgM stimulation once they had become established as cell lines, possibly due to their more mature class switched phenotype. A minority of IgM positive WT Eμ-myc tumours, such as Eμ#4, also did not undergo apoptosis following stimulation with anti-BCR mAb despite retaining IgM expression. The reasons for this are uncertain but may reflect cell anergy, gained *in vivo* or an adaptation of the cell line to *in vitro* culture.

Although most cell-lines retained the same phenotype as their parent lymphoma, on two occasions differences were observed, such as in the case with Eμ#6 and Eμ#7 which showed altered IgM expression whilst adapting to culture (Figure 3.9 and 3.10, respectively). However it has not been established whether this is due to maturation of the lymphoma cells *in vitro* or whether IgM provides a selective advantage for the cells. There is evidence that suggests the IgM expression is vital for continued survival of B cells *in vivo* [397,398,399] and as such IgM positive cells may be preferentially selected due to their IgM status. Despite this, a potential reason why the cells no longer respond to anti-IgM stimulation may be that they are continuing to mature and differentiate *ex vivo* to a more mature B cell non-responsive phenotype. In addition, it would seem that in our hands, CD32 may also be important to cell adaptation in culture, as we have observed that the WT Eμ-myc tumours adapted more readily to cell culture than those lacking CD32. Contrary to this however, it has been reported that cells cultured *in vitro* may lose CD32 expression[396] and in addition, it has been shown that both CD32 positive and CD32 negative tumours display similar levels of *in vitro* proliferation[352].

In keeping with prior reports[400] we observed that a proportion of our Eμ-Myc tumours had defects in their DNA damage response likely due to p53 mutations, although this was greater that previously described (42.6% compared with the previously reported 28%). The proportion of possible p53 mutant cell lines was also greater than that observed in general haematological malignancies[401]. Despite this, the incidence of DNA damage defects was similar in both the WT Eμ-myc and Eμ-myc/CD32$^{-/-}$ populations, 42.6% and 50% respectively (Table 3.8 and 3.9 for Eμ-myc and Eμ-myc/CD32$^{-/-}$, respectively).

We next move on to using the Eμ-myc tumours and cells to characterise a panel of unique murine anti-CD32 mAb.

CHAPTER 4 *In vitro* analysis of anti-CD32 mAb on lymphoma cells

4.1. Chapter Introduction.

In recent years the FcγR have been highlighted as important modulatory component of the immune system through engagement with mAb. It has been demonstrated that FcγR expression can regulate anti-tumour immune responses; moreover, deficiency in the inhibitory FcγR, CD32, has been shown to enhance tumour immunotherapy[83,369]. In contrast, the activatory FcγR, in particular FcγRIIIa in humans, have been shown to be essential in order to mount effective anti-tumour responses with therapeutic mAb through the induction of ADCC[83,402-404].

In order to boost ADCC in response to mAb therapy one approach that has been taken is to enhance interaction with activatory FcγR and reduce interaction with inhibitory FcγR (CD32) through glycoengineering or mutagenesis[372]. An alternative approach that could be taken involves directly blocking CD32 inhibitory function on effector cells[370]. Unfortunately, suitable reagents capable of specifically and exclusively binding mouse CD32 have been lacking. A widely used and available reagent, 2.4G2 was identified in the late 1970s as binding to FcγR on leukocytes, but has since been show to have specificity to both murine CD32 and FcγRIII[405]. Other anti-CD32 reagents have been used in xenograft models of cancer, but have been plagued by problems associated with such models as previously described (Chapter 3.1). Therefore we generated a panel of mAb which are highly specific for murine CD32 that do not cross-react with any other FcγR, allowing us to study how CD32 might be manipulated *in vivo*, with an aim to improve current immunotherapeutic strategies used for the treatment of lymphoma.

In this chapter we characterise these reagents with respects to their binding properties, ability to activate or block the receptor and assess their downstream consequences on B-cell biology.

4.2. Generation of anti-CD32 mAb.

A panel of anti-CD32 mAb were raised by Miss Alison Tutt (University of Southampton) using a mouse CD32-rat CD4 (domain 3/4) fusion protein designed and produced in 293F cells by Dr Claude Chan (University of Southampton). The CD32-CD4 fusion protein was

purified using affinity chromatography with a Sepharose 4B-anti-rat CD4 column. Immunisation was achieved using an established protocol[376]. Briefly, BALB/c $CD32^{-/-}$ mice were immunised with a dose of approximately 10 to 20 μg of the purified fusion protein in complete Freund's Adjuvant (Difco, Detroit, MI) at two sites subcutaneously. After 14 days the immunisation was repeated and a final booster of the CD32-CD4 fusion protein was injected i.v. in PBS. Spleens from the immunised mouse were fused with NS-1 myeloma cells three days after the final protein boost. Resultant colonies were screened 11 days later by ELISA against CD32, CD16 and CD64 fusion proteins. Colonies that gave a positive result against just CD32 but not CD16 and CD64 were screened against πBCL_1 cells using indirect flow cytometry analysis. Positive colonies were then cloned twice, expanded in culture and IgG purified either on Protein A or using ion exchange chromatography.

An additional anti-CD32 mAb was generated by Dr Claude Chan by molecular manipulation of the Fc domain of AT128 to create an IgG2a version of this antibody. AT128 m2a was produced as it has been shown that IgG2a mAb give better therapeutic responses *in vivo* in terms of enhanced ADCC due to a higher A/I ratio, as described by Nimmerjahn & Ravetch (2005)[166]. In addition, AT130-2 was the only IgG2a mAb generated and thus AT128 m2a acts as an isotype comparison for its activity.

4.2.1. anti-CD32 mAb binding specificity and affinity.

To confirm their specificity, the anti-CD32 mAb were first assessed for binding to WT, $CD16^{-/-}$ and $CD32^{-/-}$ CD19 positive splenocytes by flow cytometry (Figure 4.1). As expected, the anti-CD32 mAb generated in-house showed specific binding to WT and $CD16^{-/-}$ cells that express CD32, but not to $CD32^{-/-}$ cells. This is with the exception of 2.4G2, a commercially available antibody, which retained binding to both $CD32^{-/-}$ and $CD16^{-/-}$ cells in keeping with its published ability to bind both CD32 and FcγRIII[405].

It can also be observed from Figure 4.1 that although AT128 displays binding to CD32, it was at a lower level than AT130-2 and AT130-5, as demonstrated by its lower fluorescence. In order to directly compare the binding of the different anti-CD32 mAb, CD32 positive Eμ-myc cell lines were incubated with the panel of FITC-conjugated $F(ab')_2$ fragments of the anti-CD32 mAb and analysed by flow cytometry. By using $F(ab')_2$ fragments binding by the Fc portion of the antibody to CD32 is avoided. It is shown that the binding hierarchy of the anti-CD32 mAb is, 2.4G2>AT130-2>AT130-5>AT128 (Figure 4.2).

Furthermore, and to assess if the binding differences observed were due to differences in binding affinities of the anti-CD32 mAb, the K_a and K_d of the mAb were analysed using surface plasmon resonance techniques using a BIAcore T100. Two approaches were taken in order to assess the anti-CD32 mAb using the BIAcore T100. The first involved amine coupling of OX68, an anti-CD4 mAb, to the surface of a sensor chip. To this a CD4-CD32 fusion protein (ligand) was bound. Each mAb (analyte) was then run over the coated chip dynamically and binding was assessed by plasmon surface resonance[406] (Figure 4.3a – Method 1). However, due to the potential tri-meric nature of the interactions with CD32, via both Fv and Fc regions of the mAb, it was difficult to obtain an exact affinity, particularly as the binding of the anti-CD32 mAb did not fit the 1:1 mathematical binding algorithm. Figure 4.3c shows AT130-2 IgG as an example of the sensorgrams obtained from the BIAcore using this first method (affinity data not shown).

Therefore, a second approach was taken to obtain more accurate affinity values. This second method involved amine coupling the anti-CD32 mAb directly to the sensor chip and then flowing commercially obtained CD32 fusion protein over the chip at various concentrations (Figure 4.3b). Figure 4.3d demonstrates example sensorgrams for AT130-2 IgG and $F(ab')_2$ fragments. This enabled a K_D to be established for each of the anti-CD32 mAb. Both the IgG and $F(ab')_2$ fragments of the anti-CD32 mAb were analysed in this way and Table 4.1 summarises the K_D of the anti-CD32 mAb, as determined by this second method of BIAcore analysis. Using the second method the binding of the anti-CD32 mAb to fusion protein was shown to fit the 1:1 mathematical binding model better. This suggests that the second method is mimicking 1:1 binding and therefore giving us greater confidence in the values of K_D obtained from these data. The K_D was calculated using using the BIAcore T100 Evaluation Software (Version 2.0.1). The BIAcore analysis was performed by Mr C. Ian Mockridge.

From the BIAcore analysis and determination of mAb affinity, we can again see a hierarchy of anti-CD32 mAb binding, where, 2.4G2>AT130-2>AT130-5>AT128. More accurately, by examining the K_D values, 2.4G2 has ten times higher affinity for the fusion protein than the in-house anti-CD32 mAb. AT130-2 and AT130-5 have a similar magnitude of affinity and these mAb have approximately six times higher affinity than AT128. Interestingly, the $F(ab')_2$ fragments of these mAb have lower affinity for the fusion protein than the IgG fragments, suggesting that Fc engagement plays a role in their binding to CD32.

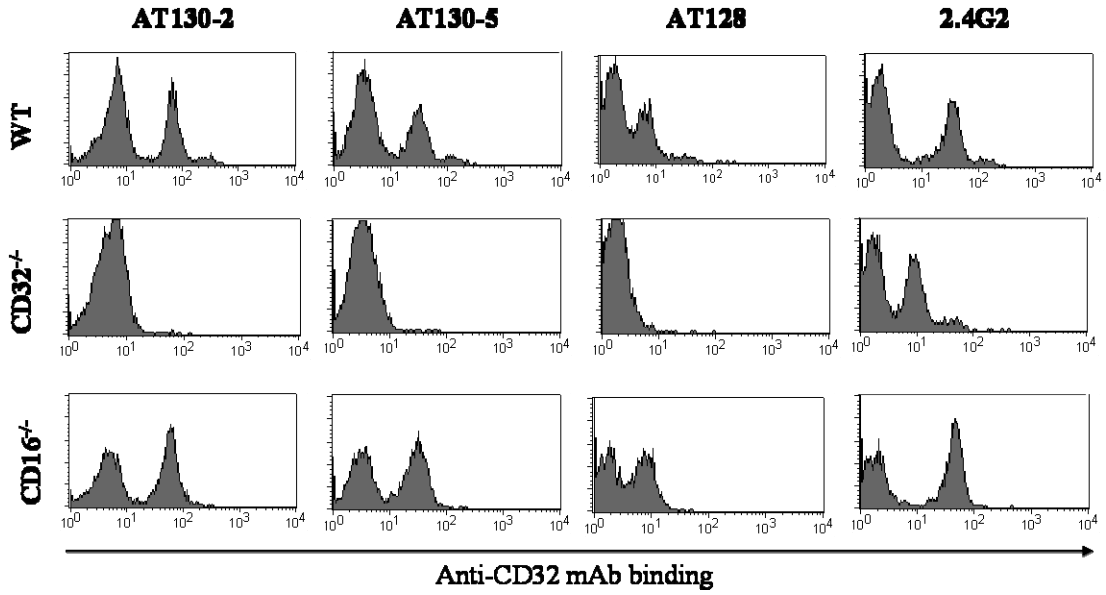

Figure 4.1, Binding profiles of anti-CD32 mAb against WT, CD32$^{-/-}$ and CD16$^{-/-}$ splenocytes.
Cells were incubated with 10 µg/ml FITC-conjugated antibodies for 30 min at 4°C and analysed by direct flow cytometry protocols. AT130-2, AT130-5 and AT128 show specific binding to WT and CD16$^{-/-}$, but not to CD32$^{-/-}$, as indicated by an increase in FL1-H MFI (anti-CD32 mAb binding).

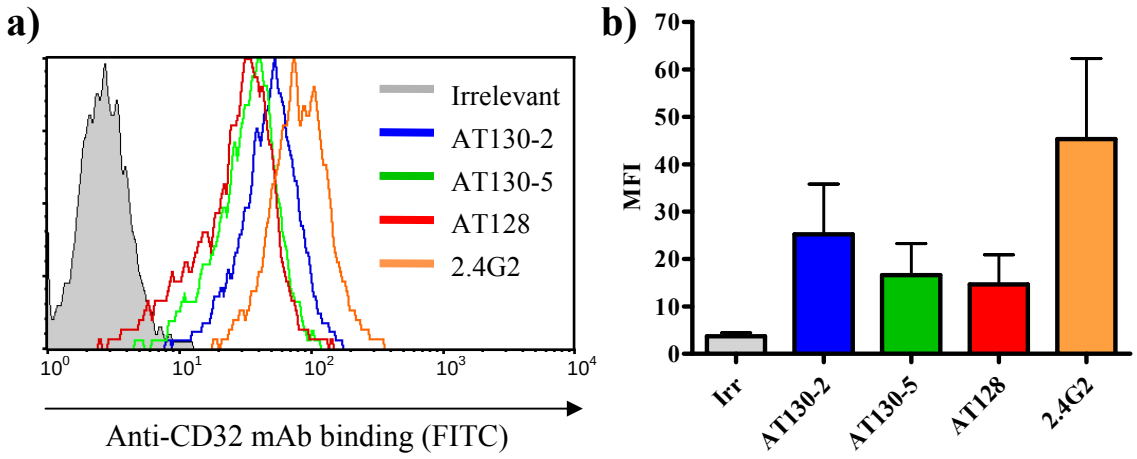

Figure 4.2. FITC-conjugated anti-CD32 mAb labelling of Eµ myc cell lines.
Cells were incubated with 10 µg/ml FITC-conjugated F(ab')$_2$ antibodies for 30 min at 4 °C and analysed by direct immunofluorescence protocol. As indicated by an increase in FL1-H MFI, the binding hierarchy is: 2.4G2>AT130-2>AT130-5>AT128. (a) is an example of the binding of the anti-CD32 mAb to Eµ#8, (b) represents the average binding of each anti-CD32 mAb to Eµ#6 to 9 and #11 to 14, error expressed as SD, where n = 3 for each cell line.

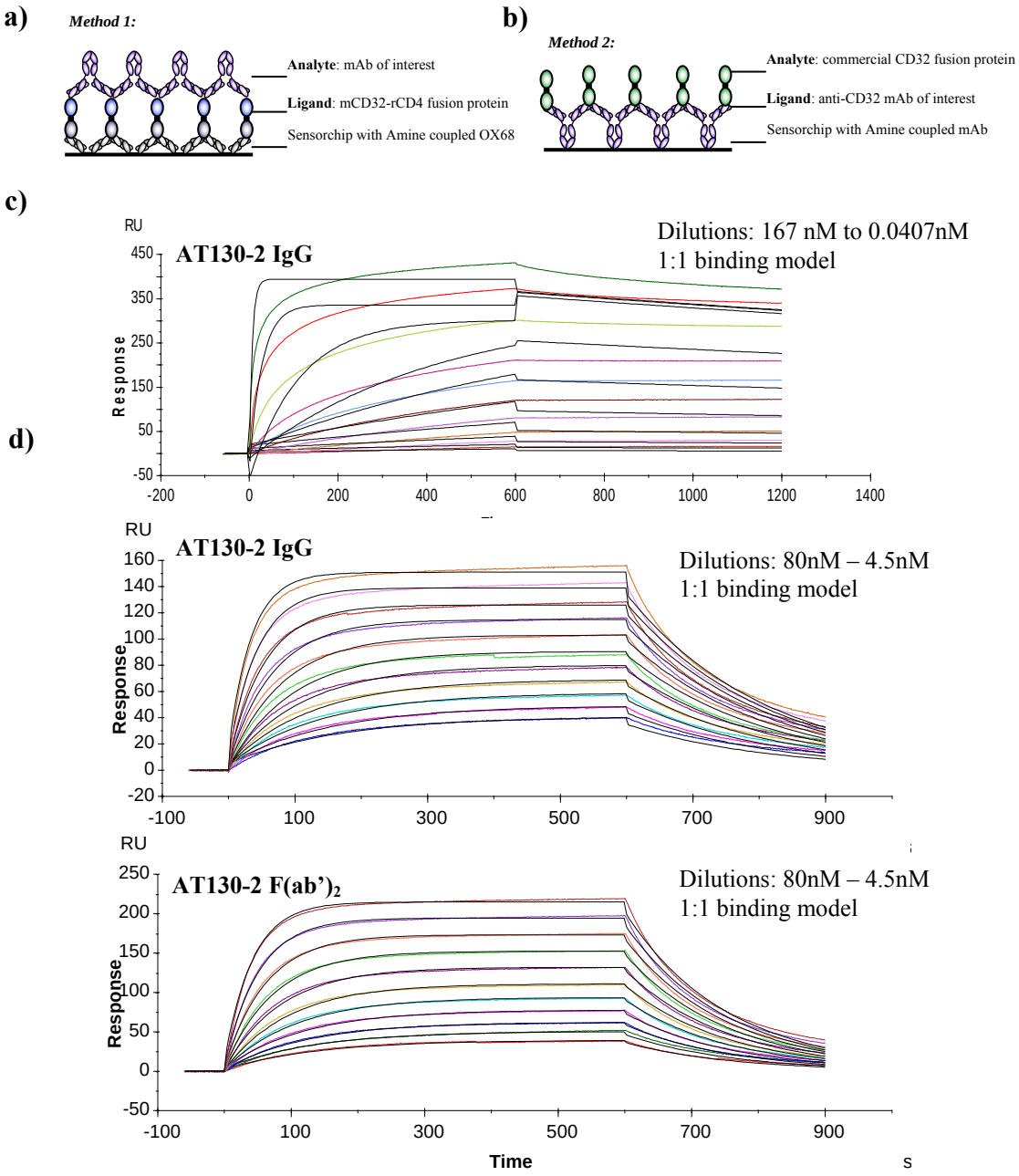

Figure 4.3. BIAcore analysis of anti-CD32 mAb.
The BIAcore system provides a unique method for analysing biospecific interactions in real time. Most commonly, the antigen of interest, in this case CD32 is immobilised onto the surface of a sensorchip by binding of fusion protein to OX68, that has been amine coupled to the sensorchip. Anti-CD32 mAb is then passed over the chip in a continuous flow and parameters of binding are determined by plasmon surface resonance (a). A second method was also used, where anti-CD32 mAb were amine coupled to the plate and a commercial CD32 fusion protein was passed over the chip at various concentrations (b). The data obtained is presented as a sensorgram (c & d). This is shown as the response units (RU) of binding over time at different concentrations of mAb (167nM to 0.0407nM) or fusion protein (from 80 nM to 4.5 nM), depending on the method. The shape of the sensorgram curve is compared alongside known binding models (1:1 binding for the anti-CD32 mAb, black lines on sensograms) and from a series of kinetic calculations the K_D can be derived and as such antibody and antigen interactions can be analysed[406]. Here, the sensograms of AT130-2 IgG are given as examples (c; using the first method & d; using the second method). Binding of AT130-2 $F(ab')_2$ fragment is also shown by the second method (d) It is clear from these graphs that the second method more closely represents the 1:1 binding model and as such more confidence is placed in the figures obtained (Table 4.1).

Table 4.1. Isotype and affinity of the anti-CD32 mAb.

Antibody	Isotype	K_D (M)
AT130-2	IgG2a	1.8×10^{-8}
AT130-5	IgG1	1.3×10^{-8}
AT128	IgG1	1.4×10^{-7}
2.4G2	Rat IgG1	8.7×10^{-11}
AT128 m2a	IgG2a	Not tested
AT130-2 $F(ab')_2$	n/a	3.1×10^{-8}
AT130-5 $F(ab')_2$	n/a	2.6×10^{-8}
AT128 $F(ab')_2$	n/a	7.5×10^{-7}
2.4G2 $F(ab')_2$	n/a	2.9×10^{-10}

The value of K_D was calculated from the 1:1 binding model, by a mathematical algorithm using the BIAcore T100 Evaluation software.

4.2.2. Identification of epitope specificity.

As a means of identifying whether the anti-CD32 mAb were binding to the same epitope on CD32, the ability of the antibodies to block the binding of each other was assessed. Splenocytes from WT mice were incubated with 50 μg/ml unlabelled anti-CD32 mAb for 15 min at room temperature. Cells were then incubated with 15 μg/ml of the FITC-conjugated anti-CD32 of interest on ice for 20 min, then with 10 μg/ml PE-conjugated anti-CD19 for 15 min at room temperature and analysed by flow cytometry. A reduction in the MFI after pre-incubation with the unlabelled anti-CD32 mAb in comparison to the FITC-conjugated mAb alone indicated that the unlabelled mAb blocked the binding of the FITC-conjugate mAb and thus blocked the binding site of that particular anti-CD32 mAb. From the results it is apparent that there are two patterns of cross-blocking. The binding of AT130-2 and AT130-5 can be blocked by each other, but not by AT128 or 2.4G2, whereas the binding of AT128 and 2.4G2 can be blocked by all of the anti-CD32 mAb (Figure 4.4).

4.2.3. The anti-CD32 mAb block immune complex binding.

IgG in the context of IC leads to activation of CD32. We reasoned that in order for the anti-CD32 mAb to manipulate CD32 activity they should be able to block engagement of CD32 by IC. To establish whether the anti-CD32 mAb were able to block IC binding, splenocytes were incubated with 50 μg/ml unlabelled anti-CD32 mAb, either whole IgG or $F(ab')_2$ fragment for 15 min at room temperature and then placed on ice. A rabbit-anti-OVA/OVA-FITC immune complex were then added to the cells at a ratio of 20:1 antibody

to antigen and then analysed by flow cytometry. It was determined that all of the anti-CD32 mAb blocked IC binding, although AT128 did so with less efficiency than AT130-2, AT130-5 and 2.4G2 (Figure 4.5a). Interestingly and with the exception of 2.4G2 the CD32 mAb did not block IC binding as $F(ab')_2$ fragments (Figure 4.5b). These data indicate that the Fc domains of AT130-2, AT130-2 and AT128 are binding to the Fc binding grove of CD32 and as such blocking Fc:CD32 interaction by IC.

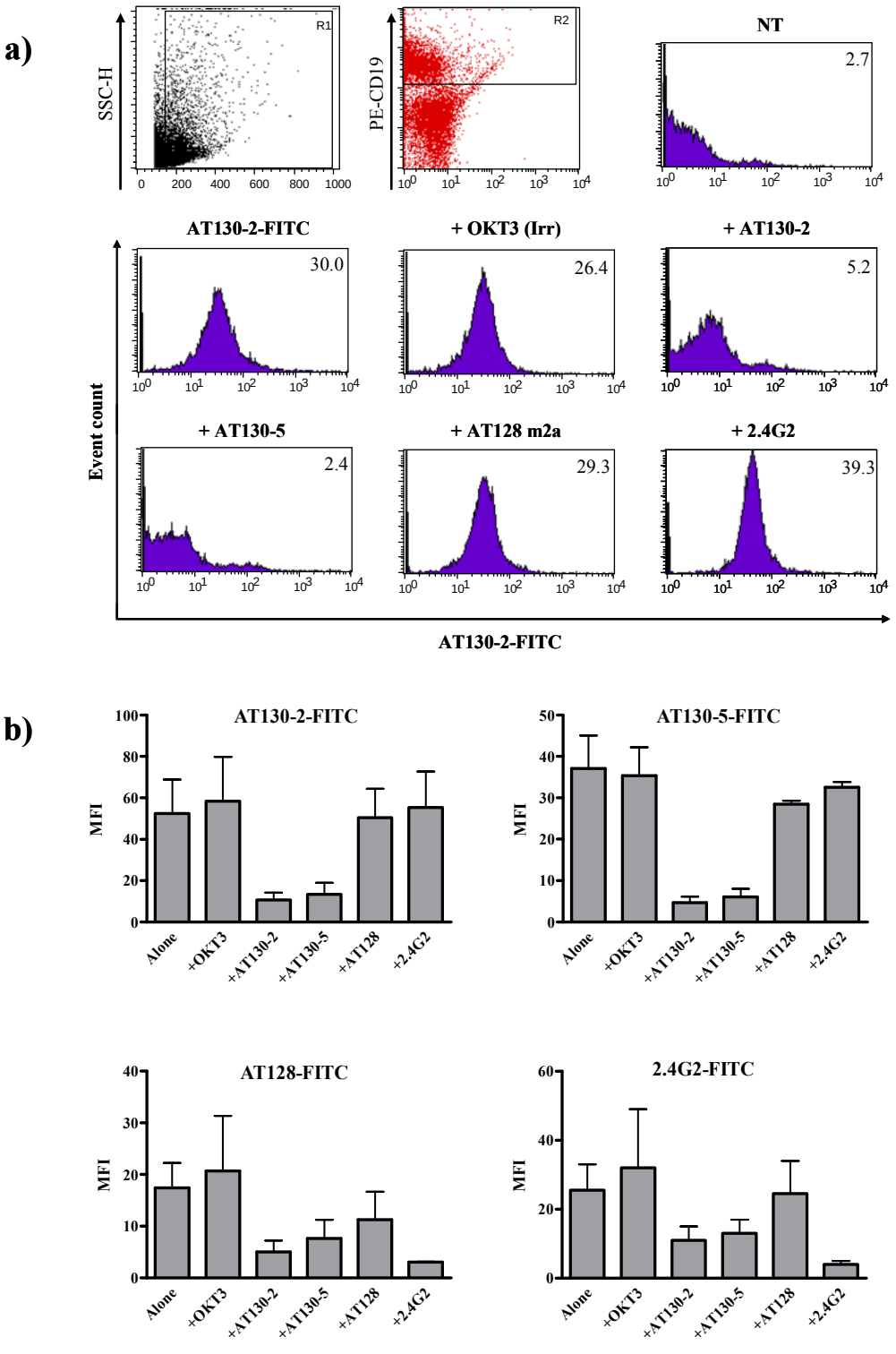

Figure 4.4. Cross-blocking by the anti-CD32 mAb.
WT splenocytes were incubated with unlabelled anti-CD32 mAb or irrelevant control (OKT3) (50 µg/ml) for 15 min at room temperature, before incubation with 15 µg/ml FITC-conjugated mAb for 20 min on ice, followed by 15 min incubation at 4 °C with PE-CD19 (R2) and then analysis by flow cytometry (a). The binding of AT130-2 and AT130-5 were blocked by themselves and each other, whereas the binding of AT128 and 2.4G2 was prevented by all of the anti-CD32 mAb (b). These data represent results from three experimental repeats, where errors was expressed as standard error of the mean (SEM). MFI is the mean florescence intensity after binding of FITC-conjugated anti-CD32 mAb.

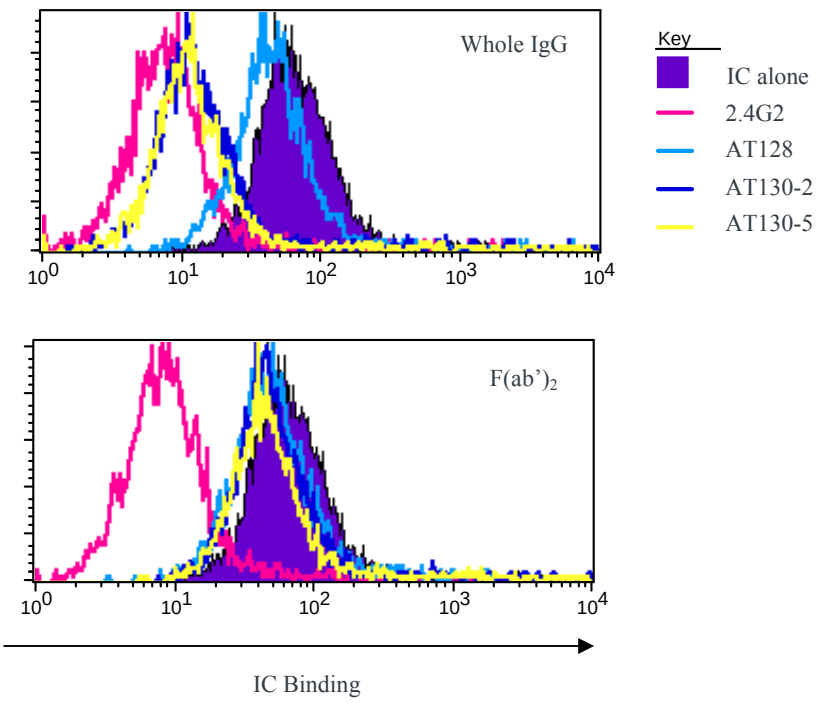

Figure 4.5. Anti-CD32 mAb block immune complex binding.
WT splenocytes were incubated with anti-CD32 mAb at 50 µg/ml, either whole IgG (a) or F(ab')$_2$ fragments (b) for 15 min at room temperature and then placed on ice. A rabbit-anti-ova/ova-FITC IC was then added at a ratio of 20:1. Cells remained on ice throughout and were analysed by flow cytometry. As can be seen, all of the anti-CD32 mAb, with the exception of AT128 effectively blocked IC binding as whole IgG. In addition, 2.4G2 also blocked IC binding as a F(ab')$_2$ fragment. Data is a representative result from three repeats

4.3. Activation of CD32.

After establishing the binding profiles of the antibodies we began to determine their functional characteristics *in vitro*.

4.3.1. Tyrosine phosphorylation of CD32, SHIP-1 and SHP by anti-BCR antibodies.

CD32 inhibition of BCR signalling has been identified as a distinctive means of regulating B cell responses. Initially we wanted to determine whether Fc engagement of CD32 on the surface of lymphoma cells would induce tyrosine phosphorylation of the receptor (a marker of CD32 activation) and also result in downstream signalling event, such as phosphorylation of SHIP-1 and SHP[312] (See Introduction section 1.8.3). To address this, πBCL1 cells were incubated with 10 µg/ml Mc39/12 (monoclonal anti-IgM) or polyclonal goat-anti-mouse anti-IgM whole IgG antibody (gαm) for 0.5, 2, 5 and 15 min at 37 °C, lysates produced and samples analysed by Western Blotting for phospho-CD32 (pCD32), phospho-SHIP-1 (pSHIP-1) and phospho-SHP (pSHP) (see Materials and Methods section 2.14). It was shown that both the monoclonal and polyclonal anti-IgM antibodies were able to induce tyrosine phosphorylation of CD32, and concurrently increase the tyrosine

phosphorylation of SHIP-1 and SHP, indicating that the anti-IgM antibodies are co-ligating with CD32 on the surface of lymphoma cells and activating the CD32 signalling pathway (Figure 4.6).

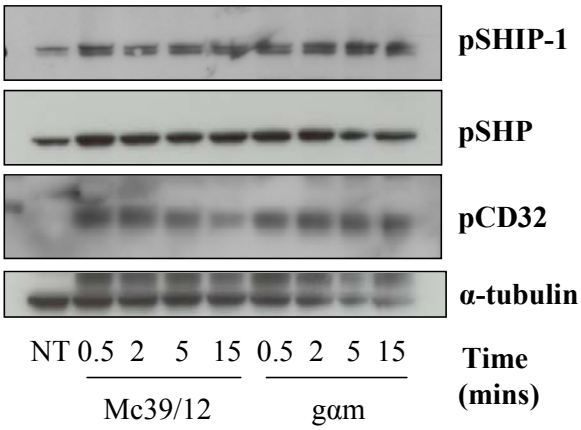

Figure 4.6. Tyrosine phosphorylation of CD32, SHIP-1 and pSHP by anti-IgM antibodies.
πBCL1 cells were stimulated for 0.5, 2, 5 or 15 min with 10 μg/ml Mc39/12 or gαm, lysates prepared and examined for pCD32 (40 kDa), pSHIP-1 (145 kDa) and pSHP (68 kDa) by Western blot. Both anti-IgM antibodies induced phosphorylation of CD32, SHIP-1 and SHP. Data is a representative result from three repeats.

4.3.2. Tyrosine phosphorylation of CD32 by the anti-CD32 mAb.

Next we wanted to determine whether the anti-CD32 mAb would activate CD32 directly and so examined the tyrosine phosphorylation of CD32 in the presence of the anti-CD32 mAb. πBCL_1 cells were incubated with 10 μg/ml anti-CD32 mAb for 30 min at 37 ˚C, lysates were produced and the samples analysed by Western blotting. Alongside the anti-CD32 mAb, πBCL_1 cells were incubated with gαm IgG (see above) or rabbit anti-mouse IgG (rαm) which contain Fc as positive controls, or with the equivalent anti-IgM $F(ab')_2$ fragment, where the Fc domains are absent, serving as a negative control. In addition, cells were also incubated with the BCL_1 specific anti-idiotype mAb (Mc106A5), serving as another positive control and potentially a better mimic of IC binding. As expected, only the whole IgG and not the $F(ab')_2$ fragments of the gαm IgG reagent elicited tyrosine phosphorylation of CD32, indicating that Fc engagement of CD32 is required to cause receptor phosphorylation and consequentially activation. Mc106A5 also engaged and caused phosphorylation of CD32, albeit to a lesser degree that the gαm IgG (Figure 4.7a). It is thought that this may be due to differences in epitope binding of gαm and anti-idiotype and thus differences in the position of binding stoichiometry of the antibodies in relation to CD32.

It was shown that alone the anti-CD32 mAb, AT130-2 and AT130-5 also caused tyrosine phosphorylation of CD32 on πBCL_1 cells, whereas AT128 and 2.4G2 did not (Figure 4.7a).

Similar results were observed with Eμ-myc cells, with Eμ#8 cells used as an example here. Phosphorylation of CD32 is a marker of activation of the receptor and therefore indicates that AT130-2 and AT130-5 induce activation of CD32. In contrast, AT128 (IgG1 or IgG2a) and 2.4G2 do not induce tyrosine phosphorylation or activation of CD32 (Figure 4.7b).

It was observed that alongside the pCD32 specific band (40 kDa), a second band, evident at approximately 60 – 70 kDa, was detected using the anti-phospho-CD32 antibody for Western blotting (see Table 2.2). The detection of this band corresponded exclusively with CD32 phosphorylation, that is to say that when phosphorylation of CD32 occurred, (e.g. after incubation with AT130-2), this band was also present, but when phosphorylation of CD32 was absent, (e.g. after incubation with AT128) the 60 - 70 kDa band was not present (see Appendix 2). Although the identity of this 60 - 70 kDa protein is unclear, its presence provided a surrogate marker for the activation of CD32 in murine cells.

4.3.3. Tyrosine phosphorylation of SHIP-1 following activation of CD32 by the anti-CD32 mAb.

In order to assess if the engagement of CD32 by the anti-CD32 mAb was producing classical activation of the CD32 receptor we further probed for downstream signalling events, as previously described. In these experiments, πBCL_1 cells were incubated with AT130-2 or AT128 m2a at 10 μg/ml for 0.5, 2, 5 or 15 min before lysates were prepared and samples analysed by Western blotting. AT128 m2a was used in these experiment rather than the IgG1 version, AT128 as it provided an isotype comparison to AT130-2. As well as inducing the phosphorylation of CD32 on πBCL1 cells, AT130-2 induced an increase in the phosphorylation of SHIP-1 in comparison to the control (Figure 4.8). In contrast, AT128 m2a did not induce phosphorylation of CD32. Rather incubation of cells with AT128 m2a seemed to correspond with inhibition of CD32 signalling, demonstrated by a reduction in phosphorylation of SHIP-1 in comparison to the control (Figure 4.8). AT128 m2a was used as an isotype comparison for AT130-2 as IgG2a have higher affinity for CD32, therefore activation of CD32 via Fc engagement could be compared.

This change in pSHIP-1 was also sustained at 15 min with both AT130-2 and AT128 m2a (Figure 4.8). Interestingly, the levels of pSHIP-1 observed as a result of AT130-2 engagement with CD32 were not as substantial as those observed after incubation with gαm whole IgG (Figure 4.9). In addition, it could be observed that pSHIP-1 levels decreased with time after gαm stimulation, with maximum phosphorylation of SHIP-1

occurring at 1 min incubation. This confirms that changes in pSHIP-1 occur as early events in the CD32 signalling cascade with regards to co-engagement between the BCR and CD32, but also as a result of direct CD32 engagement.

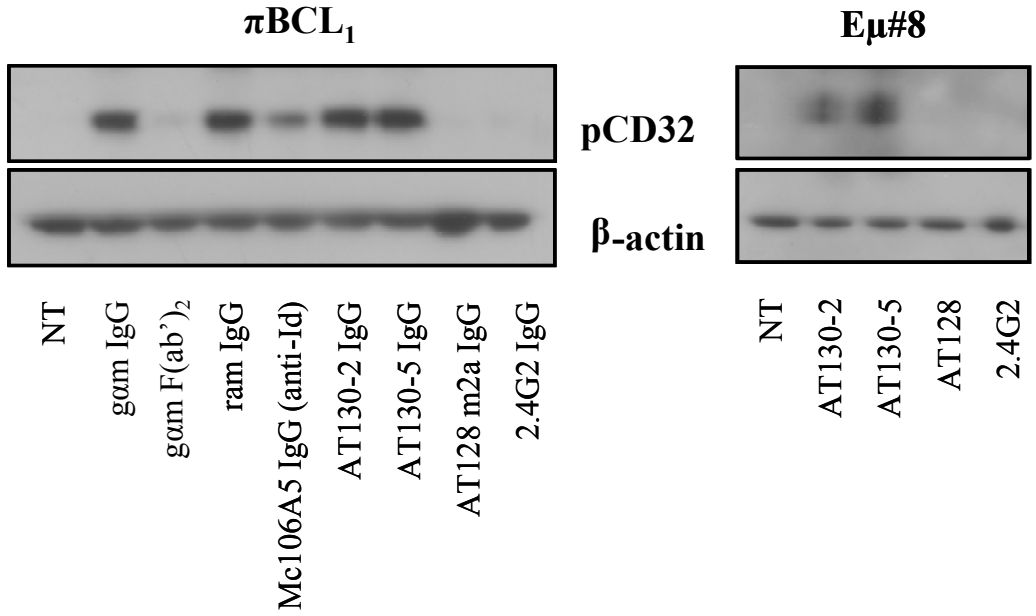

Figure 4.7. Tyrosine phosphorylation of CD32 by anti-CD32 mAb.
πBCL1 and Eμ#8 cells were stimulated for 30 min with the relevant anti-CD32 mAb or anti-IgM, lysates prepared and sample examined for CD32 and β-actin by Western blot. AT130-2 and AT130-5 cause phosphorylation of CD32, similar to treatment with polyclonal anti-IgM (gαm or rαm) whole IgG, but not gαm $F(ab')_2$ fragment. Conversely, AT128 m2a and 2.4G2 do not cause phosphorylation of CD32. Data is a representative result from three repeats.

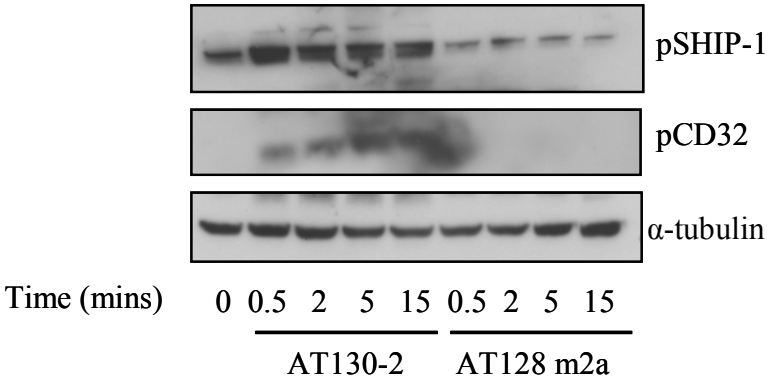

Figure 4.8. Tyrosine phosphorylation of CD32 and SHIP-1 by anti-CD32 mAb.
πBCL_1 cells were stimulated for 30 sec, 2, 5 or 15 min with 10 μg/ml AT130-2 or AT128 m2a, lysated prepared and samples examined for pCD32 and pSHIP-1 by Western blot. AT130-2 stimulation caused an increase in pCD32 and pSHIP-1, whilst in contrast, AT128 m2a stimulation did not cause phosphorylation of CD32 and caused a reduction in pSHIP-1. Data is a representative result from three repeats.

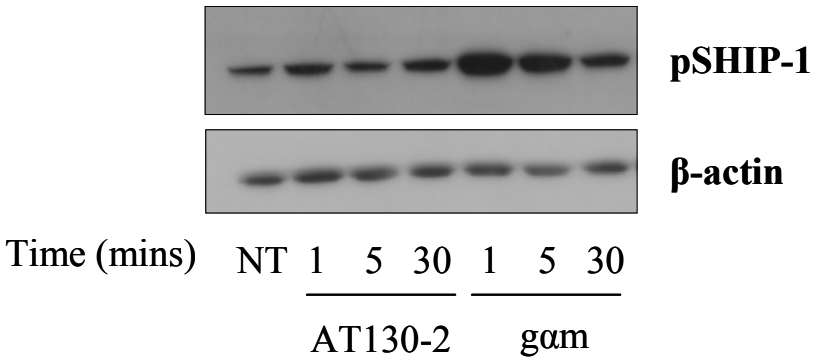

Figure 4.9. Tyrosine phosphorylation of SHIP-1 by AT130-2 and anti-IgM.
πBCL_1 cells were stimulated for 1, 5 or 30 min with 10 μg/ml AT130-2 or gαm and examined for pSHIP-1 by Western blot. Both AT130-2 and gαm stimulation caused an increase in pSHIP-1, although the anti-IgM induced a greater level of phosphorylation than AT130-2. Data is a representative result from three repeats.

4.3.4. Tyrosine phosphorylation of CD32 by the anti-CD32 mAb whole IgG and $F(ab')_2$ fragments.

Having shown that whole IgG anti-IgM is required to induce tyrosine phosphorylation of CD32 (Figure 4.6), we were interested to discover if the Fc region of the anti-CD32 mAb is also required for phosphorylation of CD32 by AT130-2 and AT130-5, or whether binding of the anti-CD32 mAb $F(ab')_2$ fragments alone were capable of causing activation of the receptor. Alongside this, we were also interested to discover if AT128 m2a and were able to elicit their inhibitory effects as $F(ab')_2$ fragments alone. We also included the commercial 2.4G2 mAb in these experiments for comparison, as we have previously demonstrated that the $F(ab')_2$ version of this mAb had different effects to the in-house generated mAb (Figure 4.5).

In these experiments, πBCL_1 cells were incubated with 10 μg/ml mAb, IgG or $F(ab')_2$ at 37 ˚C for 5 min, lysates prepared and samples analysed by Western blotting. These data again show that AT130-2 and AT130-5 cause tyrosine phosphorylation of CD32 as whole IgG. In contrast, when cells are incubated with AT130-2 and AT130-5 $F(ab')_2$ fragments, phosphorylation of CD32 was not observed (Figure 4.10), suggesting that Fc engagement by both AT130-2 and AT130-5 is essential for their activation of CD32. The BIAcore data shown in Figure 4.3, indicate that the lack of phosphorylation does not occur through lack of mAb binding and is presumably therefore due to the lack of Fc engagement.

In contrast, neither the whole IgG or $F(ab')_2$ fragments of AT128 m2a or 2.4G2 induced tyrosine phosphorylation of CD32 (Figure 4.10). As these mAb appear to inhibit phosphorylation of CD32 it is unclear from these results whether Fc engagement by AT128 m2a and 2.4G2 is important for function. However, these data suggest that the Fc

portion of these mAb did not engage with CD32 directly and as such did not induce signalling through CD32. Signalling through CD32 by Fc engagement induces inhibition of BCR signalling, however as CD32 was not activated, this suggests that the $F(ab')_2$ binding regions of AT128 m2a and 2.4G2 have a dominant inhibitory effect on CD32 activity after binding. This implies that changes in CD32 signalling due to engagement of CD32 with AT128 m2a and 2.4G2 are not through Fc engagement.

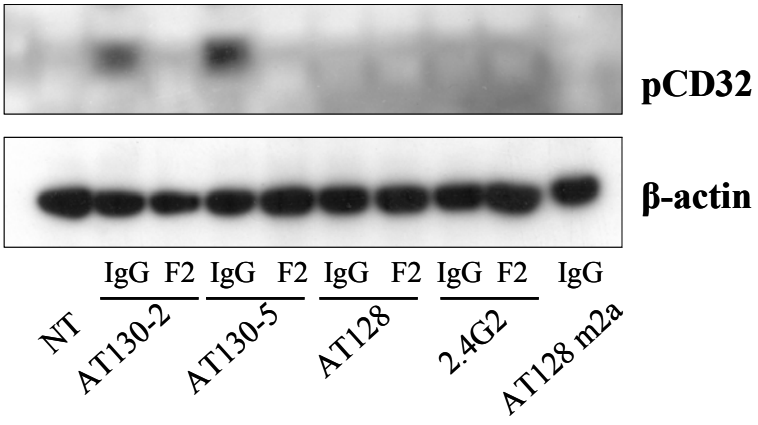

Figure 4.10. Effect of whole IgG or $F(ab')_2$ fragment CD32 mAb on tyrosine phosphorylation of CD32. πBCL_1 cells were incubated with 10 μg/ml anti-CD32 mAb, either IgG or F(ab')2 (F2) at 37˚C for 5 min, lysates prepared and samples analysed for pCD32 and β-actin by Western blot AT130-2 and AT130-5 whole IgG alone cause tyrosine phosphorylation of CD32, whilst AT128 m2a and 2.4G2 (IgG and $F(ab')_2$) and AT130-2 and AT130-5 $F(ab')_2$ do not cause tyrosine phosphorylation of CD32. Data is a representative result from three repeats.

4.3.5. Co-ligation of CD32 by AT130-2 and AT130-5 is in a *cis* fashion.

Having established that AT130-2 and AT130-5 required an Fc region in order to induce phosphorylation of CD32 and SHIP-1, we next wanted to determine whether co-ligation of CD32 was occurring on the same cell (*cis*) or on different cells (*trans*). This would indicate whether CD32 was being phosphorylated due to co-ligation of the receptor on the same cell, or by Fc engagement of the anti-CD32 mAb with FcγR on the surface of adjacent cells (Figure 4.11). To address this, πBCL_1 cells were cultured at increasing concentrations (2, 0.4 and 0.1 x 10^6 cells/ml) with 10 μg/ml IgG mAb at 37 ˚C for 5 min, images were captured by bright field microscopy, lysates prepared and samples analysed by Western blotting techniques. If the co-ligation of CD32 on the same cell was resulting in phosphorylation of the receptor then pCD32 would be consistent at all cell concentrations. Alternatively, if pCD32 was occurring due to CD32 engagement on adjacent cells then as the cell concentrations decreased so would the level of pCD32. As the cell concentrations increase the cell density also increases, the cells are closer together and the likelihood of cell contact increases, making *trans* interaction more likely, whereas

at lower cell concentrations there is less chance of cell to cell contact, making it is more likely that *cis* interactions are causing phosphorylation. Figure 4.12 demonstrates consistent phosphorylation of CD32 at all cell concentrations by the anti-CD32 mAb AT130-2 and AT130-5. This suggests that co-ligation of CD32 that resulted in phosphorylation of CD32 by the anti-CD32 mAb was occurring as a result of a *cis* interaction. Interestingly, it would seem that at the lowest cell concentration (1×10^6 cells/ml) phosphorylation of CD32 by the anti-idiotype mAb was reduced. This may suggest that anti-idiotype mAb co-ligates CD32 in a *trans* fashion, but may also reflection poor protein loading, as the β-actin is less intense in this lane (Figure 4.12). In addition, anti-idiotype phosphorylation of CD32 appeared to be of the same magnitude as phosphorylation by the anti-CD32 mAb, however this was not usually observed (Figure 4.7).

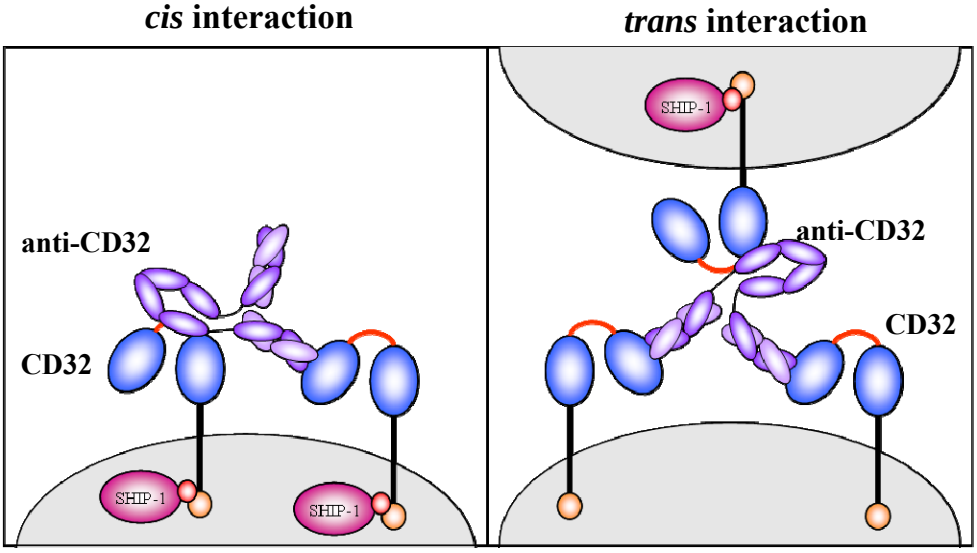

Figure 4.11. Schematic demonstrating the *cis* and *trans* engagement of CD32 by anti-CD32 mAb on CD32 expressing cells.
Engagment of CD32, resulting in phosphorylation of the receptor, could occur on the same cell (*cis*) or on different cells (*trans*). Phosphorylation of CD32 at different cell concentrations would indicate whether CD32 was being phosphorylated due to co-ligation of the receptor, or by Fc engagement by the anti-CD32 mAb with other FcγR, either another CD32 molecule or the other activatory FcγR, on the surface of adjacent cells.

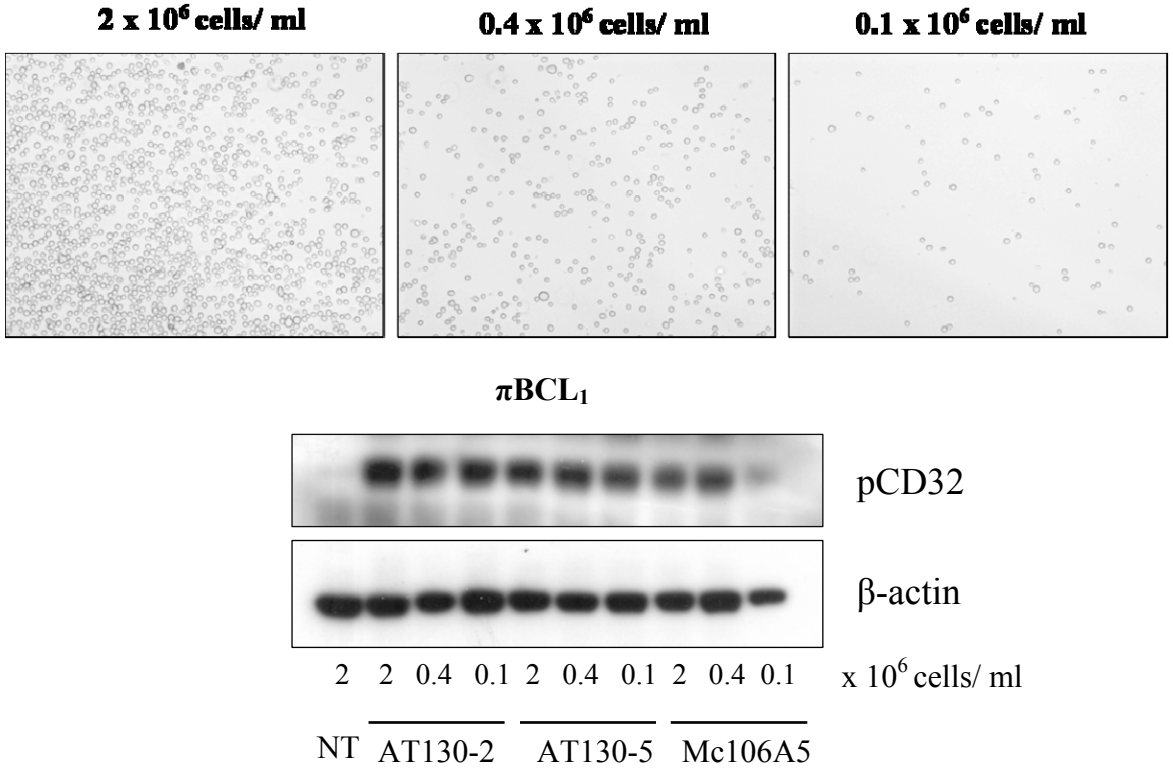

Figure 4.12. Tyrosine phosphorylation of CD32 is cis-acting rather than trans-acting.
πBCL_1 cells were cultured at 2, 0.4 and 0.1 x 10^6 cell/ml with 10 µg/ml AT130-2, AT130-5 and Mc106A5 IgG mAb at 37 ˚C for 5 min, protein lysates prepared and samples analysed for pCD32 and β-actin by Western blotting. Cell densities were demonstrated by bright field microscopy, X10 magnification (scale bar is equal to 10 µm) (a). It was shown that at varying cell densities phosphorylation of CD32 was similar with all the mAb, indicating that co-ligation of CD32 by Fc was occurring in cis fashion on the same cell (b). Data is a representative result from three repeats.

4.4. Ability of the anti-CD32 mAb to affect calcium flux.

The previous data established that the anti-CD32 mAb were able to elicit differential CD32 signalling. Next we wanted to discover whether these different signalling properties of the anti-CD32 mAb would affect cell physiology. On B cells, CD32 acts to inhibit BCR-induced Ca^{2+} flux via phosphorylation of SHIP-1 and subsequent hydrolysis and inactivation of molecules important to BCR signalling (Reviewed in [143]). Therefore, we assessed the ability of the anti-CD32 mAb to influence BCR-induced Ca^{2+} flux by labelling cells with the Ca^{2+} reporter Fluo-3-AM and then stimulating these cells with anti-BCR antibodies alone or after pre-incubation for 15 min with CD32 mAb. The reporter dye, Fluo3-AM, emits a fluorescent signal when excited by intracellular Ca^{2+} flux, consequently the magnitude and duration of the BCR-induced Ca^{2+} flux and the effects of the CD32 mAb can be determined by flow cytometry.

4.4.1. Fc engagement by anti-idotype mAb reduces the magnitude of anti-idiotype Ca^{2+} flux.

To first ascertain if CD32 engagement was able to manipulate (inhibit) BCR-induced Ca^{2+} flux we compared the Ca^{2+} flux induced by the anti-idiotype mAb, Mc106A5 as, either an IgG or $F(ab')_2$ fragment. If co-engagement of BCR and CD32 by anti-idiotype mAb leads to inhibition of cell activation the observed Ca^{2+} flux with the IgG mAb should be less than that of the $F(ab')_2$ mAb. To assess this, πBCL_1 cells stained with the intracellular dye, Fluo-3-AM were analysed by flow cytometry in the presence of Mc106A5 IgG and $F(ab')_2$ and recorded over a period of 3 minutes versus FL1-H, where Ca^{2+} flux was measured as changes in FL1-H fluorescence (Figure 4.13a). Results were analysed using FlowJo Software™. Both Mc106A5 IgG and $F(ab')_2$ were able to induce a Ca^{2+} flux in comparison to untreated cells (Figure 4.13b), with the $F(ab')_2$ fragment giving an increased Ca^{2+} flux in terms of magnitude and duration in comparison to the whole IgG mAb. These data suggest that co-ligation of CD32 and BCR via Fc interactions does in fact inhibit BCR-induced Ca^{2+} flux, as previously described[323]. However, the trend towards increased Ca^{2+} flux on cells stimulated with anti-BCR $F(ab')_2$ fragment was not significant (by Student's t-test) when the total area under the curve was analysed using the FlowJo Software™ (Figrue 4.13c).

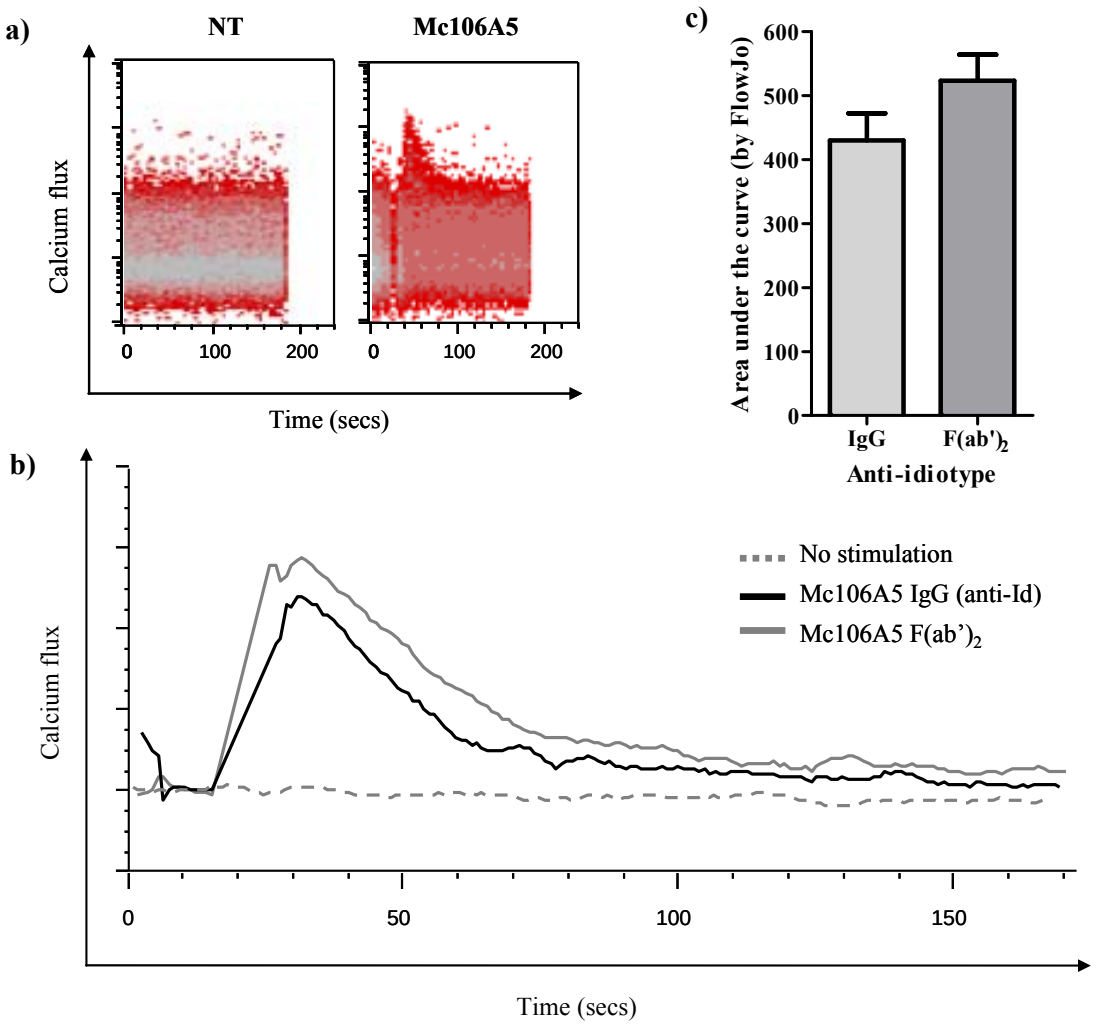

Figure 4.13. Engagement of CD32 by the Fc domain of anti-idiotype mAb reduces the magnitude of anti-idiotype Ca^{2+} signalling.
πBCL_1 cells were stained with the intracellular dye, Fluo-3-AM which becomes excited upon increased levels of intracellular Ca^{2+}. Cells were then analysed by flow cytometry for 15 sec to establish a baseline and then stimulated with buffer alone or 5µg/ml Mc106A5 (anti-idiotype) IgG or $F(ab')_2$ for a further 2 min and 45 sec. Live cell events as identified by FSC-H and SSC-H were recorded over a period of 3 minutes versus FL1-H (measure of Ca^{2+} flux) (a). Whilst untreated cells gave no Ca^{2+} flux, Mc106A5 IgG and $F(ab')_2$ both induced a Ca^{2+} flux (b). Here, Mc106A5 $F(ab')_2$ gave an amplified magnitude of Ca^{2+} flux than Mc106A5 IgG, indicating that Fc engagement with CD32 by anti-IgM antibodies inhibited Ca^{2+} flux. Although there was a trend towards increased Ca^{2+} flux when cells were stimulated with anti-idiotype whole $F(ab')_2$ fragment, this was not a significant increase (by Student t-test) (c). Area under the curve was calculated using FlowJo software. Data is a representative result from four repeats.

4.4.2. Effect of anti-CD32 on anti-idiotype induced Ca^{2+} flux.

Having established that Fc engagement of CD32 inhibits BCR-induced Ca^{2+} flux on πBCL_1 cells, we next went on to investigate whether the anti-CD32 mAb were able to manipulate BCR-induced Ca^{2+} flux. First, Fluo-3-AM stained cells were analysed by flow cytometry for 15 seconds and then stimulated with 50 µg/ml anti-CD32 mAb for a further 2 min and 45 sec to discover if the anti-CD32 mAb alone had the potential induce a Ca^{2+}. Again it was demonstrated that Mc106A5 IgG induced a Ca^{2+} flux, however there was no discernible Ca^{2+} flux when the πBCL_1 cells were stimulated with the anti-CD32 mAb alone

(Figure 4.14a). Next, to establish the effect of the anti-CD32 mAb on BCR-induced Ca^{2+} flux, πBCL_1 cells stained with Fluo-3-AM were pre-incubated with 50 μg/ml AT130-2, AT130-5, AT128 m2a or 2.4G2 for 15 min, analysed by flow cytometry for 15 seconds to establish a baseline and then stimulated with 5 μg/ml Mc106A5 IgG for a further 2 min and 45 sec.

Despite the anti-CD32 mAb not inducing their own Ca^{2+} flux, pre-incubation with the anti-CD32 mAb did alter Mc106A5 induced Ca^{2+} flux. Both AT130-2 and AT130-5 inhibited the magnitude and duration of BCR-induced Ca^{2+} flux (Figure 4.14b), whereas AT128 m2a and 2.4G2 potentiated the BCR-induced Ca^{2+} flux (Figure 4.14c), primarily by inducing an earlier Ca^{2+} flux of increased magnitude, presumably by decreasing the activation threshold of the B cells.

4.4.3. Effect of anti-CD32 mAb on anti-IgM induced Ca^{2+} flux.

We have demonstrated that anti-idiotype and anti-IgM (anti-μ) activated CD32 to different extents and we considered this related to the different binding epitopes of the antibodies. Previous observation in this laboratory have demonstrated that mAb that bind closer to the cell surface, such as the anti-IgM, Fcμ mAb (Mc39/12) initiated more potent intracellular signals than mAb that bind further away from the cell surface, such as anti-idiotype[407]. As the activatory signal received by cells after stimulation with anti-IgM Fcμ mAb would be stronger, we wanted to determine whether signalling through CD32 by our anti-CD32 mAb would be sufficient to inhibit this more potent signal.

Cells were prepared and analysed as above, cells were however stimulated with anti-IgM (Mc39/12) instead of anti-idiotype. It was shown that anti-IgM BCR-induced Ca^{2+} flux can be manipulated similarly to anti-idiotype BCR-induced Ca^{2+} flux, where AT130-2 and AT130-5 inhibit anti-IgM Ca^{2+} flux (Figure 4.15a), although the inhibition occurring as a result of pre-incubation with these mAb appeared to be reduced in comparison to their effect on anti-idiotype Ca^{2+} flux. However, potentiation of Ca^{2+} flux by AT128 m2a or 2.4G2 was not observed after anti-IgM stimulation (Figure 4.15b), potentially as the anti-IgM Ca^{2+} flux is already maximal.

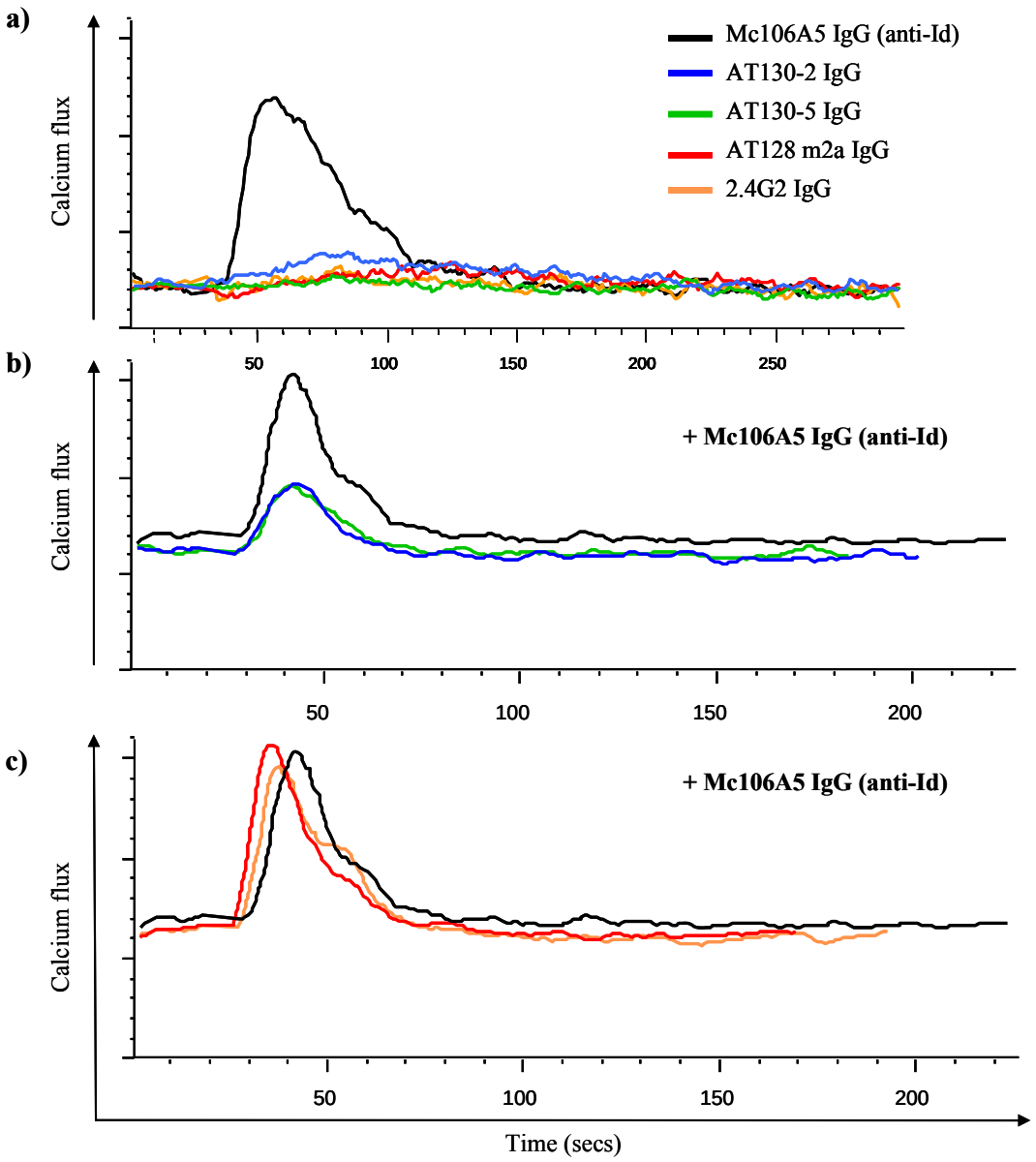

Figure 4.14. The effect on anti-idiotype induced calcium flux by pre-incubation with CD32 mAb. Cells were stained with the intracellular dye, Fluo-3-AM which becomes excited upon contact with increased levels of intracellular Ca^{2+}. Cells were pre-incubated with 50 µg/ml AT130-2, AT130-5, AT128 m2a or 2.4G2 for 15 min and analysed by flow cytometry for 15 sec to establish a baseline and then stimulated with 5 µg/ml Mc106A5 (anti-idiotype) for a further 2 min 45 sec. Live cell events, as identified by FSC-H and SSC-H, were recorded over a period of 3 min versus FL1-H and analysed using analysed using FlowJo™ software, where cells greater than the background threshold over the first 15 seconds are plotted as an average fluorescence. Alone, the CD32 mAb did not elicit a Ca^{2+} flux (a). However, pre-incubation of the πBCL_1 cells with AT130-2 and AT130-5 inhibited anti-idiotype Ca^{2+} flux (b), whereas in contrast, pre-incubation of the πBCL_1 cell with AT128 m2a and 2.4G2 potentiated anti-idiotype Ca^{2+} flux (c). Data is a representative result from three repeats.

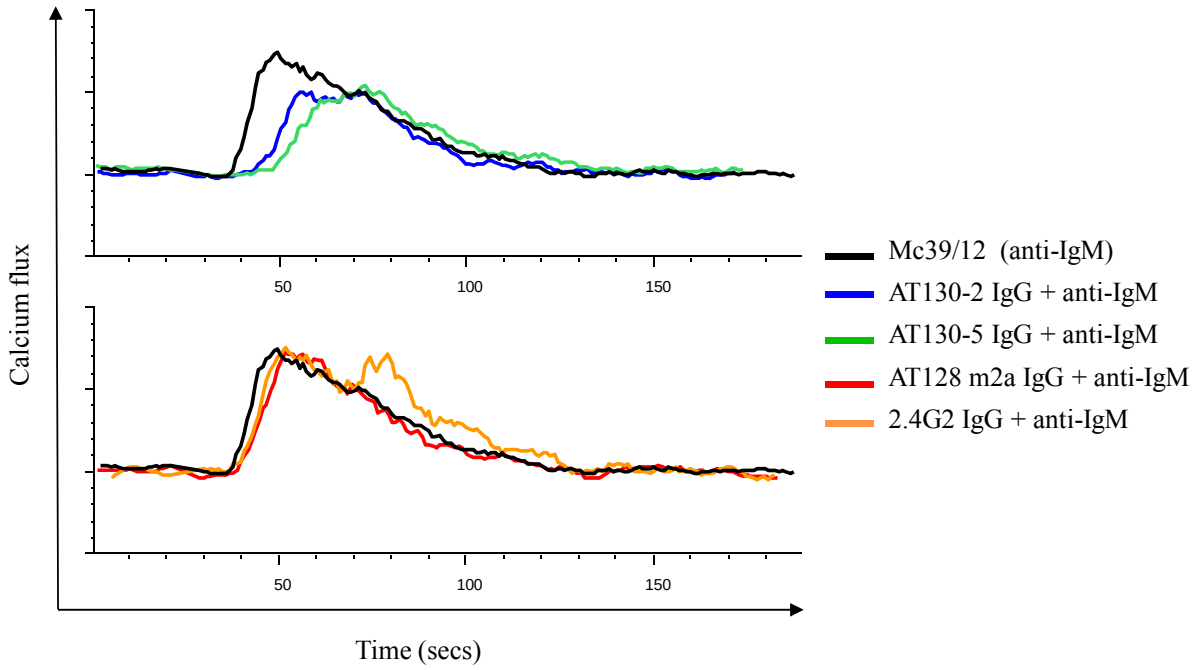

Figure 4.15. The effect on anti-IgM, Fcμ induced calcium flux by pre-incubation with CD32 mAb. Cells were stained with the intracellular dye, Fluo-3-AM which becomes excited upon contact with increased levels of intracellular Ca^{2+}. Cells were pre-incubated with 50 μg/ml AT130-2, AT130-5, AT128 m2a or 2.4G2 for 15 min and analysed by flow cytometry for 15 sec to establish a baseline and then stimulated with 5 μg/ml Mc39/12 (anti-IgM) for a further 2 min and 45 sec. Live cell events, as identified by FSC-H and SSC-H, were recorded over a period of 3 min versus FL1-H and analysed using FlowJo™ software, where cells greater than the background threshold over the first 15 seconds are plotted as an average fluorescence. It was observed that AT130-2 and AT130-5 blocked anti-IgM (Mc39/12) induced calcium flux. However there is no observed increase in Ca^{2+} flux following pre-incubation with either AT128 m2a or 2.4G2. Data is a representative result from three repeats.

4.4.4. Effect on anti-idiotype induced Ca^{2+} flux by the anti-CD32 mAb whole IgG and $F(ab)_2$ fragments.

Having discovered that whole IgG is required to induce tyrosine phosphorylation and activation of CD32 by AT130-2 and AT130-5, we next sought to discover if whole IgG anti-CD32 mAb was required to inhibit anti-idiotype induced Ca^{2+} flux. Cells were pre-incubated with either whole IgG or $F(ab')_2$ of the anti-CD32 mAb and analysed as previously described. These data show that $F(ab')_2$ fragments of AT130-2 (Figure 4.16a) and AT130-5 (Figure 4.16b) have a greatly reduced ability to inhibit Ca^{2+} flux than whole IgG. However, AT128 IgG and $F(ab')_2$ (Figure 4.16c) seem to act the same in terms of potentiating BCR-induced Ca^{2+} flux, as does 2.4G2 (Figure 4.16d), although the potentiation of anti-idiotype induced Ca^{2+} flux is slightly reduced with AT128 m2a $F(ab')_2$. These data suggests that AT128 m2a and 2.4G2 do not require engagement via the Fc portion of the antibody with CD32 to obtain an effect, whereas AT130-2 and AT130-5 do require Fc domains.

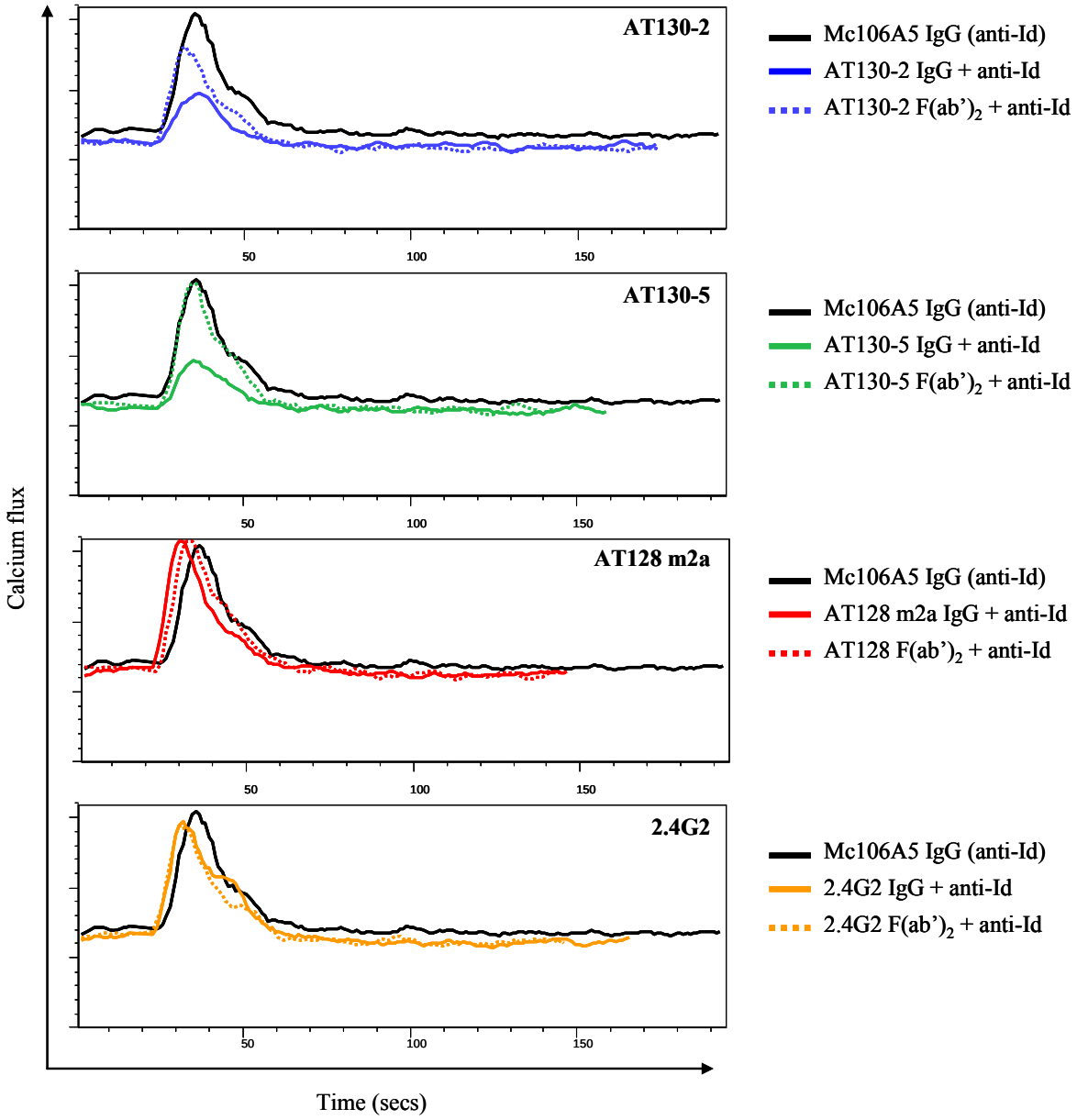

Figure 4.16. Effect on BCR-induced Ca^{2+} flux by IgG and $F(ab')_2$ fragment CD32 mAb.
Cells were stained with the intracellular dye, Fluo-3-AM. Cells were then pre-incubated with 50 µg/ml CD32 IgG or $F(ab')_2$ for 15 min and analysed by flow cytometry after the addition of 5 µg/ml Mc106A5 (anti-idiotype). Live cell events were recorded over a period of 3 min versus FL1-H and analysed using FlowJo™ software as previously detailed. $F(ab')_2$ fragments of AT130-2 and AT130-5 do not inhibit Ca^{2+} flux (a), whereas AT128 m2a and 2.4G2 functioned similarly when cells were incubated with either IgG or $F(ab')_2$. Data is a representative result from three repeats.

4.5. Induction of programmed cell death.

Next, we went on to determine whether the manipulation of B cell signalling by the anti-CD32 mAb, as described in the previous two sections, would lead to changes in functional physiology and whether this could be correlated with the differences between AT130-2/AT130-5 and AT128/AT128 m2a/2.4G2.

4.5.1. Induction of programmed cell death by the anti-CD32 mAb.

One of the reasons the Eμ-myc and Eμ-myc/CD32$^{-/-}$ LCL were generated was to facilitate the study of CD32 and the effects of the anti-CD32 mAb on CD32 and BCR biology. Initially, in order to determine if the anti-CD32 mAb would affect cell viability, πBCL1 cells were incubated with the anti-CD32 mAb at 10 μg/ml for 24 hr at 37 °C, then harvested and stained with AnV/PI for 15 min, in the dark, at room temperature and analysed by flow cytometry, as described in Materials and Methods section 2.12.

The percentage relative cell death was calculated as a percentage of non-treated (NT) cell death as described in Materials and Methods section 2.12.1. In these experiments, both AT130-2 and AT130-5 induced robust PCD of the πBCL$_1$ cells in comparion to irrelevant isotype controls ($p < 0.05$ for both by Student's t-test), whereas AT128, AT128 m2a and 2.4G2 induce limited and a non-significant level of PCD in comparion to irrelevant isotype controls (Figure 4.17a). On the πBCL$_1$ cells, AT130-2 and AT130-5 induced greater than 30 % PCD and AT128, AT128 m2a and 2.4G2 induced less than 10 % PCD (Figure 4.14a). A significance difference in levels of PDC between AT130-2 and AT130-5 and their isotype counterparts (AT128 m2a and AT128, respectively) was demonstrated for the πBCL$_1$ cell line, $p < 0.05$ cells for both AT130-2 versus AT128 m2a and for AT130-5 versus AT128 (by Student's t-test). These experiments were repeated on the Eμ-myc cell lines. In these experiments, AT130-2, AT130-5 and AT128 induced robust PCD of the Eμ-myc cells in comparion to irrelevant isotype controls ($p < 0.0001$ for both AT130-2 and AT130-5 and $p < 0.05$ for AT128, by Student's t-test), whereas AT128 m2a and 2.4G2 induce limited and a non-significant level of PCD in comparion to irrelevant isotype controls (Figure 4.17b). On the Eμ-myc cell lines, AT130-2 and AT130-5 induce greater than 40 % PCD, whereas the other anti-CD32 mAb induced less than 5 % PCD (Figure 4.17b). A significance difference in levels of PDC between AT130-2 and AT130-5 and their isotype counterparts (AT128 m2a and AT128, respectively) was also demonstrated on the Eμ-myc LCL, where $p < 0.0001$ on Eμ-myc LCL for both AT130-2 versus AT128 m2a and for AT130-5 versus AT128 (by Student's t-test).

Alongside this, in order to demonstrate the variability in the Eμ-myc cell lines response to anti-CD32 mAb we show here the relative cell death in response to incubation with AT130-2 for each of the responsive Eμ-myc cell line. Response to CD32 was measured by the induction of PCD by anti-CD32 mAb compared with the non treated control sample, where >20 % induction of cell death was considered as a response. Here, it was demonstrated that on the Eμ-myc cell lines, with one exception, incubation with anti-CD32

mAb resulted in the induction of PCD, albeit to varying degrees (Figure 4.18a). Variation in PCD recorded was unsurprising, as the level of CD32 expression on the Eμ-myc lymphoma cell lines was heterogeneous (Table 4.2). Using this assay we were also able to confirm that the Eμ-myc/CD32$^{-/-}$ cell lines would not respond to anti-CD32 mAb. The Eμ-myc/CD32$^{-/-}$ cell lines showed a relatively small or completely absent response to CD32 stimulation in comparison to the Eμ-myc LCL, as would be expected of cells lacking CD32 (Figure 4.18b) (Table 4.2). This corroborates that AT130-2 was inducing PCD through engagement of CD32.

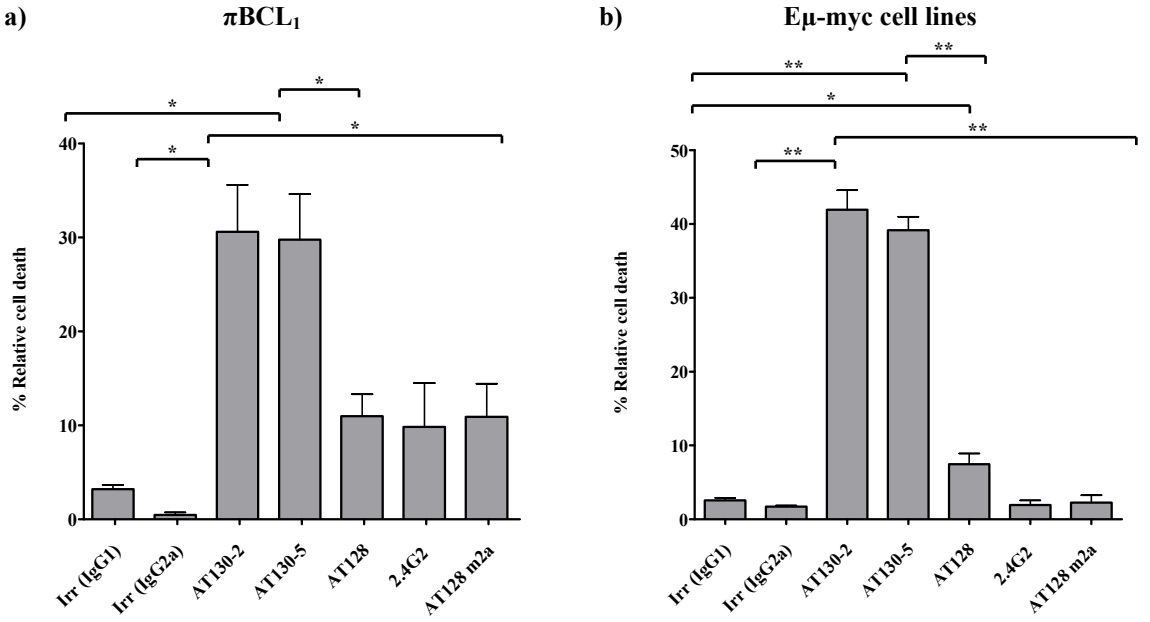

Figure 4.17. Induction of programmed cell death by anti-CD32 mAb.
The Eμ-myc cell lines (Eμ#6, 7, 8, 9, 11, 12, 13, 14 and 15) (left) and the πBCL_1 cell line (right) were incubated with mAb at 10 μg/ml for 24 hr. Where death refers to the percentage of cells that were AnV/PI positive (R2), % relative cell death was calculated as a percentage of the non-treated sample (NT) as detailed in Material and Methods. AT130-2 and AT130-5 induced robust cell death whilst AT128, AT128 m2a and 2.4G2 have relatively little effect on PCD in comparison to irrelevant isotype contols (Irr). For the Eμ-myc cell lines, the AnV/PI assay was performed on three separate occasions for each cell line, the average of the three repeats was calculated and the data pooled, where n = 9. Error for the Eμ-myc cell lines is expressed as SD. For the πBCL_1, cells the AnV/PI assay was performed on three separate occasions with the average of the three repeats calculated, error expressed as SEM. *p<0.05 and **p<0.0001.

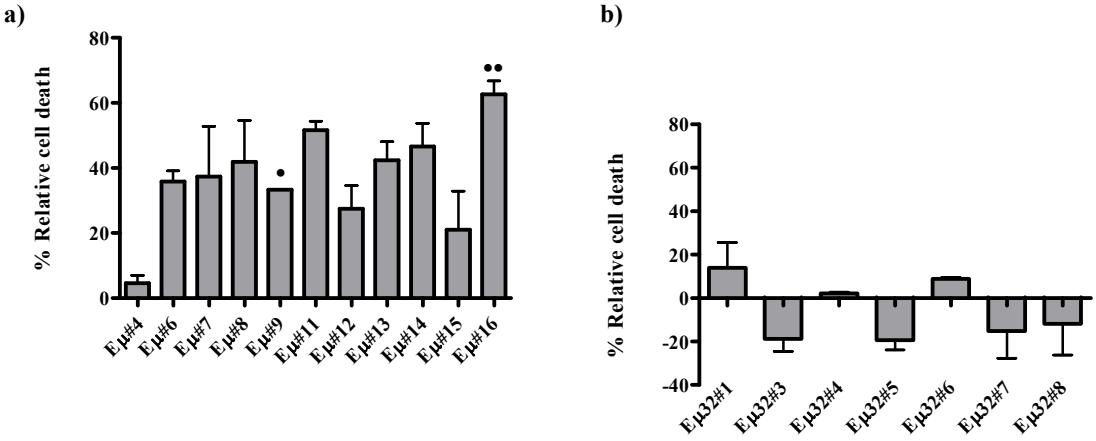

Figure 4.18. Programmed cell death induced by AT130-2 (anti-CD32 mAb) on the Eμ-myc and Eμ-myc/CD32$^{-/-}$ cell lines.
Cells were treated for 24 hr with anti-CD32 mAb (AT130-2) at 10 μg/ml. Percentage relative cell death was calculated as detailed in Material and Method 2.12. Data represents the average of three separate repeats for each cell line, with the exception of • where n=1 and •• where n =2, error bars represent SEM. A majority of the Eμ-myc cell lines (a) responded to stimulation by anti-CD32 mAb, as indicated by induction of cell death, albeit to varying degrees. In contrast, there was no induction of PCD in response to anti-CD32 mAb stimulation of the Eμ-myc/CD32$^{-/-}$ cell lines (b).

Table 4.2. Induction of programmed cell death on cell lines from Eμ-myc and Eμ-myc/CD32$^{-/-}$ mice.

1° Lymphoma (Eμ-myc)	% PCD by anti-CD32	CD32 responsive
Eμ#1	*ND	
Eμ#2	*ND	
Eμ#3		
Eμ#4	4.58	N
Eμ#5	*ND	
Eμ#6	35.81	Y
Eμ#7	46.21	Y
Eμ#8	48.04	Y
Eμ#9	33.35	Y
Eμ#10	*ND	
Eμ#11	51.62	Y
Eμ#12	27.41	Y
Eμ#13	40.02	Y
Eμ#14	46.57	Y
Eμ#15	14.27	N
Eμ#16	62.62	Y

1° Lymphoma (Eμ-myc/CD32-/-)	% PCD by anti-CD32	CD32 responsive
Eμ32#1	13.93	N
Eμ32#2	*ND	
Eμ32#3	-29.97	N
Eμ32#4	-6.90	
Eμ32#5	-20.75	N
Eμ32#6	10.57	N
Eμ32#7	-12.93	N
Eμ32#8	-16.15	N
Eμ32#9	*ND	

If the induction of PCD in response to AT130-2 was greater than 20 % these cell lines were considered responsive to anti-CD32 stimulation, as denoted with a Y (yes). If PCD following anti-CD32 stimulation was less that 20% these were denoted N (no). *ND: not determined. These data represent the average result from three experimental repeats.

4.5.2. Correlation between PCD and CD32 expression.

It was speculated that if the anti-CD32 mAb were inducing cell death by activation of CD32 then perhaps PCD would correlate with the surface expression of CD32. To assess the level of surface CD32, a panel of Eμ-myc LCLs responsive to anti-CD32 mAb stimulation were stained with FITC-conjugated AT130-2 and AT130-5 whole IgG, washed with PBS-BSA-Azide buffer and analysed by flow cytometry. The resulting MFI (equivalent to the surface expression of CD32 for each cell line) was plotted against the percentage relative PCD induced by the same anti-CD32 mAb (shown in Figure 4.18). Here, surface expression of CD32 as demonstrated by FITC-AT130-2 and FITC-AT130-5 (Figure 4.19a) correlated with percentage relative cell death, with $R^2 = 0.7477$ ($p = 0.0026$) and $R^2 = 0.6825$ ($p = 0.0061$), for AT130-2 and AT130-5, respectively by linear regression analysis. These data indicate that PCD is linked to CD32 expression, suggesting that PCD is occurring through direct receptor activation (Figure 4.19b).

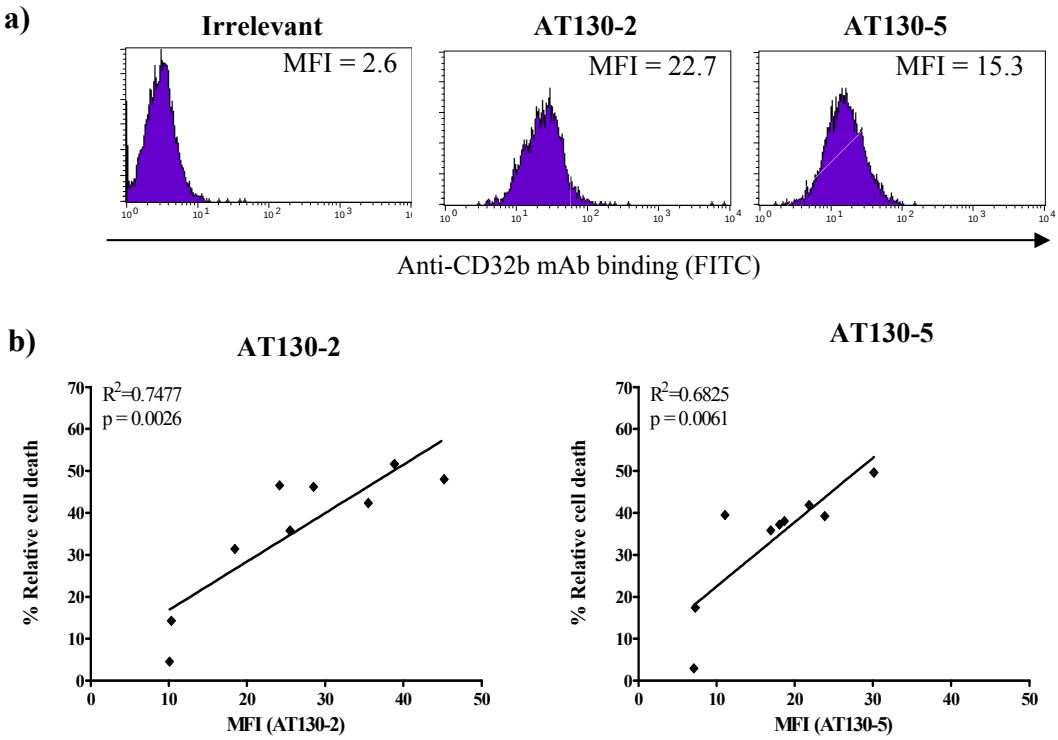

Figure 4.19. Correlation between CD32 expression and programmed cell death.
Eμ-myc cell lines (Eμ#4, 6, 7, 8, 11, 12, 13, 14, 15) were incubated at 4 ˚C for 30 min in the dark with 10 μg/ml FITC-conjugated AT130-2 or AT130-5. Samples were washed once with PBS-BSA-Azide buffer and analysed by flow cytomotery. The example flow cytometry plots shown in (a) demonstrate the staining of AT130-2 and AT130-5 on the Eμ-myc cell line, Eμ#6. MFI was plotted against % relative cell death (b). It was shown that CD32 expression positively correlated with % relative cell death (R^2 = 0.7397 for AT130-2 and R^2 = 0.6829 for AT130-5). Each dot represents the average of three repeats on a single Eμ-myc cell line.

4.5.3. Induction of PCD by anti-CD32 mAb by whole IgG and F(ab)$_2$ fragments.

Our previous data indicated that AT130-2 and AT130-5 require whole IgG to induce phosphorylation of CD32 and inhibition of BCR-induced Ca^{2+} flux. Therefore, we next assessed the ability of the anti-CD32 mAb to elicit PCD as IgG and F(ab')$_2$ fragments, using the AnV/PI assay detailed earlier. AT130-2 and AT130-5 F(ab')$_2$ fragments show a reduction in PCD induced ($p < 0.001$ and $p < 0.05$, respectively), whilst there was relatively no change in PCD induced by 2.4G2 and AT128 m2a regardless of whether whole IgG or F(ab')$_2$ fragment is used (Figure 4.20). Surprisingly, AT128 also seems to require Fc engagement as there was a significant difference ($p < 0.05$) between the relative cell death elicited by IgG and that induced by F(ab')$_2$ of this mAb. Again however, the amount of cell death induced by AT128 was not substantial in comparison with AT130-2 and AT130-5 (Figure 4.19). Regardless, these data confirm that AT130-2 and AT130-5 require Fc engagement with CD32 in order to fully activate CD32 and elicit downstream effector activities. In contrast, AT128, 2.4G2 and AT128 m2a do not require their Fc portions to elicit their effects on CD32 activity.

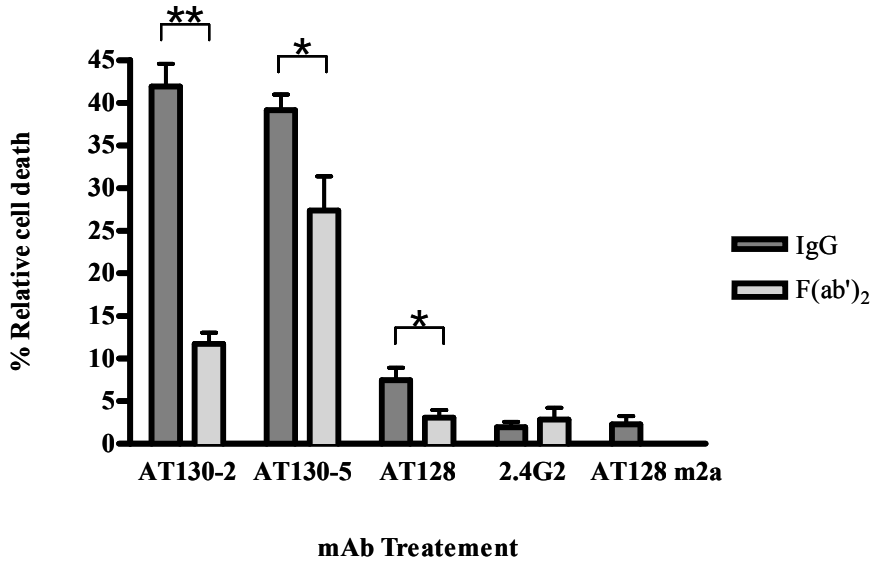

Figure 4.20. Effect of whole IgG and F(ab')$_2$ fragment on CD32 induced PCD.
Eμ-myc LCL (Eμ#6, 7, 8, 9, 11, 12, 13, 14 and 15) cells were incubated with mAb, either whole IgG or F(ab')$_2$ fragment, at 10 μg/ml for 24 hr. The percentage cell death was calculated, where % death refers to the percentage of cells that were AnV/PI positive compared to control. AT130-2 and AT130-5 whole IgG alone induced PCD, whilst AT128, AT128 m2a and 2.4G2 (IgG and F(ab')$_2$) and AT130-2 and AT130-5 F(ab')$_2$ had reduced effect on PCD. **$p<0.001$, *$p<0.05$. These data represent results from three experimental repeats, errors expressed as SD.

4.6. *In vitro* effect of anti-CD32 mAb on anti-BCR activity.

4.6.1. Correlation between CD32 and BCR expression.

As aforementioned, CD32 engagement by other mAb, such as the anti-BCR antibodies affects their ability to activate cells. We speculated that, as the function of the BCR and CD32 are linked perhaps then surface expression of BCR and CD32 would correlate. Eμ-myc LCLs were incubated for 30 min at 4 ˚C with FITC-conjugated 2.4G2 for quantification of CD32 expression and FITC-conjugated Mc39/12 for quantification of BCR expression, washed once with PBS-BSA-Azide buffer and analysed by flow cytometry (Figure 4.21a). 2.4G2 was selected as the CD32 mAb to use for staining as it showed the highest binding to CD32 and although it cross reacts with CD16, B cells do not express this FcγR and therefore the MFI recorded will be due to CD32 binding alone. These data are the average of three repeated experiments. Intriguingly, levels of CD32 and BCR on the Eμ-myc cell lines correlated, $R^2 = 0.6536$ (Figure 4.21b). This implies that as levels of BCR expression increase so does expression of associated regulatory proteins, such as CD32.

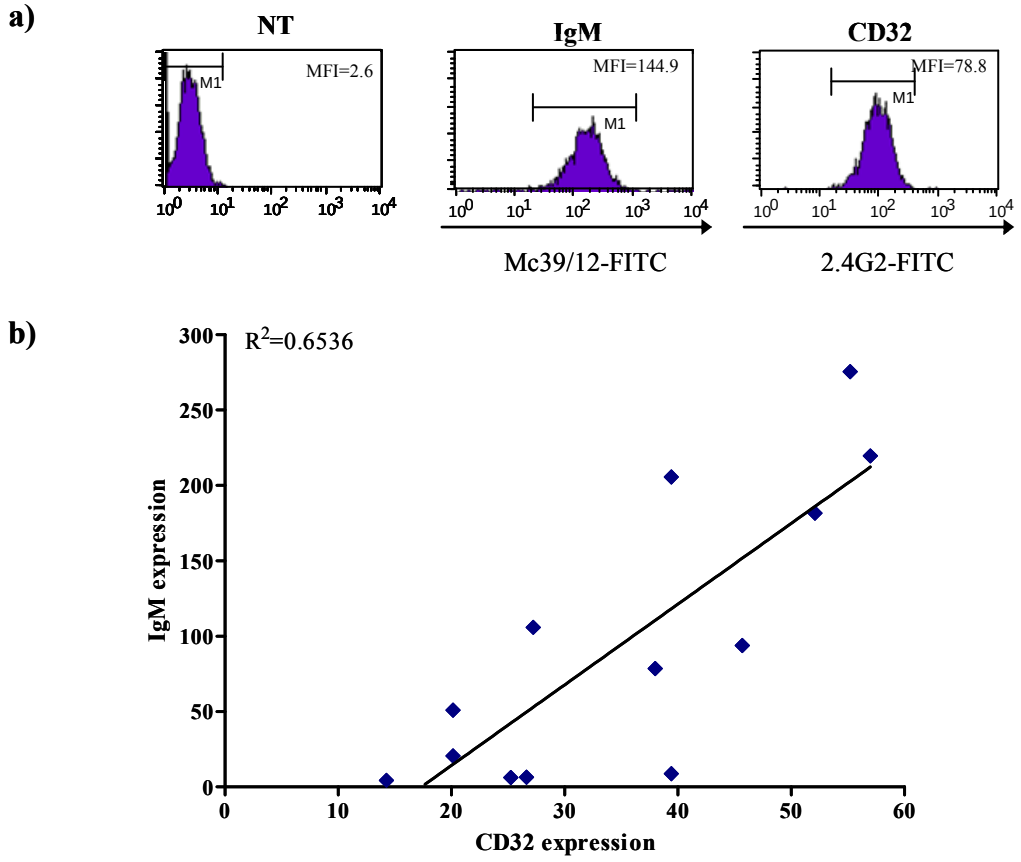

Figure 4.21. Correlation between BCR and CD32 expression on Eμ-myc LCLs.
Eμ-myc cell lines (Eμ#4, 6, 7, 8, 11, 12, 13, 14, 15) were incubated at 4 ˚C for 30 min in the dark with 10 μg/ml of either FITC-conjugated Mc39/12 (anti-IgM) or FITC-conjugated 2.4G2 (anti-CD32). Samples were washed once with PBS-BSA-Azide buffer and analysed by flow cytometry. MFI after staining was compared to an untreated sample (a). The example flow cytometry plots represent the Eμ-myc cell line, Eμ#8. It was shown that IgM expression positively correlated with CD32 expression ($R^2 = 0.6536$) (b). Each dot represents the average of three repeats on each Eμ-myc LCL.

4.6.2. Effects of BCR expression on CD32 induced cell death.

Knowing that BCR and CD32 expression correlated, next we went on to determine whether the presence of the BCR affects CD32-induced PCD. To assess this, data from Figure 4.17 was separated into Eμ-myc cell lines that expressed the BCR (IgM positive) and those that did not (IgM negative). The Eμ-myc LCL responsive to CD32 induced PCD were classed as IgM positive when surface staining of the cells with FITC-conjugated Mc39/12 was greater than 20 (i.e. greater than irrelevant control) (see Table 3.8). These data show that although the PCD induced on the IgM negative cell lines by AT130-2 and AT130-5 was marginally less than on the IgM positive Eμ-myc cell lines, there was no significant difference observed between the two groups (Figure 4.22). This indicates that PCD induced by the AT130-2 and AT130-5 occurred independently of BCR expression and signalling and was most likely due directly to engagement of CD32 on the surface of the cells rather than due to modification of the BCR signals. There was also no significant

difference between PCD induced by AT128, AT128 m2a or 2.4G2 between the IgM positive and IgM negative cell lines (Figure 4.22).

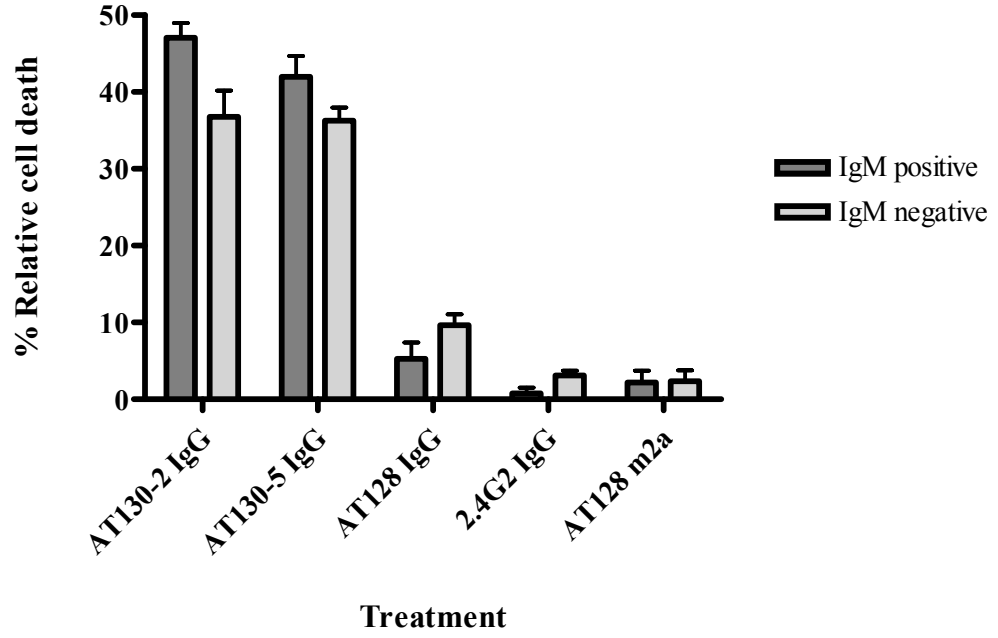

Figure 4.22. Comparison of relative cell death of IgM positive and IgM negative Eμ-myc LCL.
IgM positive Eμ-myc LCL (Eμ#6, 7, 8, 11, 13 and 15) and IgM negative LCLs (Eμ#9, 12 and 14) were incubated with mAb at 10 μg/ml for 24 hr. Where death refers to the percentage of cells that were AnV/PI positive then % relative cell death was calculated as a percentage of the NT sample as detailed in previously. On both the IgM positive and IgM negative cell lines AT130-2 and AT130-5 induce PDC, whilst AT128, AT128 m2a and 2.4G2 have shown relative little effect on PCD on either the IgM positive or IgM negative LCLs. Where there is no significant difference between PCD induced by each of the anti-CD32 mAb on IgM positive and IgM negative cell lines as determined by Student t-test. These data represent results from three experimental repeats, errors expressed as SD.

4.6.3. Additive effect of anti-IgM and anti-CD32 on PCD.

Although the anti-CD32 mAb were able to trigger cell death independent of BCR expression it was speculated whether simultaneous signalling through the BCR might augment or inhibit anti-CD32 induced cell death. The IgM positive Eμ-myc cell line Eμ#8 was incubated with CD32 mAb with the addition of increasing concentrations of polyclonal anti-IgM IgG (gαm IgG) (0.5, 2.5 and 12.5 μg/ml). Cells were incubated for 24 hr under tissue culture conditions, harvested, incubated with AnV/PI as previously described and analysed by flow cytometry. Alone, gαm IgG caused an increase in PCD in a dose dependent manner, indicating that BCR stimulation alone results in cell death. In combination, an increasing dose of gαm IgG and a single dose of AT130-2 or AT130-5 showed a trend towards increasing PCD of Eμ#8 cells, although the additive effect observed was not statistically significant. Interestingly, 2.4G2 seemed to exhibit a slight

reduction in anti-IgM induced PCD on the Eμ#8 cell line, but again this was not significant (Figure 4.23a).

In order to determine if the additive effect observed by stimulation with both anti-IgM and anti-CD32 mAb was a specific effect of BCR involvement, the above described assay was performed on the IgM negative cell line Eμ#14. By comparing an IgM positive cell line (Eμ#8) with an IgM negative cell line (Eμ#14), it can be demonstrated that the additive effect observed is a specific effect of BCR involvement, as the IgM negative cell line did not show enhanced PCD with the addition of gαm IgG (Figure 4.23b). In order to confirm that the additive effect observed was due to BCR stimulation and not Fc engagement of CD32 by the Fc region of the gαm whole IgG, the assay was repeated using an equivalent gαm $F(ab')_2$ fragment. The additive effect observed was similar whether an gαm IgG or a gαm $F(ab')_2$ fragment was used (Figure 4.23c), suggesting that engagement of CD32 by the Fc region of gαm IgG was not the reason for an increase in PCD with anti-IgM alone.

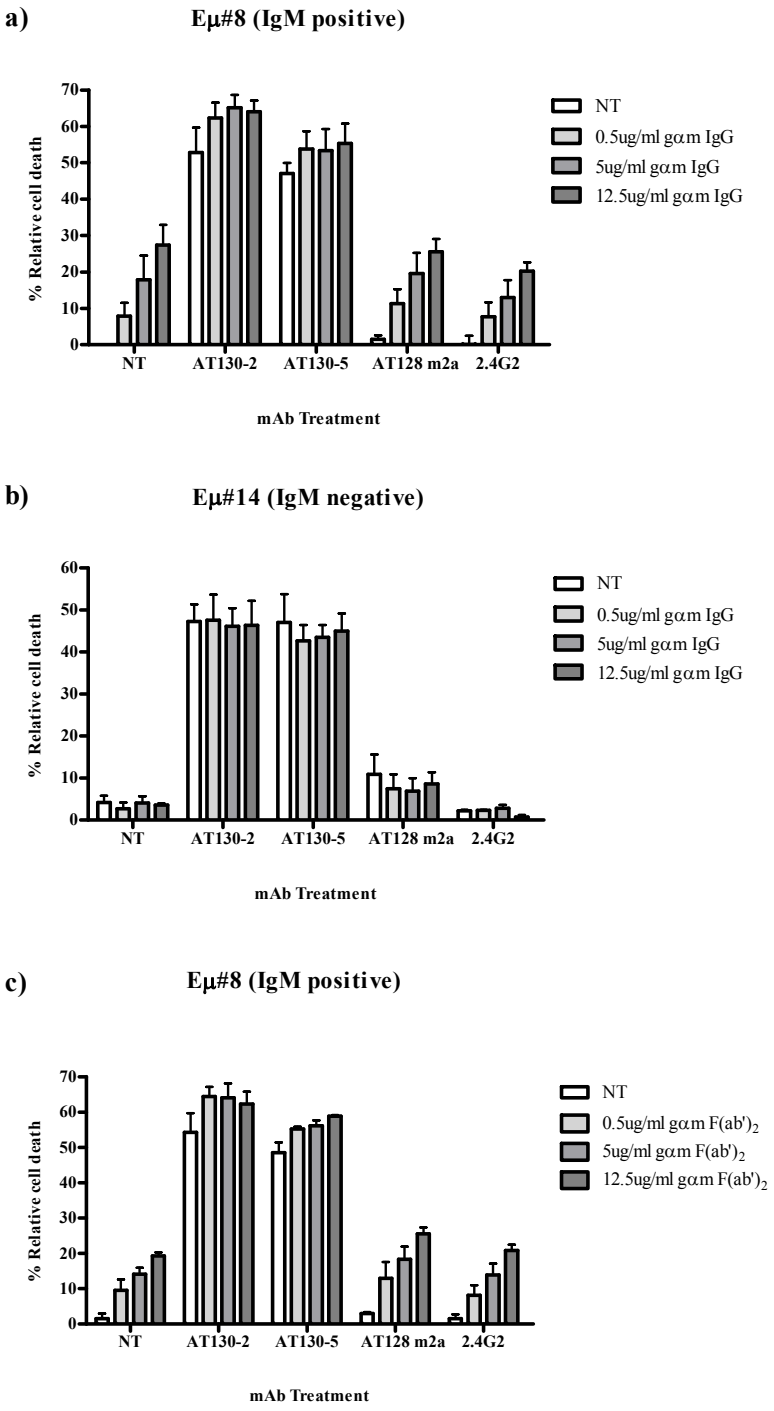

Figure 4.23. Additive effect of anti-CD32 mAb and anti-BCR stimulation on PCD.
Cells were incubated for 24 hr with 10 μg/ml AT130-2, AT130-5, AT128 m2a or 2.4G2 alone or in the presence of 0.5, 2.5 or 12.5 μg/ml anti-IgM, gαm whole IgG or $F(ab')_2$ fragments and then stained with AnV/PI as outlined in Materials and Methods section 2.12.1 to determine % relative death. The Eμ#8 LCL demonstrated an additive effect, where the PCD induced by the anti-CD32 mAb was increased with the addition of gαm whole IgG (a) and $F(ab')_2$ fragments (c). The Eμ#14 LCL, an IgM negative LCL, did not demonstrate an increase in PCD with the addition of anti-IgM (b), suggesting that there was a trend towards increased PCD due to combination between the anti-BCR and anti-CD32 mAb. These data represent results from three experimental repeats, errors expressed as SEM.

4.7. Chapter discussion.

The potential of CD32 as a therapeutic target able to modulate effector cell function and concurrent immunotherapy has, until now, been uncharacterised due to the lack of suitable reagents. However, our newly generated panel of murine specific anti-CD32 mAb are now able to facilitate such investigations. It was postulated that an antibody towards CD32 would function to block CD32 activity and thus augment anti-tumour responses, imitating enhanced immunotherapy observed in CD32 genetic knockout models[83]. Before the *in vivo* efficacy of these mAb was assessed, these mAb were first characterised *in vitro*.

The antibodies demonstrated specific binding to CD32 on WT and FcγRIII$^{-/-}$ splenocytes, but not to CD32$^{-/-}$ splenocytes (Figure 4.1). Further to this, analysis of mAb to CD32 by flow cytometry demonstrated that the anti-CD32 mAb displayed different levels of binding to the receptor (Figure 4.2) and this was confirmed, by BIAcore analysis, to be as a result of diverse antibody affinities (Figure 4.3 and Table 4.1). Further to this, AT130-2 was shown to bind specifically to CD32-CD4 fusion protein, but not to FcγRI-CD4, FcγRIII-CD4 or FcγRIV-CD4 fusion proteins by ELISA (Appendix 3).

Once the specificity and affinity of the anti-CD32 mAb had been established, initial characterisation, through a range of *in vitro* cellular and biochemical assays (summarised in Table 4.2.) on the Eμ-myc and πBcl-1 murine lymphoma cell lines demonstrated that the anti-CD32 mAb fall into two distinct categories; those which caused tyrosine phosphorylation and subsequent activation of the receptor (agonistic anti-CD32 mAb; AT130-2 and AT130-5) and those which block receptor phosphorylation, (antagonistic anti-CD32 mAb, AT128, AT128 m2a and 2.4G2) (Figure 4.7).

The phosphorylation observed with the anti-CD32 mAb, AT130-2 and AT130-5 was similar to that detected by co-ligation of the BCR and CD32 by anti-BCR whole IgG (Figure 4.6 & Figure 4.7), supporting the agonistic activity of these mAb. Alongside this, only whole IgG and not the F(ab')$_2$ fragment of the agonistic anti-CD32 mAb were able to induce phosphorylation of CD32 (Figure 4.10), suggesting that Fc engagement of CD32 by these mAb is required for activation of the receptor. It is not clear at this point whether Fc engagement by the antagonistic mAb was required as these mAb do not phosphorylated the receptor and therefore we could not monitor their activity by Western blot analysis (Figure 4.10).

In addition to phosphorylation of CD32, the agonistic and antagonistic function of the anti-CD32 mAb was further demonstrated by their effect on the phosphorylation of SHIP-1, an essential downstream signalling molecule of CD32 activation, becoming phosphorylated after CD32 activation[312]. Both the anti-BCR antibodies and the agonistic anti-CD32 mAb increased the phosphorylation of SHIP-1 (Figure 4.6, Figure 4.8 & Figure 4.9), where, on the contrary incubation of lymphoma cells with the antagonistic anti-CD32 mAb reduced SHIP-1 phosphorylation. However, pSHIP-1 was also detectable in cells that had not received stimulation through the BCR and CD32 or through CD32 alone. It is thought that there may be constitutive activation of SHIP-1 in unstimulated cells, despite undetectable phosphorylation of CD32. Although SHIP-1 is brought into the BCR:CD32 complex by the activation of CD32, it is phosphorylated by its association with Lyn[317]. Lyn, unlike CD32, has been reported to demonstrate some basal activation in the absence of BCR signalling[408]. In addition, tonic BCR signalling, occurring independently of antigen engagement, has also been demonstrated to occur[409] and this tonic signalling is sufficient to result in ITAM activation (Reviewed in [410]), which might propagate low levels of Lyn signalling. In this way it is possible that tonic BCR signalling could lead to activation of Lyn and as a result elicit basal SHIP-1 phosphorylation. Regardless, changes in pSHIP-1 as a result of incubation with the anti-CD32 mAb were consistent and regardless of tonic SHIP-1 phosphorylation, the divergent agonistic/antagonistic activity of the anti-CD32 mAb is supported by the current knowledge in the literature relating to SHIP-1 activation after CD32 engagement[312,313].

The effect of the IgG1 isotypes on SHIP-1 phosphorylation status was not established on malignant cells. Nevertheless, presuming that AT128 m2a, AT128 and 2.4G2 act similarly and AT130-2 and AT130-5 act similarly as suggested by other *in vitro* assays performed, we extrapolated that AT128 m2a and 2.4G2 activation acts to abrogate SHIP-1 activity, whereas AT130-2 and AT130-5 augment pSHIP-1. Taken together with the phosphorylation data, we were able to demonstrate that the agonistic and antagonistic mAb had divergent functional affects. Fc co-ligation of the BCR with CD32 by the anti-idiotype (Mc106A5) mAb results in a reduced Ca^{2+} flux (Figure 4.13). Next we ascertained that the agonistic mAb were able to block the magnitude and duration of Ca^{2+} signalling triggered by BCR engagement (Figure 4.14b and Figure 4.15a), whilst the antagonistic mAb are able to potentiate these responses (Figure 4.14c). This again was in keeping with an agonistic function of AT130-2 and AT130-5, as CD32 engagement has been demonstrated to inhibit BCR induced Ca^{2+} flux[323]. Alongside this, we once again established the role of the Fc portion of the agonistic anti-CD32 mAb, where the $F(ab')_2$ fragments of both AT130-2 and

AT130-5 were unable to inhibit Ca^{2+} flux (Figure 4.16a & b). Together with this, we were also able to demonstrate that the function of the antagonistic anti-CD32 mAb did not require Fc engagement with CD32, as the $F(ab')_2$ fragments of these mAb were able to augment BCR-induced Ca^{2+} flux (Figure 4.16c & d). Alongside these data and to further confirm the agonistic and antagonistic roles of the downstream signalling of the anti-CD32 mAb, we attempted to examine SHIP-1 phosphorylation after incubation with whole IgG or $F(ab')_2$ fragments of the anti-CD32 mAb. Unfortunately, due to technical difficulties with the detection of pSHIP-1 we were unable to complete these Western blots.

In conjunction with these alterations in Ca^{2+} flux, the agonistic anti-CD32 mAb were shown to trigger PCD, whilst the antagonistic anti-CD32 mAb have relatively little effect on PCD (Figure 4.17). Again it was determined that Fc engagement by the agonistic, but not the antagonistic mAb was required for the induction of lymphoma cell PCD (Figure 4.20). We were able to determine that the induction of PCD by the agonistic mAb was occurring as a direct result of CD32 engagement and that CD32-induced cell death was proportional to and correlated strongly with the level of CD32 expression (Figure 4.19). In addition, we were able to show that the agonistic anti-CD32 mAb were inducing PCD through direct CD32 signalling, as opposed to involvement of BCR co-ligaition. This was illustrated in several experiments. The PCD evoked by agonistic mAb was potentiated by anti-BCR stimulation (Figure 4.23a), but comparisons between IgM positive and IgM negative Eμ-myc LCLs showed that the agonistic anti-CD32 mAb induced PCD independently of BCR expression (Figure 4.22) or co-ligation of the BCR and CD32 (Figure 4.23b & c). Previously, it has been demonstrated by others that co-ligation of CD32 on the surface of target cells, in particular, GC B cells will lead to the induction of apoptosis independent of BCR ligation[333,272]. Here, we have demonstrated that this is also true for the co-ligation of CD32 on the surface of LCLs. Somewhat interestingly, BCR and CD32 expression correlated (Figure 4.21), suggesting that not only is the activity of CD32 linked to the BCR, but also its level of expression. A caveat here is that the correlation between CD32 and BCR expression could be explained by differences in cells size. For instance, a larger cell will have more receptors expressed at the cell surface than a smaller cell. However, analysis of the FSC-H versus SSC-H flow cytometry plots of each Eμ-myc cell line revealed negligibly difference in cell size between the different lymphomas and that smaller and larger cells of the same population expressed similar, if not identical levels of both CD32 and BCR (data not shown). Therefore it is expected that the difference in CD32 and BCR expression was not due to differences in cell size.

It was demonstrated that the anti-CD32 mAb block IC engagement with CD32 as whole IgG, but not as $F(ab')_2$ fragments, albeit to different extents. This is with the exception of 2.4G2 that can block IC binding as a $F(ab')_2$ fragment (Figure 4.5). The ability of these mAb to block Fc engagement by IC is thought to be advantageous in terms of immunotherapy. If co-administered with another therapeutic mAb, such as anti-idiotype for example that utilises FcγR-mechanisms for tumour clearance[27], then the anti-CD32 mAb could potentially block the interaction of the anti-idiotype via Fc domains *in vivo*, as such reducing inhibitory signalling on effector cells and augmenting the anti-tumour response.

Epitope mapping of the anti-CD32 mAb via their Fc suggested that AT130-2 and AT130-5 were able to block binding of each other, but not the binding of the other mAb, whilst the other anti-CD32 mAb were able to block all the anti-CD32 mAb (Figure 4.4). This distinct pattern of cross blocking suggests that the agonistic and antagonistic mAb bind to different epitopes on CD32. More recently, surface plasma resonance experiments on the BIAcore has successfully been employed in epitope mapping of a panel of anti-41BB mAb that were again generated in-house. It is hoped that a similar assay could be implemented to confirm the epitope specificity of the anti-CD32 mAb.

Altogether, data presented here suggests that AT130-2 and AT130-5 bind outside of the Fc binding domain and cross link the receptor by engaging other CD32 molecules via the Fc domain of AT130-2 and AT130-5 through their Fc binding cleft. In contrast, AT128, 2.4G2 and AT128 m2a do not appear to require similar Fc engagement with CD32, however they do block IC binding, suggesting they bind within the Fc binding cleft of CD32 (Figure 4.25). This is confirmed by CD32 phosphorylation studies on πBCL_1 cells at decreasing cell concentrations, where regardless of cell density, phosphorylation of CD32 was comparable with AT130-2 and AT130-5 (Figure 4.12), suggesting that the agonistic anti-CD32 mAb co-ligate via their Fc is a *cis* orientation rather than a *trans* orientation.

In terms of potential immunotherapy, it is proposed that both types of anti-CD32 mAb would have a function *in vivo* to enhance anti-tumour immunotherapy. The agonistic mAb would induce PCD of lymphoma cells, whilst the antagonistic anti-CD32 mAb could block CD32 function on effector cells and enhance ADCC. It has been previously demonstrated that anti-human CD32 mAb require Fc engagement with effector cells to successfully mediate anti-tumour ADCC both *in vitro* and in *in vivo* xenograft models[374]. Therefore

cross linking of CD32 through Fc:CD32 interactions may limit engagement of effector cells by AT130-2 and AT130-5. On the other hand, the Fc domain of AT128 m2a and 2.4G2 does not engage CD32, therefore the Fc domain of these mAb is available to direct anti-tumour ADCC as well as enhance ADCC though their inhibitory activity.

Having determined the activity of the panel of anti-CD32 mAb *in vitro* on malignant B-cells we next investigate their activity on normal B cells and macrophages, in particular the ability of the anti-CD32 mAb to induce effector cell responses.

Table 4.3. Summary of anti-CD32 mAb activity on lymphoma cells *in vitro*.

mAb	pCD32	pSHIP-1	Effect on BCR Ca2+ flux	Induction of PCD
AT130-2	+++	↑	↓	+++
AT130-5	+++	↑	↓	++
AT128	-	↓	↑	+
2.4G2	-	↓	↑	+
AT128 m2a	-	↓	↑	+

Key; ↑: increase; ↓: decrease; +++: high levels of pCD32 or PCD; ++: medium levels of PCD; +: low levels of PDC; -: no induction of pCD32.

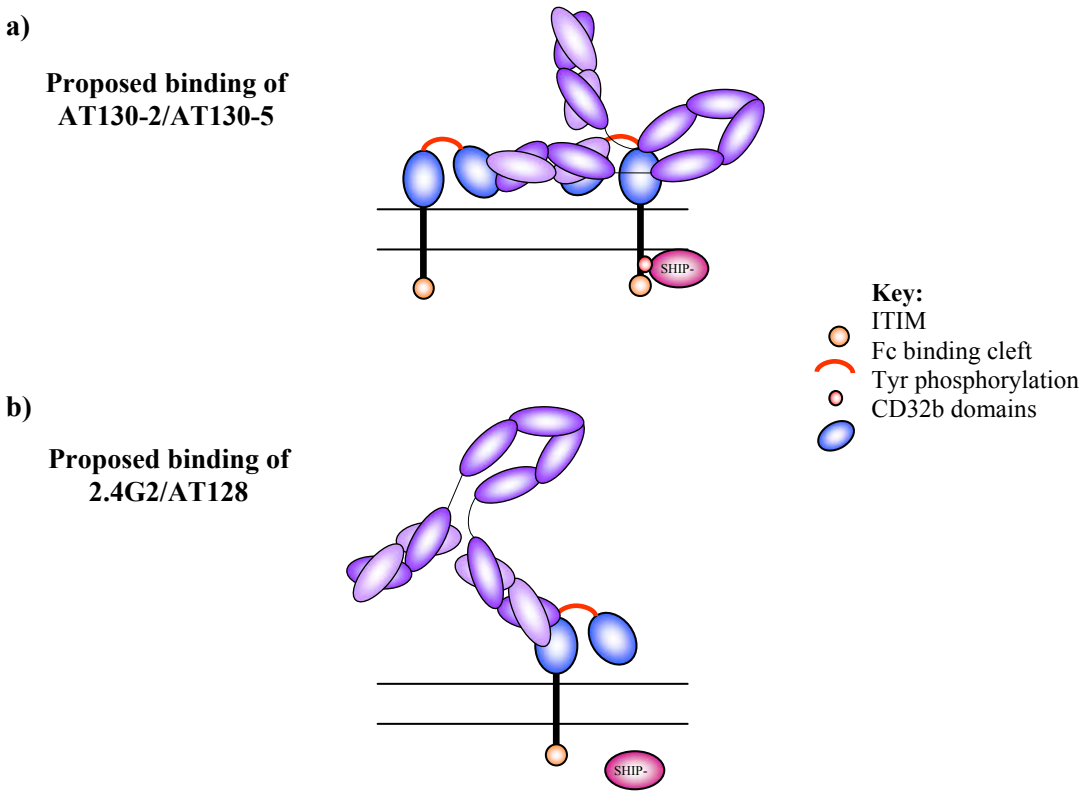

Figure 4.24. Proposed binding of agonistic and antagonistic anti-CD32 mAb.
It is proposed that AT130-2 and AT130-5 bind externally to the Fc binding cleft via CDR regions, engaging CD32 within its Fc binding cleft via their Fc binding domain of C_H2 (a). This leads to tyrosine phosphorylation of SHIP-1. In contrast, AT128, 2.4G2 and AT128 m2a do not require similar Fc engagement with CD32, however, as they do block immune complex binding, suggesting they bind via CDR regions within the Fc binding cleft of CD32 (b).

CHAPTER 5 *In vitro* analysis of anti-CD32 mAb on B cells and macrophages

5.1. Chapter introduction.

In the previous chapter we demonstrated that our panel of anti-CD32 mAb had unique properties with regards to their agonistic and antagonistic activity in lymphoma cells. *In vivo* however, the anti-CD32 mAb would not exclusively bind to tumour cells. Therefore it is important to ascertain the functional effects of receptor engagement on other cell types that express CD32, principally normal B cells and macrophages. In addition, if the anti-CD32 mAb induce cell death of B cells and macrophages in similar ways to lymphoma cells this may lead to unhelpful side effects, such as the patient becoming immunocompromised and being unable to mount an effective anti-tumour response. Consequentially, a good therapeutic agent would ideally be able to target the deletion of tumour cells, but not alter significantly the physiology of the endogenous cells (at least in a negative capacity). It has been suggested that reducing the endogenous function of CD32 on effector cells by either blocking CD32 or through an appropriate mAb isotype selection would facilitate enhanced effector cell responses by reducing the inhibitory effects of this receptor[83].

Hence, we next went on to establish whether the anti-CD32 mAb would have similar activity on normal B cells, isolated from the spleens of C57BL/6 and BALB/c mice and also on BMDMs. Assays were performed on cells from both C57BL/6 and BALB/c backgrounds as it was intended to subsequently assess the anti-CD32 mAb in the Eμ-myc (C57BL/6) and πBCL_1 (BALB/c) *in vivo* models of lymphoma. We performed similar experiments to those previously described in Chapter 4 in order to assess the effect of the anti-CD32 mAb on normal murine cells *in vitro*. In addition, we sought to discover if the anti-CD32 mAb were able augment effector cell activity, such as those required for an anti-tumour responses, i.e. phagocytosis.

5.2. *In vitro* effects of anti-CD32 mAb on normal B cells.

In order to examine the *in vitro* effects of the anti-CD32 mAb on normal B cells, B cells were isolated by MACS® separation as previously described (Materials and Methods section 2.4). The purity of the B cell yield was assessed by flow cytometry by staining with FITC-conjugated IgM (Mc39/12) and PE-conjugated CD19 (ID3). MACS separation

yielded a greater than 95 % pure B cell population as demonstrated by CD19 and IgM dual positivity (Figure 5.1a). In addition, it was also shown that the purified B cells expressed CD32, as shown by staining with FITC-conjugated AT130-2 and PE-conjugated CD19. The expression of CD32 on B cells was equivalent to CD32 expression on the Eμ-myc LCLs (Figure 5.1b).

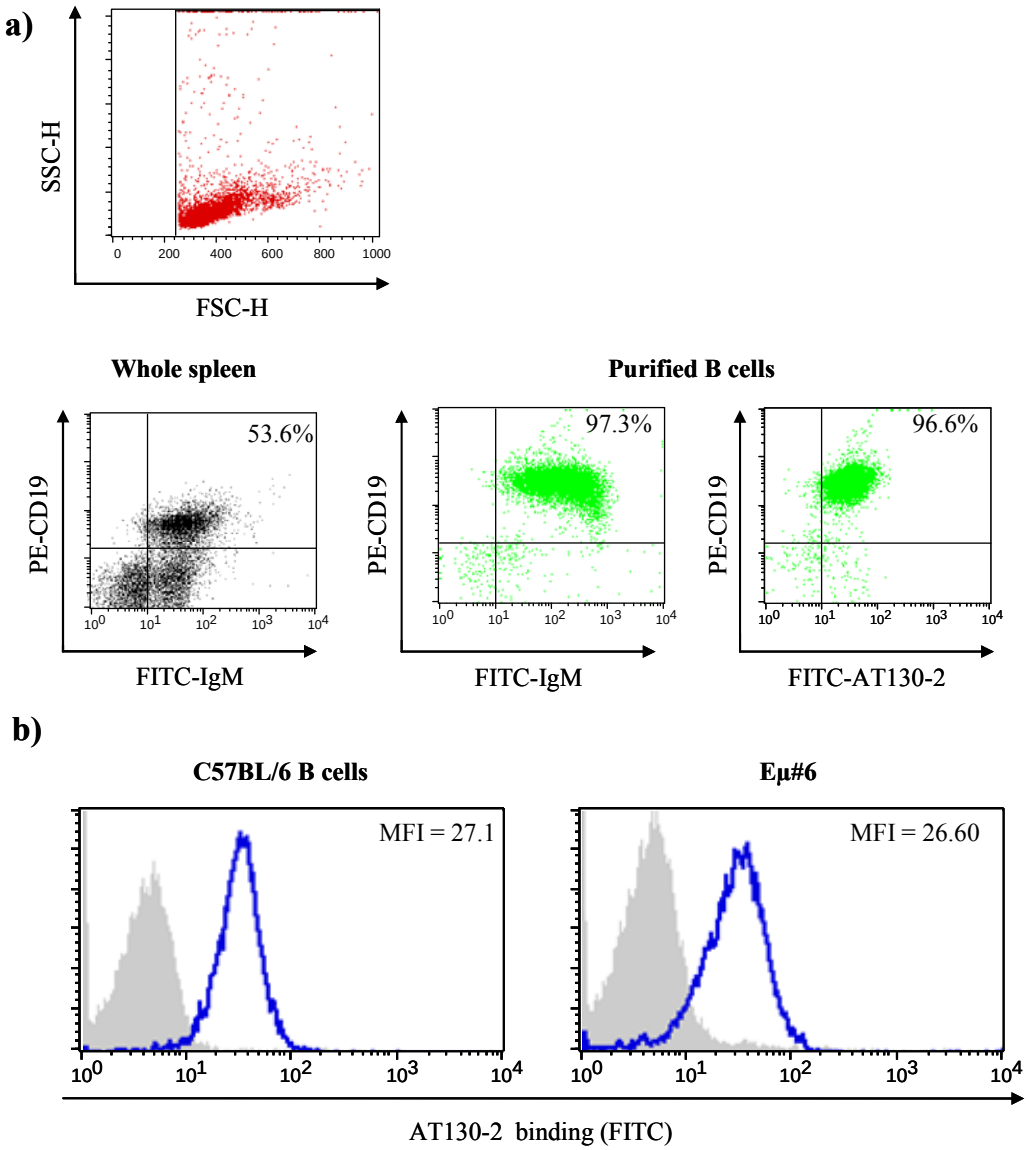

Figure 5.1. Purification of splenic B cells and their expression of CD32.
B cells from the spleen of C57BL/6 and BALB/c mice were purified using negative selection MACS® separation. The purity of the B cell population was assessed by direct flow cytometry, approximately 1 x 10^6 cells were incubated for 15 min, in the dark at room temperature with 10 μg/ml FITC-conjugated Mc39/12 (IgM) and PE-conjugated CD19 (a) The derived B cell population, as demonstrated by CD19 and IgM dual positivity, was greater than 95 % of the total cells recovered from MACS® separation. The expression of CD32 on B cells was also assessed by direct flow cytometry using FITC-conjugated AT130-2 (b). The CD32 expression on the purified B cell population was equivalent to the CD32 expression on lymphoma cells.

5.2.1. Tyrosine phosphorylation of CD32 and SHIP-1 on normal B cells.

Having established that normal B cells express CD32 and that this expression is at equivalent levels to lymphoma cells, we next went on to examine the signalling properties of the anti-CD32 mAb on normal B cells isolated from BALB/c and C57BL/6 mice. 2.5 x 10^6 purified B cells / ml (in 2 ml) were cultured at 37 °C, 10 % CO_2 with 10 µg/ml anti-CD32 for 0.5, 2, 5 and 15 min, lysates prepared and analysed by Western Blotting. On B cells purified from BALB/c mice, AT130-2 and AT130-5 induced phosphorylation of CD32 at 0.5 min and this was sustained until 15 min, where in contrast neither AT128 m2a or AT128 induced phosphorylation of CD32 (Figure 5.2). Equally, on B cells purified from C57BL/6 mice, AT130-2 and AT130-5, but not AT128 m2a or AT128 induced phosphorylation of CD32 at 0.5 min and this was sustained at 15 min (Figure 5.3). Previously we observed that, AT130-2 and AT130-5 caused tyrosine phosphorylation of CD32 on lymphoma cell lines (Figure 4.7). These data show that AT130-2 and AT130-5 induced similar tyrosine phosphorylation of CD32 and with similar kinetics to those observed on the lymphoma cell lines. Similarly, AT128 did not induce phosphorylation of CD32. It must be noted that phosphorylation with AT130-5 appear greater than with AT130-2 on these blots (Figure 5.2 & 5.3). This is likely due to differences between the membranes, i.e. differences in protein transfer or in exposure time upon development in the Xograph Compact X4 film processor. When samples for AT130-2 and AT130-5 were run alongside each other, on the same Western blotting gel, the intensity of CD32 phosphorylation was equivalent (data not shown).

Previously we also observed that in lymphoma cells the agonistic mAb demonstrated an increase in SHIP-1 phosphorylation and the antagonistic mAb inhibited SHIP-1 phosphorylation (Figure 4.8). The result with normal B cells regarding the observations of SHIP-1 phosphorylation were more difficult to interpret. On lymphoma cells we observed changes in pSHIP-1 after 0.5 min and these changes were maintained at 15 min stimulation, with both AT130-2 (increased pSHIP-1) and AT128 m2a (decreased pSHIP-1). In C57BL/6 B cells AT130-2 increased pSHIP-1 after 0.5 min, but this increased further at 2 min and had decreased again by 15 min. In contrast to AT128 m2a stimulation on lymphoma cells, AT128 m2a treatment of C57BL/6 B cells resulted in an increase in pSHIP-1 at 2 min, sustained at 5 min, but returned to background pSHIP-1 levels at 15 min. Therefore, although the trend of activation with AT130-2 and relative cell signalling with AT128 m2a was observed, the kinetics were clearly altered. In BALB/c B cells, activation of pSHIP-1 occurred more slowly, observed only after 2 min stimulation and returned to less than the NT level of phosphorylation by 15 min (Figure 5.4). In addition,

the inhibition observed with AT128 m2a stimulation in normal B cells is less marked than in lymphoma cells and in B cells there seems to be an increase rather than a decrease in SHIP-1 phosphorylation. This suggests that the anti-CD32 mAb induce similar signalling in lymphoma and B cells, but to different extents and with different kinetics.

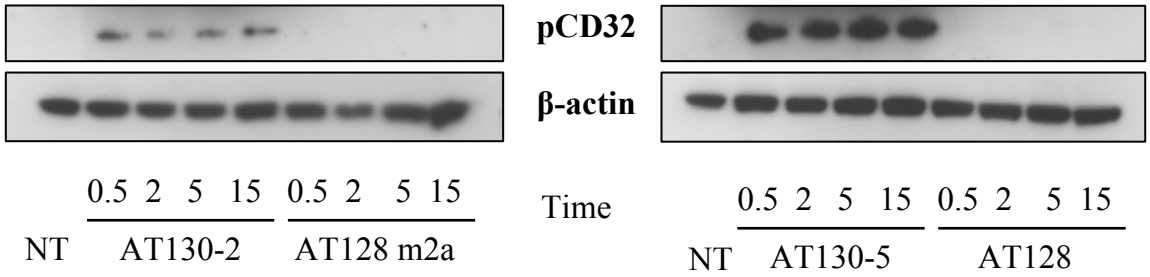

Figure 5.2.Tyrosine phosphorylation of CD32 in C57BL/6 splenic B cells.
B cells were isolated from the spleens of C57BL/6 mice using MACS® separation. Cells were plated at 2.5 x 10^6 cells / ml and incubated with the relevant anti-CD32 mAb at 10 µg/ml for the above stated period, lysates prepared and samples analysed by Western blot. AT130-2 and AT130-5 induced phosphorylation of CD32, whilst AT128 m2a and AT128 did not cause phosphorylation of CD32. Data is a representative result from three repeats.

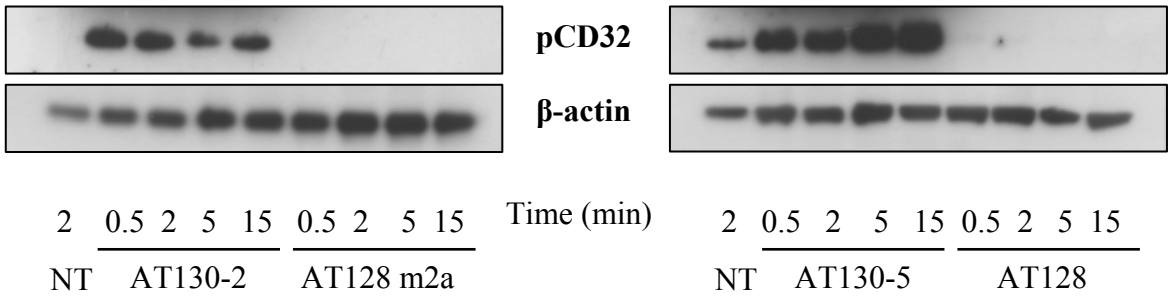

Figure 5.3. Tyrosine phosphorylation of CD32 in BALB/c splenic B cells.
B cells were isolated from the spleens of BALB/c mice using MACS® separation. Cells were plated at 2.5 x 10^6 cells /ml and incubated with the relevant anti-CD32 mAb at 10 µg/ml for the above stated period, lysates prepared and samples analysed for pCD32 and β-actin by Western blot. AT130-2 and AT130-5 induced phosphorylation of CD32, whilst AT128 m2a and AT128 did not cause phosphorylation of CD32. Data is a representative result from three repeats.

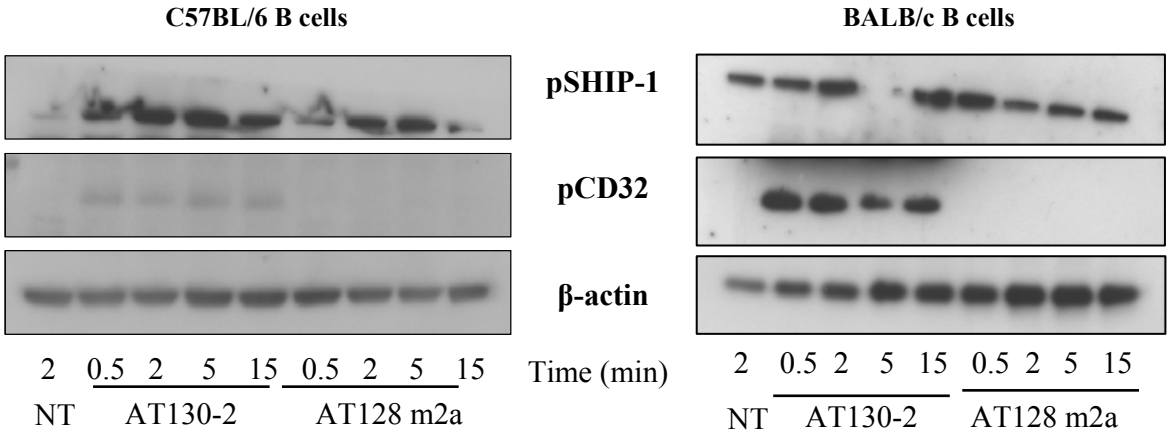

Figure 5.4. Tyrosine phosphorylation of CD32 and SHIP-1 in C57BL/6 and BALB/c splenic B cells. B cells were isolated from the spleen of C57BL/6 and BALB/c mice using MACS® separation. Cells were plated at 2.5 x10^6 cells / ml and incubated with the relevant anti-CD32 mAb for the above stated period, lysates prepared and samples analysed for pSHIP-1, pCD32 and β-actin by Western blot. AT130-2 causes an increase in pCD32, whilst AT128 m2a does not in both C57BL/6 and BALB/c splenic B cells. However, both cause an increase in tyrosine phosphorylation of SHIP-1 in C57BL/6, albeit to different extents and with different kinetics. In BALB/c splenic B cells AT130-2 increased pSHIP-1, whilst AT128 m2a decreased SHIP-1. Data is a representative result from three repeats.

5.2.2. Effect of anti-CD32 mAb on BCR-induced Ca^{2+} flux.

Next, we went on to examine the effects of pre-incubation with the anti-CD32 mAb on BCR-induced Ca^{2+} flux. In these experiments, purified B cells were stained with Fluo-3-AM, pre-incubated with 50 μg/ml AT130-2, AT130-5, AT128 m2a or 2.4G2 for 15 min, then analysed by flow cytometry for 15 sec to establish a baseline, before stimulation with 5 μg/ml Mc39/12 IgG for a further 2 min and 45 sec. On normal B cells BCR stimulation with Mc39/12 induced a sustained Ca^{2+} flux. However, unlike in lymphoma cells, there was no effect on the BCR-induced Ca^{2+} flux when cells were pre-incubated with the anti-CD32 mAb (Figure 5.4); i.e. AT130-2 and AT130-5 did not inhibit BCR-induced Ca^{2+} flux and AT128 m2a and 2.4G2 did not augment BCR-induced Ca^{2+}. These data, alongside the tyrosine phosphorylation of SHIP-1 suggests that the anti-CD32 mAb induce different signalling and functional effects in normal B cells in comparison to lymphoma cells.

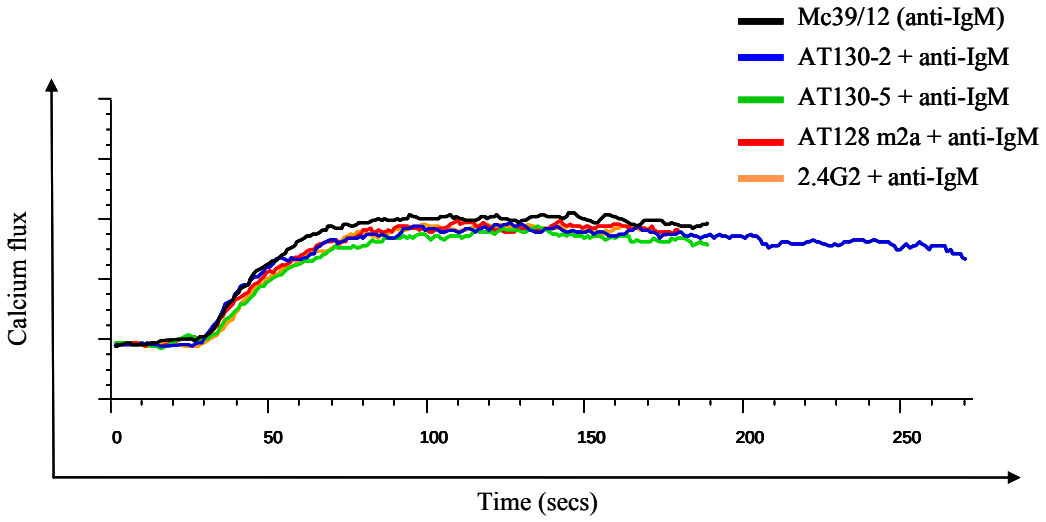

Figure 5.5. The effect of anti-CD32 mAb on BCR-induced calcium flux in normal splenic B cells. Purified B cells from the spleen of C57BL/6 mice isolated by MACS, were stained with the intracellular dye, Fluro-3-AM and pre-incubated with 50 µg/ml AT130-2, AT130-5, AT128 m2a or 2.4G2 for 15 min and analysed by flow cytometry for 2 min 45 sec after the addition of 5 µg/ml Mc39/12 (monoclonal anti-IgM) and results were analysed using FlowJo™ software. None of the anti-CD32 mAb had a substantial effect on BCR-induced Ca^{2+}. Data is a representative result from three repeats.

5.2.3. Induction of programmed cell death on B cells by anti-CD32 mAb.

Subsequently, we wanted to discover how the differences in manipulation of pSHIP-1 and Ca^{2+} flux would affect the induction of PCD in normal B cells. As previously described, 1 x 10^6 purified B cells / well were incubated with 10 µg/ml anti-CD32 mAb at 37 °C, 10% CO_2 for 24 hr, stained with AnV/PI and assessed by flow cytometry and the percentage relative death calculated. It was observed that AT130-2 induced low levels of PCD (7 to 15 %) in both splenic B cells from C57BL/6 and BALB/c mice. However, the induction of PCD by AT130-2 on normal B cells was not significantly different than that induced with the isotype counterparts, AT128 m2a (by Student's t-test). In these experiments AT130-5 did not induce cell death in B cells from either C57BL/6 or BALB/c mice. Alongside this, the antagonistic anti-CD32 mAb, AT128, AT128 m2a or 2.4G2, induced negligible PCD (Figure 5.6a).

For comparison, the levels of PCD induced in πBCL_1 cells was compared with the PCD induced in B cells from BALB/c mice (Figure 5.6b) and PCD induced in the LCL Eµ#8 was shown together with PCD in B cells from the C57BL/6 mice (Figure 5.6c). It was shown that there was a significantly higher PCD induced by the agonistic anti-CD32 mAb in the lymphoma cell in contrast with normal splenic B cells (AT130-2; $p < 0.05$ and $p < 0.01$ for πBCL_1 versus BALB/c B cells and Eµ#8 versus C57BL/6 B cells, respectively and for AT130-5; $p < 0.01$ for both comparisons). Altogether these data indicate that splenic B cells are less susceptible to PCD induced by CD32 engagement than lymphoma cell lines.

The properties of the anti-CD32 mAb on normal B cells are summarised in Table 5.1 (C57BL/6) and Table 5.2 (BALB/c).

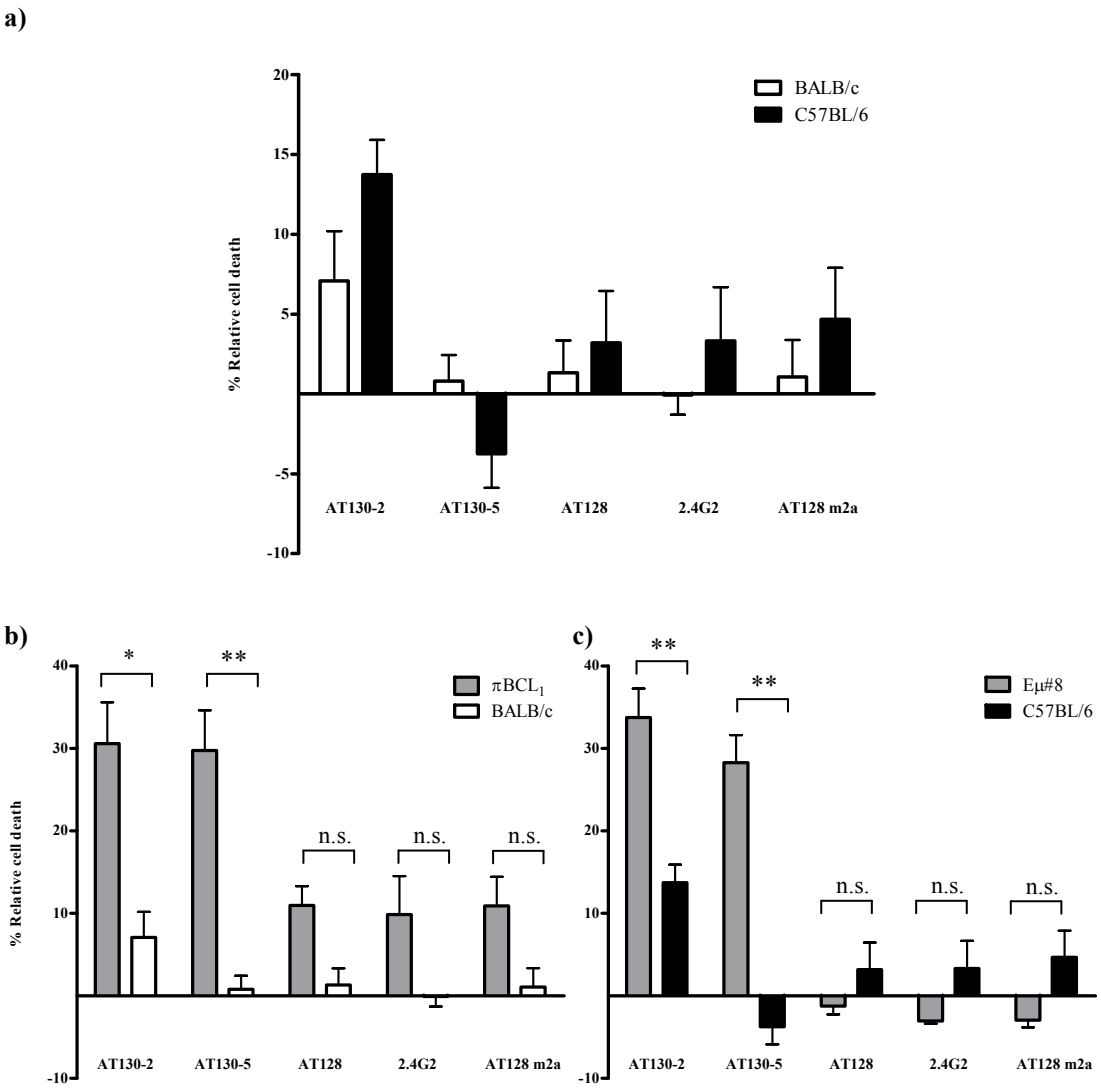

Figure 5.6. Induction of programmed cell death by the anti-CD32 mAb in normal splenic B cells and comparison with lymphoma cell lines.
B cells isolated from BALB/c and C57BL/6 mice or the πBCL_1 and Eμ#8 LCLs The were incubated with mAb at 10 μg/ml for 24 hr and PCD assessed using the AnV/PI assay. The percentage PCD was calculated as the % AnV/PI positive compared to control. In these experiments, the anti-CD32 mAb hade relatively little effect on PCD in normal splenic B cells, although there is some induction of PCD by AT130-2 (a). In πBcl_1 (b) and Eμ#8 (c) cells AT130-2 and AT130-5 induced PCD whilst AT128, AT128 m2a and 2.4G2 have relative little effect on PCD. The induction of PCD by AT130-2 on normal splenic B cells was significantly less than the induction of PCD on πBCL_1 and Eμ#8 LCLs; * $p < 0.05$; ** $p < 0.01$; n.s.: no significance by Student's t-test. These data represent results from three experimental repeats, errors expressed as SEM.

5.2.4. Summary of anti-CD32 mAb activity in splenic B cell.

Table 5.1. Summary of anti-CD32 mAb properties in normal splenic B cells from C57BL/6 mice.

mAb	pCD32	pSHIP-1 (@ 2 mins)	Alter BCR Ca^{2+}	PCD
AT130-2	↑	↑	NC	↑
AT130-5	↑	ND	NC	NC
AT128	NC	ND	NC	NC
2.4G2	NC	ND	NC	NC
AT128 m2a	NC	↑	NC	NC

Key; ↑: increase; NC: no significant change; ND; no data.

Table 5.2. Summary of anti-CD32 mAb properties in normal splenic B cells from BALB/c mice

mAb	pCD32	pSHIP-1 (@ 2min)	Alter BCR Ca^{2+}	PCD
AT130-2	↑	↑	ND	↑
AT130-5	↑	ND	ND	NC
AT128	NC	ND	ND	NC
2.4G2	NC	ND	ND	NC
AT128 m2a	NC	↓	ND	NC

Key; ↑: increase; ↓: decrease; NC: no change; ND; no data.

5.3. *In vitro* effect of anti-CD32 mAb in BMDMs.

As well as establishing the affects of the anti-CD32 mAb on normal B cells, it is also important to assess the direct targeting effects the anti-CD32 mAb will have on effector cells, such as macrophages. Macrophages were isolated from the bone marrow of C57BL/6 and BALB/c mice, denoted bone marrow derived macrophages or BMDMs. The BMDMs were cultured at 37 °C, 5 % CO_2 in the presence of L929 cell supernatant, which contains M-CSF as described in Materials and Methods section 2.2. After approximately 7 days in culture a differentiated macrophage population was observed, as indicated by changes in cell morphology (Figure 5.7). First, we assessed the expression of CD32 on these macrophage populations. We were able to establish that the anti-CD32 mAb were able to bind to both C57BL/6 and BALB/c macrophages (Figure 5.8), by flow cytometry

and that the level of expression of CD32 on BMDMs is similar to that on lymphoma and B cells (Figure 5.1).

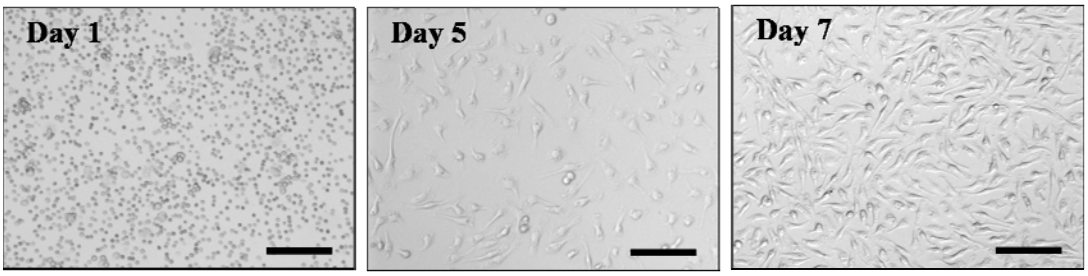

Figure 5.7. BMDM differentiation during adaption to culture
5 x 10^6 cells isolated from the bone marrow of C57BL/6 mice were culture in enriched RPMI-1640 and 20 % L929 cell conditioned medium (see Material and Methods section 2.2) in 6-well tissue culture plates. Bright field microscopy images were obtained at X10 magnification to demonstrate changes in cell morphology over a seven day period, demonstrating differentiation from small, round cells (day 1) to fully confluent flat, elongated cells (day 7). Scale bar represents 10 µm.

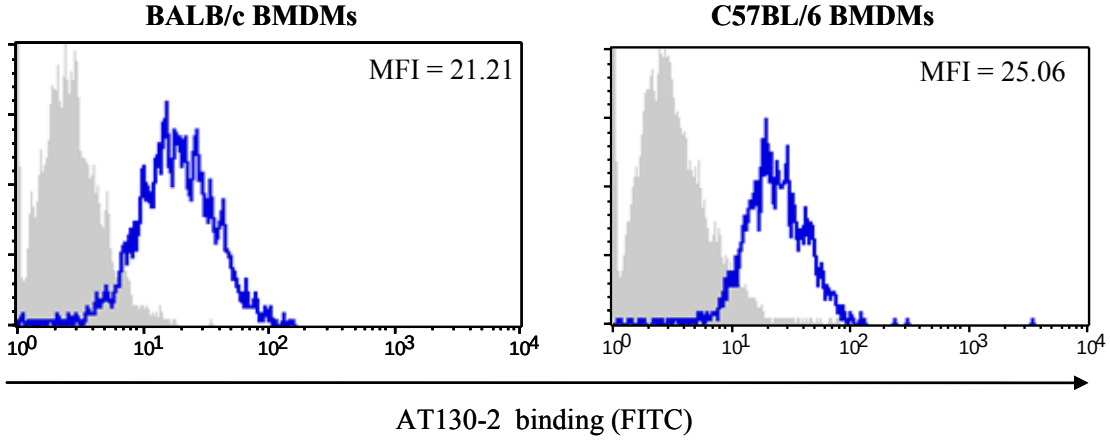

Figure 5.8. Expression of CD32 on C57BL/6 and BALB/c BMDMs.
1 x 10^6 BMDM from C57BL/6 and BALB/c mice were incubated for 15 min, in the dark at room temperature with 10 µg/ml APC-conjugated F480 and 10 µg/ml FITC-conjugated anti-CD32 mAb, washed once with PBS-BSA-Azide buffer and analysed by flow cytometry. Again, the expression of CD32 on BMDMs was similar to CD32 expression on lymphoma cells and splenic B cells.

5.3.1. Tyrosine phosphorylation of CD32 and SHIP-1 in BMDMs.

Next we wanted to determine whether the anti-CD32 mAb would cause activation of CD32 similar to that demonstrated on lymphoma and B cells. To assess this, 2.5 x 10^6 cells / ml BALB/c BMDMs were incubated with 10 µg/ml anti-CD32 mAb for 0.5, 2, 5 and 15 min, lysates prepared and samples analysed by Western blotting (Figure 5.9). Here, the agonistic mAb (AT130-2) induced tyrosine phosphorylation of CD32 whilst the antagonistic mAb (AT128 m2a) did not, similar to that observed on both normal B cells and lymphoma cell lines. However, in contrast with the lymphoma and normal B cells, the phosphorylation of CD32 was much more transient in BMDMs. On cells of lymphoid

lineage CD32 phosphorylation was sustained at 15 min, however on BMDMs CD32 phosphorylation had decreased to almost background levels by 15 min. SHIP-1 phosphorylation on the BMDMs follows the same pattern as CD32 phosphorylation, which is again transient in comparison to that observed on the lymphoma cell lines. Furthermore, the agonistic mAb increased phosphorylation of SHIP-1 and the antagonistic mAb decreased phosphorylation of SHIP-1 (Figure 5.9); similar to the action of these mAb on lymphoma cell lines.

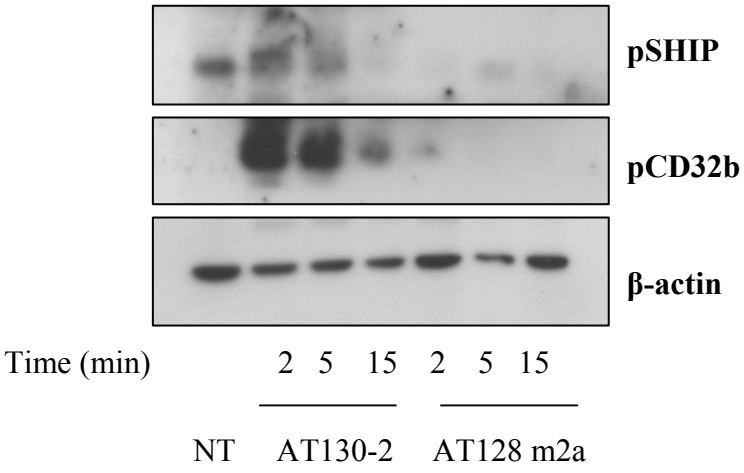

Figure 5.9. Tyrosine phosphorylation of CD32 and SHIP-1 on BMDMs.
BMDMs derived from BALB/c mice were plated at 2.5 x 10^6/ml and incubated with the anti-CD32 mAb for 0.5, 2, 5 or 15 min, protein lysates prepared and samples analysed for pCD32 and pSHIP-1 by Western blot. AT130-2 induced phosphorylation of CD32 and SHIP-1, whilst AT128 m2a did not cause phosphorylation of CD32 and SHIP-1. Data is a representative result from three repeats.

5.3.2. Induction of programmed cell death on BMDMs by anti-CD32 mAb.

We next went on to ascertain whether the anti-CD32 mAb induced PCD of BMDMs. Briefly, 2 x 10^6 cell/ml in a 48-well plate were incubated for 24 hr under tissue culture conditions with 10 μg/ml anti-CD32 mAb. NB; in these experiments 2.4G2 was excluded as this mAb also interacts with CD16 expressed by macrophages. Cells were stained in the tissue culture plate with AnV/PI as previously described, harvested by incubation with TE for 10 min at 37 °C, assessed by flow cytometry and the percentage relative cell death calculated. Surprising, the induction of PCD by the agonistic and antagonistic mAb in the BMDMs was equivalent. Here, all the anti-CD32 mAb induced comparable levels of PCD in the BMDMs and there was a trend towards greater induction of PCD on BMDMs than that observed in normal B cells (Figure 5.10). However, the induction of PCD on BMDMs was not significantly different to that induced on normal B cells. We would suggest that this may be because of variation between experimental repeats.

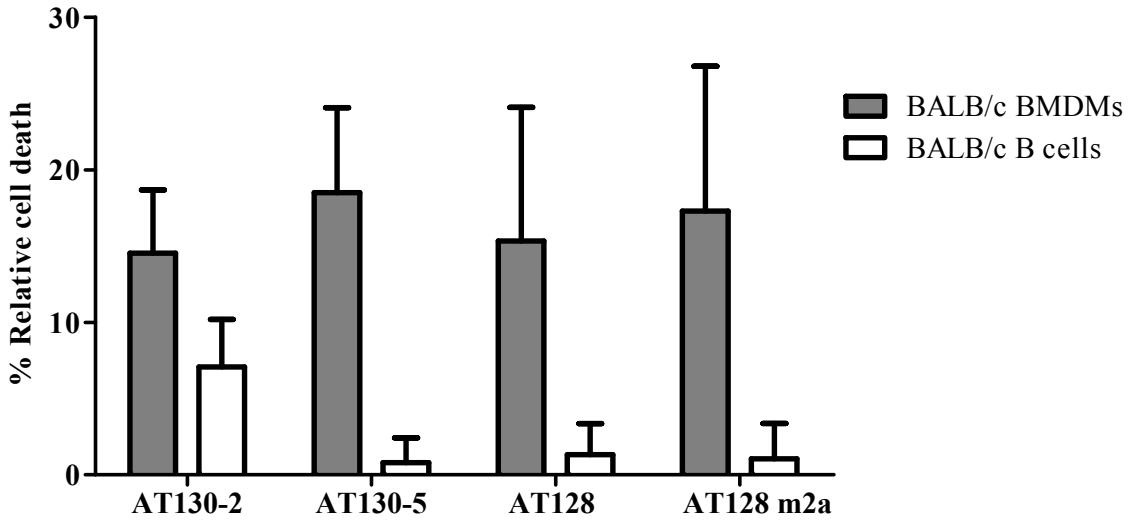

Figure 5.10. Induction of PCD by the anti-CD32 mAb on BMDMs.
200 µl of BMDMs at 2 x 10^6 cell/ml in a 48-well plate were incubated for 24 hr under tissue culture conditions with 10 µg/ml anti-CD32 mAb. Cells were stained with AnV/PI as previously described, harvested by incubation with TE for 10' at 37 °C, assessed by flow cytometry and the percentage relative cell death calculated. The agonistic and antagonistic anti-CD32 mAb do not show differential activity and induce equivalent levels of PCD on BMDMs. The level of PCD induced in BMDMs (n = 4) appears to be greater than that induced on normal B cells (n = 3), although this was not significant (by Student's t-test), presumably due to variation between experiments for the BMDMs. These data represent results from four experimental repeats for BMDMs and three experimental repeats for B cells, errors expressed as SEM.

5.4. The anti-CD32 mAb induce phagocytosis of opsonised B cells by BMDMs.

Macrophages have been demonstrated to be key regulators of the anti-tumour response *in vivo*, particularly in response to mAb therapy (see Introduction section 1.3.3). Having determined that the anti-CD32 mAb were able to engage with CD32 on the surface of cultured BMDMs, but that they did not induce high levels of PCD, we went on to establish whether target cells coated with anti-CD32 mAb were able to interact with effector cells. Here we used phagocytosis as a measure of macrophage engagement, as this is one of the major mechanisms by which effector cells, such a macrophages aid in the clearance of tumour cells.

5.4.1. The anti-CD32 mAb induce phagocytosis of opsonised B cells.

In order to measure phagocytosis, we cultured 5 x 10^4 BMDM / well in 96-well plates at 37 °C, 5 % CO_2 for 2 hr. Concurrently, CD20 Tg B cells were purified, stained with 5 µM CFSE and opsonised by incubation for 20 min at room temperature with 10 µg/ml anti-CD32 mAb or anti-CD20 mAb (as a positive control). 2.5 x 10^5 purified, CFSE labelled and opsonised CD20 Tg B cells were then incubated with the BMDMs for 1 hr under the

same tissue culture conditions. These were then harvested, stained with APC-conjugated F480 to identify macrophages for 15 min at room temperature, washed, before being harvested and analysed by flow cytometry for the percentage of dual positive (F480 and CFSE) cells. A schematic of the phagocytosis assay is shown in Figure 5.10. Routinely, viable cell lymphocyte and macrophage events were collected, as identified by the FSC-H and SSC-H threshold parameters and 5000 macrophage (APC-conjugated $F480^{+}$) cells were collected for analysis (Figure 5.11).

CD20 Tg B cells were used for the phagocytosis assays as previous work in our laboratory has demonstrated that the anti-CD20 mAb, such as B1, rituximab and rit m2a, are able to induce phagocytosis of opsonised B cells[364] and served as positive controls for the assay. The phagocytosis assays were performed using BMDMs and purified CD20 Tg B cells on the BALB/c background.

There were no double positive events recorded when BMDMs were not incubated with B cells and there was a low level of double positive events recorded when non-opsonised B cells were incubated with the BMDMs (Figure 5.12a & c). In contrast, these data demonstrate specific engulfment of CD20 Tg B cells opsonised with both anti-CD20 and anti-CD32 mAb, with the exception of AT128 m2a. Together, these data indicated that most of the anti-CD32 mAb were able to directly target the B cells towards the BMDMs. However, the level of phagocytosis induced by the anti-CD20 mAb was greater than that induced by the anti-CD32 mAb. In the case of AT128 m2a, we have previously shown that this mAb binds CD32 weakly and has a low affinity for CD32 and this is a likely explanation as to why AT128 m2a was unable to induce a significant amount of phagocytosis. Phagocytosis can also be examined microscopically, as demonstrated by Figure 5.12b, where an unlabelled BMDM can be seen engulfing CFSE labelled B cells (Figure 5.12b; courtesy of Dr Stephen Beers, University of Southampton).

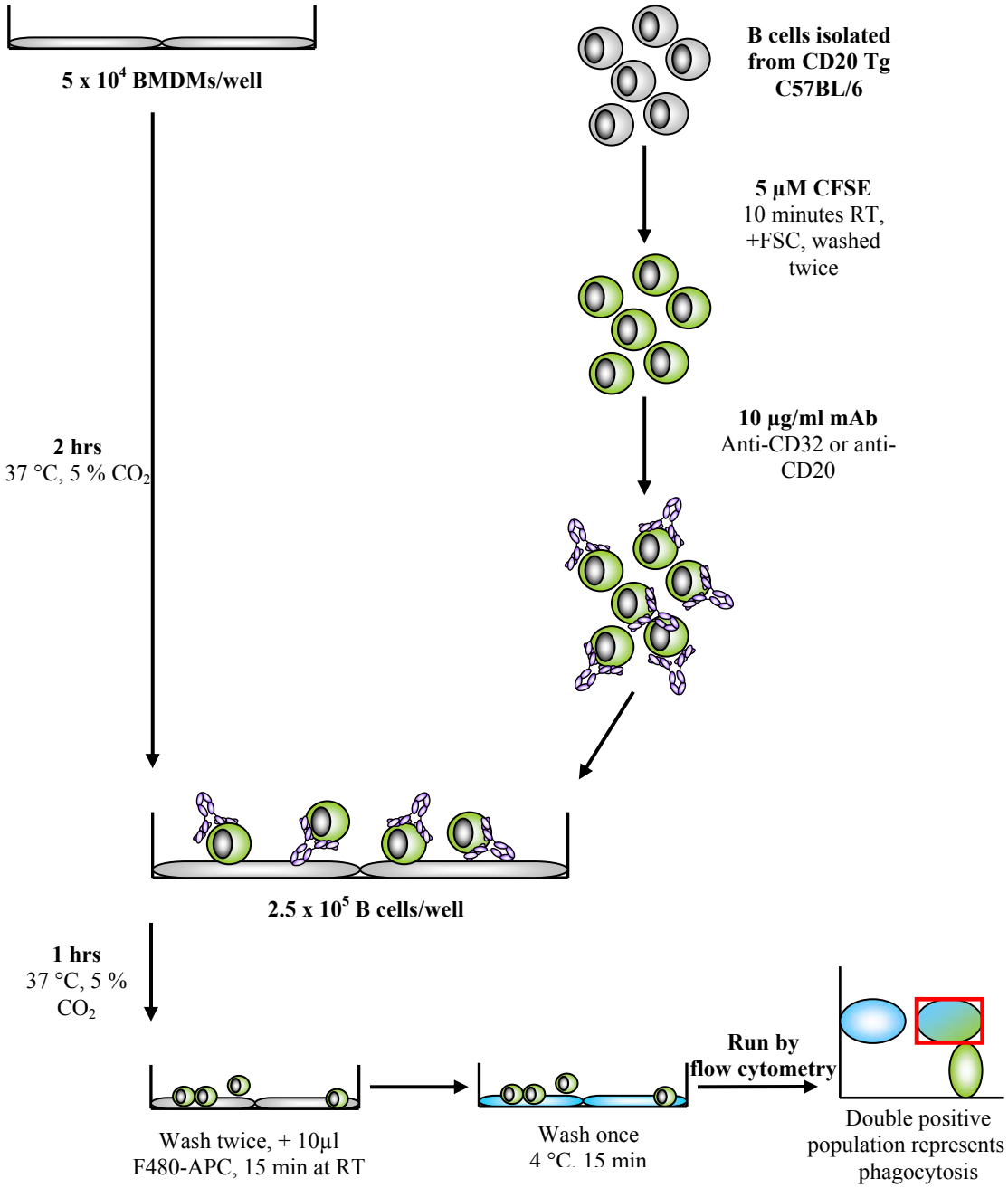

Figure 5.11. Schematic of the phagocytosis assay.
5 x 10^4 BMDM / well were incubated in 96-well plates at 37 °C, 5 % CO_2 for 2 hr before the addition of 2.5 x 10^5 purified, CFSE labelled and opsonised CD20 Tg B cells for 1 hr under the same tissue culture conditions. These were then harvested, stained with 10 µl of 1:10 diluted APC-conjugated macrophage marker F480 for 15 min at room temperature, washed once with PBS-BSA-Azide buffer before being harvested and analysed by flow cytometry.

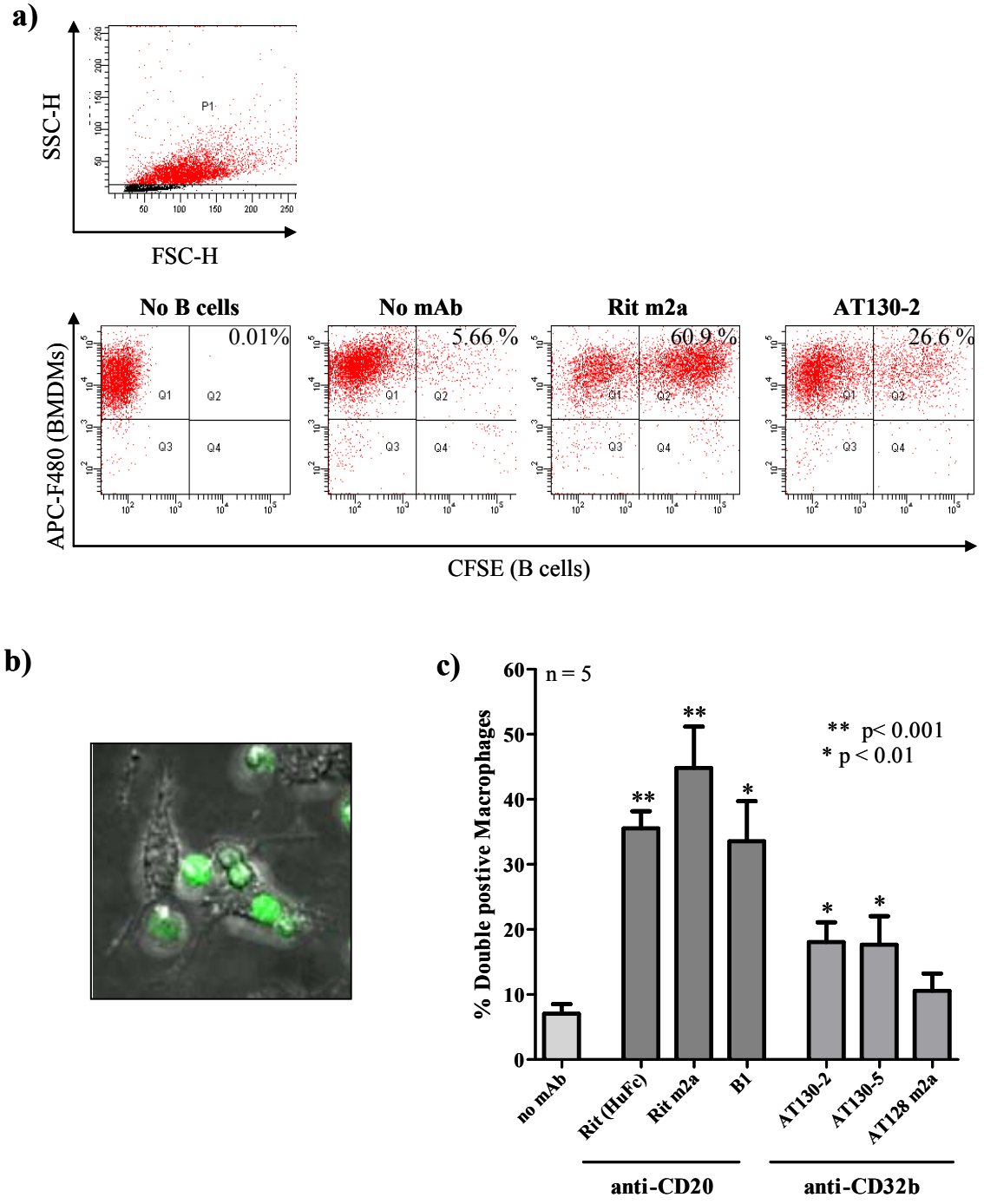

Figure 5.12. The anti-CD32 mAb are able to induce phagocytosis of opsonised B cells.
5 x 10^4 BMDM / well were incubated in 96-well plates at 37 °C, 5 % CO_2 for 2 hr before the addition of 2.5 x 10^5 purified, CFSE labelled and opsonised CD20 Tg B cells for 1 hr under the same tissue culture conditions. These were then harvested, stained with APC-conjugated F480 for 15 min at room temperature, washed once, before being harvested and analysed by flow cytometry for presence of double positive cells ($F480^+CFSE^+$)(a). Confocal examination of BMDMs shows engulfment of CFSE labelled B cells opsonised with rituximab. For confocal microscopy, samples were mounted in Vectashield (VectorLaboratories) and images collected equentially on a Leica TCS SP5 (LeicaMicrosystems). Images were acquired using Leica software (LAS-AF v2) and processed using Adobe Photoshop CS2 Version 9.0.2. (b). The anti-CD32 mAb, AT130-2 and AT130-5 were able to induce a significant level of phagocytosis of opsonised B cells in comparison to non-opsonised B cells (no mAb) (* $p < 0.01$, by Student's t-test). The induction of phagocytosis by the anti-CD32 mAb was less than that induced by the anti-CD20 mAb in comparison to non-opsonised B cells (no mAb) (** $p < 0.001$, by Student's t-test) (c).

5.4.2. The anti-CD32 mAb induce phagocytosis of opsonised B cells in a dose dependent manner.

The relative expression levels of CD32 and CD20 differs on the surface of B cells. There are more CD20 molecules per cell than CD32 molecules; therefore it is plausible that more anti-CD20 mAb will bind to the surface of the cell and be accessible for engagement with activatory FcγR on BMDMs. In order to determine whether it was the expression level of CD32 on B cells that is limiting the amount of phagocytosis observed with anti-CD32 mAb in comparison to the anti-CD20 mAb, a titration of mAb binding and phagocytosis was performed. Unlabelled CD20 Tg B cells were incubated with 10, 3, 1, 0.3 or 0.1 μg/ml anti-CD32 or anti-CD20 mAb for 20 min at room temperature and processed according to indirect immunofluorescence protocols (Materials and Methods section 2.11) (Figure 5.13a). Alongside this, CFSE labelled CD20 Tg B cells were opsonised with 10, 3, 1, 0.3 or 0.1 μg/ml anti-CD32 or anti-CD20 mAb as previously described prior to incubation with BMDMs and then levels of phagocytosis were assessed by flow cytometry (Figure 5.13b). These data show that there is a titration effect on the binding of the anti-CD20 mAb and AT128 m2a, where a lower concentration of mAb results in reduction in the detectable mAb bound to CD20 Tg B cells (Figure 5.13c). The titration effect on mAb binding correlates with the level of induction of phagocytosis (Figure 5.13d). In contrast however, there was no titration effect with regards to mAb binding or phagocytosis with AT130-2; both binding of the mAb and induction of phagocytosis seemed to alter little across the dose range, meaning that CD32 on the B cell surface was most likely saturated with mAb and that we were observing maximal phagocytosis induced by AT130-2.

From these data it was also observed that at 0.3 μg/ml and 3 μg/ml, where Rit m2a and AT130-2, respectively, demonstrate comparable surface binding, as determined by MFI, there is not a significant difference between the percentage of phagocytosis ($p = 0.2613$ by Student's t-test). These data indicate that the anti-CD20 mAb and the anti-CD32 mAb have equivalent abilities to induce phagocytosis of opsonised B cells, but that this is limited with regards to the lower expression level of CD32 in comparison to CD20. To explore the role of mAb isotype in these assays, we also included the mouse IgG1 Rit γ1 mAb in these assays. Although it demonstrated similar binding levels by MFI to Rit m2a, Rit γ1 was relatively poor at inducing phagocytosis. It has previously been reported that murine IgG1 has lower affinity for the activatory FcγR than the other IgG subclasses[166] and as a consequence the IgG1 isotype mAb may not induce efficient effector cell responses. These data allude to a dependence on activatory FcγR engagement for the induction of

phagocytosis in response to surface bound mAb. Therefore, we subsequently went on to determine the extent of this phenomenon.

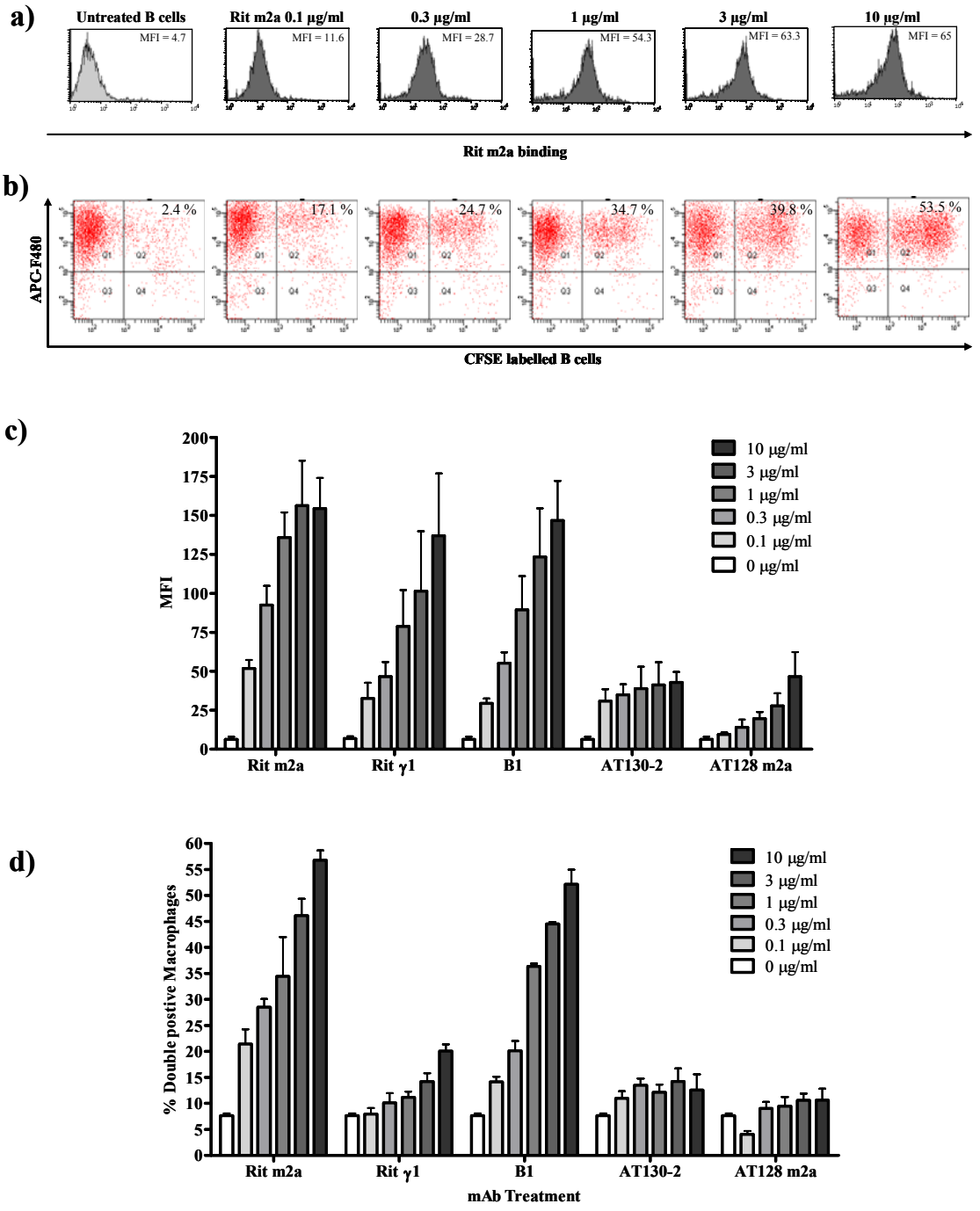

Figure 5.13. Induction of phagocytosis is dependent on mAb binding.
Unlabelled CD20 Tg B cells were incubated for 20 min at room temperature with 10, 3, 1, 0.3 and 0.1 µg/ml of either anti-CD20 or anti-CD32 mAb, washed twice, incubated for 15 min at room temperature with 10 µg/ml PE-conjugated anti-mouse Fc, washed once and analysed by flow cytometry (a) Phagocytosis was measured as previously described (b). mAb binding to CD20 Tg B cells showed a titration effect (c) and this correlated with the level of phagocytosis induction (d). mAb binding to CD32 on the B cells showed a titration effect, but induction of phagocytosis was similar at all concentrations of mAb. However, at comparable mAb binding levels Rit m2a (0.3 µg/ml) and AT130-2 (> 0.1 µg/ml), the mAb induced comparable induction of phagocytosis, indicating that the level of phagocytosis induced by the anti-CD32 mAb is limited by CD32 expression of B cells.

5.4.3. CD32$^{-/-}$ BMDMs induce an enhanced level of phagocytosis than WT BMDMs and this is dependent on the presence of activatory FcγR.

To confirm the requirement of activatory FcγR for the induction of phagocytosis in our assays we next examined the response of γ-chain$^{-/-}$ BMDMs to opsonised B cells. The γ-chain$^{-/-}$ mice lack the common γ-chain molecule that associates with extracellular domain of some human and all mouse activatory Fc receptors and is required for their function[143]. Alongside this and in order to assess the induction of phagocytosis in mice lacking inhibitory signals, we also examined the phagocytic ability of CD32$^{-/-}$ BMDMs. As previously mentioned (Introduction section 1.5.2), the balance between the activatory and inhibitory FcγR will determine the magnitude of cell activation. If cells are lacking the inhibitory FcγR, then the predominant signal induced by Fc engagement will be activatory. It is therefore expected that phagocytosis induced in CD32$^{-/-}$ BMDMs will be increased in comparison with the WT BMDMs.

WT, γ-chain$^{-/-}$ and CD32$^{-/-}$ BMDMs were cultured and assessed for phagocytosis of opsonised B cells as previously described. Rituximab and rit m2a were both able to induce phagocytosis of target B cells by WT and CD32$^{-/-}$ BMDM, but this was not observed with the γ-chain$^{-/-}$ BMDMs (Figure 5.14a), confirming that induction of phagocytosis in our assay is dependent upon activatory FcγR. In addition, these data demonstrate that BMDMs that lack CD32 show no increase in background phagocytosis (no mAb), but show enhanced phagocytic properties in the presence of anti-CD20 mAb opsonised B cells (Figure 5.14a) ($p < 0.05$, by Student's t-test) and in a dose dependent manner (Figure 5.14b). This is also true when B cells are opsonised with anti-CD32 mAb (Figure 5.14a – only AT130-2 shown here). These data suggest that CD32 deficiency leads to increased activation potential on BMDMs. Next we went on to determine whether this enhanced activation potential could be recapitulated using our anti-CD32 mAb on WT BMDMs.

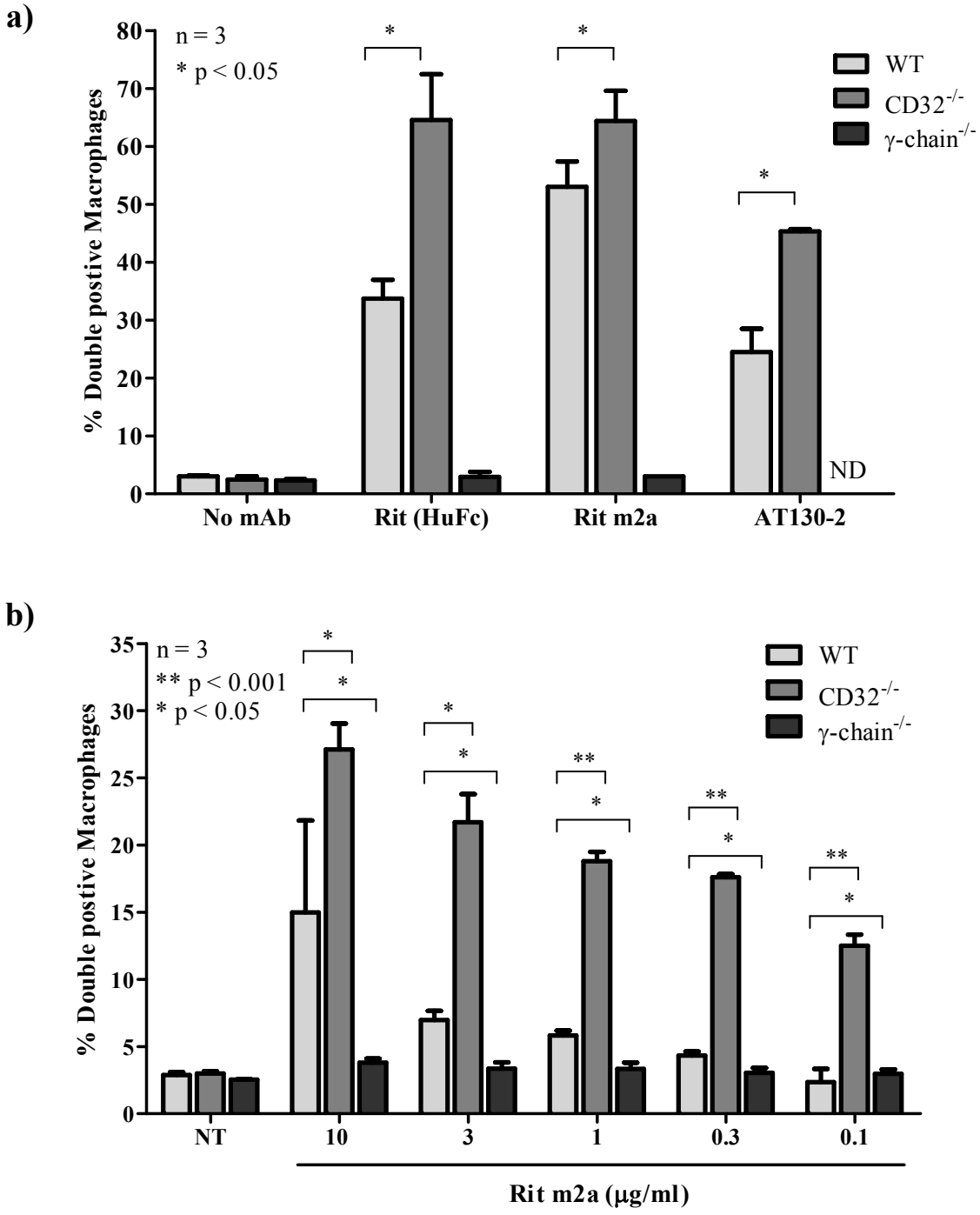

Figure 5.14. Phagocytosis is dependent on expression of activatory FcγR and is enhanced in CD32$^{-/-}$ BMDMs.

5 x 10^4 WT, CD32$^{-/-}$ or γ-chain$^{-/-}$ BMDM / well were incubated in 96-well plates at 37 °C, 5 % CO_2 for 2 hr before the addition of 2.5 x 10^5 purified, CFSE labelled CD20 Tg B cells opsonised with 10 μg/ml mAb (a) or 10, 3, 1, 0.3 or 0.1 μg/ml mAb (b) for 1 hr under the same tissue culture conditions. These were then harvested, stained with 10 μl of 1:10 diluted APC-conjugated macrophage marker F480 for 15 min at room temperature, washed once with PBS-BSA-Azide buffer before being harvested and analysed by flow cytometry. Activatory FcγR are required for mAb-induced phagocytosis by the anti-CD20 mAb (a), whilst the absence of CD32 results in enhanced levels of phagocytosis by anti-CD20 and anti-CD32 mAb in comparison to BMDMs that express CD32 (a). The induction of phagocytosis on WT and CD32$^{-/-}$ BMDMs was in a dose dependent manner (b). * $p < 0.05$, ** $p < 0.001$. ND; no data.

5.4.4. Pre-treatment of macrophages with anti-CD32 mAb enhances phagocytic activity of WT BMDMs.

Having determined that the anti-CD32 mAb were capable of binding to target B cells and inducing phagocytosis, we next went on to determine whether the anti-CD32 mAb would influence the activity of BMDMs directly. In order to accomplish this, prior to incubation with CFSE labelled, opsonised (with rituximab or rit m2a) CD20 Tg B cells, the BMDMs were incubated with 10 μg/ml AT130-5 or AT128 m2a IgG or $F(ab')_2$ or relevant isotype controls (LOB.74 – human IgG1, WR17 – mouse IgG2a) for 1 hr under tissue culture conditions, washed once and media replaced with complete RPMI. Here, phagocytosis induced by non-opsonised B cells was equivalent in all conditions. After BMDMs were pre-incubated with the isotype control, AT128 m2a IgG or $F(ab')_2$, there is no significant difference in phagocytosis (by Student's t-test). However, treatment with AT130-5 IgG but not $F(ab')_2$ increased phagocytosis of Ritux and rit m2a opsonised B cells. ($p = 0.0114$ and $p = 0.0465$, respectively by Student's t-test) (Figure 5.15a).

In addition, comparable experiments were performed using $CD32^{-/-}$ and γ-$chain^{-/-}$ BMDMs (Figure 5.15b and c, respectively). These data demonstrate that the enhancement in phagocytosis observed after AT130-5 IgG treatment of WT BMDMs is specific to blocking CD32 Fc engagement in conjunction with activatory FcγR engagement on the BMDMs, as there is no observed enhancement of phagocytosis in the $CD32^{-/-}$ or γ-$chain^{-/-}$ BMDMs in these assays. The properties of the anti-CD32 mAb on BMDMs are summarised in Table 5.3.

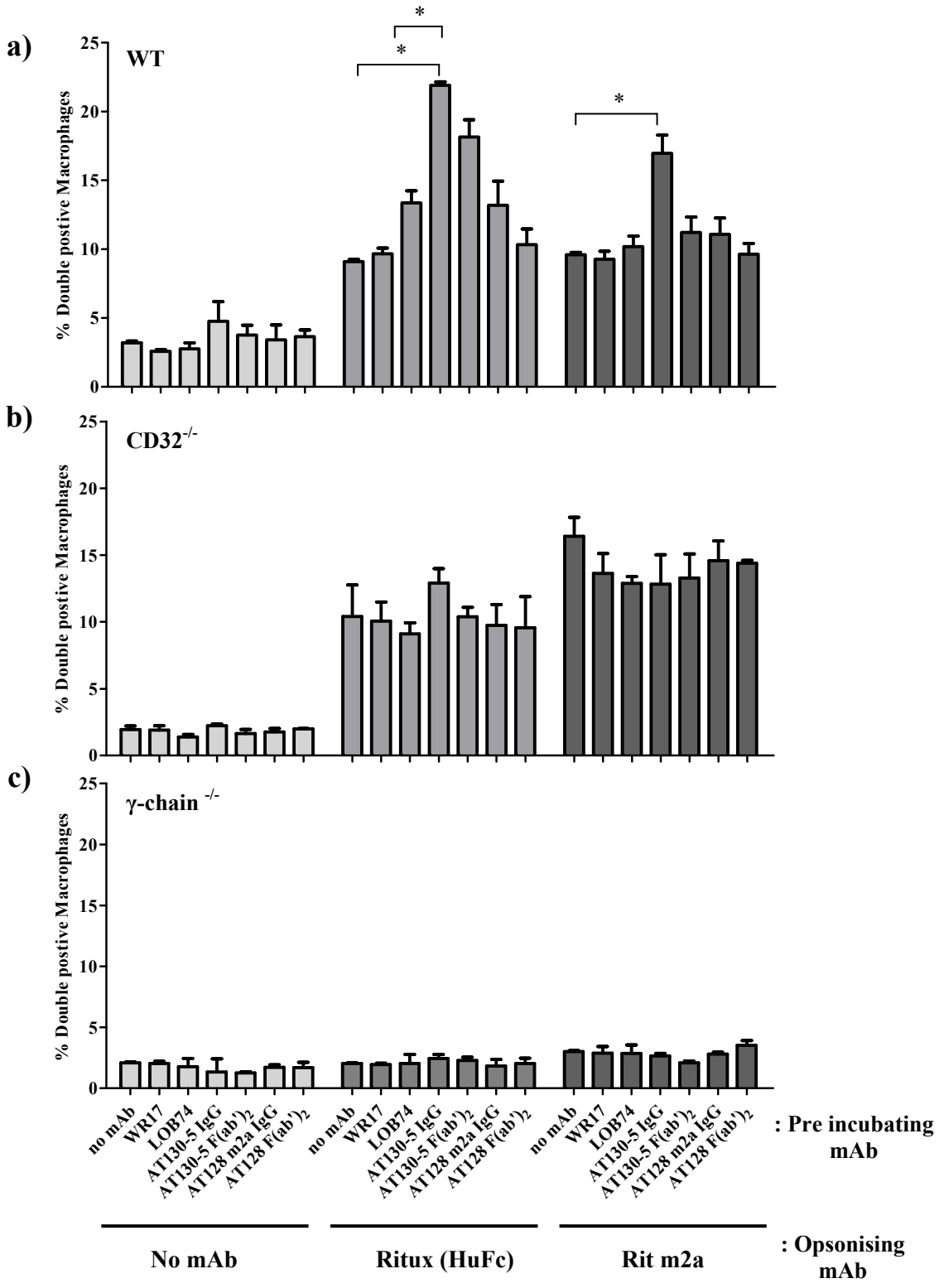

Figure 5.15. Treatment of BMDMs with anti-CD32 mAb leads to augmented phagocytosis.
5 x 10^4 WT, CD32$^{-/-}$ or γ-chain$^{-/-}$ BMDM / well were cultured in 96-well plates at 37 °C, 5 % CO_2 for 2 hr, then incubated with 10 μg/ml AT130-5, AT128 m2a IgG or F(ab')$_2$ or isotype controls (LOB7.4 or WR17), washed once, then incubated with 2.5 x 10^5 purified, CFSE labelled CD20 Tg B cells opsonised with 10 μg/ml rituximab or rit m2a for 1 hr under the same tissue culture conditions. These were then harvested, stained with APC-conjugated macrophage marker F480 for 15 min at room temperature and washed once, before being harvested and then analysed by flow cytometry. Only AT130-5 IgG significantly augmented (*$p < 0.05$) phagocytosis in WT BMDMs to both rituximab and rit m2a opsonised B cells (a). There were no observed effects of anti-CD32 mAb treatment of CD32$^{-/-}$ BMDMs (b) and γ-chain$^{-/-}$ BMDMs (c).

5.4.5. Summary of anti-CD32 activity on BMDMs.

Table 5.3. Summary of anti-CD32 mAb properties on BALB/c BMDMs.

mAb	pCD32	pSHIP-1	Phagocytosis of opsonised B cell	Effect on phagocytic ability of BMDMs
AT130-2	↑	↑	+	++ (data not shown)
AT130-5	ND*	ND*	+	+
AT128	ND*	ND*	ND*	ND*
2.4G2	ND*	ND*	ND*	ND*
AT128 m2a	↓	↓	-	-

Key; ↑: increase; ↓: decrease; ++: medium effect; +: low effect; -: no effect

5.5. Chapter discussion.

The aim of this chapter was to establish the possible effects of the anti-CD32 mAb on key CD32 expressing cells of the immune system, with the aim of determining any potential detrimental effects of anti-CD32 mAb therapy. We have focused on splenic B cells and BMDMs, although the expression of CD32 has been reported on a much wider range of cells, including epithelial cells[143]. Initially, we demonstrated that the anti-CD32 mAb bound both splenic B cells and BMDMs and that the expression levels of CD32 on these tissues were similar to CD32 expression on lymphoma cells (Figure 5.1 & Figure 5.8).

We next examined the ability of the anti-CD32 mAb to elicit tyrosine phosphorylation. It was observed that the agonistic anti-CD32 mAb were able to induce tyrosine phosphorylation of CD32 on normal B cells, (Figure 5.2 & 5.3) and BMDMs (Figure 5.9), albeit with slightly different kinetics to those observed on lymphoma cells (Figure 4.8), whereas the antagonistic anti-CD32 mAb did not induce phosphorylation of CD32, as previously seen on lymphoma cells. A caveat here is the lack of an isotype control in the experiments on the BMDMs. However, mAb of the same isotype were assessed on the same membranes and a differential phosphorylation pattern was still observed between the angonistic and antagonistic anti-CD32 mAb, suggesting that there were limited non-specific interactions on these cells. The differential phosphorylation of CD32 was consistent between both C57BL/6 and BALB/c mouse strains. This is important as the C57BL/6 and BALB/c mice were both to be used for examination of *in vivo* effects on the anti-CD32 mAb in both the Eμ-myc and BCL_1 syngeneic tumour models. Alongside this, we were able to demonstrate that SHIP-1 phosphorylation in the BMDMs at least was

similar to that on lymphoma cells, where the agonistic anti-CD32 mAb enhanced pSHIP-1 and the antagonistic anti-CD32 mAb reduced pSHIP-1 (Figure 5.9; BMDMs & Figure 4.8; lymphoma cells). The phosphorylation of SHIP-1 on splenic B cells however was different to that observed on lymphoma cells in terms of the kinetics of phosphorylation and the fact that pSHIP-1 was induced after incubation with the antagonistic anti-CD32 mAb (Figure 5.4). On the lymphoma cells, the differential phosphorylation of CD32 and SHIP-1 seems to correlate with contrasting functional activity, i.e. differences in Ca^{2+} flux. However, the anti-CD32 mAb did not inhibit (agonistic) or augment (antagonistic) Ca^{2+} flux on normal B cells from C57BL/6 mice (Figure 5.5; normal B cells & Figure 4.14; lymphoma cells), in fact it was evident that the anti-CD32 mAb had no effect on BCR-induced Ca^{2+} flux on normal B cells. The Ca^{2+} flux in lymphoma cells appeared to be transient, rather than prolonged as in the normal B cells. This would suggest that BCR-induced signalling between B cells and lymphoma cells is distinct. Observations by Dr Kathleen Potter (University of Southampton) have also demonstrated this. Unpublished data from her laboratory has previously shown that purified B cells show extend Ca^{2+} flux, whilst cell lines demonstrate a transient Ca^{2+} flux, similar to that observed through this thesis (personal communication). Alongside this, it was suggested that the phosphorylation of CD32 was greater on cells from BALB/c mice compared with those from C57BL/6 mice and therefore the strength of signal mediated by the anti-CD32 mAb on cells from C57BL/6 mice would be less than that on cells from BALB/c mice, meaning that inhibition of BCR-induced Ca^{2+} flux would be more difficult to detect. Densitometry analysis of the Western blots in Figure 5.2 and Figure 5.3 revelled this not to be the case (Appendix 4). In addition, we did not assess the effect of the anti-CD32 mAb alone on Ca^{2+} flux on normal B cells so can not conclude that the anti-CD32 mAb alone would not have an effect on Ca^{2+} flux.

In conjunction with this signalling assay, we observed that neither AT130-2 nor AT130-2 induced a significant level of PCD in the WT B cells, from either C57BL/6 or BALB/c mice (Figure 5.6), unlike on lymphoma cells where these mAb did induce PCD (Figure 4.18). Much the same as the observations on lymphoma cells, the antagonistic mAb did not induce PCD on normal B cells. This suggests that the induction of direct cell death of normal B cells *in vivo* by the anti-CD32 mAb will be limited, which is promising for their use *in vivo* and may allow tumour selectivity. Altogether these data indicate that splenic B cells are less susceptible to PCD induced by CD32 engagement that lymphoma cell lines, although there is a significant if small induction of AT130-2 induced cell death on C57BL/6 splenic B cells. However, we have only analysed the effect of the anti-CD32

mAb on splenic B cells and it is not implausible that the anti-CD32 mAb would have detrimental effects on other B cell subsets, such as circulating naïve, memory B cells or plasma cells. Alongside this, there was a trend towards greater induction of PCD induced by the anti-CD32 mAb on BMDMs than on B cells, however, this was less than on the lymphoma cell lines (Figure 5.10). Taken together, these data therefore indicates that despite differences in CD32 and SHIP-1 activation, perhaps the agonistic and antagonistic mAb do not demonstrate differential function on normal B cells and BMDMs as they do on lymphoma cell lines and as such are unlikely to deplete CD32 expressing cells *in vivo*.

Having established that the effects of direct PCD on CD32 expressing cells *in vivo* are likely to be relatively small, we next went on to establish if the anti-CD32 mAb had the potential to affect the function of CD32 expressing effector cells, in particular macrophages *in vivo*. As previously mentioned, FcγR expressing effector cells are a key components of the anti-tumour response, by instigating ADCC and phagocytosis of opsonised tumour cells. This process is regulated by co-ligation with the inhibitory FcγR, CD32, where CD32 engagement dampens anti-tumour responses. Our anti-CD32 mAb therefore have two potential means of augmenting anti-tumour responses through effector cells *in vivo*; by engaging the activatory FcγR, much as any other mAb, inducing ADCC and phagocytosis or by blocking CD32 on the effector cells and therefore limiting inhibitory signalling. We were able to assess these activities via the use of a phagocytosis assay, described in Figure 5.11. It was shown that the anti-CD32 mAb were able to induce phagocytosis of opsonised B cells, although to a lesser extent than other therapeutic mAb, i.e. the anti-CD20 mAb (Figure 5.12). Alongside this, we were able to demonstrate that the difference in the extent of phagocytosis was on account of mAb binding, where the use of lower concentrations of anti-CD20 lead to equivalent levels of cell surface binding of the AT130-2 mAb and equivalent phagocytosis (Figure 5.13). This suggests that the anti-CD32 mAb alone or in combination with other clinically relevant mAb immunotherapeutics would be able to interact with effector systems and provide further focus to the anti-tumour response. A caveat here however is that we were unable to determine whether B cells underwent phagocytosis or merely clustering with the macrophages via FcγR interactions. In order to rule this out, a cell surface marker, such as B220 or CD19 conjugated to PerCP could be used to detect B cells within the F480+/CFSE+ population. If the B cells were being engulfed then minimal B220 staining would be observed, but if clustering of opsonised B cells with BMDMs was occurring then B220 staining would be evident. Regardless, these phagocytosis assays determined the phagocytic potential of the mAb of interest.

Specifically and as described by others[83], we were able to further demonstrate the requirement of the activatory FcγR and Fc receptor engagement in the initiation of these phagocytosis, where deficiency in either abrogated the phagocytosis observed (Figure 5.14). Alongside this we were also able to show that CD32 deficient BMDMs demonstrated augmented phagocytosis of opsonised B cells in comparison to WT BMDMs (Figure 5.14). This suggests that CD32 expression abrogates BMDM activity *in vitro* and presumably *in vivo*. However, it could be suggested that the augmented phagocytic response of the $CD32^{-/-}$ BMDMs may be due to altered activatory FcγR expression on these cells in comparison to WT BMDMs. In order to address this, the FcγR profile of WT and $CD32^{-/-}$ BMDMs would need to be established. Up until recently we have not had access to a full panel of anti-FcγR mAb and currently, as a result of the MHV infection in the Tenovus Biomedical Research Unit, resulting in a lack of the required animals, we were are unable to address this issue through this thesis.

After establishing that the anti-CD32 mAb were able to induce phagocytosis we next went on the confirm reports that the use of anti-CD32 mAb augment effector cell responses[372]. Pre-incubation of BMDMs with the antagonistic anti-CD32 mAb resulted in no significant change in levels of phagocytosis. However, treatment with agonistic anti-CD32 mAb increases phagocytosis of opsonised B cells (Figure 5.15). This is intriguing, as on lymphoma cells agonistic anti-CD32 mAb led to an increase in CD32 activation and antagonistic anti-CD32 mAb led to a reduction in CD32 activation. In theory, this would lead to an increase and decrease in CD32 activation, respectively, if the mAb were acting the same way on BMDMs. However, we previously demonstrated that, in terms of PCD at least, the anti-CD32 mAb do not have the same activity on BMDMs as on lymphoma cells. It is therefore proposed that, rather than inducing changes in CD32 signalling on BMDMs, the agonistic anti-CD32 mAb are blocking Fc engagement between CD32 on the surface of BMDM and the anti-CD20 mAb. As a result, the predominant signal received by the BMDMs after Fc engagement will be activatory. In this way, blocking of CD32 augments phagocytosis, as observed (Figure 5.15).

Taken together, all these data suggest that the agonistic anti-CD32 at least, have potential to augment anti-tumour responses but without negative effects on normal CD32 expressing cells. We next go on to examine the effects of the anti-CD32 mAb in our B cell lymphoma murine models.

CHAPTER 6 Manipulation of immunotherapy by anti-CD32 mAb.

6.1. Chapter introduction.

CD32 has been shown to modulate *in vivo* cytotoxicity against tumour targets; where CD32 deficiency seems to enhance therapeutic mAb anti-tumour responses[83]. There are two potential mechanisms by which anti-CD32 mAb may improve anti-tumour activity, first by enhancing effector cell activation, i.e. ADCC, by blocking CD32 inhibitory function on effector cells and secondly by inducing direct apoptosis on CD32 expressing target cells. Anti-human CD32b monoclonal antibodies (mAb) have been shown by some to have anti-tumour effects[374] but can show cross-reactivity, as CD32 is greater than 95 % homologous to the activatory FcγR, FcγRIIa (CD32a)[293,146]. Our murine anti-CD32 mAb have been show to be specific to murine CD32 (mice lack the CD32a member of the FcγR family) and can be used to study the *in vivo* potential of anti-CD32 mAb, alone or in combination with other known immunotherapeutics.

In Chapter 4 we established that there are two types of anti-CD32 mAb. The agonistic anti-CD32 mAb (AT130-2 and AT130-5) induced phosphorylation of CD32 and SHIP-1, caused an inhibition of BCR-induced Ca^{2+} and induced PCD in LCLs. All of these functions require an Fc portion for CD32 cross-linking. On the other hand, the antagonistic anti-CD32 mAb (AT128, AT128 m2a and 2.4G2) do not cause phosphorylation of CD32, block phosphorylation of SHIP-1, potentiate calcium flux and have relatively little effect on PCD. In chapter 5 we established that the anti-CD32 mAb induce only small amount of PCD in B cells and BMDMs and in addition, it was shown that the agonistic anti-CD32 mAb, at least, were able to induce phagocytosis of opsonised B cells and enhance the phagocytic capacity of BMDMs. The properties of the anti-CD32 mAb described in both chapters 4 and 5 elucidate the potential use of these antibodies *in vivo* as immunotherapy modulatory reagents.

Here, we wished to ascertain the *in vivo* efficacy of the anti-CD32 mAb and assess their potential to enhanced anti-tumour responses, similar to that described by others[374,372]. We compared only AT130-2 and AT128 m2a as these are both IgG2a isotype, which has been shown to have a greater therapeutic effect with regards to mAb treatment *in vivo*[411]. Mouse IgG2a is equivalent to human IgG1 which preferentially engages the activatory FcγR in comparison to the inhibitory FcγR[166].

6.2. Manipulation of Immunotherapy *in vivo.*

6.2.1. Anti-idiotype immunotherapy in WT and CD32$^{-/-}$ BALB/c mice.

Initially we wished to recapitulate previously published data [83] and confirm the original hypothesis, that CD32$^{-/-}$ mice display increased survival following administration of tumour and subsequent mAb immunotherapy. We compared BCL_1 anti-idiotype immunotherapy in BALB/c WT and CD32$^{-/-}$ mice. Mice were injected i.v. with 1 x 10^4 fresh BCL_1 cells on day 0. The mice were then treated on days 4 to 7 or on days 7 to 10 with a total of 0.5 mg (125 μg/day) anti-idiotype (Mc106A5), as previously described[27]. In both mouse strains anti-idiotype therapy improved survival in comparison to the non-treated mice ($p < 0.05$, by Mantel-Cox statistical testing).

In these experiments the WT mice that were left untreated succumbed to disease within approximately 21 days. Treatment with anti-idiotype increased survival of animals in these groups to between 28 and 32 days, which was significantly different in comparison to the untreated mice ($p < 0.05$, by Mantel-Cox statistical testing). The survival in WT mice was equivalent whether anti-idiotype mAb was administered from day 4 until day 7 or if treatment was from day 7 to day 10; i.e. there was not significant difference between the different treatment regimes (Figure 6.1). Likewise, the survival of untreated CD32$^{-/-}$ was approximately 21 days and the survival of mice treated with anti-idiotype was also increased to a significant level ($p < 0.05$, by Mantel-Cox statistical testing) in both treatment groups. Although there was a trend towards increased survival in the CD32$^{-/-}$ mice as a result of anti-idiotype treatment from day 4 to day 7, there was no significant difference between the survival of WT and CD32$^{-/-}$ mice treated from day 4 to day 7 with anti-idiotype. Nevertheless, in the CD32$^{-/-}$ mice that were treated from day 7 to day 10 there was a significant increase in survival compared with the same treatment in WT mice ($p<0.05$, by Mantel-Cox statistical testing), (Figure 6.1). This indicates that CD32 expression or lack of expression can alter immunotherapy; in part confirming previously published literature that shows improved immunotherapy in CD32$^{-/-}$ mice [83]. We next went on to examine this potential using anti-CD32 mAb in our models of lymphoma.

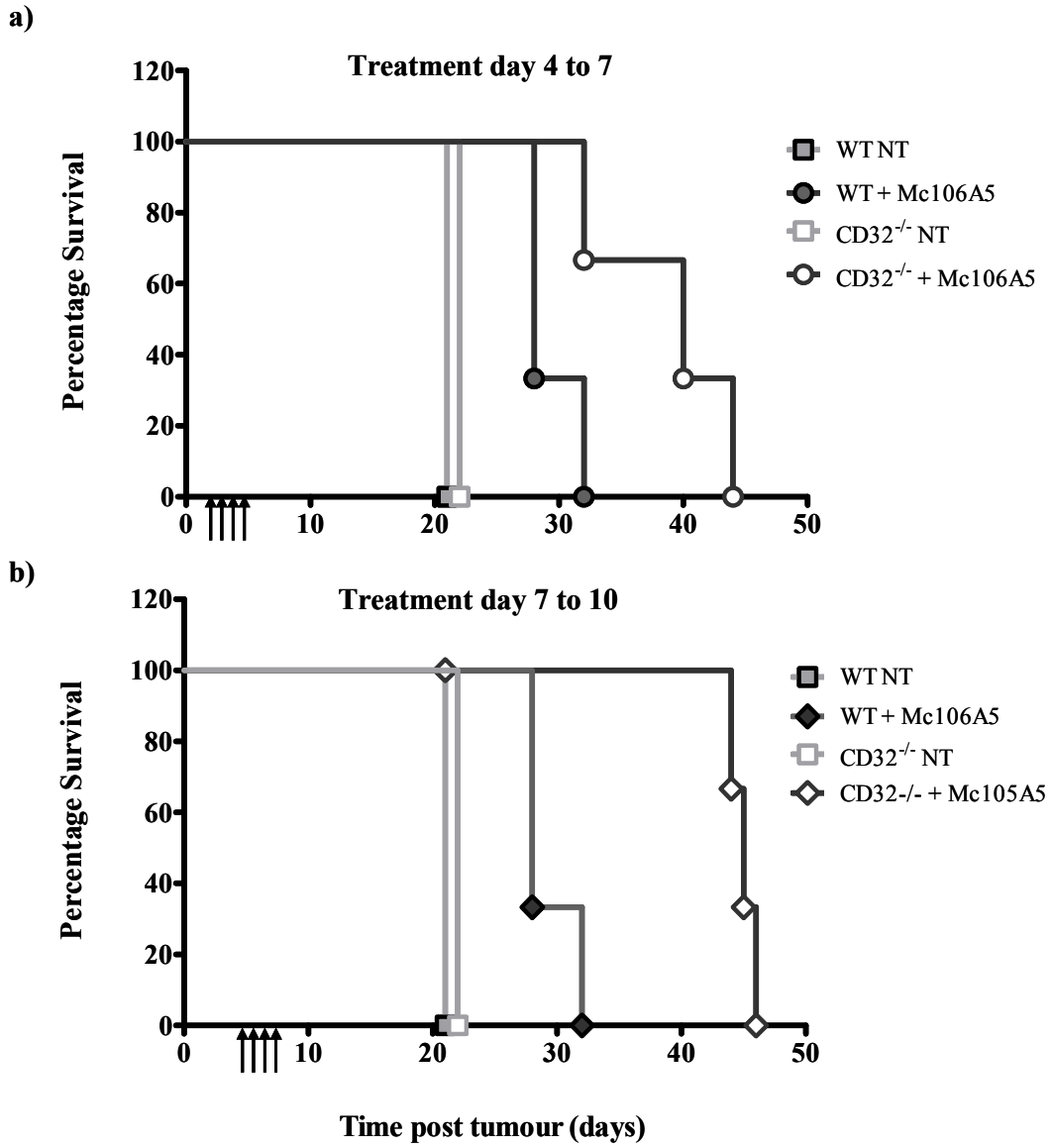

Figure 5.16. Anti-idiotype BCL_1 immunotherapy shows improved efficacy in $CD32^{-/-}$ mice compared with WT mice.
Mice were inoculated with 1 x 10^4 BCL_1 cells on day 0 and then treated with 125 µg/day (total 0.5 mg) anti-idiotype on days 4 to 7 (circle) or days 7 to 10 (diamond). Arrows indicated the anti-idiotype treatment regime. There is an increased survival with anti-idiotype treatment compared with the untreated mice (square) in both WT (closed) and $CD32^{-/-}$ (open) mice and this survival is significantly increased in the $CD32^{-/-}$ mice (open) treated day 7 to 10 (◇) (p= 0.0224) (b) but not when treated day 4 to7 (○) (p= 0.0628) (a), although there was a clear trend towards increased survival in these mice. Data is a representative result from three repeats, where n = 4 mice per group.

6.2.2. *In vivo* efficacy of anti-CD32 mAb on anti-idiotype therapy.

In order to examine *in vivo* efficacy of the anti-CD32 mAb we examined long term survival of WT BALB/c mice that were inoculated with the syngeneic BCL_1 tumour and then treated with anti-CD32 mAb alone or in combination with anti-idiotype mAb. Mice were inoculated i.v. with 1 x 10^4 fresh BCL_1 cells on day 0. Mice were then treated with a 0.5 mg dose of irrelevant control (WR17), AT130-2 or AT128 m2a i.v. on day 3 and then

treated on day 4 through to day 7 with 125 µg/day (0.5 mg total mAb) anti-idiotype or irrelevant control (Mc39/16) (Figure 6.2).

Anti-idiotype treatment improved survival in comparison to the untreated mice (p = 0.0023, by Mantel-Cox), as seen in Figure 6.1. When administered as a single therapeutic agent, AT130-2 and AT128 m2a had no effect on increasing survival compared with irrelevant control (Figure 6.2a), as determined by Mantel-Cox statistical testing. In combination with anti-idiotype therapy AT130-2 and AT128 m2a also had no significant effect on increasing survival in comparison to anti-idiotype treatment alone (Figure 6.2b). These results indicate that in this BCL_1 lymphoma model the anti-CD32 mAb did not improve therapy.

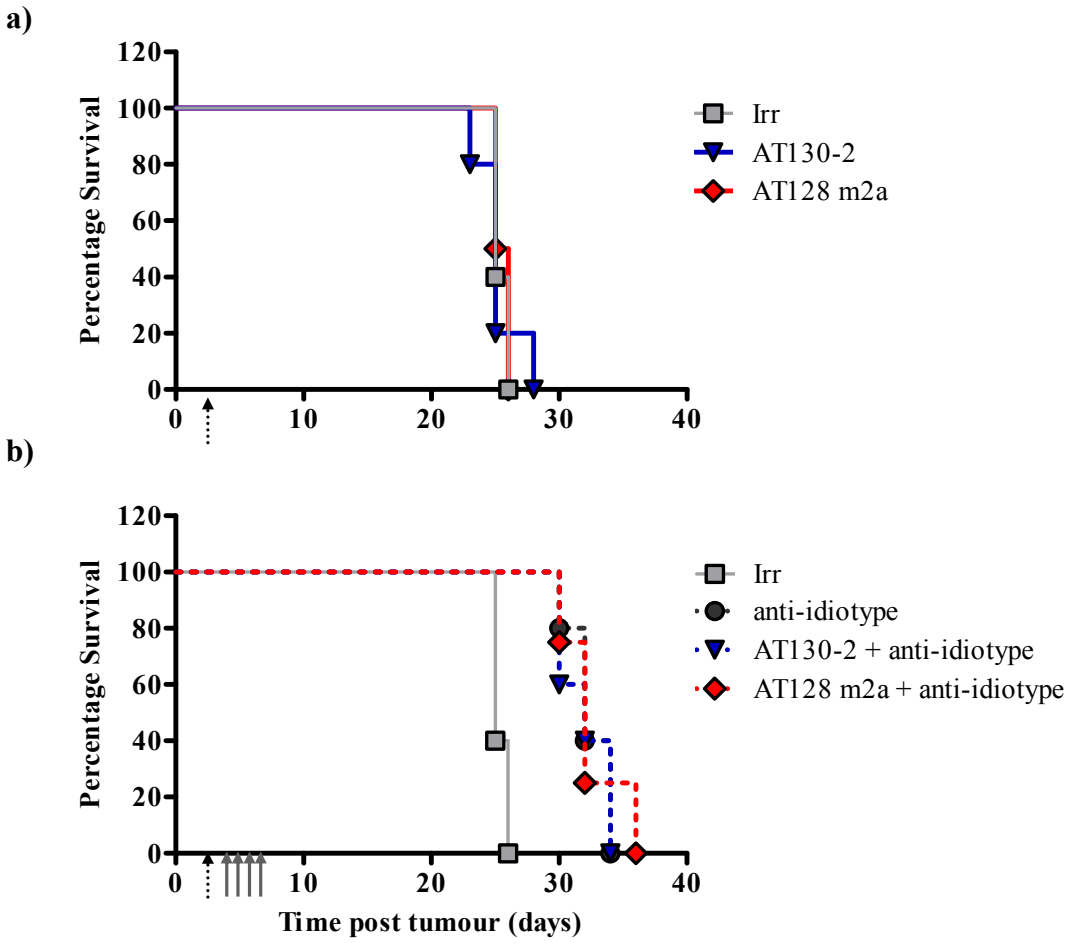

Figure 5.17. Effect of anti-CD32 mAb alone and in conjunction with anti-idiotype therapy of BCL_1 tumour.
WT mice were inoculated with 1 x 10^4 BCL_1 cells on day 0, 0.5mg AT130-2, AT128m2a or irrelevant control (WR17, Irr) on day 3 (dotted arrow) and 125µg of anti-idiotype (Mc106A5) or irrelevant control (Mc39/16) per day on days 4 to 7 (solid grey arrows). AT130-2 and AT128m2a alone did not significantly increase survival (a). Anti-idiotype therapy alone did improve survival in comparison to the untreated controls (p = 0.0023, Mantel-Cox). However, the anti-CD32 mAb did not improve survival with anti-idiotype immunotherapy (b). Data is a representative result from three repeats, where n = 4 mice per group.

6.2.3. Effect of anti-CD32 mAb on tumour growth.

The data from Figure 6.1 indicates that deficiency in CD32 can lead to improved immunotherapy and implies that this might be mimicked with anti-CD32 mAb. However, the data in Figure 6.2 indicates that the anti-CD32 mAb have negligible effect on survival alone or in combination with anti-idiotype therapy. This is an extreme assessment of mAb efficacy, therefore we next examined whether the anti-CD32 mAb were able to slow tumour growth we next went on to examine the effects on the CD32 mAb in short term *in vivo* tumour growth assays, using two syngeneic tumour models of lymphoma, BCL_1 and A31[27].

In these experiments, BALB/c mice were inoculated with 2 x 10^7 BCL_1 cells or CBA/H mice were inoculated with 2 x 10^7 A31 tumour (day 0). Mice were treated on day 4 with 0.5 mg mAb, either irrelevant control (WR17), anti-idiotype (Mc106A5 or Mc39/16 for BCL_1 and A31, respectively), AT130-2 or AT128 m2a. The spleens were harvested from two mice per treatment group on day 6 and day 8 (48 hr and 96 hr post treatment, respectively). Using a Coulter counter the total number of cells per spleen was established and the percentage tumour cells per spleen determined, by flow cytometry after staining with FITC-conjugated anti-idiotype and PE-conjugated CD19 (ID3), as outlined in the Material and Method section 2.12.1. From the percentage of anti-idiotype/CD19 positive cells and the total spleen cell number the total number of tumour cells per spleen was calculated.

As one of the mAb treatments in this experiment included the anti-idiotype mAb used for detection of tumour cells, we initially needed to establish whether the binding of anti-idiotype mAb to the tumour cells *in vivo* was blocking detection of tumour cells *ex vivo* in the anti-idiotype treated animals, CD19 positive cells were plotted against FSC-H. In all treatments, a population of large (FSC-H high) CD19 positive cells (lymphoma cells) were detected and this corresponded with detection of a CD19/anti-idiotype double positive population. This provided confidence that we were detecting the tumour cell population correctly (Figure 6.3a, top panels).

In both the BCL_1 and A31 tumour tracking experiments (Figure 6.3b and 6.4, respectively) treatment with anti-idiotype significantly reduced tumour growth ($p < 0.05$). In comparison with the other treatment groups, anti-idiotype treatment resulted in smaller spleen size and fewer tumour cells, both in terms of total number and percentage per spleen. In contrast, AT130-2 and AT128 m2a had no significant effect on tumour growth.

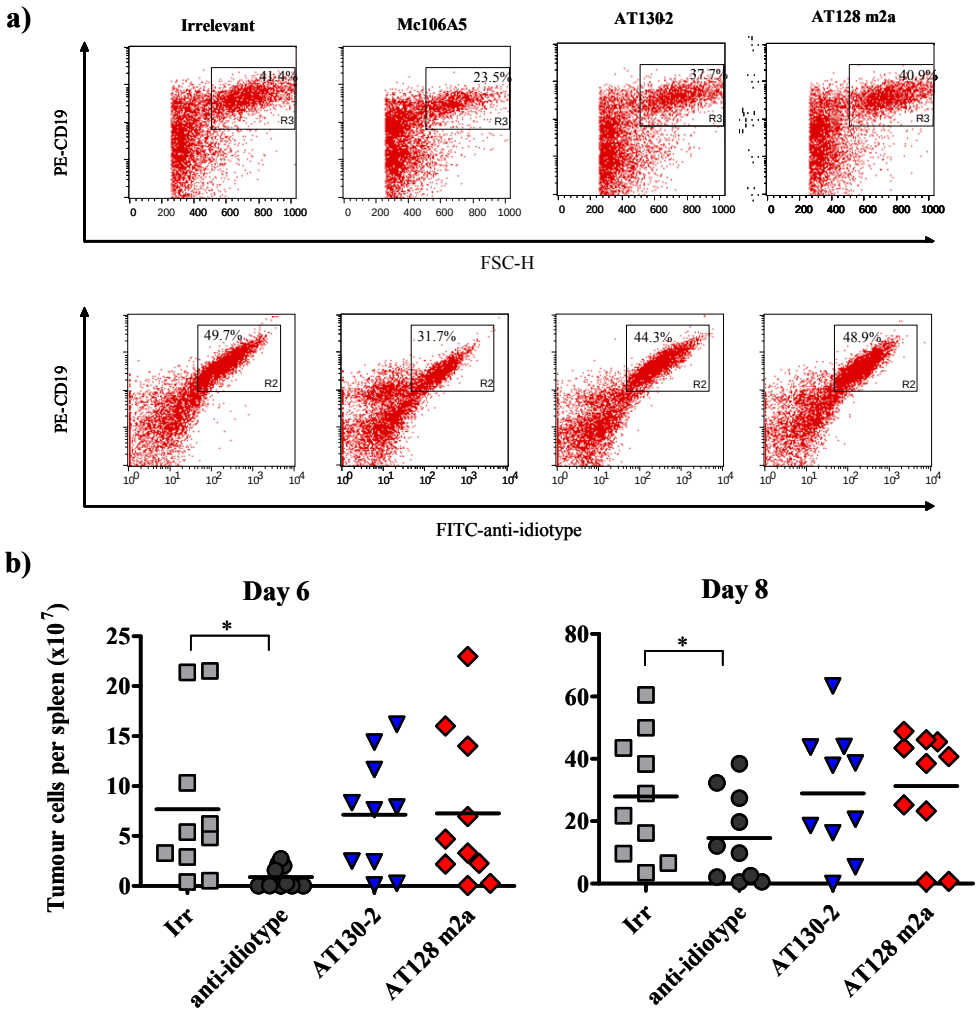

Figure 5.18. BCL_1 tumour tracking assay.
WT mice were inoculated with 2 x 10^7 fresh BCL_1 cells i.v. on day 0. Mice were treated i.p. on day 4 with 0.5 mg AT130-2, AT128 m2a, anti-idiotype or irrelevant control (WR17). Spleens were harvested on days 6 and 8. Splenocytes were counted using the Coulter cell counter (see Materials and Methods section 2.3) and stained with 10 µg/ml PE-conjugated CD19 and FITC-conjugated anti-idiotype. Lymphocyte events, including tumour cells, as identified by FSC-H and SSC-H were collected. The percentage of tumour cell within the live cell gate were collected and expressed as CD19 (FL2-H) versus anti-idiotype (FL1-H). The data shown in (a) represents the typical flow cytometry results obtained from day 8 of these experiments, four days post mAb treatment. The percentage of tumour cells per spleen was calculated as ((total cell number/100) x % CD19/anti-idiotype positive cells (R2)). Typically, treatment with anti-idiotype slowed tumour growth ($p < 0.05$) (b) and although AT130-2 seems to reduce the number of tumour cells this is not significant compared with the control or anti-idiotype treatment which showed fewer total cells per spleen ($p > 0.05$) (b). AT128 m2a however seemed to enhance tumour growth, although again this was not significant ($p > 0.05$). CD19 positive cells were plotted against FSC-H to show that the antibodies were detecting a specific tumour cell population (a – top panels). These data represent five independent experiments, with two animals per experiment.

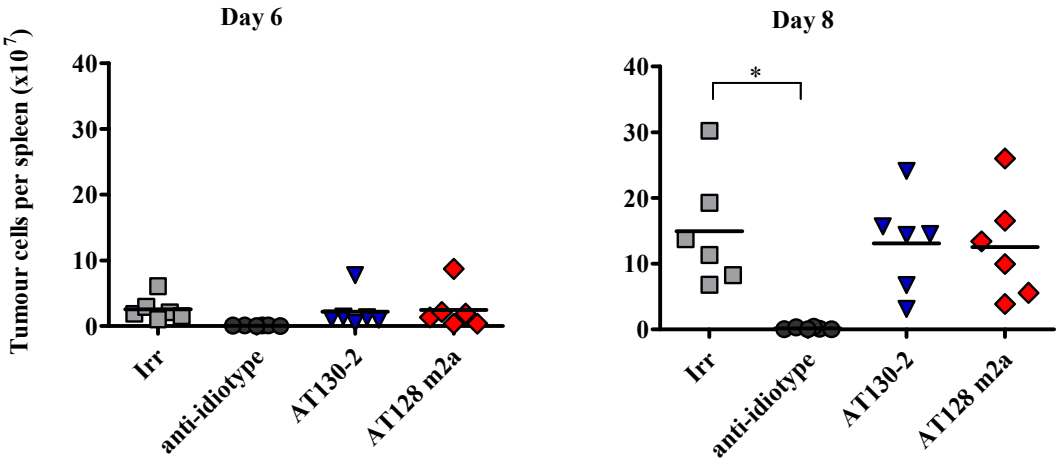

Figure 5.19. A31 tumour tracking assay.
CBA/H mice were inoculated with 2 x 10^7 fresh A31 cells i.v. on day 0. Mice were treated i.p. on day 4 with 0.5mg AT130-2, AT128 m2a, anti-idiotype (Mc39/16) or irrelevant control (WR17). Spleens were harvested on days 6 and 8. Splenocytes were counted using the Coulter cell counter (see Materials and Methods section 2.3) and stained with 10 µg/ml PE-conjugated CD19 and FITC-conjugated anti-idiotype. The percentage of tumour cells per spleen was determined and calculated as described above. Anti-idiotype treatment significantly reduced the number of tumour cells in the spleen four days after treatment ($p < 0.05$) and although AT130-2 and AT128m2a seems to reduce the number of tumour cells compared with the control this is not significant ($p > 0.05$). These data represent three experiments, with two animals per experiment.

6.3. *In vivo* consumption of mAb.

6.3.1. *In vivo* consumption of mAb in BCL_1 and A31 treated mice.

Previous published experiments have demonstrated increased mAb immunotherapy in $CD32^{-/-}$ mice in comparison with similar therapy in WT mice[374] and our own data has confirmed these findings in the BCL_1 immunotherapy model (Figure 6.1). However, there was little or no effect on survival in animals treated with the anti-CD32 mAb. Given these unexpected findings we considered several possible reasons for the failure of the anti-CD32 mAb to improve therapy. First we wished to establish whether there was adequate mAb in the serum of treated mice as we considered it possible that the amount of mAb given may not be sufficient to elicit an effect, particularly in the short term, high tumour load experiments. To assess consumption of mAb in the BCL_1 tumour model we performed a cellular bioassay using mouse serum from tumour bearing mice described in the previous experiments at 48 hr and 96 hr post treatment (Figure 6.3 & 6.4). Here, serum was diluted to an appropriate level and incubated with πBCL_1 cells for 30 min at 4 ˚C in the dark, washed twice with PBS-BSA-Azide buffer and incubated with 10 µg/ml PE-conjugated anti-mouse anti-Fc. Alongside these a standard curve of doubling dilutions was performed for each of the mAb (i.e. anti-idiotype, AT130-2 and AT128 m2a). All samples were analysed by flow cytometry and the concentration of serum mAb was calculated from

the appropriate linear area of the standard curve. Using the equation from the relevant linear area of the standard curve (Figure 6.5b) the mAb concentration is calculated from the MFI of the bound serum (Figure 6.5c).

Our results clearly demonstrated that whilst levels of anti-idiotype remained high at both 48 hr and 96 hr post treatment, the CD32 mAb were rapidly consumed *in vivo* within 48 hr of administration (Figure 6.5c). However through these experiments we observed difficulties with the cellular bioassay, mainly in obtaining a good and consistent standard curve for the anti-CD32 mAb, in particular AT128 m2a. It would seem that the lower affinity of this particular anti-CD32 mAb posed a problem when trying to establish a standard curve and serum mAb concentrations in that at 10 μg/ml, usually a saturating dose of mAb, a plateau of mAb binding had not been achieved and as such, the linear portion of the curve could not be established. Therefore, an alternative method to that previously described was therefore used to determine serum mAb levels. We utilised an ELISA based method to determine serum concentrations of the anti-CD32 mAb, as outlined in Materials and Methods section 2.22. In brief, immunomaxisorb 96-well plates were coated with a $F(ab')_2$ rat anti-CD4 mAb (OX68) at 5 μg/ml, then with a CD32-CD4 fusion protein (in house, Dr Stephen Beers) and incubated with the diluted serum and mAb standards before the addition of a goat anti-mouse HRP reagent and ELISA substrate (Figure 6.6). This method was used to establish the serum mAb levels in tumour bearing WT and $CD32^{-/-}$ mice, discussed below.

6.3.2. *In vivo* consumption of mAb in WT and $CD32^{-/-}$ mice.

By examining the serum levels of the anti-CD32 mAb in tumour bearing WT and $CD32^{-/-}$ mice we can ascertain the extent to which endogenous CD32 expression limits serum mAb levels and as a result could limit mAb immunotherapy. Serum from WT and $CD32^{-/-}$ tumour bearing mice treated for 48 and 96 hr with 0.5 mg AT130-2 was obtained and then analysed by this ELISA method. The ELISA results plainly show that serum mAb levels were dissimilar at 48 hr post treatment in the WT and the $CD32^{-/-}$ mice. There was trend towards increased serum mAb in the $CD32^{-/-}$ mouse compared to the WT mouse, although there was a significant difference in mAb serum levels between the two mouse strains at 96 hr ($p < 0.05$, by Student's t-test) (Figure 6.7b). There was a dramatic difference in consumption by 96 hr post treatment. AT130-2 was undetectable in the serum of WT mouse at 96 hr, whilst the serum level of this mAb remained reasonably unchanged at 96 hr in the $CD32^{-/-}$ mouse (no significant difference between serum levels at 48 and 96 hr post treatment in the $CD32^{-/-}$ mice, by Student's t-test) (Figure 6.7b). This suggests that

anti-CD32 mAb is rapidly consumed within the WT, but not the $CD32^{-/-}$ tumour bearing mouse. On top of this, a photograph of an immunomaxisorb 96-well plate from a completed ELISA assay clearly demonstrates that there is a dramatic difference in the colour reaction in the WT and $CD32^{-/-}$ at 96 hr post treatment. The titrations from the 96 hr time point from the serum of WT mice show a weak colour development, whilst the titrations of serum from the 96 hr time point of the $CD32^{-/-}$ mice show a deep colour development (Figure 6.7a) These data further supports the implication that the rapid consumption of mAb may account for a decrease efficacy in therapy in our BCL_1 long term survival and tumour tracking experiments.

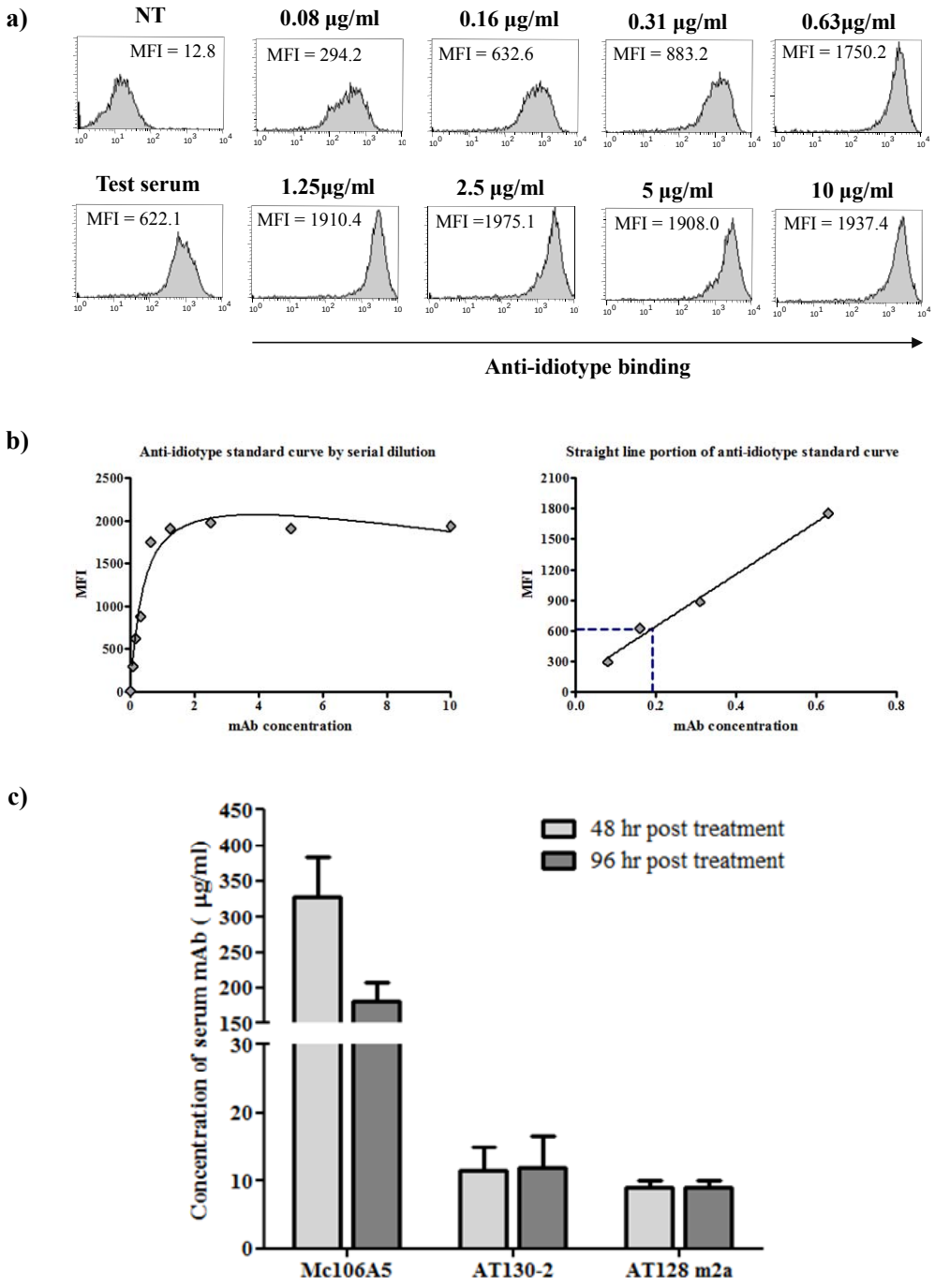

Figure 5.20. Antibody serum levels in WT mice after inoculation with BCL_1 and treatment with mAb. Blood was taken and serum prepared from mice inoculated with 2 x 10^7 fresh BCL_1 cells on day 0 and sequentially treated i.p. on day 4 with 0.5 mg AT130-2, AT128 m2a, anti-idiotype or irrelevant control for 48 and 96 hr. 10 µl of diluted serum was added to 90 µl πBCL_1 cells at 1 x 10^6 cells / ml and incubated for 30 min in the dark at 4 °C before staining by indirect immunofluorescence and analysis by flow cytometry. Example flow cytometry plots are shown for the standard curve of anti-idiotype, which was run along the serum samples (test serum) (a). A standard curve for each mAb was established and this was used to determine the serum concentration of each mAb (b). The graph represents the average of duplicate mice for each condition, from two separate BCL_1 tumour tracking experiments (c). It shows that serum levels of anti-idiotype (Mc106A5) remained high, whereas serum levels of AT130-2 and AT128 m2a were reduced to almost undetectable levels. .

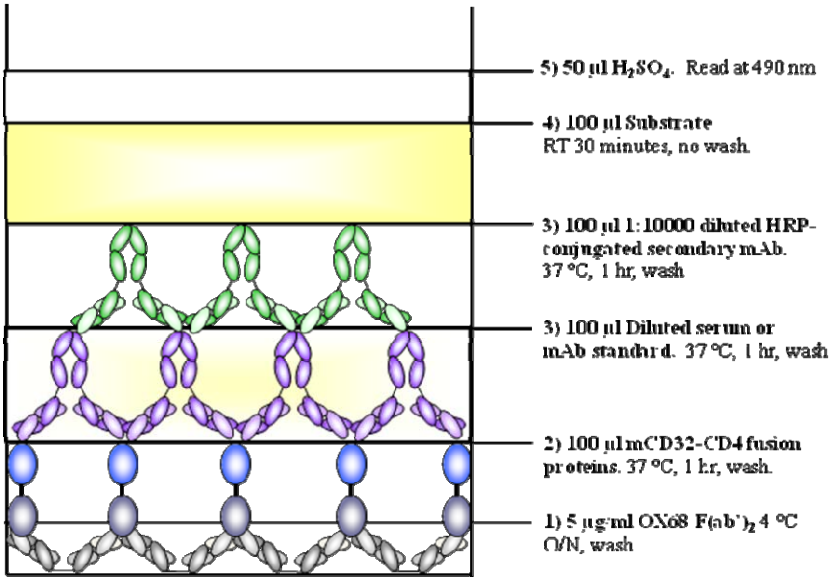

Figure 5.21. Schematic for anti-CD32 mAb detection in murine serum by ELISA.
(1) A 96-well immunomaxisorb plate was coated with 100 µl / well of OX68 F(ab')$_2$ at 5 µg/ml in ELISA coating buffer and incubated for 1 hr at 37 °C, then at 4 °C overnight. (2) Coating solution was discarded and replaced with 100 µg/ml CD32-CD4 fusion protein diluted 1:2 with 1% BSA/PBS and incubated at 37 °C for at least 1 hr. (3) Standard dilution of the mAb of choice commenced at 100 ng/ml and a standard curve produced through doubling dilution, with sample dilutions starting at 1:100 from neat serum and diluted 1:10 down the ELISA plate and incubated at 37 °C for 90 min. (4) 100 µl / well goat anti-mouse FcγR-HRP diluted 1:10000 in 1% BSA/PBA was dispensed into all wells and incubated for a further 90 min. (5) In order to stop the reaction 50 µl of 2.5 M H_2SO_4 was added to each well. The ELISA results were then read at an absorbance of 495 nm and serum concentration of mAb was calculated against the standard curve.

a)

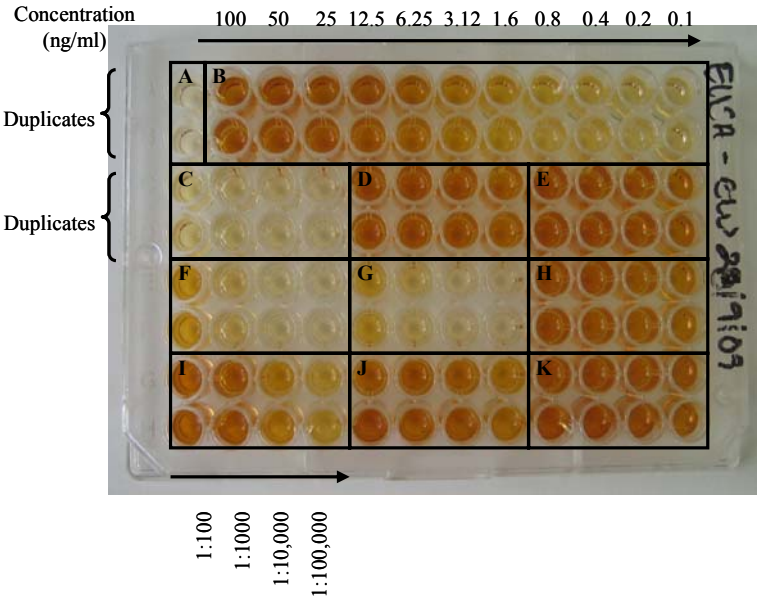

Key:

A: 1% BSA/PBS

B: Standard curve for AT130-2

C: Normal mouse serum

D: WT 48 hr post AT130-2

E: WT 48 hr post AT130-2

F: WT 96 hr post AT130-2

G: WT 96 hr post AT130-2

H: CD32$^{-/-}$ 48 hr post AT130-2

I: CD32$^{-/-}$ 48 hr post AT130-2

J: CD32$^{-/-}$ 96 hr post AT130-2

K: CD32$^{-/-}$ 96 hr post AT130-2

b)

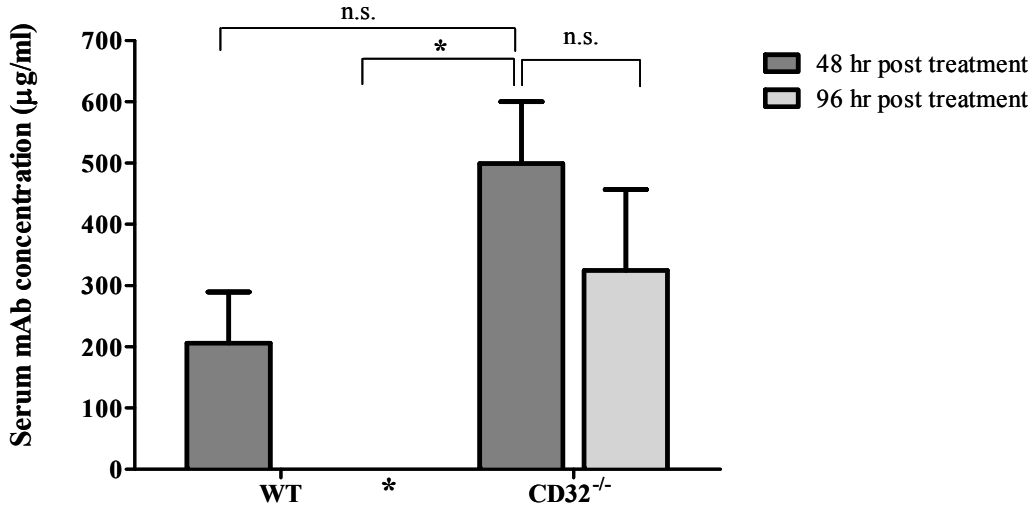

Figure 5.22. Serum levels of AT130-2 in BALB/c mice inoculated with 2 x 10^7 BCL_1.
The serum of WT and CD32$^{-/-}$ mice from the tumour tracking experiments, described previously (Figure 6.6), was serum levels of AT130-2 were determined by ELISA as described in Figure 6.7. At 48 hr post treatment, serum levels of AT130-2 are greater in the CD32$^{-/-}$ mice than in the WT mice. At 96 hr post treatment, there is no detectable AT130-2 in the WT mice (*), whereas levels of AT130-2 in the CD32$^{-/-}$ mice remained comparable to those at 48 hr post treatment. Data represents the average of four mice from two experiments, error expressed as SD.

6.3.3. Comparing the rate of AT130-2 consumption in WT, CD32$^{-/-}$ and γ-chain$^{-/-}$ mice.

Having established that there was a difference in the mAb consumption between WT and CD32$^{-/-}$ mice we next wished to determine the rate of anti-CD32 mAb consumption in non-tumour bearing mice. As activatory FcγR are also capable of binding mAb we also performed these experiments in γ-chain$^{-/-}$ mice which only express CD32. This allowed us to directly measure mAb consumption by CD32 and determine the contribution of the activatory FcγR to this process. In these experiments, mice were injected i.v. with 0.5 mg AT130-2 and tail bled on days 1, 2, 7 and 14. Serum was obtained and serum mAb levels were determined by ELISA, as previously described (Section 6.3.1). In addition, we also included an anti-CD20 mAb (rit m2a) for comparison to determine the half-life of other murine IgG2a mAb. This data was courtesy of Dr Stephen Beers (University of Southampton)[364]. We compared the serum levels of rit m2a in WT, CD20 Tg and CD20 Tg/γ-chain$^{-/-}$ mice, with the aim to address consumption when the mAb doesn't bind to its target antigen (WT), when it does bind to its target antigen (CD20 Tg) and consumption of mAb through activatory FcγR engagement (CD20 Tg/γ-chain$^{-/-}$).

In the WT mouse AT130-2 was consumed rapidly within 48 hr and was undetectable by day 7. In comparison AT130-2 was still detectable in the serum of CD32$^{-/-}$ mice at day 14 ($p < 0.0001$, by ANOVA statistical test). Consumption of AT130-2 in the γ-chain$^{-/-}$ mouse was identical to that in the WT mice, indicating that it is exclusively CD32 expression in the WT mouse that is responsible for anti-CD32 mAb consumption *in vivo* (Figure 6.8a). When examining the data obtained from the CD20 Tg experiments the picture is very different. In WT, CD20 Tg or CD20 Tg/γ-chain$^{-/-}$ mice rit m2a was still detectable after 14 days and even at 28 days (data not shown), although the levels of rit m2a are slightly less in mice expressing CD20, there was no significant difference between these groups ($p = 0.4721$, by ANOVA statistical test) (Figure 6.8b). This was in stark contrast to the rapid depletion of serum levels of AT130-2, suggesting that the precipitously lose of anti-CD32 mAb in mice expressing CD32 is a unique property of these antibodies and the receptor. We next endeavoured to discover whether this loss of mAb could be overcome.

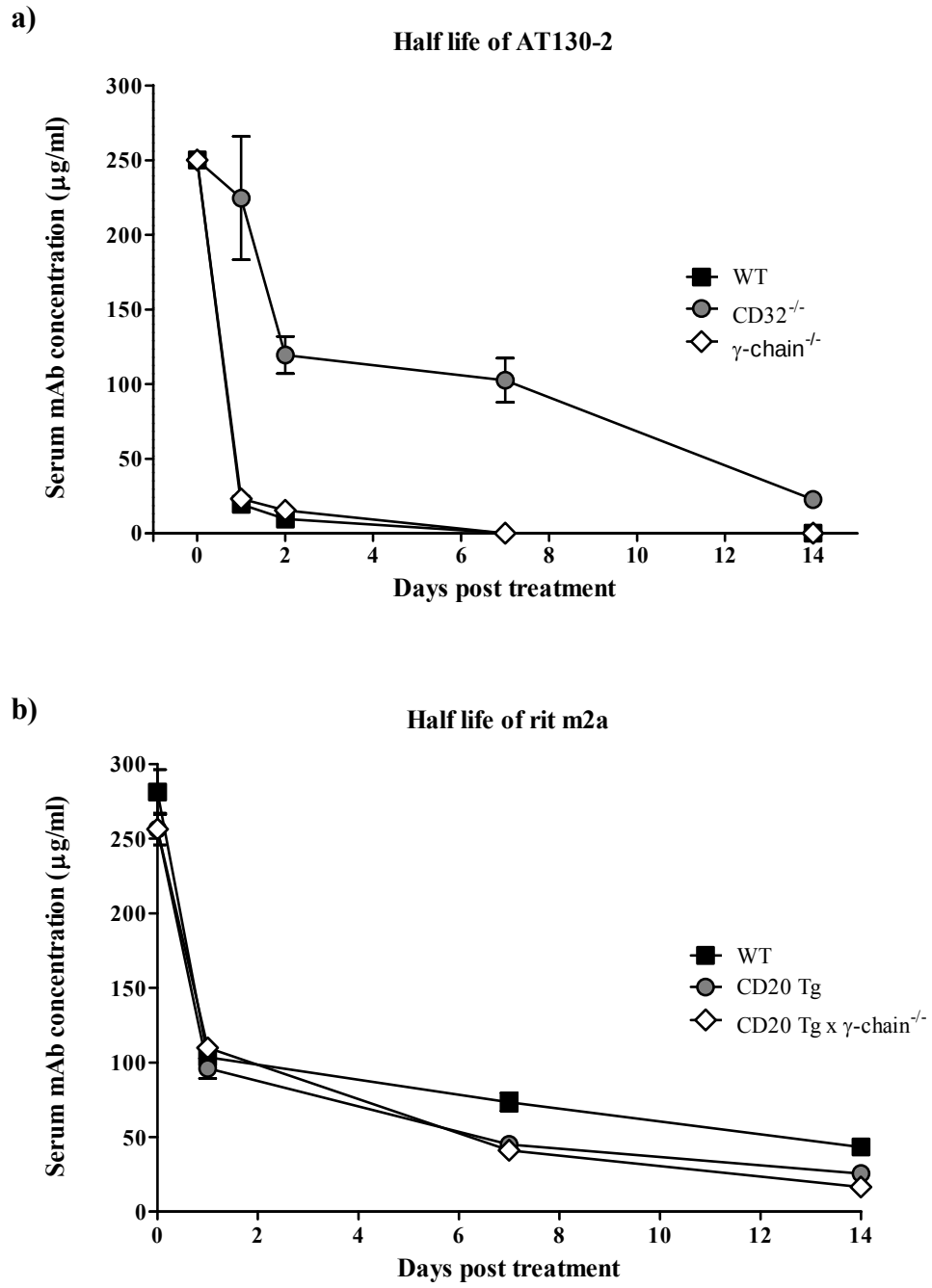

Figure 5.23. Serum mAb levels of AT130-2 in WT, CD32$^{-/-}$ and γ-chain$^{-/-}$ mice and rit m2a in WT, CD20 Tg and CD20 Tg/γ-chain$^{-/-}$ mice.
Mice were injected i.v. with 0.5 mg AT130-2 or rit m2a on day 0. Serum was then obtained and the levels of AT130-2 present were determined by ELISA and serum levels of rit m2a determined by cellular bioassay (section 6.3.1). AT130-2 was rapidly consumed in the WT and γ-chain$^{-/-}$ mice after 24 hr and was undetectable by day 7. In contrast, AT130-2 serum levels were maintained up to 14 days in the CD32$^{-/-}$ mice ($p < 0.0001$, by ANOVA statistical test) (a). This is in stark contrast to the gradual depletion of serum mAb in CD20 Tg expressing mice, where CD20 Tg expression did not significantly change mAb consumption ($p = 0.4721$, by ANOVA statistical test) (b). Data is a representative result from three experimental repeats, where n = four animals per group, error is expressed as SEM.

6.3.4. Repeated doses of AT130-5 *in vivo.*

We were interested to determine whether repeated doses of mAb would increase the longevity of mAb in the serum of WT mice and as such provide a potential means to improve immunotherapy. Mice were given one, two or three doses of AT130-5 (0.5 mg, i.v.) and tail bled 1, 2, 4 and 7 days after the final dose of the mAb. It was determined that multiple doses of mAb could marginally increase the longevity of the mAb in the serum, but this was still far less than in the $CD32^{-/-}$ mouse, as shown by comparison 2 days after the final dose of mAb. Although there was an observable difference between the serum mAb levels in the WT mice administered different doses of AT130-5 on day 1 (Figure 6.9a), there was no significant difference between serum mAb irrespective of dose by day 2 (Figure 6.9b). However, there was a significant difference between the serum mAb levels in the $CD32^{-/-}$ mouse after a single 0.5 mg dose of AT130-5 in comparison to single, double or triple i.v. doses in the WT mouse ($p < 0.001$, $p < 0.001$ and $p < 0.05$, respectively).

6.3.5. Tissue specific consumption of mAb *in vivo*.

Given the remarkable consumption of anti-CD32 mAb in our previous experiments we were interested to establish which tissues were responsible for the consumption of the anti-CD32 mAb *in vivo*. CD32 is predominately expressed by B cells and macrophages, although other cell and tissue types such as FDCs have also been shown to express CD32[146], therefore we postulated that rapid mAb consumption could be reduced, if not completely diminished, by depletion of B cells and macrophages. To examine this we depleted B cells from CD20 Tg BALB/c mice using a single, 250 μg dose of the type II anti-CD20 mAb, FGM6 (Tenovus). This mAb completely depleted CD20 Tg B cells from the spleen and peripheral blood seven days post treatment and depletion was maintained for up to a month. To demonstrate B cell depletion, the spleens of B cell depleted mice were stained with Peridinin-chlorophyll-protein complex (PerCP)-conjugated B220 (BD Biosciences, UK) and APC-conjugated CD19 and analysed by flow cytometry (Figure 6.10a).

In order to deplete macrophages clodronate liposomes were prepared as described in Materials and Methods section 2.23 and administered by i.v. injection to WT BALB/c mice. These liposomes are artificially prepared spheres, consisting of concentric phospholipid bilayers, separated by aqueous compartments. During formation of the vesicles, small molecules such as clodronate can become encapsulated within these

structures and this facilitates the uptake of such small molecules that otherwise would not be engulfed by phagocytic cells[412]. The i.v. injection of clodronate containing liposomes has been shown to deplete phagocytic cells in both the spleen and liver within 24 hr[413].

Cells are depleted after clodronate liposomes accumulate within the phagocytic cells, where the clodronate induced irreversible metabolic damage and resulting apoptosis[414]. Clodronate itself is not toxic and when released from apoptotic cells has a relatively short half life *in vivo*[415]. Importantly, apoptosis does not induce inflammation in surrounding tissues, so depletion of phagocytic cells in this way should be fairly innocuous to the animal and most importantly should not activate the immune system. PBS liposomes were prepared alongside the clodronate liposomes as a control for macrophage depletion. Macrophage depletion was detected in the clodronate liposome treated mice, but not in the PBS liposome treated mice, three days post injection and was maintained for at least seven days, as determined by splenic staining with PE-conjugated CD11b and APC-conjugated F480 and analysis by flow cytometry (Figure 6.10b).

Having depleted both B cells or macrophages, mice were then injected with 0.5 mg i.p. AT130-2 and tail bled on days 1, 2, 4, and 7, serum prepared and sample analysed by ELISA. As previously described (section 6.3.1 & 6.3.2), AT130-2 in the WT mouse was rapidly consumed, with less than 50 µg/ml detectable after 2 days (Figure 6.10c &d). In contrast, serum levels of AT130-2 in $CD32^{-/-}$ mice remains high, even after 7 days ($p < 0.0001$, by ANOVA statistical testing) (Figure 6.10c & d). When B cells were depleted serum levels of AT130-2 persisted at high levels in comparison to WT mice at day 1 and 2 (approximately 200 µg/ml in the CD20 Tg mouse versus approximately 80 µg/ml in the WT mouse at day 1 and approximately 150 µg/ml versus approximately 30 µg/ml by day 2; $p = 0.0007$, by ANOVA statistical test), but these had rapidly depleted at day 4, similar to levels of serum AT130-2 in WT mice (Figure 6.10c). Similarly, macrophage depletion also resulted in increased serum AT130-2 levels at days 1, 2 and 4 in comparison to both WT and PBS liposome treated mice ($p < 0.0001$ for both, by ANOVA statistical testing) (Figure 6.10d), however serum levels of AT130-2 were undetectable by day 7. PBS liposome treated mice shown similar consumption of AT130-2 to WT mice ($p = 0.3970$, by ANOVA statistical test), suggesting that the PBS liposomes had little effect on mAb consumption (Figure 6.10d). These data suggest that both B cells and macrophages are involved in the consumption of anti-CD32 mAb *in vivo* and depletion of these cell subsets would lead to increased serum longevity of these mAb.

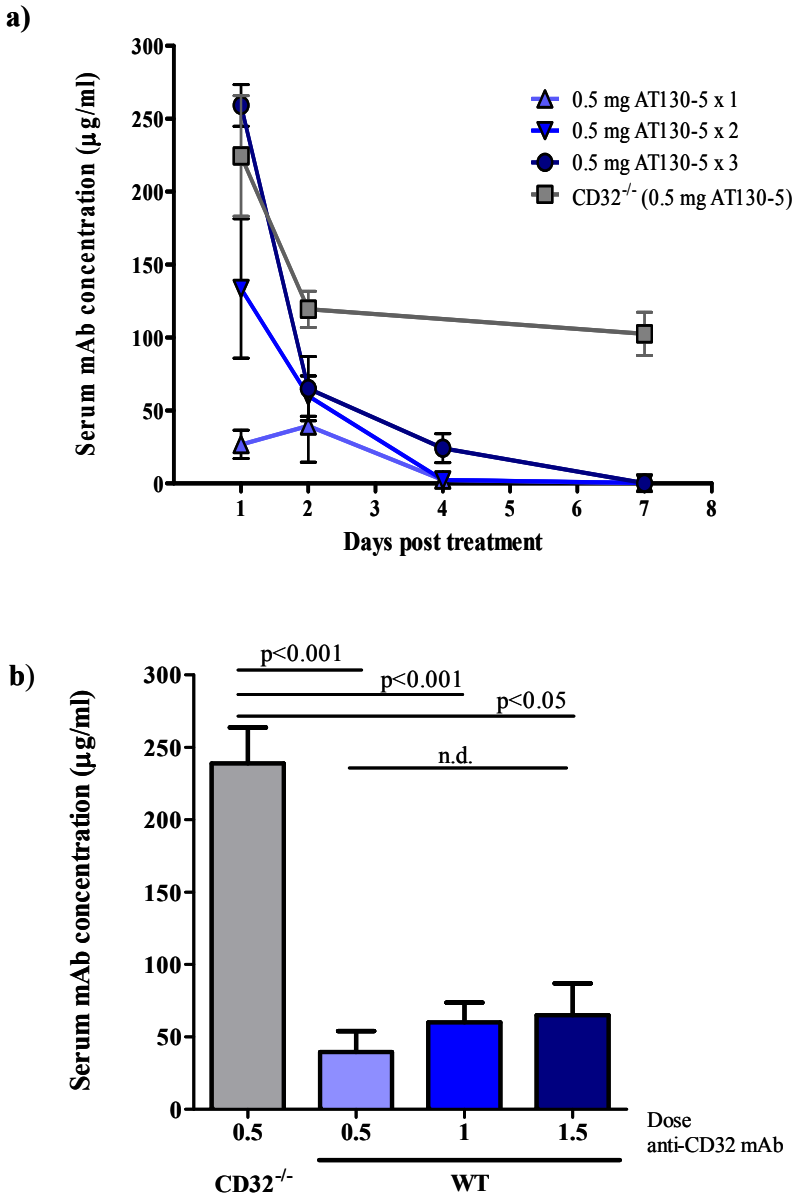

Figure 5.24. Serum mAb levels of AT130-5 in WT mice injected with multiple 0.5 mg doses of anti-CD32 mAb.

WT mice were injected i.v. with one, two or three shots of AT130-5, serum was obtained after the final dose of mAb and serum mAb levels determined by ELISA. These data show that although serum levels of AT130-5 were greater with multiple doses of the mAb at 24 hr after the final dose (a) there is no significant different by day 2 irrespective of mAb dose (b) and serum mAb was undetectable by day 7 in all cases. In contrast, a single dose of anti-CD32 mAb resulted in maintained serum mAb which was significantly greater at day 2 in the $CD32^{-/-}$ mouse in comparison with the WT mouse receiving either one, two or three doses of AT130-5 ($p < 0.001$, $p < 0.001$ and $p < 0.05$, respectively) (b). Data is a representative result from two experimental repeats, where n = three animals per group, error is expressed as SEM.

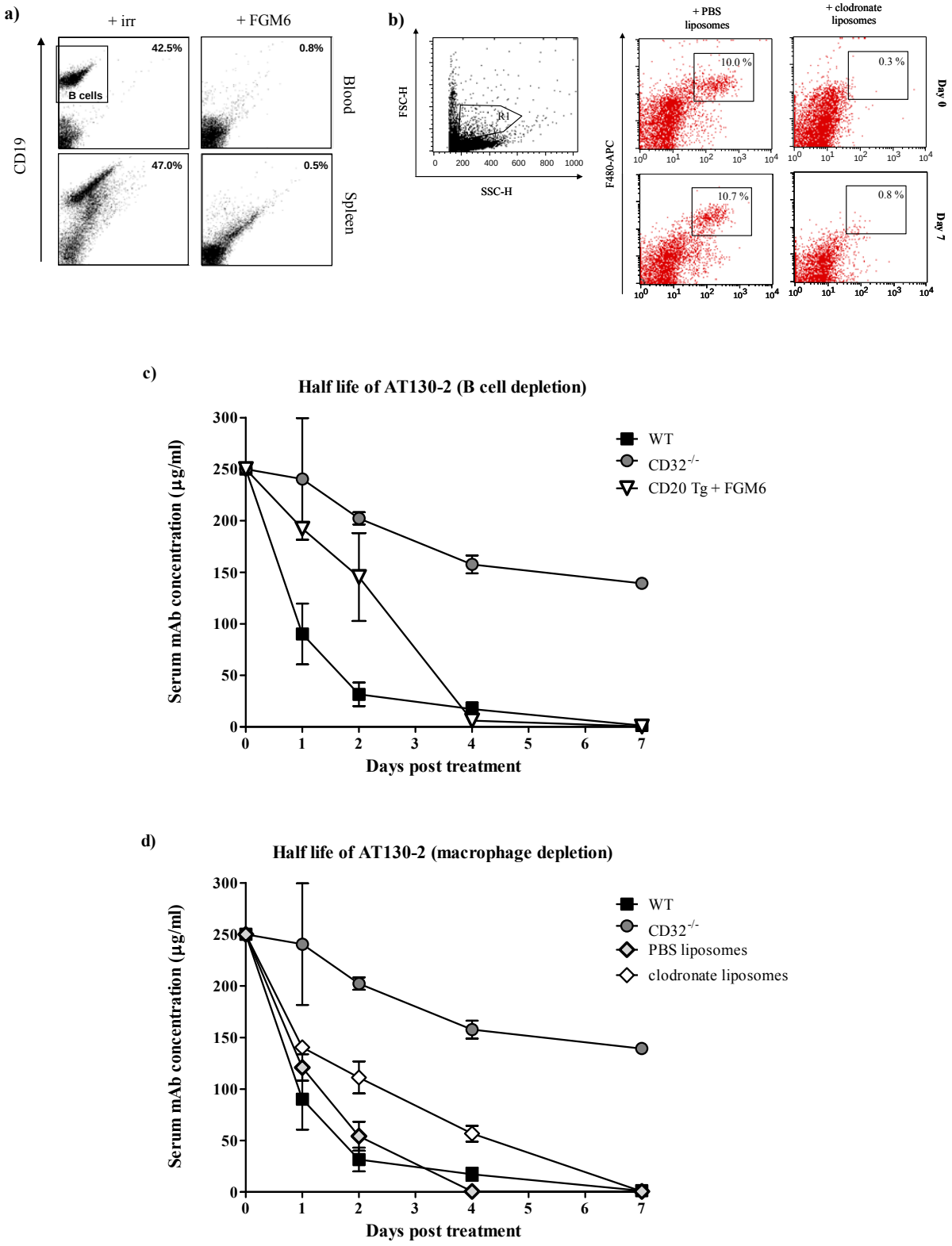

Figure 5.25. Serum mAb levels of AT130-2 in WT, B cell and macrophage depleted mice.
CD20 Tg mice were depleted of B cells by administration of a 250 µg dose of FGM6.WT mice were depleted of macrophages by administration of clodronate liposomes, 200 µl i.v. day – 3 and -1. B cell (a) and macrophage (b) depletion was determined by flow cytometry on day 7. Mice were then injected i.v. with 0.5 mg AT130-2 day 0, serum obtained day 1, 2, 4 and 7 and serum mAb levels assessed by ELISIA (previously described). Here, AT130-2 was rapidly consumed from the serum of the WT (c & d – black squares) and PBS liposome treated controls (d- grey diamonds). As previously seen, serum levels of AT130-2 were sustain in the $CD32^{-/-}$ mice ($p < 0.0001$, by ANOVA) (c & d – grey circles). Both B cell (c) and macrophage (d) increased serum longevity of AT130-2 compared to the appropriate controls ($p = 0.0007$ & $p < 0.0001$, respectively, by ANOVA). Data are the result from one experiment, where n = four animals per group, error is expressed as SEM.

6.4. *In vivo* antigenic modulation of CD32.

6.4.1. *In vivo* antigenic modulation of CD32 in the WT mouse.

Having established that the anti-CD32 mAb were rapidly consumed *in vivo*, leading to a precipitous loss from the serum we next went on to determine how exactly this consumption was occurring. Other work in this laboratory has recently discovered that anti-CD20 mAb can become internalised and consumed *in vivo*, thus limiting its immunotherapeutic capacity ([364] & unpublished observations). B cells incubated with the type I anti-CD20 mAb lose surface CD20 expression and this has been demonstrated to be due to receptor and mAb internalisation. It was speculated that this may also be true for the anti-CD32 mAb, where CD32 and bound anti-CD32 mAb maybe be internalised and as such reduce serum mAb levels.

In order to assess CD32 modulation on normal B cells we treated non-tumour bearing WT BALB/c mice with 0.5mg AT130-2 and AT128 m2a i.v. for 48 hours. Splenocytes were assessed for CD32 levels using indirect immunofluorescence methods as outlined in Material and Methods section 2.7. Briefly, the spleen from mice that had been treated with irrelevant mAb (WR17) were incubated with excess (10 μg/ml final concentration), AT130-2 or AT128 m2a to establish the maximal binding of the antibodies to untreated cells. The spleens of mice treated with, AT130-2 or AT128 m2a were processed in two ways. Cells were left untreated to assess surface bound mAb after treatment, or the cells were incubated with mAb in excess to determine antigen expression after treatment. Cells from mice treated with AT130-2 were incubated with AT130-2 at 10 μg/ml and cells from mice treated with AT128 m2a were incubated with AT128 m2a at 10 μg/ml. It was shown that splenocytes from WT mice treated with mAb demonstrated a down regulation of CD32 on splenocytes with AT130-2 treatment and with AT128 m2a treatment (Figure 6.11). It is also apparent from these data that there is some divergence between the total amount of mAb bound on untreated splenocytes and the surface bound mAb after treatment, suggesting that by some, as yet undetermined process, mAb is being removed from the cell surface. We were somewhat perplexed by the observed changes in CD32 expression after treatment with the anti-CD32 mAb as the CD32 isoform predominately expressed on B cells (CD32b1) has been reported to lack endocytic properties, supposedly due to a nineteen amino acid insertion in the transmembrane domain of the human receptor[293] and a 47 amino acid insertion in the murine receptor in comparison to the endocytic isoform (CD32b2) expressed in macrophages and as such, should not become internalised upon engagement.

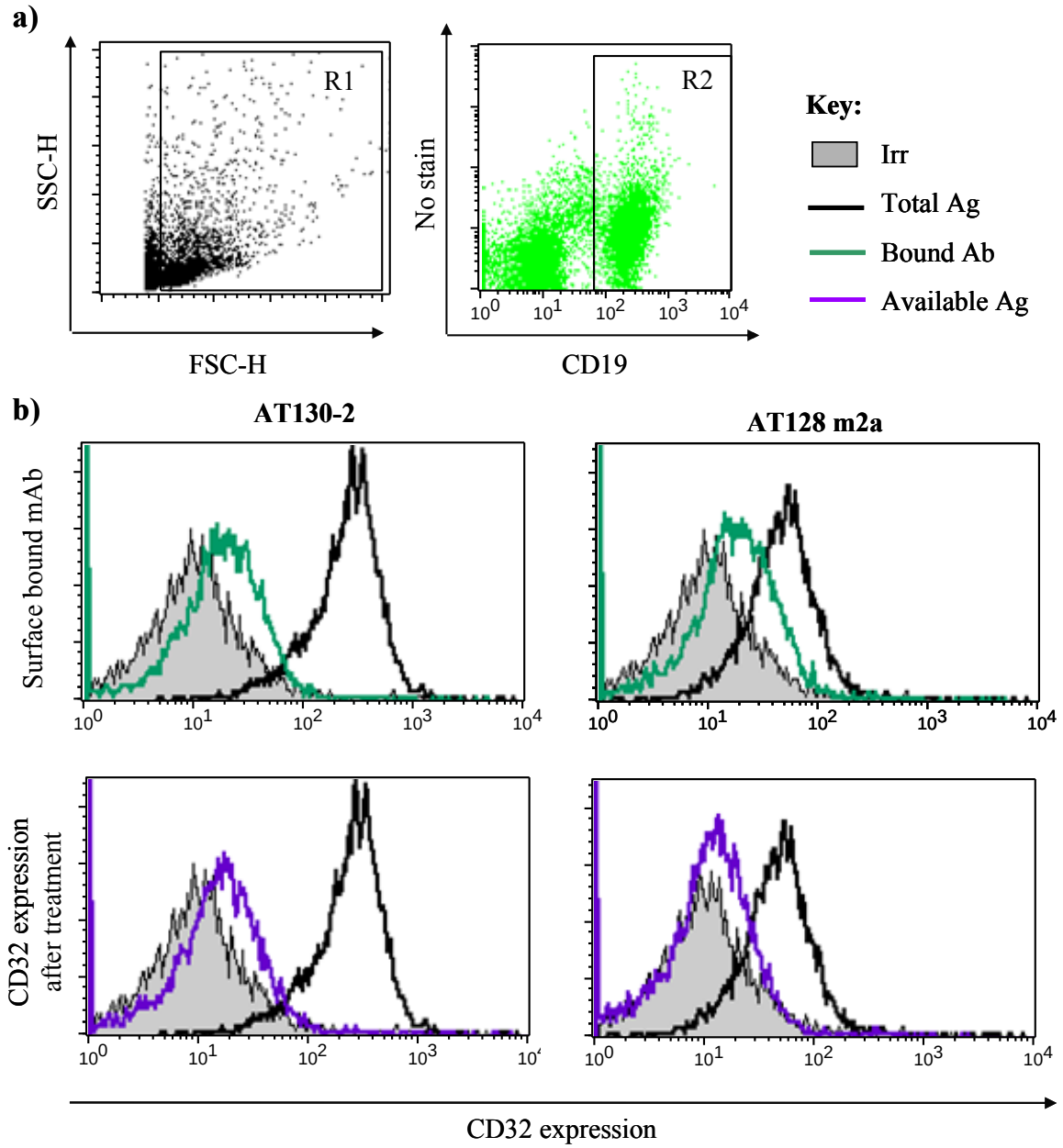

Figure 5.26. *In vivo* antigenic modulation of CD32 in WT mice.
WT mice were injected i.v. with 0.5 mg AT130-2 or irrelevant control (WR17). 48 hr after treatment the spleens of these mice were excised. 100 µl of splenocytes were incubated with or without excess mAb (10 µg/ml) and incubated for 30 min at 4 °C in the dark and stained according to indirect immunofluorescence protocol (Materials and Methods 2.11). These were then incubated with APC-conjugated CD19 for 15 min before being washed once and analysed by flow cytometry. Live B cell events were collected as identified by FSC-H versus SSC-H (R1) and CD19 positivity (R2) (a). CD32 expression was expressed as cell number versus FL-2 fluorescence. Total CD32 expression is shown in the black histogram, these were WR17 treated splenocytes incubated with excess anti-CD32 mAb. The mAb retained at the cell surface is shown in the green histogram and CD32 expression after treatment with mAb is shown in the purple histogram (b). Here, in both the AT130-2 and AT128 m2a there is a reduction in surface bound mAb (green histograms) and a decrease in CD32 expression after treatment (purple histograms). Data is a representative result from three experimental repeats.

6.4.2. Loss of surface CD32 *in vivo* is not a result of FcγR-dependent macrophage shaving.

One potential mechanism that could lead to loss of CD32 binding after anti-CD32 mAb treatment *in vivo* is macrophage shaving as described by Beum *et al* (2006). During shaving, CD20 is lost from the surface of B cells due to the removal and uptake of rituximab/CD20 complexes by effector cells (in this case THP-1 monocytes differentiated to a macrophage-like phenotype using retnoic acid). Beum *et al* (2006) illustrated that macrophage shaving was an Fc dependent function that leads to the removal of antibody bound receptors from the surface of the cell membrane after Fc engagement with activatory FcRs (in particular FcγRI) on macrophages [416].

To address whether, in our assays, macrophage shaving was a plausible mechanism leading to changes in CD32 levels after treatment with the anti-CD32 mAb, we analysed CD32 expression after administration of AT130-2 or AT128m2a to WT and γ-chain$^{-/-}$ BALB/c mice. As γ-chain$^{-/-}$ mice lack activatory FcγR macrophage shaving of mAb/CD32 complexes cannot occur. CD32 expression was measured by indirect immunofluorescence, as previously described. Almost identical modulation of CD32 expression occurred in WT and γ chain$^{-/-}$ mice treated for 48 hr with AT130-2 or AT128 m2a; where treatment with the anti-CD32 mAb results in a reduction in CD32 expression (Figure 6.12). This suggests that the process by which we see a reduction in CD32 surface levels is independent of activatory FcR engagement and therefore not due to macrophage shaving. In addition there is a loss of surface bound mAb, suggesting that the process of CD32 expression loss could be through antigenic modulation. In order to address this we next examined *in vitro* changes in CD32 expression after treatment with the anti-CD32 mAb.

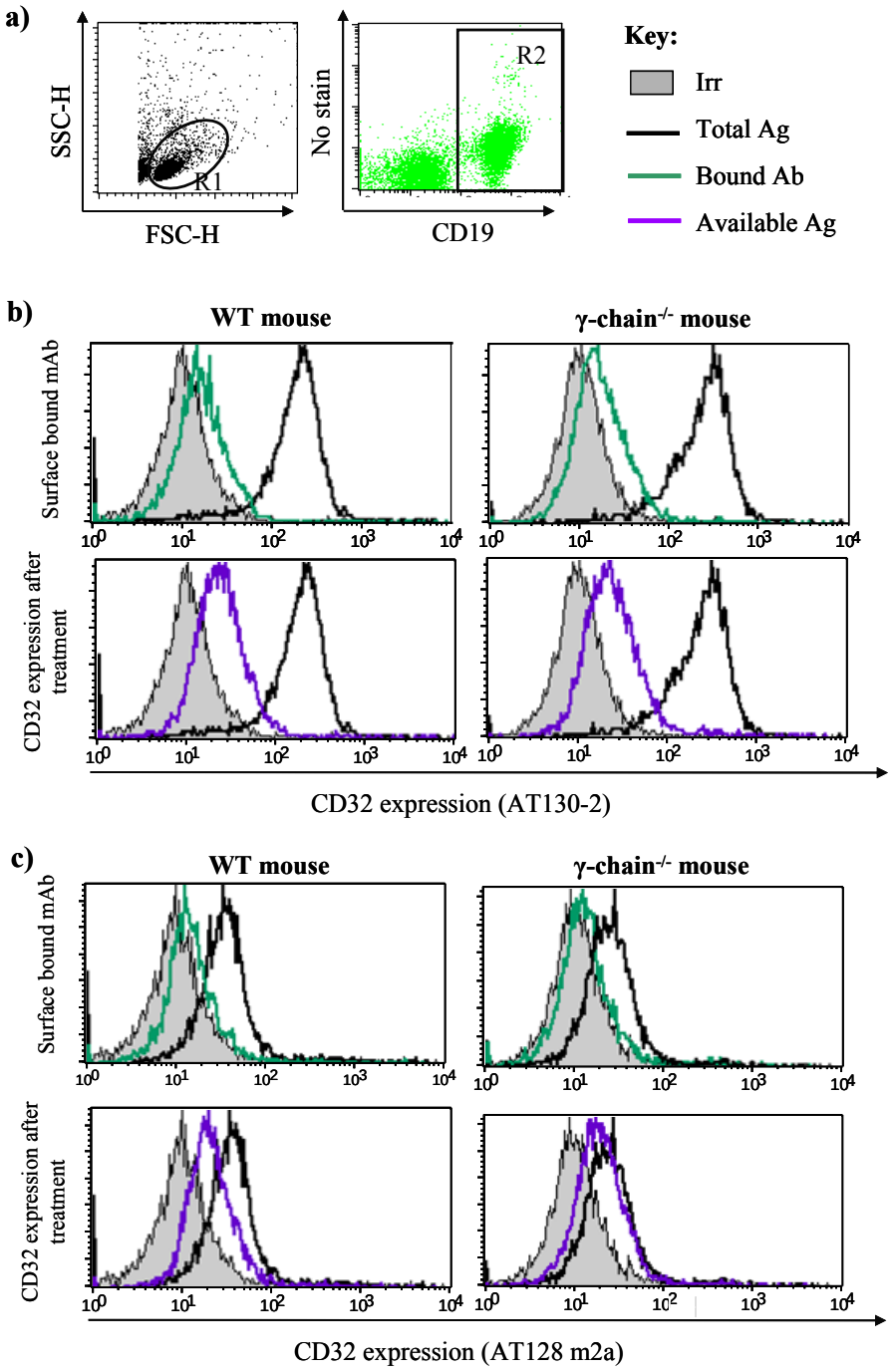

Figure 5.27. *In vivo* antigenic modulation of CD32 on B cells from WT and γ chain$^{-/-}$ mice after treatment with anti-CD32 mAb.

WT and γ-chain$^{-/-}$ mice were injected i.v. with 0.5 mg AT130-2 or irrelevant control (WR17). 48 hr after treatment the spleens of these mice were excised. 100 µl of splenocytes at approximately 1 x 10^6 cells / ml, from both the irrelevant and anti-CD32 mAb treated mice were incubated with or without excess AT130-2 or AT128 m2a (10 µg/ml), incubated for 30 min in the dark at 4 °C, stained according to indirect immunofluorescence protocols and analysed by flow cytometry. Live B cell events were collected as identified by FSC-H versus SSC-H (R1) and CD19 positivity (R2) (a). CD32 expression was expressed as cell number versus FL-2 florescence. Total CD32 expression is shown in black, mAb retained at the cell surface is shown in green and CD32 expression after treatment with AT130-2 is shown in green. In both the WT and γ-chain$^{-/-}$ mice surface mAb is reduced after treatment, as is CD32 expression. These data demonstrate that surface bound mAb and CD32 expression decreased after 48 hr of treatment with AT130-2 (b) or AT128 m2a (c) and these are identical in both WT and γ-chain$^{-/-}$ mice, indicating that FcγR dependent shaving is unlikely the explanation for loss of CD32 expression after treatment. Data is a representative result from three experimental repeats.

6.5. *In vitro* antigenic modulation of lymphoma cell lines and WT B cells.

The previous data suggested that antigenic modulation was not due to macrophage shaving, leaving the possibility that the anti-CD32 mAb was binding to target cells and then being internalised. We went on to examine the effect of anti-CD32 mAb treatment on various B cell types *in vitro*. Cells from either lymphoma cell lines or B cells isolated from BALB/c and C57BL/6 spleens were incubated for 2, 6 or 24 hr with 10 μg/ml mAb and then stained with excess (10 μg/ml) mAb prior to incubation with an anti-mouse Fc PE-conjugated mAb. It was shown that AT130-2 causes a down regulation of CD32, whilst surprisingly AT128 m2a caused an up regulation of CD32. The change in CD32 expression followed similar trends on WT B cells from BALB/c and C57BL/6 mice (Figure 6.13), Eμ-myc LCLs and πBCL_1 cells (Figure 6.14). The modulation occurred independently of the BCR, as the Eμ#14, IgM negative cell line, showed similar modulation of CD32 to the IgM positive cell line, Eμ#8 (Figure 6.14). In addition, we assessed the modulation capacity of the entire panel of murine anti-CD32 mAb on πBCL_1 cells (Figure 6.15). It was observed that the agonistic mAb (AT130-2 and AT130-5) down-regulated CD32 expression, whilst the antagonistic mAb up-regulated CD32 expression, again confirming that there are two distinct sub-types of anti-CD32 mAb and they seemingly act in opposition to each other.

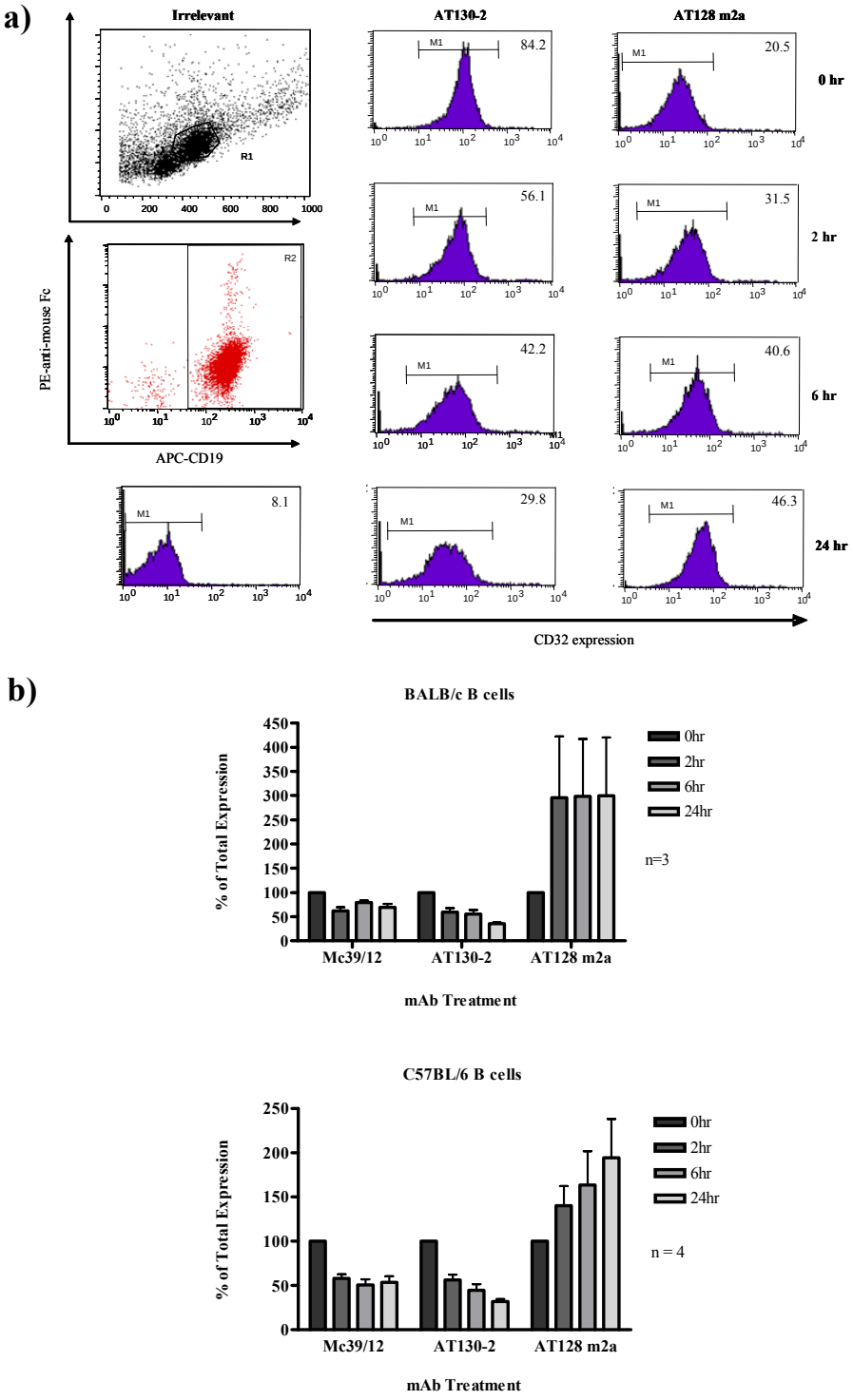

Figure 5.28. *In vitro* modulation of CD32 on WT B cells.
B cells were isolated from BALB/c and C57Bl/6 mice by MACS® separation as described in Materials and Methods section 2.4. Purified B cells (200 µl of cells at 1 x 10^6 cells / ml) were incubated with 10 µg/ml Mc39/12 (anti-BCR (µ)), AT130-2 or AT128 m2a for 2, 6 or 24 hr. Cells were harvested, stained in accordance with indirect immunofluorescence protocols and then incubated with 10 µg/ml APC-conjugated CD19. Live B cell events were collected as identified by FSC-H versus SSC-H (R1) and CD19 positivity (R2) (a). FL2-H MFI versus cell number was taken as a measure of antigen expression and expressed as a percentage of total antigen expression at 0 hr. Mc39/12 and AT130-2 showed a down-regulation of antigen expression over time, whilst AT128 m2a showed increase antigen expression over time (b). This is true for both mouse stains. These data represent results from three experimental repeats for BALB/c mice and four experimental repeats for C57BL/6 mice, error expressed as SEM.

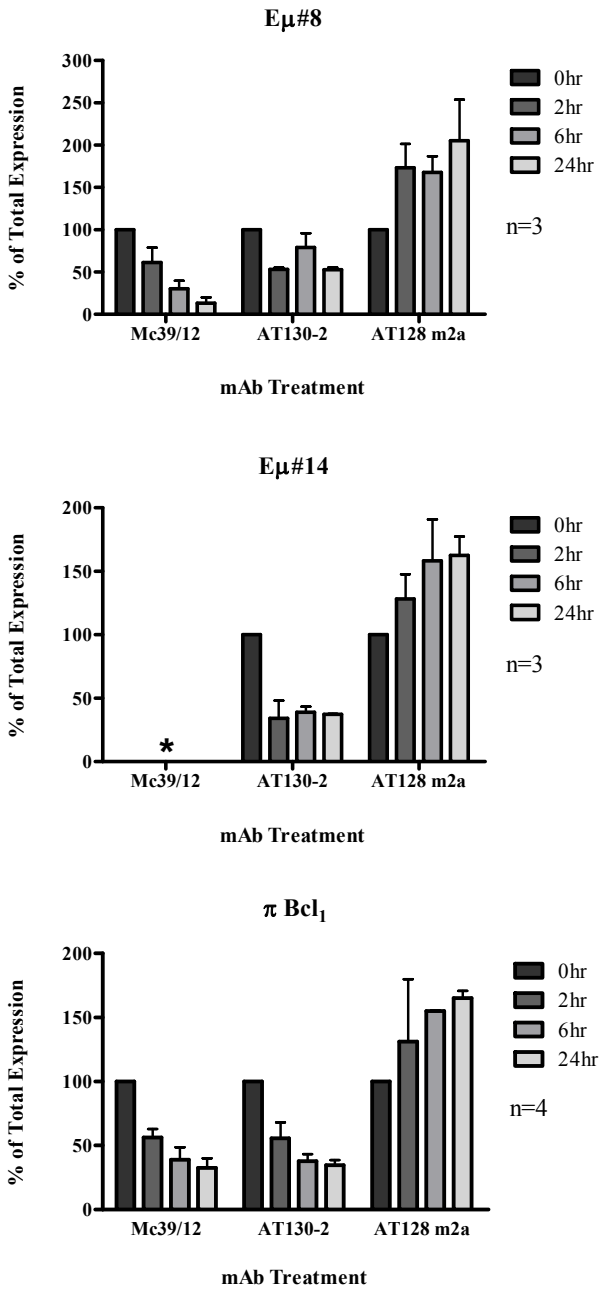

Figure 5.29. *In vitro* modulation of CD32 on lymphoma cell lines.
1 x 10^6 /ml cells were treated with 10 μg/ml Mc39/12, AT130-2 or AT128 m2a for 2, 6 or 24 hr with NT control being used to determine normal physiological antigen levels. Cells were stained in accordance with indirect immunofluorescence protocols. Antigen levels were determined as described above. Mc39/12 and AT130-2 showed a down-regulation of antigen expression over time, whilst AT128 m2a showed increase antigen expression over time (b). This is true for all three cell lines examined. These data represent results from three experimental repeats for Eμ#4 and Eμ#8 LCL and four experimental repeats for πBCL_1 cells, error is expressed as SEM. *Not determined as Eμ#14 is an IgM negative cell line.

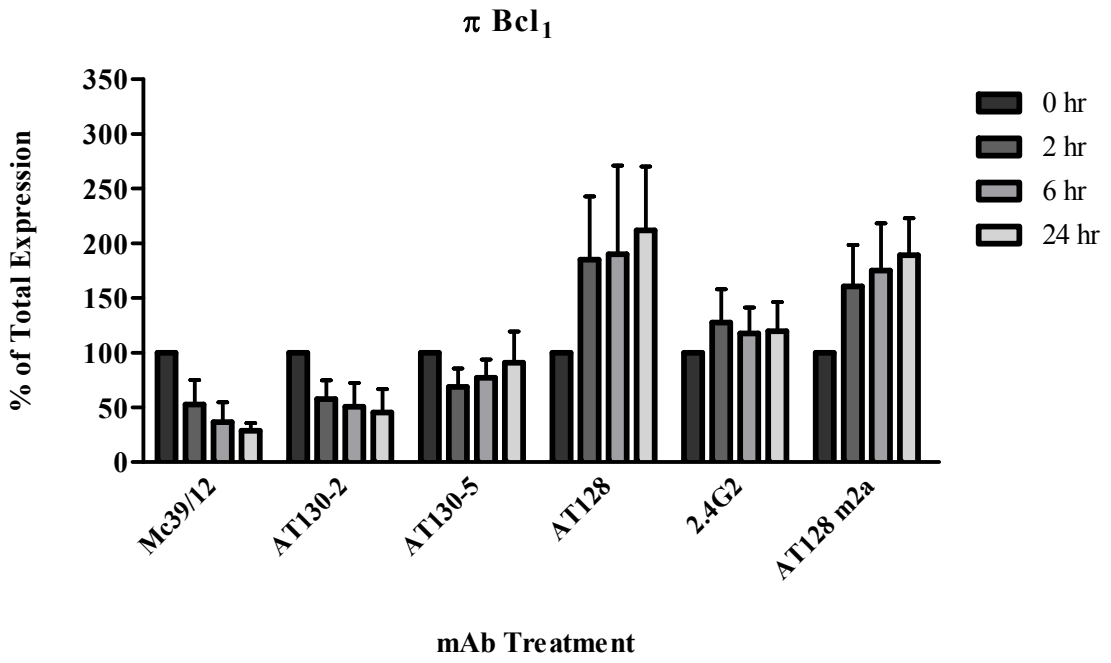

Figure 5.30. The agonistic and antagonistic anti-CD32 mAb show divergent CD32 modulation on πBCL_1 cell *in vitro*.
πBCL_1 cells were treated with 10 μg/ml Mc39/12 or anti-CD32 mAb for 2, 6 or 24 hr with NT control being used to determine normal physiological antigen levels. Cells were stained in accordance with indirect immunofluorescence protocols. 10,000 live cell events were collected as identified by FSC-H and SSC-H (a). FL2-H MFI versus cell number was taken as a measure of antigen expression and expressed as a percentage of total antigen expression at 0 hr. Mc39/12 and AT130-2 showed a down-regulation of antigen expression over time, whilst AT128 m2a showed increase antigen expression over time (b). This is true for all three cell lines examined. These data represent results from three experimental repeats, error expressed as SEM.

6.6. Alexa-488 quenching assays demonstrate internalisation of CD32 by agonistic anti-CD32 mAb *in vitro*.

In order to verify that AT130-2 was becoming internalised at the cell surface we used an Alexa-488 quenching assay. This assay uses Alexa-488 labelled mAb which lose fluorescence when bound by a quenching anti-Alexa-488 mAb reagent. If Alexa-488 conjugated mAb is retained at the cell surface the Alexa-488 fluorescence becomes quenched by anti-Alexa-488 and is therefore detected as a decrease in FL1-H fluorescence when analysed by flow cytometry. In contrast, if an antigen is internalised (modulated) it will be protected from anti-Alexa-488 quenching and will retain FL1-H fluorescence. Samples were therefore analysed before and after the addition of the anti-Alexa-488 mAb and this allowed an assessment of the percentage of Alexa-488 conjugated mAb that was internalised. Prior work within this laboratory has shown that CD20 becomes internalised on CD20 Tg B cells using this assay when bound by the CD20 mAb rituximab, but not by another CD20 mAb, tositumomab (tosit)[364]. Therefore, to provide both positive and

negative controls, CD20 Tg B cells were examined, with rituximab and tosit anti-CD20 mAb, acting as comparisons for CD32 quenching by AT130-2 and AT128 m2a.

It was found that AT130-2 was protected from quenching, much like rituximab, indicating it becomes internalised. Conversely, AT128 m2a became quenched in these assays, much like tosit, implying retention at the cell surface (Figure 6.16). This conclusion was confirmed by fluorescence microscopy. Here, AT130-2 and rituximab were seen to form punctate clusters whilst AT128 m2a and tosit remained diffusely stained on the cell surface, although the latter is not clear from the produced images probably due to the low level of binding of AT128 m2a mAb (Figure 6.17).

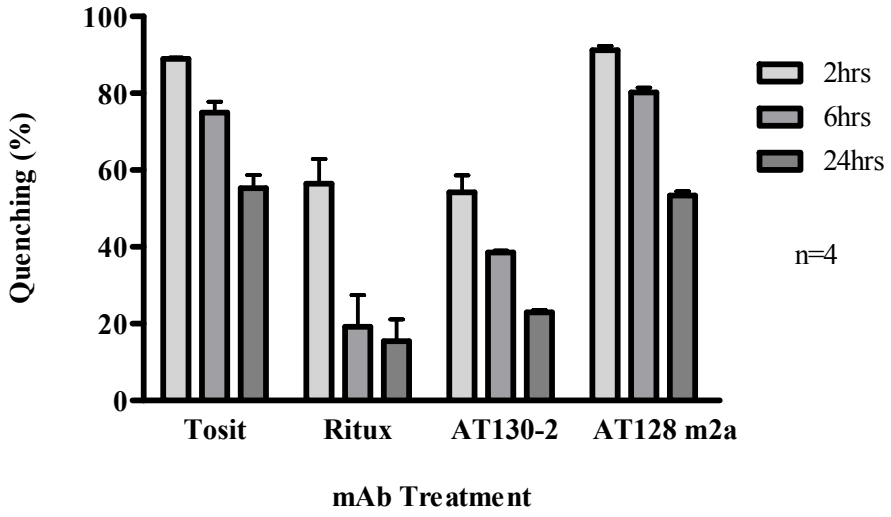

Figure 5.31. Alexa-488 quenching of C57BL/6 CD20 Tg B cells by anti-CD20 and CD32 mAb.
B cells isolated by MACS® separation were incubated with Alexa-488 labelled mAb at 5µg/ml for 2, 6 or 24 hr. Unquenched and quenched (+anti-alexa-488) samples were analysed by flow cytometry. Live B cell events were collected as identified by FSC-H and SSC-H and CD19 staining. FL1-H MFI was taken as a measure of Alexa-488 labelling. Percentage quenching was calculated by (((MFI unquenched sample – background MFI)-(MFI quenched sample-background MFI))/(MFI unquenched sample – background MFI)). AT130-2 and ritux showed a reduction in fluorescence after quenching as shown by a decrease in percentage quenching, indicating internalisation, whereas AT128 m2a and tosit show no decrease in fluorescence after quenching as shown by a smaller decrease in percentage quenching, indicating continued cell surface expression, even at 24 hr. These data represent results from four experimental repeats, where each sample was performed in duplicate, error is expressed as SEM.

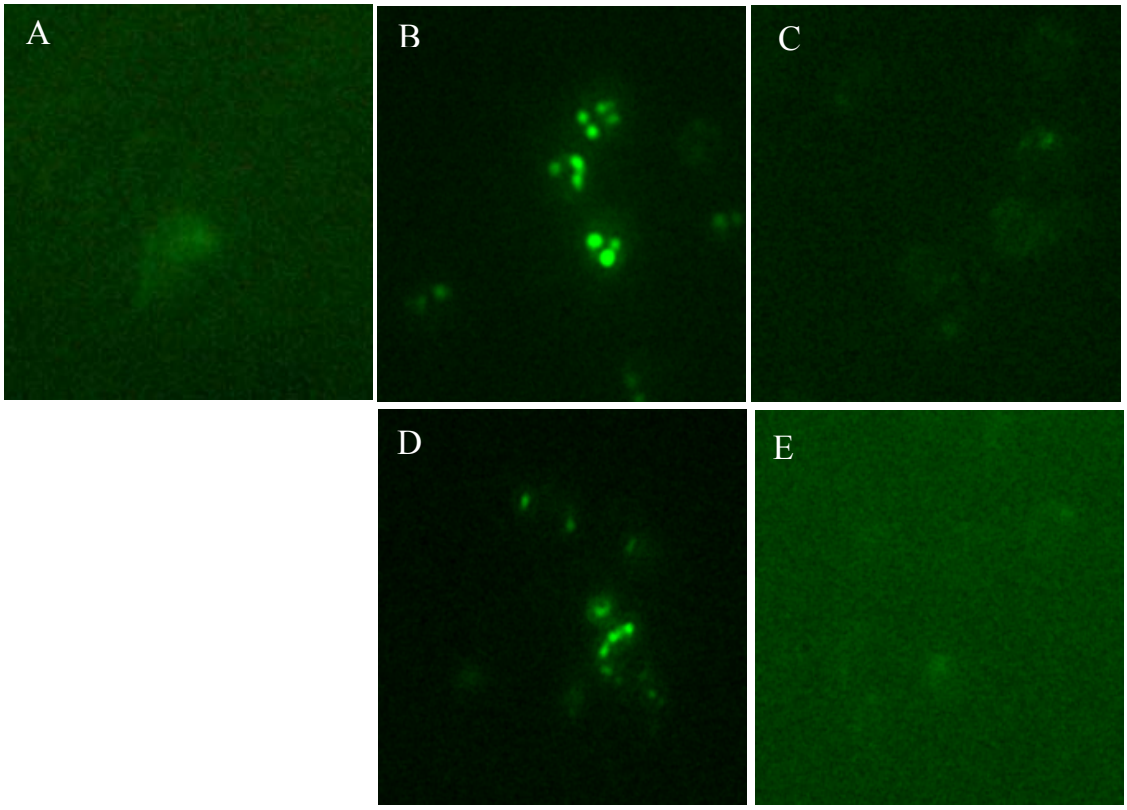

Figure 5.32. Fluorescence microscopy of C57BL/6 CD20 Tg B cells stained with anti-CD20 and CD32 mAb.
CD20 Tg B cells were isolated by MACS® separation were incubated with Alexa-488 labelled mAb at 5 μg/ml for 2, 6 or 24 hr. Unquenched samples were examined by fluorescence microscopy after two washes with BSA-PBS-Azide. Irreverent staining is shown in A. Rituximab (B) and AT130-2 (D) show punctate staining, whereas tosit (C) and AT128m2a (E) show diffuse staining with Alexa-488 at 24 hr. Staining with irrelevant and AT128 m2a conjugated mAb was very weak and required gain of the microscope had to be increased to see any labelling of the cells. These data are a representative result from three experimental repeats.

6.7. CD32 modulation on non-B cells (BMDMs).

6.7.1. Modulation of CD32 on BMDMs *in vitro.*

We next went on to determine if CD32 on macrophages was modulating in a similar fashion to CD32 on lymphoma and B cells. In the macrophages this becomes more difficult as there is the compounding factor of activatory FcγR, which will bind to the Fc portion of the CD32 mAb and potentially undergo endocytosis through endogenous pathways associated with activatory FcγR signalling. We therefore performed our experiments in both WT (BALB/c and C57BL/6) and γ-chain$^{-/-}$ BMDMs.

Similar to the results with B cells, we observed that on WT and γ-chain$^{-/-}$ BMDMs there is a decrease in CD32 expression after AT130-2 treatment and an increase in CD32 expression after treatment with AT128 m2a, demonstrating that the anti-CD32 mAb can modulate CD32 expression on both B cells and macrophages (Figure 6.18). However, surprisingly the IgG1 isotype mAb (AT130-5 and AT128) showed different effects

between WT and γ-chain$^{-/-}$ BMDMs. On WT BMDMs incubation with AT130-2 resulted in a decrease in CD32 expression and incubation with AT130-5, AT128, or 2.4G2 resulted in an increase in CD32 expression. However, incubation with AT128 m2a had relatively little effect on CD32 expression. On γ-chain$^{-/-}$ BMDMs, incubation with both AT130-2 and AT130-5 resulted in a decrease of CD32 expression, whereas pre-incubation with AT128, 2.4G2 or AT128 m2a resulted in an increase in CD32 expression. On B cells incubation with AT130-5 caused a decrease in CD32 expression, whilst AT128 caused an increase in CD32 expression. This is true for CD32 on γ-chain$^{-/-}$ BMDMs, but not on the WT BMDMs. Therefore the interaction of the Fc of the IgG1 mAb with the activatory FcγR is affecting the modulation of CD32 on BMDMs. Presumably this indicates that there is an effect of isotype on CD32 modulation on macrophages. On the WT macrophages, the Fc portion of the anti-CD32 mAb will engage with the activatory FcγR on the surface of these cells. As IgG1 mAb have a higher affinity for the activatory FcγR than the IgG2a mAb, it is expected that the interaction between the activatory FcγR and the IgG1 anti-CD32 mAb and not the interaction between activatory FcγR and the IgG2a mAb will regulate the internalisation of CD32 observed on B cells or γ-chain$^{-/-}$ BMDMs *in vitro*.

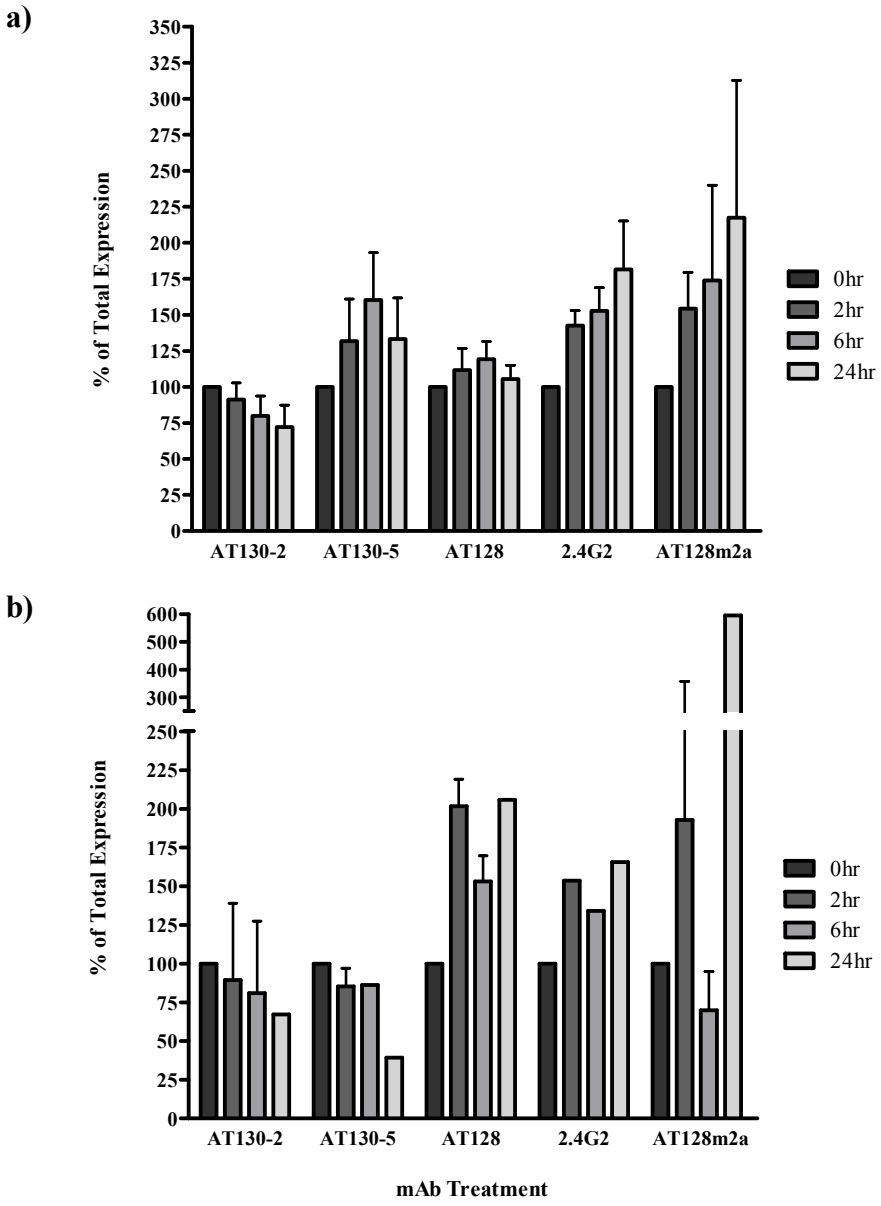

Figure 5.33. *In vitro* modulation of CD32 on BMDMs.
2 x 10^6 /ml cells in a 48-well plate were treated with 10 μg/ml anti-CD32 mAb for 2, 6 or 24 hr or untreated to determine normal physiological antigen levels. Cells were stained in accordance with indirect immunofluorescence protocols, then stained with APC-conjugated F480 before analysis by flow cytometry. Live macrophage events were collected as identified by FSC-H and SSC-H and F480 positivity. FL2-H MFI was taken as a measure of antigen expression and expressed as a percentage of total antigen expression of the untreated sample. On WT (a) and γ-chain$^{-/-}$ (b) BMDMs AT130-2 showed a down-regulation of antigen expression over time, whilst AT128 m2a showed increased antigen expression over time. In contrast however, the IgG1 anti-CD32 mAb show divergent effects on WT and γ-chain$^{-/-}$ BMDMs and this was also different to changes observed on lymphoma cell lines and normal B cells. These data represent results from four experiments, where error is expressed as SEM.

6.8. B cells express the CD32b1 isoform and macrophages express the CD32b2 isoform.

We were surprised that CD32 on the surface of B cells was able to internalise. It was reported by Minstkoff *et al* (1989) and confirmed by others[302,294] that the CD32b1 isoform, predominantly expressed on cells of lymphocyte lineage, did not undergo endocytosis upon

engagement by IC, whilst the CD32b2 isoform, predominately expressed by cells of myeloid lineage, underwent endocytosis upon engagement by IC in both humans and mice. We were therefore surprised that we consistently demonstrated that CD32 on the surface of cells of lymphocyte lineage, both normal B cells and lymphoma cells, internalised CD32 upon engagement. In order to confirm that our B cells and BMDMs were expressing the expected isoforms of CD32 we performed a PCR as described in Materials and Methods section 2.24.3. Briefly, RNA was isolated from purified splenic B cells and BMDMs from both BALB/c and C57BL/6 mice and πBCL_1 cells, converted into cDNA before PCR was performed using primers that had been to detect both CD32 isoforms. PCR products were separated by gel electrophoresis, giving products of 335 bp for mCD32b1 and 194 bp for mCD32-2. The PCR primers were designed flanking the sequence for the intracellular tail of CD32, where there is an extension of 19 amino acids in murine CD32b1, resulting in a larger product for this particular isoform (Figure 6.19). These data demonstrate that, as in accordance with the literature cells of lymphocyte origin predominately express CD32b1 and cells of monocyte origin express CD32b2. However, these data also show that B cells express the CD32b2, whereas macrophages do not seem to express CD32b1. In addition, a third isoform, apparent between the products of CD32b1 and CD32b2 was also observed. This is believed to the CD32b1' isoform as described by Latour *et al* (1996) and was demonstrated to have similar properties to the CD32b1 isoform and is a splice-form of CD32 which contained an extension in the cytoplasmic domain shorter than that observed in CD32b1.

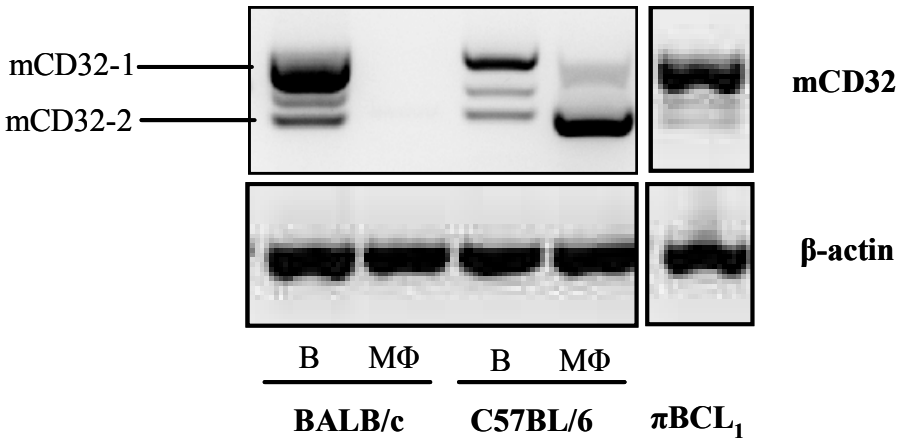

Figure 5.34. Expresssion of CD32 isoforms in normal murine B cells, macrophages and lymphoma cells.
RNA was extracted from approximately 5 x 10^6 normal murine B cells (B), BMDMs (MΦ) and πBCL_1 cells using the PureLink™ Micro-to-Midi Total RNA Purification System. RNA was quantified and converted to cDNA. Primers, designed by Dr. Claude Chan (University of Southampton) were used to give PCR products of 335bp for mCD32-1 and 194bp for mCD32-2. These data show that B cells, including lymphoma cells in this instance, predominately express mCD32-1, whilst C57BL/6 macrophages at least, express mCD32-2; confirming previously published reports on isoform expression. A third PCR product was also visible after electrophoresis, it is believed this was the CD32-1' isoform as described by Latour *et al* (1996).

6.9. The effects of anti-CD32 mAb in adoptive transfer assay.

6.9.1. The anti-CD32 mAb can deplete target B cells in adoptive transfer depletion assays in $CD32^{-/-}$ but not WT recipients.

Having determined that anti-CD32 mAb immunotherapy was limited by mAb consumption as a result of receptor internalisation *in vivo* we next wanted to compare the ability of WT and $CD32^{-/-}$ mice to deplete CD32 positive target cells and thus demonstrate the affect that these two factors may have on anti-CD32 mAb therapy. To address this, we performed an adoptive transfer experiment of CFSE labelled splenocytes into WT and $CD32^{-/-}$ mice and treated these mice with anti-CD32 mAb. In order to distinguish between our non-target (NT) and target (T) populations, $CD32^{-/-}$ splenocytes (NT) were labelled with 0.5 μM CFSE to give low FL-1 fluorescence and WT (CD32 positive) splenocytes (T) were labelled with 5μM CFSE to give high FL-1 fluorescence (Figure 6.20a). These cells were injected i.v. into mice at a 1:1 NT:T ratio on day -1 and treated on day 0 with 100μg mAb, either WR17, AT130-2 or AT128 m2a. After a further 24 hr the spleens of these animals were excised, processed and stained with APC-conjugated CD19. The percentage of non-target (NT) and target (T) cells was determined and expressed as a normalised NT:T ratio (outlined in Materials and Methods section 2.20.2). In the WT and $CD32^{-/-}$ mice there was no deletion of target cells when mice were treated with an irrelevant mAb, nor was there deletion of target cells in the WT mice treated with anti-CD32 mAb. However, in the $CD32^{-/-}$ recipients there was approximately 50 % deletion of target B cells with either of the anti-CD32 mAb used (Figure 6.20b). These data indicate that anti-CD32 mAb consumption in the WT mouse limits the capacity of these mAb to deplete CD32 positive target cells *in vivo*.

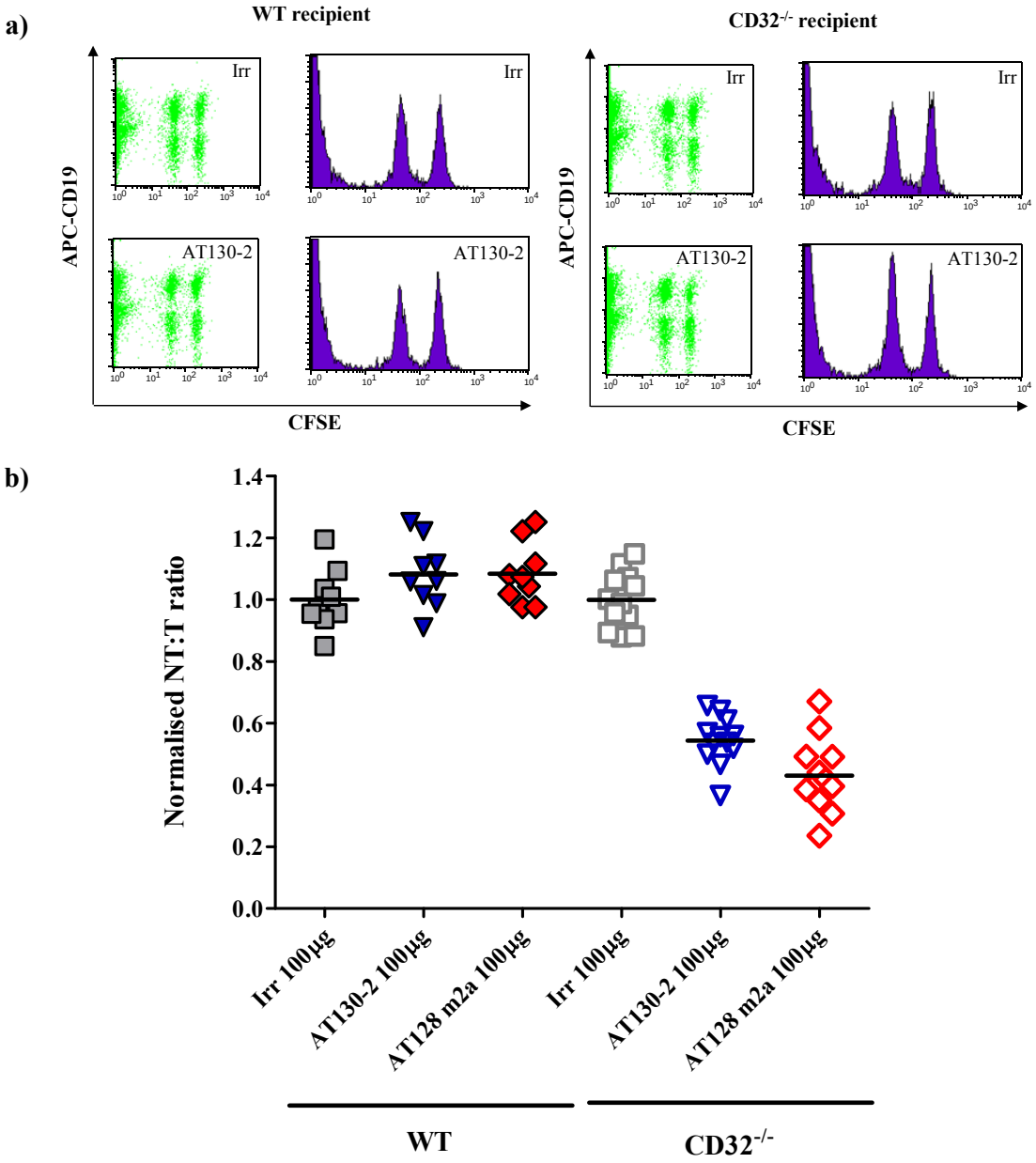

Figure 5.35. Depletion of target cells by anti-CD32 mAb in WT and CD32$^{-/-}$ recipients.
WT (target) and CD32$^{-/-}$ (non-target) splenocytes were labelled with 5 µM and 0.5 µM CFSE, respectively and injected i.v. into WT and CD32$^{-/-}$ BALB/c mice. After 24 hr 100 µg AT130-2, AT128m2a or irrelevant control (Irr) was administered i.v. After a further 24 hr the spleens of these animals were excised, processed and stained with APC-conjugated anti-CD19. The percentage non-target (NT) and target (T) cells was determined (a) and expressed as a normalised NT:T ratio as described in Materials and Methods section 2.20.2 (b). In the WT mice there was minimal deletion of target cells, in comparison with the same experiment in the CD32$^{-/-}$ mice, where there was approximately 50 % deletion of cells with either of the anti-CD32 mAb used. Data represents the results from three repeats, with three mice per group per experiment.

In other work performed by Dr Ruth French in our laboratory, CD20 Tg (target) cells and WT cells (non-target) were transferred into WT and CD20 Tg recipients. In a similar series of experiments examining CD20 as a target antigen and the capacity of antigen expression by endogenous cells to limit deletion of target cells it was shown that expression of the target receptor on endogenous cell in the recipient mice, in this case human CD20, reduced the efficacy of the mAb (rituximab) with regards to depletion of CD20 positive target cells (Figure 6.21). However, the disparity in target cell deletion due

to endogenous antigenic expression in the CD20 system is much less prominent than in the CD32 system, presumable due to the larger range of cell types that express CD32 in comparison to CD20, especially as the observed depletion was achieved with only a tenth of the anti-CD32 mAb dose. These data also indicate that the consumption of the anti-CD32 mAb observed in mice expressing CD32 prevents effective deletion of target cells and that this is specific to these mAb.

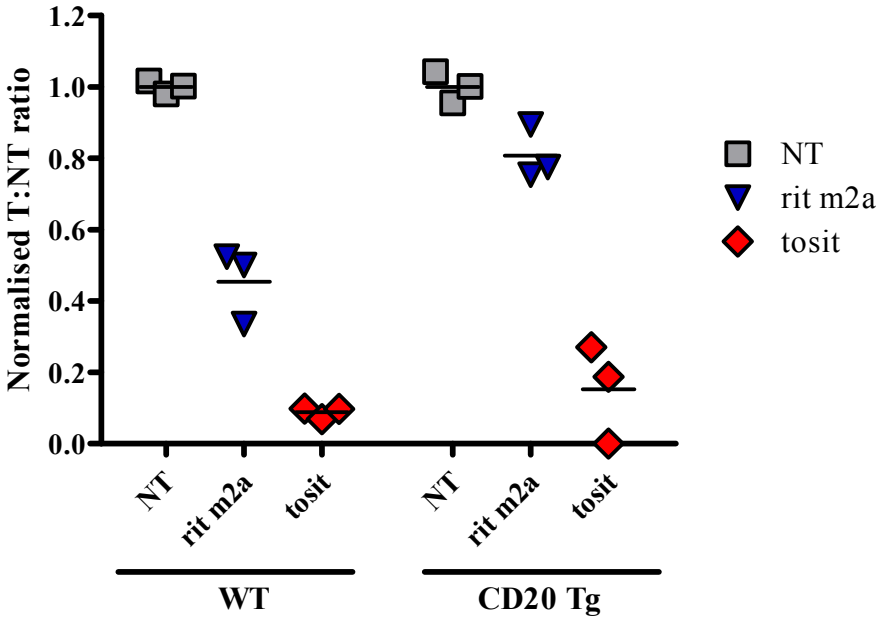

Figure 5.36. Target cells depletion by the anti-CD20 mAb is greater than that by the anti-CD32mAb. CD20 Tg (target) and WT (non-target) splenocytes were labelled with 5 µM and 0.5 µM CFSE, respectively and injected i.v. into WT and CD20 Tg BALB/c mice. After 24 hr 10 µg rit m2a or tosit was administered i.v. or mice were left untreated (NT). After a further 24 hr the spleens of these animals were excised, processed and stained with APC-conjugated anti-CD19. The percentage non-target (NT) and target (T) cells was determined and expressed as a normalised NT:T ratio as described in Materials and Methods section 2.20.2. Here, both rit m2a and tosit depleted target cells expressing human CD20, although tosit was more efficient at this that rit m2a. Transfer of cells into mice expressing human CD20 on endogenous cells resulted in a small reduction in target cell depletion. Data represents the results from three repeats, with three mice per group per experiment. Data courtesy of Dr Ruth French (University of Southampton).

6.10. Effect of anti-CD32 mAb consumption on CD32 expression *in vivo*.

We have discerned that the rate of mAb consumption *in vivo* is less rapid in the $CD32^{-/-}$ mouse than in the WT mouse and that this consumption diminishes the therapeutic potential of the anti-CD32 mAb to deplete target cells. In order to ascertain the extent to which CD32 modulation affects mAb consumption we further analysed the target cell population from the CFSE transfer experiments. To ascertain the extent of CD32 modulation of CD32 positive target cells in the WT and $CD32^{-/-}$ recipients we performed the *ex vivo* antigenic modulation assay (described in section 6.5) and gated on the target B cells from the adoptive transfer assays. Target cells transferred into the WT recipients

demonstrated no surface bound mAb but did express measurable levels of CD32. This is in contrast to the target B cells transferred into the $CD32^{-/-}$ mice. In these mice there was no cell surface bound mAb or CD32 expression after treatment, indicating total modulation of the receptor in the $CD32^{-/-}$ mice (Figure 6.22b). These results were entirely in keeping with a very low level of mAb gaining access to the target cells in the WT recipients and thus limiting depletion of target cells in these mice. In addition, the reduction of CD32 expression on the CD32 positive target cells in the $CD32^{-/-}$ recipients after treatment means that the target antigen was no longer expressed. In order for a mAb to elicit a response it must first bind to its target Ag. Receptor internalisation in these assays consequently limits the efficacy of the anti-CD32 and suggests, that in these assays at least, AT130-2 and AT128 m2a have a maximal depletion potential of 50% in the $CD32^{-/-}$ recipients. This level of direct target cell death is reflected in the death detected *in vitro* on lymphoma cell lines (Figure 4.17).

Alongside this, it was shown that the non-B cell target population (CFSE HI and CD19 negative) did not bind anti-CD32 mAb or express the receptor and nor was this modulated in these assays (Figure 6.22c). Although this does not elucidate whether CD32 is modulated on non-B cell populations *in vivo*, this does confirm that the only cells in the $CD32^{-/-}$ mice capable of binding anti-CD32 mAb were the target B cells.

We postulated that a 100 μg dose of anti-CD32 mAb in the WT mouse was insufficient to reach the target cells *in vivo* due to the mAb being consumed by endogenous tissues prior to its binding to the target cells. We therefore increased the dose of AT130-2 in our adoptive transfer assay to 500 μg per mouse, to determine whether this would induce the deletion of target cells. Interestingly, even when the dose of mAb was increased to 500 μg per mouse (only AT130-2 was tested) target cell deletion was not any more efficient in either the WT or in the $CD32^{-/-}$ recipients (Figure 6.23). These data indicates in the first instance that consumption of mAb in the WT mouse in these experiments was still too great to facilitate depletion of the target cells, providing a clear rationale as to why we see no therapeutic effect on our BCL_1 tumour model. Secondly these data indicate that the maximal amount of depletion achievable by AT130-2 in the $CD32^{-/-}$ mouse is approximately 50 %, most likely due to complete modulation of CD32 on the target cells after treatment, based on the assumption that 100 % of the target B cell population expressed CD32 (Figure 6.23). We therefore have been able to elucidate that the therapeutic potential of the anti-CD32 mAb is limited by both mAb consumption and receptor modulation.

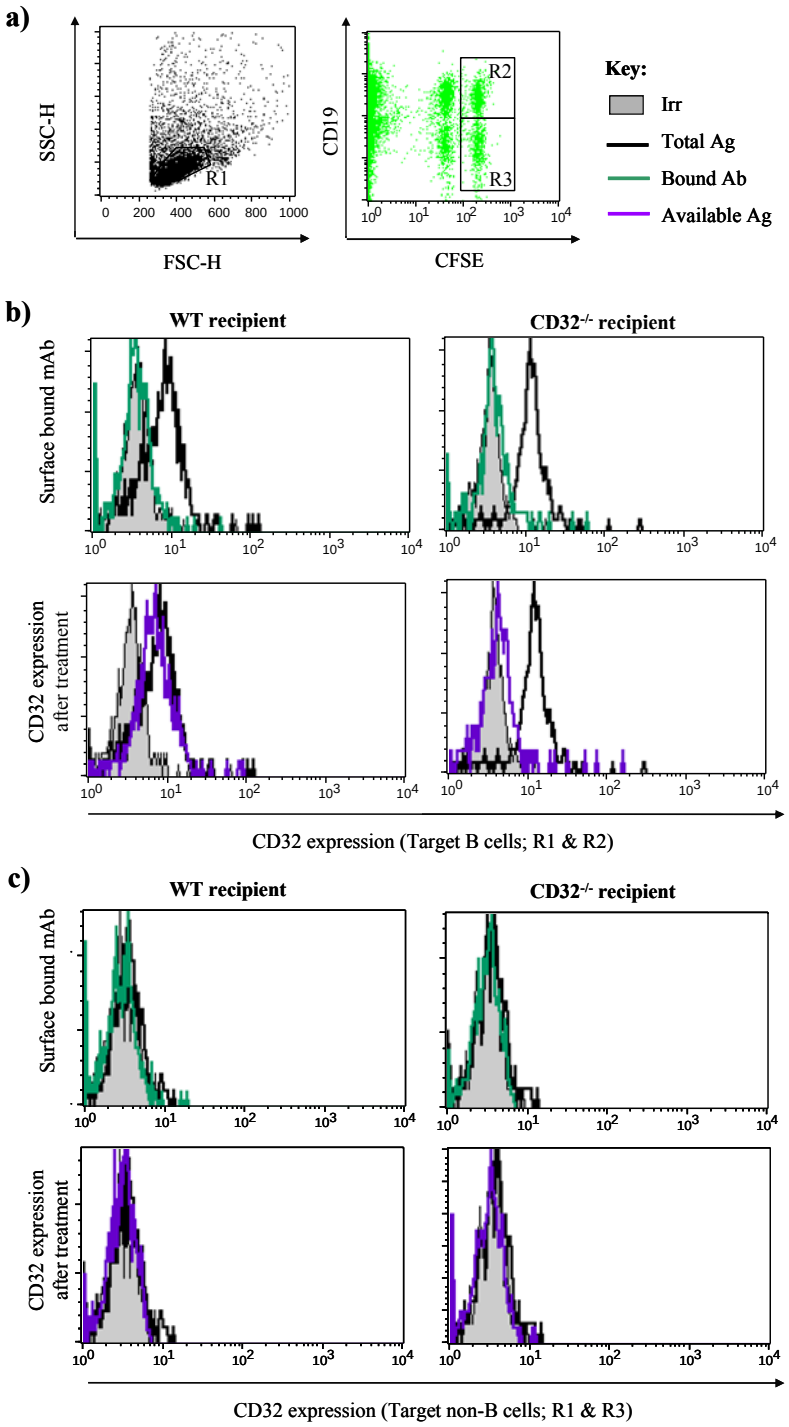

Figure 5.37. Antigenic modulation on target cells in adoptive transfer experiments in WT and CD32$^{-/-}$ mice.

100 µl of splenocytes at approximately 1 x 10^6 cells / ml, from the adoptive transfer experiments were incubated with or without excess anti-CD32 mAb (10 µg/ml), incubated for 30 min in the dark at 4 °C, stained according to indirect immunofluorescence protocols and analysed by flow cytometry. Target B cell events were collected as identified by FSC-H versus SSC-H (R1) and CD19 positivity (R2) (a). CD32 expression was expressed as cell number versus FL-2 florescence. Total CD32 expression is shown in black, mAb retained at the cell surface is shown in green and CD32 expression after treatment with AT130-2 is shown in purple. These data indicate that in the WT recipient anti-CD32 mAb did not bind to the target cells and as a result CD32 is not modulated on the cell surface. In contrast, there is total modulation of CD32 in the target cells within the CD32$^{-/-}$ recipient mice, resulting in removal of mAb from the cells surface (b). Alongside this, these data indicate that in the WT and CD32$^{-/-}$ recipient anti-CD32 mAb did not bind to then non-B cell targets, confirming that the only target within the CD32$^{-/-}$ mice for the anti-CD32 mAb were the target B cells in the adoptive transfer experiments (c). Data is a representative result from three repeats.

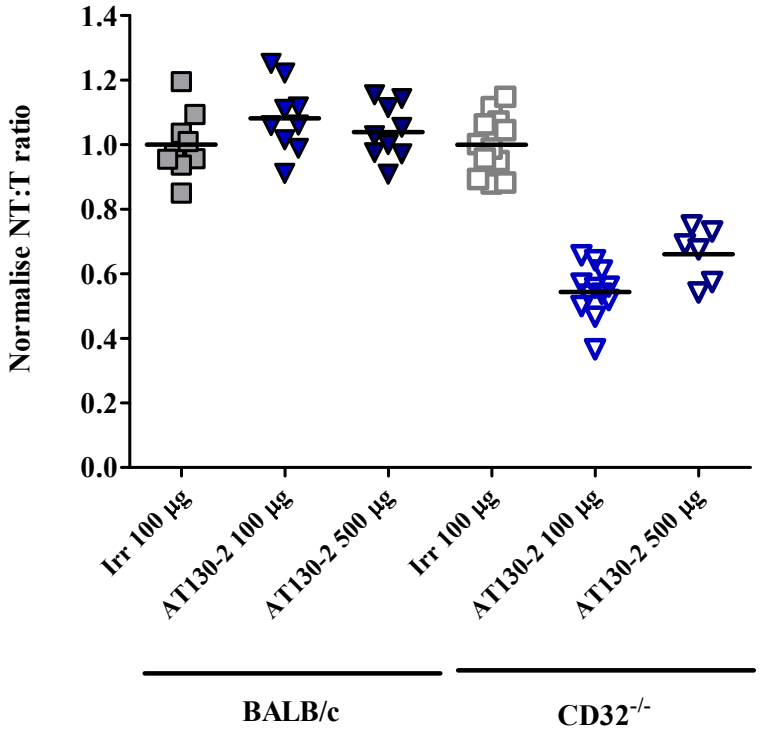

Figure 5.38. Increasing the dose of AT130-2 does not increase deletion of target cells in adoptive transfer experiments in WT or CD32$^{-/-}$ mice.
WT (target) and CD32$^{-/-}$ (non-target) splenocytes were labelled with 5 µM and 0.5 µM CFSE respectively and injected i.v. into WT and CD32$^{-/-}$ BALB/c mice. After 24 hr 100 µg or 500 µg AT130-2 irrelevant control (Irr) was administered i.v. After a further 24 hr the spleens of these animals were excised, processed and stained with anti-CD19 conjugate to APC. The percentage non-target (NT) and target (T) cells was determined and expressed as a normalised NT:T ratio. In the WT mice there was minimal deletion of target cells, even with the increase in mAb dose, in comparison there was approximately 50% deletion of cells with either of the anti-CD32 mAb in the CD32$^{-/-}$ recipients, although this level of target cell depletion was increased with the larger 500 µg AT130-2 dose. . Data represents the results from three repeats, with three mice per group per experiment.

6.11. Anti-CD32 mAb immunotherapy in CD32$^{-/-}$ mice inoculated with BCL$_1$.

In order to demonstrate the magnitude to which mAb consumption affects the immunotherapeutic potential of the anti-CD32 mAb we again employed the syngeneic BCL$_1$ lymphoma model and examined the survival of mice treated with AT130-2 alone or in combination with anti-idiotype (Mc106A5) in WT or CD32$^{-/-}$ mice. WT and CD32$^{-/-}$ mice were inoculated with 1 x 10^4 BCL$_1$ cells on day 0 and treated with either no mAb or a single, double or triple 0.5 mg dose of AT130-2 administered i.p. on days 2, 4 and 6 (total 0.5 mg/1 mg/1.5 mg depending on dosage regime) and either no mAb or 125 µg / day anti-idiotype from day 4 to day 7. In the WT mice the AT130-2 alone or in combination with anti-idiotype gave no increase in survival compared to non-treated or anti-idiotype treated mice alone (Figure 6.24a). As previously observed (Figures 6.1 & 6.2), anti-idiotype treatment increased the survival of WT mice by approximately 7 to 10 days ($p = 0.0011$, by Mantel-Cox test) (Figure 6.24b). In contrast to that which was observed in the WT mice, AT130-2 treatment in the CD32$^{-/-}$ mice increased survival as a single therapeutic agent and

in a dose dependent manner, i.e. single dose $p = 0.0143$, double dose $p = 0.0082$, triple dose $p = 0.0047$ (Mantel-Cox test) (Figure 6.24c). Alongside this, survival of the $CD32^{-/-}$ mice also increased when treated with AT130-2 in combination with anti-idiotype compare to anti-idiotype treatment alone ($p < 0.05$, by Mantel-Cox test) (Figure 6.24d). In fact, in one of the experimental repeats of this particular BCL_1 therapy, 50 % (2 of 4) of mice treated with 1.5 mg AT130-2 in combination with 0.5 mg anti-idiotype survived, tumour free for over 100 days. When rechallenged with 1×10^4 fresh BCL_1 cells i.v. these mice succumbed to the tumour within 21 days. This again demonstrates that the anti-CD32 mAb alone or in combination with another therapeutic agent e.g. anti-idiotype, do have potential to augment immunotherapy if the compounding factor of mAb consumption demonstrated previously in this chapter could be overcome.

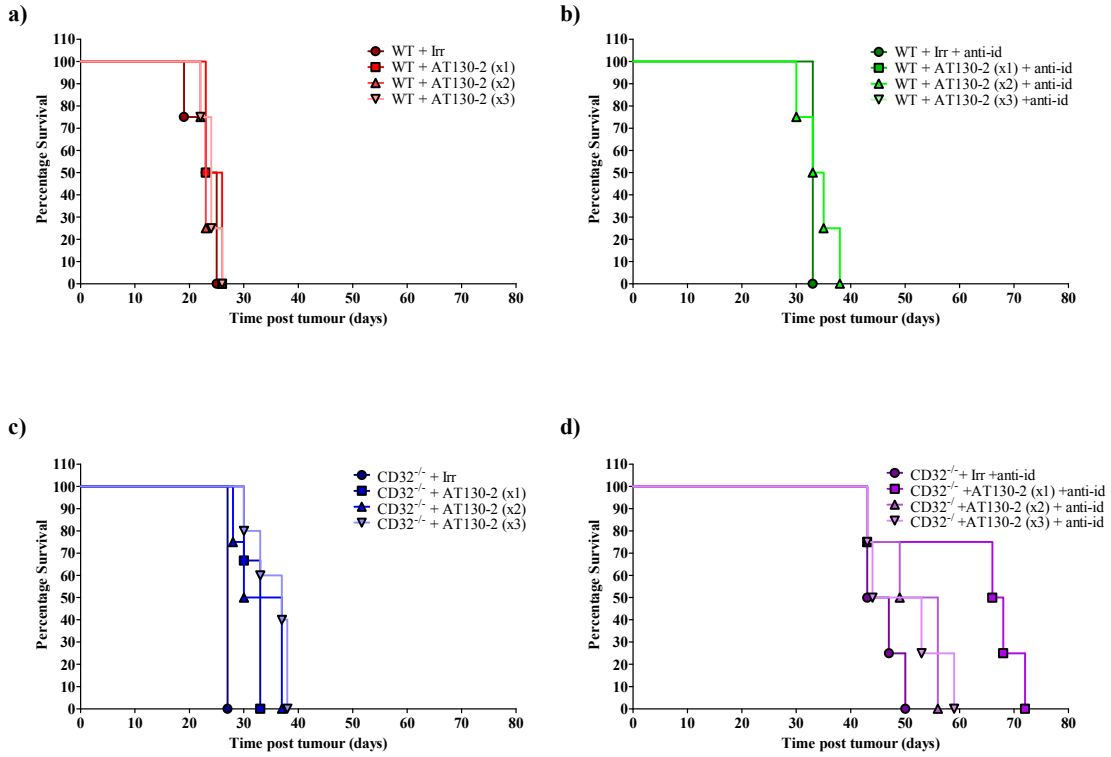

Figure 5.39. Anti-CD32 mAb improve survival alone and in combination with anti-idiotype therapy in CD32$^{-/-}$ mice.
WT and CD32$^{-/-}$ mice were inoculated with 1 x 10^4 BCL_1 cells on day 0, then administered either a single, double or triple dose 0.5mg AT130-2 i.p. on day 2, 4 and 6 and 125 µg of anti-idiotype (anti-id; Mc106A5) per day on days 4 to 7. In the WT mice AT130-2 did not significantly increase survival as a single immunotherapeutic (a) or in combination with anti-idiotype (b), although anti-idiotype therapy alone did improve survival in comparison to the untreated controls ($p = 0.0011$, Mantel-Cox). In contrast however, in the CD32$^{-/-}$ mice AT130-2 either single, double or triple dose increased (single dose $p = 0.0143$, double dose $p = 0.0082$, triple dose $p = 0.0047$ by Mantel-Cox test) alone (c) and in combination with anti-idiotype therapy (d). These data indicate the potential of the anti-CD32 mAb if the issue of mAb consumption could be overcome. Data is a representative result from three repeats.

6.12. Depletion of B cells and macrophages in the BCL_1 model of lymphoma.

Having earlier established that depletion of B cells and macrophages can increase levels of serum mAb (section 6.3.5), we next went on to determine whether similar depletion would improve immunotherapy in the WT mouse by limiting mAb consumption. Although previously we have discussed that such depletion would be detrimental to patient's immune response to cancer we still wished to establish whether mAb could be overcome to provide effective immunotherapy alone or as a boost to existing regimes. Depletion of B cells is currently used in the treatment of B cell cancers, for example the use of human anti-CD20 mAb in combination with CHOP in the treatment of NHL[62] and as such these experiments would provide a rational towards use in combination with anti-CD20 therapy. In addition, depletion of macrophages does not completely obliterate the effector cell compartment. Commonly, NK cells remain in the circulation after clodronate depletion as these cells do not partake in phagocytosis. NK cells have, by some been demonstrated to

have anti-tumour activity *in vitro*, where NK cell can induce ADCC of mAb coated tumour cells[417,418]. Therefore, B cells and macrophages were depleted from CD20 Tg and WT BALB/c mice, respectively as previously described in section 6.5.4 by the administration of 250 µg i.v. human anti-CD20 (FGM6, day -7) or two 200 µl i.v. doses of clodronate liposomes (days -3 and -1). Mice were inoculated with 1 x 10^4 BCL_1 cells on day 0, then treated with either irrelevant (WR17) or 0.5 mg AT130-2 administered i.p. on days 2 , 4 and 6 (total 1.5mg dose) and anti-idiotype 125 µg from day 4 to day 7 (Figure 6.25).

In this experiment, there was no statistical difference in survival in the irrelevant treated mice in any group ($p = 0.1226$, by Mantel-Cox statistical test). As previously demonstrated, anti-idiotype treatment prolonged survival in the WT mice and this survival ($p = 0.0100$ by Mantel-Cox statistical test) was not increased by co-administration of AT130-2 ($p = 0.1266$, by Mantel-Cox statistical test) (Figure 6.25a). This was also similar in the WT mice pre-treated with PBS liposomes ($p = 0.6186$, by Mantel-Cox statistical test, irrelevant versus anti-idiotype/AT130-2) (Figure 6.25d). In this experiment however, treatment with anti-CD32 mAb alone also seemed to improve mouse survival in both the WT and PBS liposome treated mice, although this was not significant in either case. In the $CD32^{-/-}$ mice, irrelevant mAb did not improved survival and was comparable to survival of irrelevant treatment in the WT mice. In the $CD32^{-/-}$ mice, treatment with AT130-2 significantly improve survival of mice greater than the control ($p = 0.0069$, by Mantel-Cox statistical test), as did treatment with anti-idiotype ($p = 0.0082$, by Mantel-Cox statistical test), although the latter seemed improved survival to a greater extent than the former ($p = 0.0058$, by Mantel-Cox statistical test). Again and as previously observed, treatment with AT130-2 and anti-idiotype increased survival more than treatment with either AT130-2 or anti-idiotype alone ($p = 0.0058$ & 0.0414, respectively, by Mantel-Cox statistical test) (Figure 6.25b).

This pattern of improved survival was also observed in the B cell depleted CD20 Tg mice, where AT130-2 in combination with anti-idiotype treatment improved survival beyond treatment and as a single therapeutic mAb ($p = 0.0062$ & $p = 0.0388$, respectively, by Mantel-Cox statistical test) (Figure 6.25c). There was no significant difference between improved survival in both the $CD32^{-/-}$ and CD20 Tg mice with combined anti-idiotype and AT130-2 treatment ($p = 0.5457$, by Mantel-Cox statistical test). These data indicate that B cell depletion improves immunotherapy in this model, similar to that observed in the $CD32^{-/-}$.

Alongside this, WT mice pre-treated with clodronate liposomes, resulting in the depletion of macrophages, also showed improved survival under all treatment conditions. Although the survival in these mice with combined anti-idiotype and AT130-2 treatment did not to appear to be as great as that demonstrated in the $CD32^{-/-}$ or B cell depleted mice, there was no significant difference between survival between $CD32^{-/-}$ or CD20 Tg mice after treatment with anti-idiotype and AT130-2 ($p = 0.2662$ & 0.4371, respectively, by Mantel-Cox statistical test) (Figure 6.25e). These data indicate that macrophage depletion improves survival of AT130-2 treated mice, presumably due to reduced mAb consumption.

Alongside this and to reiterate, anti-idiotype and AT130-2 treatment in $CD32^{-/-}$, CD20 Tg B cell depleted mice and clodronate liposome treated mice significantly improved survival compared to that observed in WT mice ($p = 0.0416$, 0.0389 & 0.069, respectively, by Mantel-Cox statistical test). These data therefore suggest that both B cells and macrophages are important in mAb consumption and depletion of either cell type can significantly improve survival after anti-CD32 mAb combination therapy with anti-idiotype.

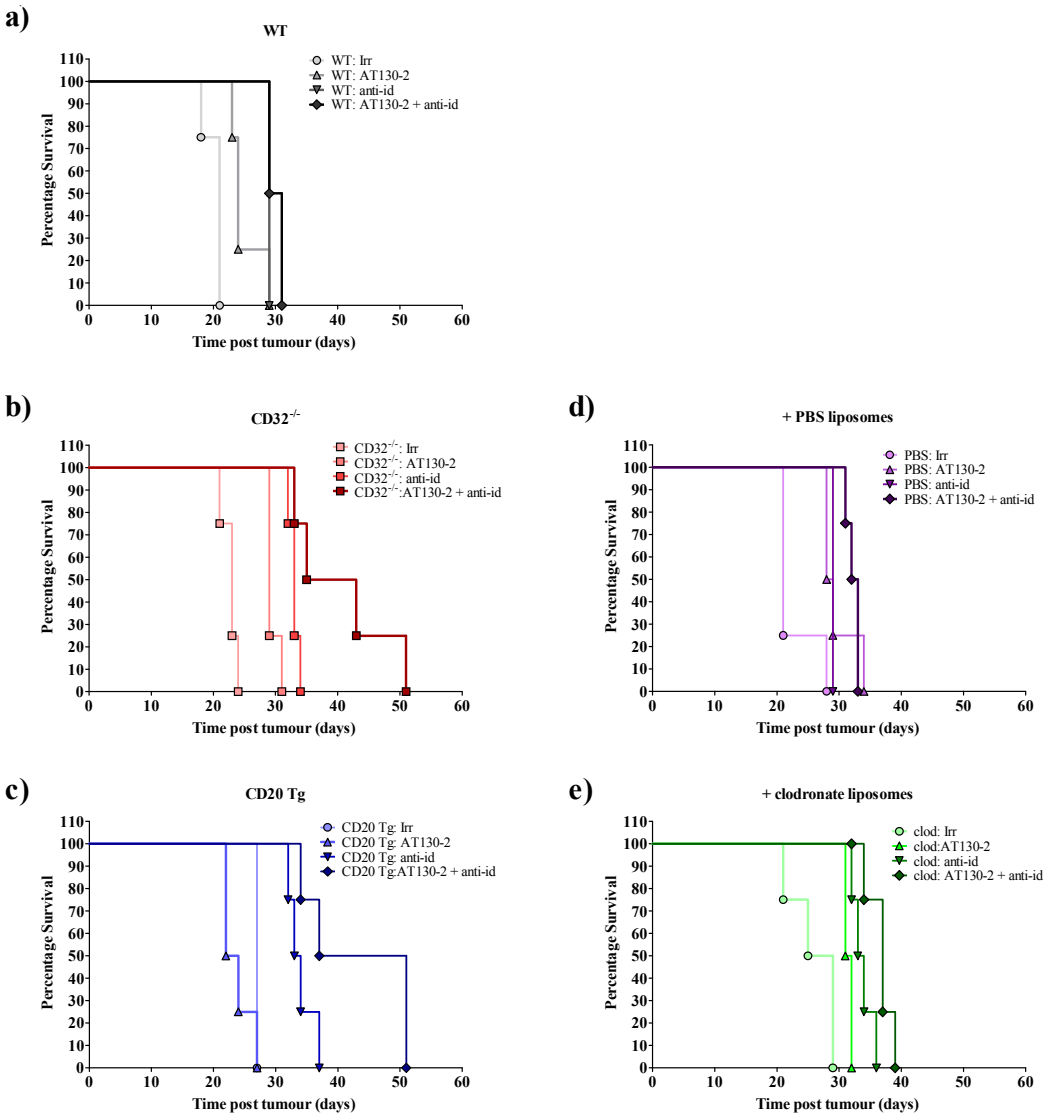

Figure 5.40. The effects of B cell and macrophage depletion on anti-CD32 mAb therapy in combination with anti-idiotype therapy.
WT mice were depleted of macrophages by administration of clodronate liposomes, 200 µl i.v. day – 3 and -1. CD20 Tg mice were depleted of B cells by administration of a 250 µg dose of FGM6. All mice were inoculated with 1 x 10^4 BCL_1 cells on day 0, then either left untreated or administered a triple 0.5mg dose AT130-2 i.p. on day 2, 4 and 6, and 125 µg of anti-idiotype (anti-id; Mc106A5) per day on days 4 to 7. Treatment with AT130-2 in the WT, PBS liposome treated or CD20 Tg mice did not significantly increase survival, however, AT130-2 treatmetn in the $CD32^{-/-}$ or clodronate liposome treated mice did significantly improve survival ($p = 0.0069$ & 0.0091, respectively. Further to this, anti-idiotype and AT130-2 treatment in $CD32^{-/-}$, CD20 Tg B cell depleted mice and clodronate liposome treated mice significantly improved survival compared to that observed in WT mice ($p = 0.0416$, 0.0389 & 0.069, respectively, by Mantel-Cox statistical test).

6.13. Chapter discussion.

In this chapter we sought to establish the efficacy of our panel of anti-CD32 mAb in a range of immunotherapy models of B cell lymphoma. By examining the survival of WT and $CD32^{-/-}$ mice inoculated with BCL_1 tumour cells and treated with specific anti-idiotype mAb we were able to demonstrate that survival was significantly augmented in the $CD32^{-/-}$

mice (Figure 6.1). This indicates that CD32 expression can alter immunotherapy; in part confirming previously published literature that shows improved immunotherapy in $CD32^{-/-}$ mice[83]. These data also highlight the potential of anti-CD32 mAb therapy. However, when WT mice were treated with anti-idiotype mAb in combination with anti-CD32 mAb there was no significant increase in survival (Figure 6.2). This was also reflected in preliminary data gained in a second lymphoma model (CBA/H mice inoculated with the A31 B cell tumour and treated with anti-CD32 mAb in combination with the specific A31 anti-idiotype (Mc39/12))(data not shown).

Alongside this, we showed that the anti-CD32 mAb had no direct effect on tumour growth in the BCL_1 model (Figure 6.3). Treatment with anti-idiotype mAb led to a reduction of tumour growth, demonstrated by reduced total number and percentage of tumour cells and also a reduction in spleen size and weight. However, the anti-CD32 mAb did not significantly reduce tumour growth in either short-term tumour growth assays or in a long term survival experiments.

Our initial results, in the $CD32^{-/-}$ mice mirrored previously published data. Clynes *et al* (2000) showed that mAb therapy of B16 melanoma with TA99 and BT474MI human breast cancer cells by 4D5 and trastuzumab in $CD32^{-/-}$ mice almost completely abrogated tumour growth compared with WT controls. There are however several problems associated with the models used. For example, B16, although of mouse origin is an established tumour line which has been subject to extensive re-passage both in vitro and in vivo. As previously described (Chapter 3.1) such tumour models are likely to develop a range of additional oncogenic mutations and are commonly retrovirally infected. As such, these models have increased immunogenicity. Asides from this, treatment of the B16 tumours occurs on the same day as administration of the tumour load, where in contrast we attempt to treat established tumours, again making it harder to treat the tumours in our model. In addition the tumour growth in the B16 model is only examined after day 14, where the authours examined the number of tumour metastases in the lungs, rather than overall animal survival. It would have been interesting to establish the effect of the mAb in WT and $CD32^{-/-}$ on actual animal survival in these studies.

The second model Clynes *et al* (2000) used was a xenograft model of human breast cancer where cells are injected subcutaneously into nude mice and treated with 4D5 or trastuzumab. Again they demonstrated an almost complete reduction in tumour growth in the treated $CD32^{-/-}$ mice compared to WT counterparts. However there are also issues with

the use of xenograft models. Primarily these models require immuno-compromised animals and as such, they do not mimic the complex relationship between the tumour and immune system. Nude and SCID mice lack components of the adaptive immune system, but still have some elements of the innate immune systems. Therefore, the human breast cancer cells are still likely to be immunogenic within the mouse, by stimulating components of the innate immune system. Furthermore, it is not yet clear whether the human breast cancer cells receive the same stromal microenvironment support in the mouse. Alongside this and as described with the B16 model, treated occurred on the same day as tumour innoculation, again this is in comparison with our model that attempts to treat a systemic, non-immnuogenic established tumour, that is more closely reminiscent of the situation in humans.

Interestingly however, others have demonstrated little improvement in mAb therapy in $CD32^{-/-}$ mice[419]. Takade *et al* (2004) treated TNF-related apoptosis-inducing ligand (TRAIL) sensitive 4T1 murine mammary carcinoma with an anti-mouse anti-DR5 mAb (MD5-1). They showed that MD5-1 almost completely abrogated tumour growth in WT mice, but that this therapy was not improved in $CD32^{-/-}$ mice. However, MD5-1 mAb is a hamster mAb and unpublished observations in this laboratory (Dr Stephen Beers) have also demonstrated that the hamster anti-mouse BCL_1 idiotype, AT65, did not shown enhanced immunotherapy in the $CD32^{-/-}$ mice. It is possible that hamster mAb do not interact with murine CD32 and if not, the level of immunotherapy observed in the WT mouse will be maximal and not improved in the $CD32^{-/-}$ mouse. This theory could be tested using the BIAcore analyser to assess the ability of AT65 and Mc106A5 (anti-rat anti-idiotype) to interact with recombinant CD32.

Despite this, we were unable to demonstrate increased efficacy in our models of lymphoma by using an anti-CD32 blocking mAb. Nevertheless, our tumour tracking experiments did provide a useful tool for examining what was happening to the anti-CD32 mAb. It was demonstrated, by cellular bioassay, that serum levels of the anti-CD32 mAb dropped rapidly and become almost negligible in comparison to anti-idiotype mAb serum levels, suggesting that the anti-CD32 mAb may be limited by its consumption from the serum (Figure 6.5). Further to this, we were able to demonstrate that there was a dramatic difference in serum mAb levels between the WT and $CD32^{-/-}$ mouse strains. Serum longevity of AT130-2 was improved in the $CD32^{-/-}$ mice 48 hr and 96 hr post-treatment compared with levels in the WT mice (Figure 6.7). The complete loss of mAb in the WT

mice offers a potential explanation as to why anti-CD32 mAb efficacy was limited in these animals.

It was plausible that the other FcγR were consuming anti-CD32 mAb through Fc:FcγR engagement. We were able to rule this out by examining the serum mAb levels of AT130-2 in γ-chain$^{-/-}$ mice, which lack activatory FcγR, but still express CD32. When comparing serum longevity of AT130-2 in WT and γ-chain$^{-/-}$ mice we were able to demonstrate that the consumption of mAb was identical, with sustained serum levels of the mAb only evident in the CD32$^{-/-}$ mice as previously demonstrated (Figure 6.8a). This precipitous loss of mAb in mice expressing the endogenous receptor was not seen in the CD20 Tg system (Figure 6.8b), alluding to the fact that there was something unique about CD32 engagement by the anti-CD32 mAb *in vivo*. In the CD20 Tg serum the half life of anti-CD20 mAb (rit m2a) in WT, CD20 Tg and CD20 Tg/γ-chain$^{-/-}$ was comparable and changed little with expression of the CD20 Tg. In comparison, the half life anti-CD32 mAb was greatly extending in mice lacking CD32 expression in comparison to WT or γ-chain$^{-/-}$ mice, suggesting that there was something particular about CD32 expression that leads to rapid mAb consumption. Furthermore, as CD32 on placenta endothelium cells has been shown to transport and recycle IgG it is plausible that CD32 may also function in a similar manner on other tissues. Therefore, it could be suggested that as binding of monomeric IgG *in vivo* to CD32 leads to recycling of the IgG (possible in co-operation with FcRn[420]) and at high serum IgG levels or in the presence of IC, IgG is internalised and degraded, binding by the anti-CD32 mAb could potentially mimick the binding of IC, thereby accounting for the rapid consumption of mAb in CD32 expressing animals.

Recently, Dr Sonya James (University of Southampton) has stained murine tissue, including haemopoietic and non-haemopoietic tissues, for their expression of CD32. These experiments have highlighted CD32 expression in tissues, such as the liver (sinusoidal lining cells), colon (lamina propria) and ileum (lamina propria and peyers patches), further confirming and identifying early literature that demonstrates widespread expression of CD32 in non-haemapoietic tissues[289,288]. In the case of the transgenic CD20, this antigen is only expressed by B cells. Therefore it is possible that the consumption of anti-CD32 mAb in WT mice is greater that the consumption of anti-CD20 in the CD20 Tg mouse, due to the greater quantity of tissues in the WT mouse that express CD32.

We next theorised that due to the extensive expression of CD32 on a variety of tissues and cells within the mouse[139] perhaps a repeated dose of mAb would overcome this problem of

rapidly diminishing mAb levels. Repeated administration of AT130-2 in the WT mouse did not improve overall serum mAb longevity, although initially it did seem that mAb levels were improved 24 hr after the final dose of mAb was administered, however this was not sustained and was again rapidly abridged by 48 hr (Figure 6.9). Furthermore, we were able to demonstrate that depletion of two of the main cell types that have been reported to express CD32, B cells and macrophages, increase serum longevity of mAb, but again this was not to the levels seen in the $CD32^{-/-}$ mouse (Figure 6.10). One point that must be made about this experiment is that mAb was administered i.p. due to occasional adverse reaction in mice administered i.v. with AT130-2 at the time of these particular experiments being performed. This may have limited the serum mAb detectable. However, work by Dr Ruth French (University of Southampton) has previously demonstrated that serum mAb levels are comparable 24 hr after administration by a range of injection routes, including i.p., i.v. and s.c. (unpublished observations).

As a result of our observations, we went on to determine the method by which the anti-CD32 mAb were being consumed *in vivo*. We determined that after treatment with anti-CD32 mAb (either AT130-2 or AT128 m2a) there was diminution of CD32 expression both *in vivo* (Figure 6.11). Having established that anti-CD32 mAb and CD32 were not being removed from the cell surface by FcγR-dependent shaving[416] (Figure 6.12), we were able to determine that CD32 was being modulated from the cell surface both *in vivo* (Figure 6.11 & 6.12) and *in vitro* (Figure 6.13 & 6.14) by internalisation. We could confirm the absence of FcγR-dependent shaving as half-life experiments in WT and γ-$chain^{-/-}$ mice showed identical rate of mAb consumption (Figure 6.8), indicating that the process of mAb consumption was not dependent on FcγR, suggesting that anti-CD32 mAb was being lost from the serum by mechanisms aside from those dependent on FcγR, further confirming that modulation of CD32 as a candidate for this process. In Figure 6.12 due to the low affinity of AT128 m2a it was difficult to ascertain whether CD32 was being modulated after treatment with AT128 m2a in the γ-$chain^{-/-}$ mice. To overcome this, another anti-CD32 mAb, such as AT130-2 could be used to detect CD32 expression before and after treatment *in vivo* with AT128 m2a.

Interestingly, we observed that *in vitro* as least, the anti-CD32 mAb demonstrated distinct effect on CD32 expression. The agonistic mAb decreased receptor expression, whilst the antagonistic mAb increased receptor expression (Figure 6.13, 6.14 & 6.15). This did not correlate with the observations that AT130-2 and AT128 m2a lead to a decrease in CD32 *in vivo*, but we do expect the *in vitro* observation to also be correct as they were consistent

between both mouse strains and in three repeats for the BALB/c B cells and four repeats for the C57BL/6 B cells, where samples were run in duplicate each time. This suggests that perhaps, for AT128 m2a at least, there are different mechanisms of modulation occurring *in vivo* and *in vitro* as increase in CD32 after AT128 m2a treatment was not observed *in vivo*. This further corroborates data obtained in Chapter 4 that suggests that the two types of anti-CD32 mAb affect lymphoma cells in different way with regards to CD32 phosphorylation, affect of BCR-induced Ca^{2+} flux and induction or not of cell death. We were able to verify that CD32 was being internalised after AT130-2 treatment, but not after treatment with AT128 m2a though comparisons with CD20 modulation by performing Alexa-488 quenching assays on CD20 Tg B cells (Figure 6.16 & 6.17). Alongside this we confirmed that our murine lymphoid cells predominantly express the CD32-1 isoform and that murine myeloid cells express the CD32-2 isoform[294] (Figure 6.19), further refuting claims that the CD32 on B cells does not undergo endocytosis. In addition, a third PCR product, which separated during electrophoresis between the two expected PCR products, was also visible. We believe this product to be CD32b1', as described by Latour *et al* 1996. Sequencing of this PCR product would confirm that B cells also express CD32b1'.

Examination of CD32 modulation on BMDMs showed that these cells also modulated CD32 in response to anti-CD32 mAb stimulation, similar to our lymphoid cells (Figure 6.18). There were however difficulties with these BMDMs assays in terms of consistency between batches of BMDMs and even between different periods of *ex vivo* growth. Regardless, these data do suggest that macrophages modulate CD32 and as such confirm that these cells would consume mAb *in vivo*. In the previous chapter we demonstrated that pre-incubation of macrophages with the anti-CD32 mAb increased the phagocytic ability of these cells (Figure 5.11). It seems reasonable, in light of the modulation data, that increased phagocytosis may be due to the down regulation of cell surface CD32. However, due to the short pre-incubation period (1hr) of the BMDMs with anti-CD32 mAb prior to the phagocytosis assays it is possibly more likely that simple blocking of the inhibitory receptor enhances BMDMs.

In summary, our data indicate that CD32 on B cells and macrophages is capable of endocytosis when engaged by mAb. This was in stark contrast to several reports in the literature that show that the isoform predominately expressed on B cells has been reported to lack endocytic properties[294,302,298] and therefore we expected that anti-CD32 mAb and CD32 was not being internalised by the splenic B-cells *in vivo*. We anticipate that we

observe differences in reported behaviour of the two isoforms due to differences between engagement of IC and mAb. In the initial studies that described the contrasting endocytic properties between the CD32b1 and CD32b2 isoforms, IC, formed from heat agglutinated human IgG was used to engage CD32. IC, in this case would have bound exclusively to CD32 via Fc:FcγR interactions. Conversely, the agonistic anti-CD32 mAb (which cause receptor internalisation), as demonstrated in Chapter 4, bind to an epitope on the receptor and then crosslinks the receptors on the cell surface by Fc engagement. As endocytosis (or lack of) has been demonstrated by others in the context of IC[294,302], we would suggest that the induction of endocytosis in our assays may be as a direct result of antibody engagement alone and therefore differs from that previously reported. We have also examined internalisation of CD32 at longer time points (2, 6 and 24 hr) to those previously reported (up to 30 mins), suggesting that the kinetics of receptor internalisation may vary between the two isoforms and the earlier publish literature does not account for this. This could be in part to the aspects of the cell membrane with which the two isoforms associate with (CD32b1 contains a cytoskeletal binding site, whereas CD32b2 contains a domain that associates with clathrin coated pits).

In addition, it is unclear from the published literature whether CD32 on murine cells lack the endocytic properties described in human cells. Early papers do suggest that murine CD32b1 lacks endocytic properties, however, most of the published data is in human and transgenic mouse cell lines or murine cells transfected with CD32 isoforms. There is a subtle difference between the structures of murine and human CD32b1, demonstrated by a shortened cytoplasmic tail of the human receptor[196]. Perhaps this is enough to account for the proposed differences in endocytic properties between the species. For example, it has however been reported that levels of CD32b expression do not alter in human lymphoma cell lines *in vivo* after treatment with a humanised anti-CD32b mAb[374]. Therefore, the modulation we detect on the murine lymphoma cells after treatment with murine CD32b mAb both *in vitro* and *in vivo* may be a species dependent observation. There are human anti-CD32 mAb available to us (AT10 (Tenovus), IV.3[421] and KB61[422]) that could be used to address this inconsistency between species and determine whether similar modulation of CD32b occurs *in vitro* on human cell lines in our hands. In fact, initial data has determined that the human anti-CD32 mAb do not induce modulation of CD32b *in vitro* on human cell lines and also in CD32 Tg mice models. This is part of a continuing project in the laboratory to determine the differences between modulation of the murine and human CD32 isoforms. In addition, it could be suggested that as B cells express both isoforms of CD32 (see Figure 6.19) then crosslinking by anti-CD32 mAb could be inducing

internalisation of CD32b2 and cosequentually CD32b1 is being interanlised in complex with CD32b2 and may be being internalising independently. This theory could be tested by co-transfection of both isoforms, with either one of the isoformed conjugated to FLAG tag, YFP or GFP to look at the locations of the isoforms at the cell surface and within intracellular compartments.

However, despite having determined the limitations of anti-CD32 mAb therapy in the WT mouse we still wanted to determine the extent to which the consumption of anti-CD32 mAb affected immunotherapy. In order to establish if the anti-CD32 mAb had the potential to deplete cells *in vivo* we performed adoptive transfer assays of CFSE labelled target and non-target splenocytes and established the level of target cell depletion in WT and $CD32^{-/-}$ mice. When recipient mice lacked endogenous expression of CD32, then there was a 50 % depletion of target splenocytes after treatment with the anti-CD32 mAb. This was in contrast to no depletion of target cells in WT mice (Figure 6.20), even with a five times larger dose of mAb (Figure 6.23). Again, with reference to the CD20 Tg systems, where endogenous CD20 expression limited but did not completely abolish depletion of target cells (Figure 6.21), endogenous CD32 expression entirely abrogated the activity of the anti-CD32 mAb. Furthermore, we were able to demonstrate in our transfer experiments that the activity of the anti-CD32 mAb was limited in the $CD32^{-/-}$ by modulation of CD32 on target cells (Figure 6.22).

We were also able to determine how the absence of anti-CD32 mAb consumption would effect long term survival in the $CD32^{-/-}$ mice. It would seem that in the absence of mAb consumption the anto-CD32 mAb are able to significantly increase mAb immunotherapy, i.e. in the $CD32^{-/-}$ mice as a single therapeutic, but more impressively in combination with anti-idiotype (Figure 6.24). Indeed, in one repeat of this experiment we observed that 50 % of the animals treated with anti-CD32 and anti-idiotype mAb exceeded 100 days survival. Re-challenge of these mice with BCL_1 resulted in the animals succumbing to their disease, suggesting that survival occurred through direct mAb effect rather than development of a memory response against the tumour.

Alongside this we were also able to demonstrate that removing B cells and macrophages *in vivo* extended the half live of AT130-2 in the WT mice, although plasma longevity of mAb was still less than in the $CD32^{-/-}$ mice (Figure 6.10). When this was extrapolated into therapy, we were able to demonstrate that depletion of B cells gave increased survival of mice inoculated with BCL_1, similar to that seen in the $CD32^{-/-}$ mouse (Figure 6.25). In fact

the survival of CD20 Tg mice with B cell depletion and CD32$^{-/-}$ mice that were treated with a combination of anti-CD32 and anti-idiotype was almost exactly the same. However, some cautious must be taken interpreting these results, as B cells in the CD20 Tg mouse were depleted using administration of mAb, which utilises a variety of mechanisms as described in introduction section (1.3.3). The type II anti-CD20 mAb used, specifically engages with FcγR-dependent mechanisms to deplete B cells[115] and as such will already by mediating cellular clearance prior to treatment with anti-CD32 mAb. The anti-CD32 mAb will therefore target these already activated cells towards the tumour, rather than initiating a specific anti-tumour response. In contrast, depletion of macrophages could limit the induction of FcγR-dependent mechanisms. However, NK cells, which have been demonstrated to be involved in mAb mediated anti-tumour ADCC in the therapeutic setting are not depleted after clodronate liposome treatment as they are not phagocytic and as such will be able to mediate anti-tumour responses. Interestingly, two days after administration of AT130-2, there is approximately 120 μg/ml more mAb in the CD20 Tg mice versus the WT mice and approximately 90 μg/ml more mAb in the clodronate treated mice versus the WT mice. This indicates that approximately 210 μg/ml mAb could be rescued from consumption with both B cell and macrophage depletion in comparison to the WT mouse. This is comparable with levels of mAb observed in the CD32$^{-/-}$ mice (220 μg/ml) two days after mAb administration. It would be interesting to examine serum mAb levels in mice depleted of both B cells and macrophages to determine whether mAb consumption could be completely rescued under these conditions. This would also limit the role of CD32 expressing tissues in mAb consumption.

In conclusion, we have successfully demonstrated the potential of our anti-CD32 mAb in models of B cell lymphoma, although alongside this we have also demonstrated that, in our models at least, consumption of anti-CD32 mAb by receptor internalisation limits the therapeutic efficacy. However, this can be overcome by limiting the expression of endogenous CD32, either by depletion of cell subsets or genetic knockout and can lead to long-term animal survival.

CHAPTER 7 Concluding remarks and future directions

Through a range of cellular and biochemical assays we were able to establish that a panel of novel murine anti-CD32 mAb could be categorised into two types with regards to their activity of LCL, the agonistic and antagonistic anti-CD32 mAb. The agonistic mAb, as the name would suggest, activate CD32 as seen through phosphorylation of the receptor and also the downstream signalling molecule SHIP-1, correlating with inhibition of BCR-induced Ca^{2+} flux and interestingly induction of PCD. In contrast, the antagonistic mAb inhibit CD32 activation as seen through inhibition of SHIP-1 phosphorylation and augmented BCR-induced Ca^{2+} flux.

It has been reported that co-aggregation of CD32 leads to induction of direct PCD through mechanisms independent of SHIP-1 phosphorylation, but dependent on the membrane dissociation of Btk in murine lymphoma cell lines[333,334]. Here, in contrast to this published data, we observed a correlation between SHIP-1 phosphorylation and induction of PCD in our lymphoma cell lines. Despite our data refuting previous reports, other B cell subsets, such as pre-B cells, demonstrate that CD32-dependent PCD does correlate with phosphorylation of SHIP-1[343], suggesting that in some instances pSHIP-1 does play a role in the induction of PCD after CD32 coaggregation. The anti-CD32 mAb did not however seem to induce significant levels of PCD in normal splenic B cells and BMDMs, an advantage for their use as immunotherapeutic agents. The success of rituximab therapy has come from its ability to specifically deplete CD20 positive cells. CD20 is expressed by B cells throughout B cells development, excluding haematopoietic stem cells and plasma cells[423]. This enables targeted depletion of cells whilst retaining both immunological memory and the ability to reconstitute the B cell population, meaning that the patient does not suffer from an impaired immune system[424]. Therefore, it is of great advantage that our anti-CD32 mAb do not seem to deplete normal B cells and macrophages.

Alongside this, studies in melanoma models support the potential induction of direct PCD by signalling through CD32 by the agonistic anti-CD32 mAb in our models of lymphoma. It was shown that the use of murine anti-GD2 in the treatment of melanoma was not limited by CD32 expression[359]. It has been proposed that crosslinking between GD2 and CD32 via Fc interaction by anti-GD2, induced cell signalling that leads to growth inhibition, through activation of SHP-2 and associated signalling pathways[359]. Potentially, this is what is occurring with the agonistic anti-CD32 mAb on B lymphoma cells were

crosslinking by Fc is providing inhibitory signalling to the lymphoma cells, resulting in growth inhibition and subsequent death.

It would therefore be interesting to dissect out the signalling pathways leading to PCD in our LCL to determine the contribution of pSHIP-1 and proteins involved in downstream signalling pathways, in this process. For example, compare PCD in WT cells with $SHIP^{-/-}$ cells or cells containing truncated CD32, lacking cytoplasmic domains, both of which will result in abrogated CD32 signalling. Further to this, examination by Western blot for downstream signalling proteins, such as Btk and the use of specific inhibitors towards these proteins would further tease out pathway leading to PCD in lymphoma cells.

The Eμ-myc LCLs generated are heterogeneous and as such we possess lymphomas arising at different stages of B cell development. It would therefore also be interesting to examine the differences in SHIP-1 signalling and PCD at these various stages of B cell development, with the expectation that the signalling involved in the induction of PCD in pre-B cell lymphomas may differ from that observed in mature B cell or class-switch lymphomas, as previously described for normal B cell subsets[333, 334, 272, 343]. However, our current data in lymphomas from the Eμ-myc model demonstrates that pre-B cell lymphomas respond similarly to anti-CD32 mAb induced PCD as B cell lymphomas.

It has also been shown that PCD occurs through apoptotic pathways involving Bim, where CD32-induced PCD was reduced in plasma cells from $Bim^{-/-}$ mice. Preliminary data from this laboratory examining PCD induced by the anti-CD32 mAb in splenic B cells from WT and $Bim^{-/-}$ mice has shown that there was a significant reduction in PCD, although PCD in WT C57BL/6 B cells was only approximately 10 %. Bim becomes up-regulated in response to cellular stress; either withdrawal of growth factors or with the addition of drugs or stimuli (i.e. treatment with anti-IgM)[337,425]. Signalling through the MAPK pathway (i.e. Ras/Raf1) and ERK1/2 have been indicated in leading to a reduction in Bim. A splice variant of Bim, Bim_{EL} contains an exon that encodes the ERK1/2 docking domain and phosphorylation site (at Ser69)[425]. As a result, activation of ERK1/2 leads to the phosphorylation and subsequent ubiquintation and protesomal degradation of BIM[426,427,428]. Therefore it is plausible, that as CD32 signalling has been implicated in the diminution of MAPK signalling[249,250], CD32 coaggregation would limit ERK1/2 targeting of Bim and therefore Bim would accumulate in the cell and mediate PCD. Again, this signalling pathway could be investigated through Western blot analysis. Preliminary data

suggests that after CD32 coaggregation (using AT130-2) Bim is not phosphorylated, unlike that observed after BCR ligation (anti-IgM) (data not shown).

Alongside the induction of PCD on LCL by the anti-CD32 mAb *in vitro*, we were also able to demonstrate that the anti-CD32 mAb had further anti-tumour activity, the ability to induce phagocytosis of opsonised B cells. Altogether, the anti-CD32 mAb showed promising *in vitro* activity on LCL. However, this was not extrapolated into our *in vivo* models. Despite our observations that in $CD32^{-/-}$ mice, anti-idiotype immunotherapy significantly increased survival in comparison with WT mice, combination therapy of the anti-CD32 mAb and anti-idiotype mAb did not have any influence on survival in WT mice. Having established this was through mAb consumption, which we presume is occurring as a result of CD32 internalisation and not FcγR-dependent shaving, we were able to partly overcome this. Where there is limited consumption, i.e. in macrophage or B cell depleted animals, therapy is comparable to that seen in the $CD32^{-/-}$ mice and the anti-CD32 mAb have measurable impact on therapy. Further to this, this laboratory has recently obtained conditional CD32 knock-out animals, where CD32 has been selectively deleted from either B cells or macrophages. Therefore, the impact of mAb consumption by B cells and macrophages could more easily be investigated, without the compounding issues mentioned earlier, i.e. the anti-CD32 mAb potentially utilising already activated effector systems as a result of B cell depletion by anti-CD20 mAb. A caveat to the use of this system however in that *in vitro* at least, $CD32^{-/-}$ BMDMs have heightened phagocytosis of opsonised B cells, suggesting that survival in BCL_1 therapy in a macrophage-specific $CD32^{-/-}$ animal might occur as a result of enhanced activation (on account of a lack of CD32) and not due to reduced mAb consumption.

Impressively however, the anti-CD32 mAb improved survival in the $CD32^{-/-}$ mice in comparison to untreated animals, similar to that which was observed in combination with anti-idiotype in the $CD32^{-/-}$ mice. This suggests that in these animals, the anti-CD32 mAb are working to either induce PCD of tumour cells or recruit anti-tumour effector systems towards anti-CD32 mAb coated cells via Fc engagement with activatory FcγR expressing cells. This confirms the observations by others that anti-CD32 mAb have potential as therapeutic agents[374].

When combined with anti-idiotype therapy, there are various potential mechanisms by which anti-CD32 mAb may be augmenting therapy. Anti-CD32 mAb may be improving the presentation of Fc to activatory FcγR expressing effector cells in two ways. Firstly by

blocking anti-idiotype engagement with CD32 via Fc interactions, or secondarily, by increasing the total amount of surface bound mAb, and consequentially the number of Fc presented. Both of these will enhance the number of Fc available for engagement with activatory FcγR expressing cells, thus augmenting effector cell function. This second mechanisms is particularly attractive, as human anti-CD32b mAb have been demonstrated by others to direct anti-tumour FcγR-dependent effector function[374].

In order to dissect out whether the anti-CD32 mAb are acting to simple block CD32 engagement with therapeutic mAb or acting to recruit effector cells a N297Q mutated anti-CD32 mAb could be used. As the asparagine residue at 297 has been implicated in the binding of Fc to FcγR, mutation in this amino acid (replacing it with a glutamine) perturbs this interaction. As such, the anti-CD32 mAb will be able to bind to CD32 on the surface of the tumour cell, but will not be able to engage the activatory FcγR on effector cells. We would favour this method over the use of a $F(ab')_2$ fragment as our *in vitro* studies advocated that the $F(ab')_2$ fragment version of the agonists anti-CD32 mAb did not function in the same way as the IgG, presumably by crosslinking the receptor. However, the N297Q mutation would also prevent this crosslinking, but will retain the structural integrity of the IgG. We would hope that this would be sufficient for the function of the mAb. A flow cytometry assay could then be employed to determine the relative interaction of the anti-idiotype mAb with activatory FcγR fusion proteins in the presence or absence of the un-mutated and N297Q mutated anti-CD32 mAb, thus determining the amount of Fc available for effector cell interaction *in vivo*. The effective use of these combinations could also be employed in a therapeutic setting depending on the outcome of these preliminary experiments.

Other work within this laboratory has demonstrated that interactions by therapeutic mAb (rituximab) with CD32, limit its efficacy by increasing internalisation of the receptor and bound mAb. It would be proposed to investigate the affect of CD32 engagement with anti-idiotype on modulation of the BCR and how this could be altered by blocking CD32 with anti-CD32. This could be investigated using the Alexa-488 quenching assay, as previously discussed, (Materials and Methods section 1.19). Through examining modulation of Alexa-488 labelled anti-idiotype in the presence and absence of anti-CD32 mAb we would be able to determine the contribution of CD32 to BCR internalisation, with implications for therapy.

Alongside this and having demonstrated *in vitro* that these anti-CD32 mAb have a least two potential anti-tumour mechanisms, either through direct PCD or through phagocytosis, we would next aim to use the recently generated complete FcγR knockout mice produced from crossing the γ-chain$^{-/-}$ with CD32$^{-/-}$ mice (denoted FcγR$^{-/-}$) to evaluate the contribution of these two anti-tumour mechanisms for the anti-CD32 mAb immunotherapy of BCL_1. The FcγR$^{-/-}$ mice will not suffer from mAb consumption (due to lack of CD32) and as a result of lacking the activatory FcγR expressed by effector cells such as phagocytes, we would be able to tease out the contribution of FcγR dependent anti-tumour mechanisms (discussed in Introduction section 1.3.3) to this BCL_1 immunotherapy.

Preliminary data from these animals initially suggested that the predominant mechanism of anti-tumour effect was through activatory FcγR engagement, as the FcγR$^{-/-}$ mice showed almost completely attenuated survival (similar to that seen in the WT mice) in comparison to the CD32$^{-/-}$ mice. However, when this experiment was repeated the attenuation of survival after anti-CD32 mAb was diminished. Although survival was not comparable to that seen in the CD32$^{-/-}$ animals, this suggested that in this case anti-tumour effect was occurring through PCD and activatory FcγR-dependent mechanisms, rather than in the initial experiment where anti-tumour effect seemed to be occurring through activatory FcγR-dependent mechanism. This, of course, needs further exploration, but hopefully in combination with the abovementioned investigations will delineate the potential anti-tumour mechanisms of our anti-CD32 mAb. During the second experiment using the FcγR$^{-/-}$ our animal house became infected with mouse hepatitis virus (MHV), which may have affected the outcome of this particular experiment. As a result the animals needed to be re-derived through an external company and the animal house facilities were quarantined. Therefore, we were lacking mice and the facilities to repeat this experiment. The MHV infection may also account for the differences observed between experimental repeats, although the extent to which MHV affects immunotherapy has not been fully reported.

Further to this, having mention in introduction section 1.3.3.2 the importance of CDC in the function of therapeutic mAb we have not, through this thesis, elucidated the potential of complement involvement in the anti-tumour response mediated by the anti-CD32 mAb. We would suggest, given the modulation of the anti-CD32 mAb from the cell surface after treatment, it is unlikely that complement activation would be a major anti-tumour effector mechanism in reponse to our anti-CD32 mAb, primarily as this modulation would prevent sufficient accumulation of complement at the cell surface for effective induction of CDC.

In addition, using the example of the anti-CD20 mAb, complement activation seems to be dependent of accumulation of the CD20 molecule within lipid rafts, where the type II anti-CD20 mAb do not accumulate in lipid raft domains nor do they induce CDC, whilst in contrast the type I anti-CD20 mAb do accumulate in lipid rafts and consequentially induce CDC[112]. Preliminary studies in this laboratory using Triton X-100 insolubility assays to assess raft-associated antigen have demonstrated that the anti-CD32 mAb are excluded from lipid rafts domains. This suggests that the anti-CD32 mAb are likely to induce limited amounts of CDC.

The mouse models used and the experiments performed do not determine the affects of the anti-CD32 mAb on CD32 expressing effector cells *in vivo*. It has been postulated and demonstrated by others that anti-CD32 mAb reagents are able to attenuate CD32 activity on effector cells and sequentially enhance activatory FcγR activity *in vitro*[373,374]. We have been able to demonstrate *in vitro* that the anti-CD32 mAb augment FcγR-dependent phagocytosis and we would assume that this would also be true *in vivo*, although we do not, at this time have a system in which we could test this theory, i.e. a $CD32^{-/-}$ mouse with conditional expression of CD32 only on effector cells.

Despite the set-backs we have encountered in investigating the use of anti-CD32 mAb in our murine models of lymphoma, the research of this thesis has highlighted many areas for future investigation. Included in this, would be establishing the similarities in CD32 modulation between species, discussed at length in Chapter 6 (section 6.13). For example, here we have shown that CD32 on murine cells is differentially modulated depending on the anti-CD32 mAb used. This is contrast to the observed lack of CD32b1 internalisation observed by others[298,299,294,302]. Preliminary data from this laboratory and others[374], have demonstrated that CD32b expression in human lymphoma cell lines is not significantly altered after incubation with human anti-CD32b mAb. As mentioned, establishing the differences between modulation of the murine and human CD32b isoforms is part of an existing project in this laboratory. Preliminary data from this project has demonstrated that modulation of CD32 after incubation with anti-CD32 mAb is consistent irrespective of the isoform expressed by lymphoma cells, suggesting that modulation of CD32 was as a result of engagement by mAb rather than by IC. This does however require further investigation.

Alongside this, work by Dr Sean Lim within this laboratory has shown that on human B cell malignancies, CD32 expression correlates with modulation of CD20 after rituximab treatment and this may have clinical impact for rituximab treatment (Manuscript

submitted). We know that CD32 expression limits immunotherapy in many cases, the example of rituximab being just one. Therefore co-administration of anti-CD32 mAb in a situation where CD32 expression hampers therapy may be advantageous, particularly if modulation as seen in our *in vivo* murine models reduces CD32 expression alongside blocking the Fc interaction with CD32 on the surface of tumour cells. In addition, consumption of anti-CD32 mAb would be limited in patients treated with rituximab as a result of systemic B cell depletion. However, we first would need to establish if modulation of CD32 and consumption of anti-CD32 mAb holds true for the human system and human anti-CD32 mAb. As published data has shown anti-tumour efficacy in human pre-clinical models[129,372,373,374] it would be expected that this would not be the case. However, a limitation to these studies is that human CD32b was expressed on specific cell types and not systemically, as observed in our mice with murine CD32. We would suggest that if we are able to elucidate that human CD32b isoforms modulate in a similar manner to the murine CD32 isoforms as a result of mAb engagement, then the rate of mAb consumption in patients would need to be assessed before the instigation of clinical trials, particularly as work within this laboratory has shown that human CD32b is expressed by a plethora of non-haemopoietic tissues.

In conculsion, although the data in this thesis had highlighted the possible complications of using anti-CD32 mAb, we have also demonstrated the potential of these reagents in augmenting mAb immunotherapy of cancer.

APPENDICES.

Appendix 1: Common Stock buffers

Tail lysis buffer:
Requires: 50 mM Tris (pH 8.0)
200 mM NaCl
0.5 % SDS
5 mM EDTA

For 100 ml of stock:

- 1 M Tris: 5 ml
- 5 M NaCl: 4 ml
- 0.5g SDS or 5 ml of 10 % SDS solution (5 g SDS in 50 ml dH_2O).
- 500 mM EDTA: 1 ml of warmed solution.

Buffer should be autoclaved after preparation.

0.2M TE8 buffer
Consists of:

- 0.2 M Tris base
- 10 mM Na_2EDTA, in ultrapure water, and titrated to pH 8.

PBS-BSA-AZIDE (FACS wash):
Phosphate buffered saline (PBS) was made up of:

- 8.768 g NaCl, 2.3 g Na_2HPO4
- 0.456 g NaH_2PO_4 per litre dH_2O.

With the addition of:

- 1 % w/v BSA
- 0.1 % w/v sodium azide

AnV/PI stock:

- AnV: 50 µl of a 50 mM stock solution.
- PI: 100 µl of a 1 mg/ml stock solution

Made up in 1 ml sterile PBS or FACS binding buffer (see below). Add 10 µl AnV/PI stock to 200 µl of cells.

FACS binding buffer:
10X stock buffer consists of:

- 100 mM Hepes buffer, pH 7.4
- 1.4 M NaCl
- 25 mM $CaCl_2$

Onyx Lysis Buffer:

100 ml of stock buffer consists of:

- 1 M Tris
- 5 M NaCl
- 1 M $MgCl_2$
- 1 M EGTA
- 1 ml Triton-X 100
- 10 ml Glycerol

Made up to 100 ml with dH_20

For use, an aliquot of was made containing specific inhibitors and placed immediately on ice.
To 3ml of above add:

- Protease inhibitor PI: 6µl (1:500)
- Phosphatase inhibitors NaF: 150 µl (1M, 41.99mg/ml) and NaV: 7.2 µl (700mM, 36.8mg/ml Na_3VO_4)

4 X Loading Buffer for Western blot:

- 5 ml 0.5M Tris HCl pH 6.8
- 4 ml glycerol
- 4 ml 20% SDS solution or 0.8 g SDS
- Bromophenol blue , until solution turns blue or at 1%
- MQW to 10mls.

For use (reduced):

- 900 µl 4x LB plus 100 µl 2-ME. Can be stored at RT.

NuPAGE® MOPS SDS running buffer (Invitrogen system):

- 50 mM MOPS
- 50 mM Tris base
- 0.1 % SDS
- 1 mM EDTA

For 500 ml of 20x stock:

- 104.6 g MOPS
- 60.6 g Tris base
- 10 g SDS
- 3.0 g EDTA

Made up to 500 ml with dH_2O. 1x stock made up with 100 ml 20X buffer with1.9 L dH_2O.

TBS-Tween (TBS-T) 0.05%
In dH_2O this buffer consists of :

- 150 mM NaCl
- 50 mM Tris
- 0.05 % Tween 20

50X TAE buffer
1 L of 50X buffer contains,

- 242 g Tris
- 57.1 ml glacial acetic acid
- 100 ml 0.5 M EDTA (pH 8.0)

Appendix 2: 60 – 70 kDa band detected by Western blot associated with phosphorylation of CD32.

As mentioned in Chapter 4, section 1.3.2, alongside the pCD32 specific band (40 kDa), a second band at approximately 60 – 70 kDa, was detected using the anti-phospho-CD32 antibody for Western blotting. The detection of this band corresponded exclusively with of CD32 phosphorylation and provided a surrogate marker for the activation of CD32 in murine cells. This was valuable for analysis of the Western blot data as the anti-phospho-CD32 specific antibody was specific for detection of human CD32, specifically the intracellular domains of the receptor, which differed between species[146,293,294]. As a result, the detection of pCD32 in our murine cells was sometimes limited and the surrogate marker therefore indicated whether CD32 has been phosphorylated. Below are detailed two examples.

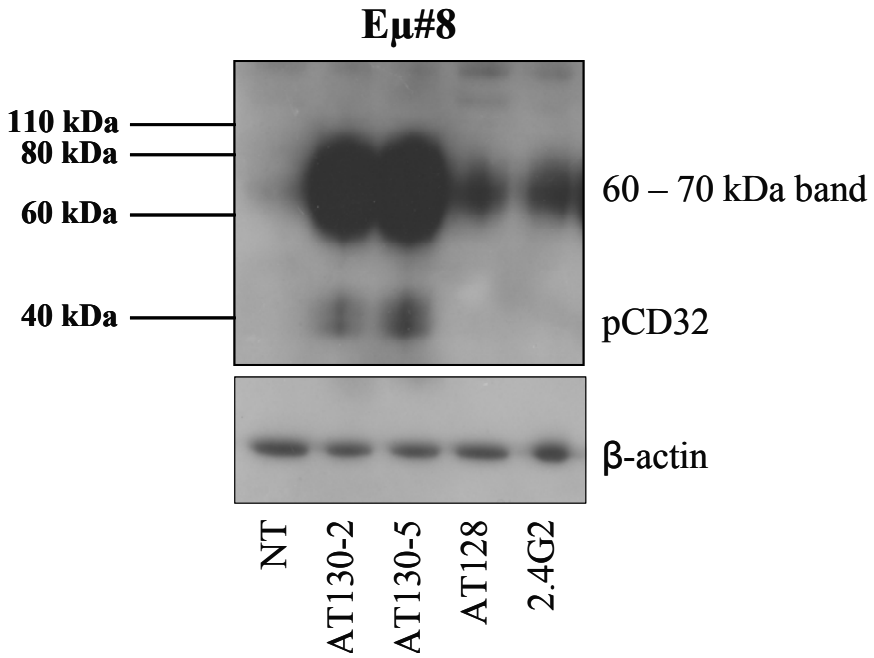

Appendix figure 1: Tyrosine phosphorylation of CD32 by anti-CD32 mAb and detection of a surrogate marker for pCD32 in Eμ-myc cells.
Eμ#8 cells were stimulated for 30 min with the relevant anti-CD32 mAb, lysates prepared and sample examined for CD32 and β-actin by Western blot. The use of the anti-phospho-CD32 antibody for detection of pCD32 in murine cells also resulted in the detection of a surrogate marker for pCD32 at approximately 60 -70 kDa. Where, we observed a phosphorylation of CD32 by AT130-2 and AT130-5, we observed a dramatic increase in the intensity of this band compare to instances where we did not observe phosphorylation of CD32, such as after incubation with AT128 m2a and 2.4G2.

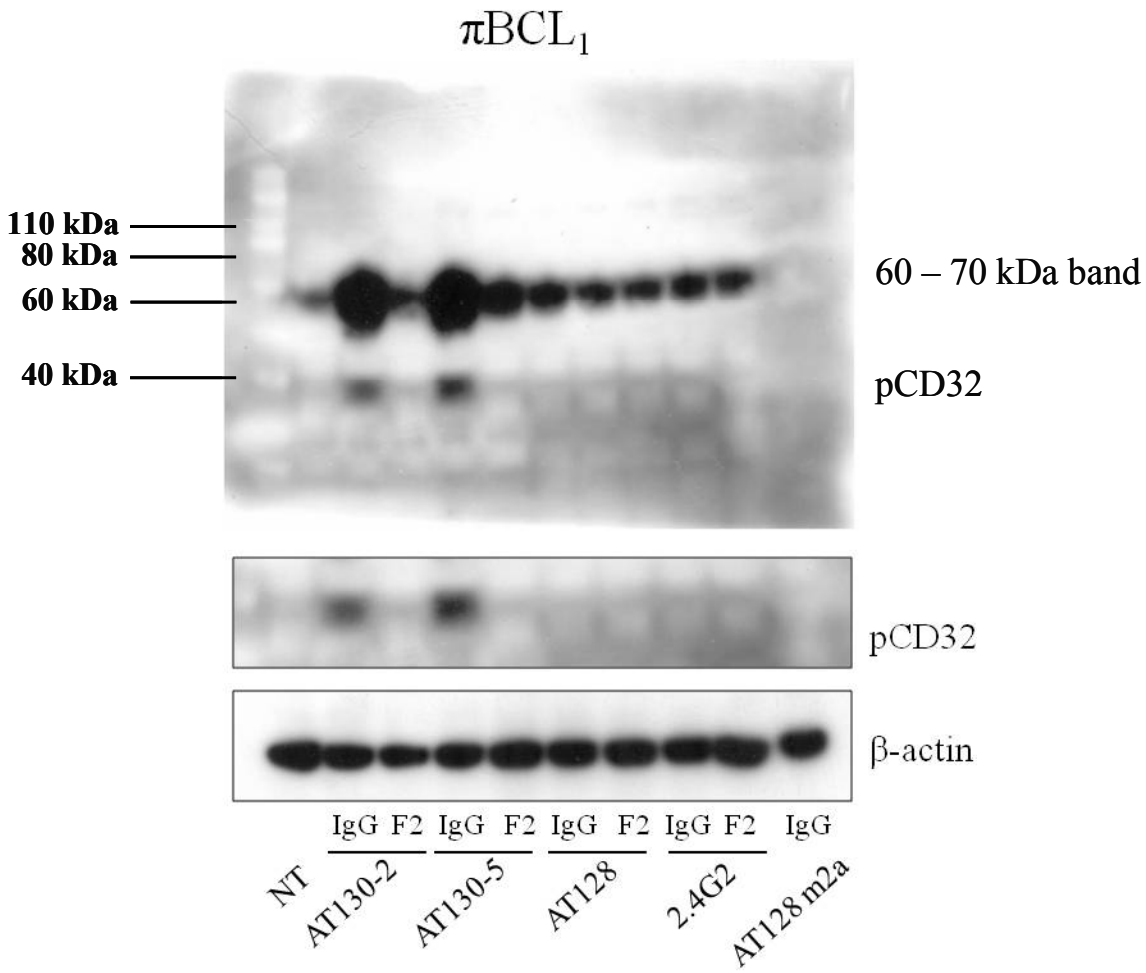

Appendix figure 2. Effect of whole IgG or F(ab')$_2$ fragment anti-CD32 mAb on tyrosine phosphorylation of CD32 and detection of surrogate marker of pCD32.
πBCL$_1$ cells were incubated with 10 μg/ml anti-CD32 mAb, either IgG or F(ab')2 (F2) at 37˚C for 5 min, lysates prepared and samples analysed for pCD32 and β-actin by Western blot. When the entire membrane exposure is examined, again we can clearly see an increase in intensity of the surrogate marker of CD32 phosphorylation.

Appendix 3: Binding of anti-FcγR mAb to FcγR fusion proteins by ELISA.

Further to the generation of specific murine anti-CD32 mAb, reagents were also raised by Miss Alison Tutt against the other FcγR. The specificity of these reagents to their specific FcγR was assessed by ELISA. Briefly, an immunomaxisorb 96-well plate were coated with 10 µg/ml anti-FcγR mAb at 37 °C for 1 hr. A 1:15 dilution of normal mouse serum to fusion protein was incubated overnight at 4 °C before 100 µl added to the plate and incubated at 37 °C for 2 hrs. In order to detect bound fusion protein, 100 µl of a 1:4000 dilution of HRP-conjugated anti-CD4 (OX68) was added to the plate and the reaction stopped by the addition of 5 M sulphuric acid. Results were read at a wavelength of 495 nm. It was demonstrated that the anti-FcγR mAb had specific binding to the relevant FcγR fusion protein. In particular, the anti-CD32 mAb bound only the CD32 fusion protein and did not demonstrate binding to FcγRI, FcγRIII or FcγRIV.

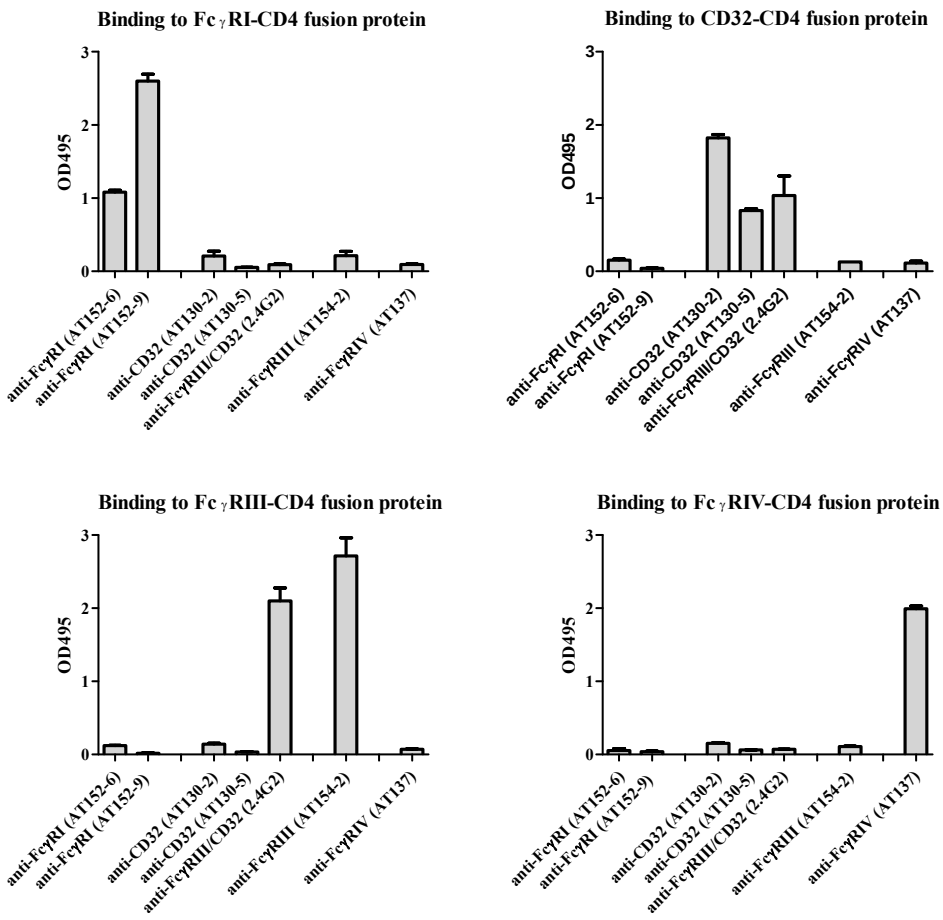

Appendix figure 2. Binding of anti-FcγR mAb to FcγR fusion proteins byELISA.
Immunomaxisorb 96-well plate were coated with 10 µg/ml anti-FcγR mAb at 37 °C for 1 hr, these were then incubated at 37 °C for 2 hr, before incubation with HRP-conjugated anti-CD4 (OX68). Here, it has been shown that the anti-FcγR mAb bind specific FcγR fusion proteins. For example, the anti-CD32 mAb only bind to the CD32 fusion protein and not to the FcγRI, FcγRIII or FcγRIV.

Appendix 4: Densitomerty analysis of Figure 5.2 and Figure 5.3.

In order to demonstrate whether the lack of inhibition of BCR-induced Ca^{2+} flux by the anti-CD32 mAb on C57BL/6 cells was due to differences in CD32 activation (phosphorylation) densitometry analysis was performed on the Western blots from Figures 5.2 & 5.3 using Photoshop C4S histogram analysis and normalised against the actin control (see below tables). Here, the densitometry analysis demonstrates that for AT130-2 the level of phosphorylation was more significant on B cells from the BALB/c mice than on cells from C57BL/6 mice ($p = 0.01$, by Student's t-test), but that there was no significant difference between phosphorylation of CD32 by AT130-5 on cells from the different mouse strains (by Student's t-test). This suggests that the lack of anti-CD32 mAb inhibition of BCR-induced Ca^{2+} flux was unlikely due to lack of CD32 activation.

Sample	C57BL/6	BALB/c
NT	0.01	0.09
AT130-2 0.5 min	0.51	1.48
AT130-2 2 min	0.51	1.35
AT130-2 5 min	0.56	0.81
AT130-2 15 min	0.48	0.87
AT128 m2a 0.5 min	0.14	0.11
AT128 m2a 2 min	0.09	-0.02
AT128 m2a 5 min	0.04	-0.06
AT128 m2a 15 min	0.01	-0.07

Sample	C57BL/6	BALB/c
NT	0.46	1.35
AT130-5 0.5 min	1.43	1.75
AT130-5 2 min	1.59	1.86
AT130-5 5 min	1.44	1.83
AT130-5 15 min	1.14	2.20
AT128 0.5 min	0.32	0.43
AT128 2 min	0.17	0.17
AT128 5 min	0.08	0.04
AT128 15 min	0.04	0.01

References:

1. WHO. http://www.who.int/cancer/en/. In: Organisation WH ed; 2009.

2. Llewelyn MB, Hawkins RE, Russell SJ. Discovery of antibodies. BMJ. 1992;305:1269-1272.

3. Migkou M, Dimopoulos MA, Gavriatopoulou M, Terpos E. Applications of monoclonal antibodies for the treatment of hematological malignancies. Expert Opin Biol Ther. 2009;9:207-220.

4. Leukaemia-Lymphoma USA. 2008.

5. CRUK. 2009.

6. Sato N, Hirohashi Y, Tsukahara T, et al. Molecular pathological approaches to human tumor immunology. Pathol Int. 2009;59:205-217.

7. Jain KK. Personalized cancer vaccines. Expert Opin Biol Ther;10:1637-1647.

8. Celluzzi CM, Mayordomo JI, Storkus WJ, Lotze MT, Falo LD, Jr. Peptide-pulsed dendritic cells induce antigen-specific CTL-mediated protective tumor immunity. J Exp Med. 1996;183:283-287.

9. Nestle FO, Alijagic S, Gilliet M, et al. Vaccination of melanoma patients with peptide- or tumor lysate-pulsed dendritic cells. Nat Med. 1998;4:328-332.

10. Koido S, Kashiwaba M, Chen D, Gendler S, Kufe D, Gong J. Induction of antitumor immunity by vaccination of dendritic cells transfected with MUC1 RNA. J Immunol. 2000;165:5713-5719.

11. Palucka AK, Ueno H, Connolly J, et al. Dendritic cells loaded with killed allogeneic melanoma cells can induce objective clinical responses and MART-1 specific CD8+ T-cell immunity. J Immunother. 2006;29:545-557.

12. Mackensen A, Herbst B, Chen JL, et al. Phase I study in melanoma patients of a vaccine with peptide-pulsed dendritic cells generated in vitro from CD34(+) hematopoietic progenitor cells. Int J Cancer. 2000;86:385-392.

13. Thurner B, Haendle I, Roder C, et al. Vaccination with mage-3A1 peptide-pulsed mature, monocyte-derived dendritic cells expands specific cytotoxic T cells and induces regression of some metastases in advanced stage IV melanoma. J Exp Med. 1999;190:1669-1678.

14. Koido S, Hara E, Homma S, et al. Cancer vaccine by fusions of dendritic and cancer cells. Clin Dev Immunol. 2009;2009:657369.

15. Anderson KS. Tumor vaccines for breast cancer. Cancer Invest. 2009;27:361-368.

16. Antonia SJ, Mirza N, Fricke I, et al. Combination of p53 cancer vaccine with chemotherapy in patients with extensive stage small cell lung cancer. Clin Cancer Res. 2006;12:878-887.

17. Arlen PM, Gulley JL, Parker C, et al. A randomized phase II study of concurrent docetaxel plus vaccine versus vaccine alone in metastatic androgen-independent prostate cancer. Clin Cancer Res. 2006;12:1260-1269.

18. Baxevanis CN, Perez SA, Papamichail M. Combinatorial treatments including vaccines, chemotherapy and monoclonal antibodies for cancer therapy. Cancer Immunol Immunother. 2009;58:317-324.

19. Finn OJ. Cancer vaccines: between the idea and the reality. Nat Rev Immunol. 2003;3:630-641.

20. Chang Y, Brewer NT, Rinas AC, Schmitt K, Smith JS. Evaluating the impact of human papillomavirus vaccines. Vaccine. 2009;27:4355-4362.

21. Stanley M. Prevention strategies against the human papillomavirus: the effectiveness of vaccination. Gynecol Oncol. 2007;107:S19-23.

22. Gray JC, Johnson PW, Glennie MJ. Therapeutic potential of immunostimulatory monoclonal antibodies. Clin Sci (Lond). 2006;111:93-106.

23. French RR, Taraban VY, Crowther GR, et al. Eradication of lymphoma by CD8 T cells following anti-CD40 monoclonal antibody therapy is critically dependent on CD27 costimulation. Blood. 2007;109:4810-4815.

24. Gray JC, French RR, James S, Al-Shamkhani A, Johnson PW, Glennie MJ. Optimising anti-tumour CD8 T-cell responses using combinations of immunomodulatory antibodies. Eur J Immunol. 2008;38:2499-2511.

25. Hodi FS, O'Day SJ, McDermott DF, et al. Improved survival with ipilimumab in patients with metastatic melanoma. N Engl J Med;363:711-723.

26. Suntharalingam G, Perry MR, Ward S, et al. Cytokine storm in a phase 1 trial of the anti-CD28 monoclonal antibody TGN1412. N Engl J Med. 2006;355:1018-1028.

27. Tutt AL, French RR, Illidge TM, et al. Monoclonal antibody therapy of B cell lymphoma: signaling activity on tumor cells appears more important than recruitment of effectors. J Immunol. 1998;161:3176-3185.

28. Funakoshi S, Longo DL, Beckwith M, et al. Inhibition of human B-cell lymphoma growth by CD40 stimulation. Blood. 1994;83:2787-2794.

29. Luqman M, Klabunde S, Lin K, et al. The antileukemia activity of a human anti-CD40 antagonist antibody, HCD122, on human chronic lymphocytic leukemia cells. Blood. 2008;112:711-720.

30. Tai YT, Li X, Tong X, et al. Human anti-CD40 antagonist antibody triggers significant antitumor activity against human multiple myeloma. Cancer Res. 2005;65:5898-5906.

31. Hussein M, Berenson JR, Niesvizky R, et al. A phase I multidose study of dacetuzumab (SGN-40; humanized anti-CD40 monoclonal antibody) in patients with multiple myeloma. Haematologica;95:845-848.

32. Advani R, Forero-Torres A, Furman RR, et al. Phase I study of the humanized anti-CD40 monoclonal antibody dacetuzumab in refractory or recurrent non-Hodgkin's lymphoma. J Clin Oncol. 2009;27:4371-4377.

33. Furman RR, Forero-Torres A, Shustov A, Drachman JG. A phase I study of dacetuzumab (SGN-40, a humanized anti-CD40 monoclonal antibody) in patients with chronic lymphocytic leukemia. Leuk Lymphoma;51:228-235.

34. Disis ML, Bernhard H, Jaffee EM. Use of tumour-responsive T cells as cancer treatment. Lancet. 2009;373:673-683.

35. Falkenburg JH, Wafelman AR, Joosten P, et al. Complete remission of accelerated phase chronic myeloid leukemia by treatment with leukemia-reactive cytotoxic T lymphocytes. Blood. 1999;94:1201-1208.

36. Bishop MR, Fowler DH, Marchigiani D, et al. Allogeneic lymphocytes induce tumor regression of advanced metastatic breast cancer. J Clin Oncol. 2004;22:3886-3892.

37. Yee C, Thompson JA, Byrd D, et al. Adoptive T cell therapy using antigen-specific CD8+ T cell clones for the treatment of patients with metastatic melanoma: in vivo persistence, migration, and antitumor effect of transferred T cells. Proc Natl Acad Sci U S A. 2002;99:16168-16173.

38. Marijt E, Wafelman A, van der Hoorn M, et al. Phase I/II feasibility study evaluating the generation of leukemia-reactive cytotoxic T lymphocyte lines for treatment of patients with relapsed leukemia after allogeneic stem cell transplantation. Haematologica. 2007;92:72-80.

39. Muranski P, Boni A, Wrzesinski C, et al. Increased intensity lymphodepletion and adoptive immunotherapy--how far can we go? Nat Clin Pract Oncol. 2006;3:668-681.

40. Klebanoff CA, Gattinoni L, Torabi-Parizi P, et al. Central memory self/tumor-reactive CD8+ T cells confer superior antitumor immunity compared with effector memory T cells. Proc Natl Acad Sci U S A. 2005;102:9571-9576.

41. Bruggemann M, Williams GT, Bindon CI, et al. Comparison of the effector functions of human immunoglobulins using a matched set of chimeric antibodies. J Exp Med. 1987;166:1351-1361.

42. Riechmann L, Clark M, Waldmann H, Winter G. Reshaping human antibodies for therapy. Nature. 1988;332:323-327.

43. van de Winkel JG, Anderson CL. Biology of human immunoglobulin G Fc receptors. J Leukoc Biol. 1991;49:511-524.

44. Gergely J, Medgyesi GA, Wang AC, Fudenberg HH. IgG myeloma subclass-typing by tryptic digestion of whole sera. Immunochemistry. 1972;9:589-592.

45. Turner MW, Bennich HH, Natvig JB. Pepsin digestion of human G-myeloma proteins of different subclasses. I. The characteristic features of pepsin cleavage as a function of time. Clin Exp Immunol. 1970;7:603-625.

46. Lucisano Valim YM, Lachmann PJ. The effect of antibody isotype and antigenic epitope density on the complement-fixing activity of immune complexes: a systematic study using chimaeric anti-NIP antibodies with human Fc regions. Clin Exp Immunol. 1991;84:1-8.

47. Wang SY, Weiner G. Complement and cellular cytotoxicity in antibody therapy of cancer. Expert Opin Biol Ther. 2008;8:759-768.

48. Burton DR. Immunoglobulin G: functional sites. Mol Immunol. 1985;22:161-206.

49. Bruggemann M, Teale C, Clark M, Bindon C, Waldmann H. A matched set of rat/mouse chimeric antibodies. Identification and biological properties of rat H chain constant regions mu, gamma 1, gamma 2a, gamma 2b, gamma 2c, epsilon, and alpha. J Immunol. 1989;142:3145-3150.

50. Kohler G, Milstein C. Continuous cultures of fused cells secreting antibody of predefined specificity. Nature. 1975;256:495-497.

51. Jones PT, Dear PH, Foote J, Neuberger MS, Winter G. Replacing the complementarity-determining regions in a human antibody with those from a mouse. Nature. 1986;321:522-525.

52. Iannello A, Ahmad A. Role of antibody-dependent cell-mediated cytotoxicity in the efficacy of therapeutic anti-cancer monoclonal antibodies. Cancer Metastasis Rev. 2005;24:487-499.

53. Marks JD, Hoogenboom HR, Bonnert TP, McCafferty J, Griffiths AD, Winter G. By-passing immunization. Human antibodies from V-gene libraries displayed on phage. J Mol Biol. 1991;222:581-597.

54. Winter G, Griffiths AD, Hawkins RE, Hoogenboom HR. Making antibodies by phage display technology. Annu Rev Immunol. 1994;12:433-455.

55. Clackson T, Hoogenboom HR, Griffiths AD, Winter G. Making antibody fragments using phage display libraries. Nature. 1991;352:624-628.

56. Almagro JC, Fransson J. Humanization of antibodies. Front Biosci. 2008;13:1619-1633.

57. Lonberg N. Human antibodies from transgenic animals. Nat Biotechnol. 2005;23:1117-1125.

58. Fisher RI, LeBlanc M, Press OW, Maloney DG, Unger JM, Miller TP. New treatment options have changed the survival of patients with follicular lymphoma. J Clin Oncol. 2005;23:8447-8452.

59. Sehn LH, Donaldson J, Chhanabhai M, et al. Introduction of combined CHOP plus rituximab therapy dramatically improved outcome of diffuse large B-cell lymphoma in British Columbia. J Clin Oncol. 2005;23:5027-5033.

60. Salles GA. Clinical features, prognosis and treatment of follicular lymphoma. Hematology Am Soc Hematol Educ Program. 2007:216-225.

61. Molina A. A decade of rituximab: improving survival outcomes in non-Hodgkin's lymphoma. Annu Rev Med. 2008;59:237-250.

62. Coiffier B, Lepage E, Briere J, et al. CHOP chemotherapy plus rituximab compared with CHOP alone in elderly patients with diffuse large-B-cell lymphoma. N Engl J Med. 2002;346:235-242.

63. Boland A, Bagust A, Hockenhull J, Davis H, Chu P, Dickson R. Rituximab for the treatment of relapsed or refractory stage III or IV follicular non-Hodgkin's lymphoma. Health Technol Assess. 2009;13 Suppl 2:41-48.

64. Bagust A, Boland A, Hockenhull J, et al. Rituximab for the treatment of rheumatoid arthritis. Health Technol Assess. 2009;13 Suppl 2:23-29.

65. Emery P, Fleischmann R, Filipowicz-Sosnowska A, et al. The efficacy and safety of rituximab in patients with active rheumatoid arthritis despite methotrexate treatment: results of a phase IIB randomized, double-blind, placebo-controlled, dose-ranging trial. Arthritis Rheum. 2006;54:1390-1400.

66. Leget GA, Czuczman MS. Use of rituximab, the new FDA-approved antibody. Curr Opin Oncol. 1998;10:548-551.

67. Goldenberg MM. Trastuzumab, a recombinant DNA-derived humanized monoclonal antibody, a novel agent for the treatment of metastatic breast cancer. Clin Ther. 1999;21:309-318.

68. Pagano L, Fianchi L, Caira M, Rutella S, Leone G. The role of Gemtuzumab Ozogamicin in the treatment of acute myeloid leukemia patients. Oncogene. 2007;26:3679-3690.

69. Gribben JG, Hallek M. Rediscovering alemtuzumab: current and emerging therapeutic roles. Br J Haematol. 2009;144:818-831.

70. Kaminski MS, Zasadny KR, Francis IR, et al. Radioimmunotherapy of B-cell lymphoma with [131I]anti-B1 (anti-CD20) antibody. N Engl J Med. 1993;329:459-465.

71. Kaminski MS, Zelenetz AD, Press OW, et al. Pivotal study of iodine I 131 tositumomab for chemotherapy-refractory low-grade or transformed low-grade B-cell non-Hodgkin's lymphomas. J Clin Oncol. 2001;19:3918-3928.

72. Saltz LB, Meropol NJ, Loehrer PJ, Sr., Needle MN, Kopit J, Mayer RJ. Phase II trial of cetuximab in patients with refractory colorectal cancer that expresses the epidermal growth factor receptor. J Clin Oncol. 2004;22:1201-1208.

73. Bernier J. Cetuximab in the treatment of head and neck cancer. Expert Rev Anticancer Ther. 2006;6:1539-1552.

74. Hurwitz H, Fehrenbacher L, Novotny W, et al. Bevacizumab plus irinotecan, fluorouracil, and leucovorin for metastatic colorectal cancer. N Engl J Med. 2004;350:2335-2342.

75. Gridelli C, Maione P, Rossi A, De Marinis F. The role of bevacizumab in the treatment of non-small cell lung cancer: current indications and future developments. Oncologist. 2007;12:1183-1193.

76. Marty M, Pivot X. The potential of anti-vascular endothelial growth factor therapy in metastatic breast cancer: clinical experience with anti-angiogenic agents, focusing on bevacizumab. Eur J Cancer. 2008;44:912-920.

77. Friedman HS, Prados MD, Wen PY, et al. Bevacizumab alone and in combination with irinotecan in recurrent glioblastoma. J Clin Oncol. 2009;27:4733-4740.

78. Bellmunt J. Future developments in renal cell carcinoma. Ann Oncol. 2009;20 Suppl 1:i13-17.

79. Gibson TB, Ranganathan A, Grothey A. Randomized phase III trial results of panitumumab, a fully human anti-epidermal growth factor receptor monoclonal antibody, in metastatic colorectal cancer. Clin Colorectal Cancer. 2006;6:29-31.

80. Coiffier B, Lepretre S, Pedersen LM, et al. Safety and efficacy of ofatumumab, a fully human monoclonal anti-CD20 antibody, in patients with relapsed or refractory B-cell chronic lymphocytic leukemia: a phase 1-2 study. Blood. 2008;111:1094-1100.

81. Weiner GJ. Monoclonal antibody mechanisms of action in cancer. Immunol Res. 2007;39:271-278.

82. Papamichail M, Perez SA, Gritzapis AD, Baxevanis CN. Natural killer lymphocytes: biology, development, and function. Cancer Immunol Immunother. 2004;53:176-186.

83. Clynes RA, Towers TL, Presta LG, Ravetch JV. Inhibitory Fc receptors modulate in vivo cytoxicity against tumor targets. Nat Med. 2000;6:443-446.

84. Sliwkowski MX, Lofgren JA, Lewis GD, Hotaling TE, Fendly BM, Fox JA. Nonclinical studies addressing the mechanism of action of trastuzumab (Herceptin). Semin Oncol. 1999;26:60-70.

85. Golay J, Cortiana C, Manganini M, et al. The sensitivity of acute lymphoblastic leukemia cells carrying the t(12;21) translocation to campath-1H-mediated cell lysis. Haematologica. 2006;91:322-330.

86. Fearon DT, Wong WW. Complement ligand-receptor interactions that mediate biological responses. Annu Rev Immunol. 1983;1:243-271.

87. Kennedy AD, Solga MD, Schuman TA, et al. An anti-C3b(i) mAb enhances complement activation, C3b(i) deposition, and killing of CD20+ cells by rituximab. Blood. 2003;101:1071-1079.

88. Cragg MS, French RR, Glennie MJ. Signaling antibodies in cancer therapy. Curr Opin Immunol. 1999;11:541-547.

89. Slamon DJ, Clark GM, Wong SG, Levin WJ, Ullrich A, McGuire WL. Human breast cancer: correlation of relapse and survival with amplification of the HER-2/neu oncogene. Science. 1987;235:177-182.

90. Slamon DJ, Godolphin W, Jones LA, et al. Studies of the HER-2/neu proto-oncogene in human breast and ovarian cancer. Science. 1989;244:707-712.

91. Tandon AK, Clark GM, Chamness GC, Ullrich A, McGuire WL. HER-2/neu oncogene protein and prognosis in breast cancer. J Clin Oncol. 1989;7:1120-1128.

92. Seshadri R, Firgaira FA, Horsfall DJ, McCaul K, Setlur V, Kitchen P. Clinical significance of HER-2/neu oncogene amplification in primary breast cancer. The South Australian Breast Cancer Study Group. J Clin Oncol. 1993;11:1936-1942.

93. Izumi Y, Xu L, di Tomaso E, Fukumura D, Jain RK. Tumour biology: herceptin acts as an anti-angiogenic cocktail. Nature. 2002;416:279-280.

94. Marty M, Cognetti F, Maraninchi D, et al. Randomized phase II trial of the efficacy and safety of trastuzumab combined with docetaxel in patients with human epidermal growth factor receptor 2-positive metastatic breast cancer administered as first-line treatment: the M77001 study group. J Clin Oncol. 2005;23:4265-4274.

95. Marty M, Espie M, Llombart A, Monnier A, Rapoport BL, Stahalova V. Multicenter randomized phase III study of the cardioprotective effect of dexrazoxane (Cardioxane) in advanced/metastatic breast cancer patients treated with anthracycline-based chemotherapy. Ann Oncol. 2006;17:614-622.

96. Slamon DJ, Leyland-Jones B, Shak S, et al. Use of chemotherapy plus a monoclonal antibody against HER2 for metastatic breast cancer that overexpresses HER2. N Engl J Med. 2001;344:783-792.

97. Cooley S, Burns LJ, Repka T, Miller JS. Natural killer cell cytotoxicity of breast cancer targets is enhanced by two distinct mechanisms of antibody-dependent cellular cytotoxicity against LFA-3 and HER2/neu. Exp Hematol. 1999;27:1533-1541.

98. Heath WR, Carbone FR. Cross-presentation, dendritic cells, tolerance and immunity. Annu Rev Immunol. 2001;19:47-64.

99. Weiner LM, Dhodapkar MV, Ferrone S. Monoclonal antibodies for cancer immunotherapy. Lancet. 2009;373:1033-1040.

100. Schicher N, Paulitschke V, Swoboda A, et al. Erlotinib and bevacizumab have synergistic activity against melanoma. Clin Cancer Res. 2009;15:3495-3502.

101. McMahon G. VEGF receptor signaling in tumor angiogenesis. Oncologist. 2000;5 Suppl 1:3-10.

102. Carmeliet P. Mechanisms of angiogenesis and arteriogenesis. Nat Med. 2000;6:389-395.

103. Jenab-Wolcott J, Giantonio BJ. Bevacizumab: current indications and future development for management of solid tumors. Expert Opin Biol Ther. 2009;9:507-517.

104. Miller K, Wang M, Gralow J, et al. Paclitaxel plus bevacizumab versus paclitaxel alone for metastatic breast cancer. N Engl J Med. 2007;357:2666-2676.

105. Sandler A, Gray R, Perry MC, et al. Paclitaxel-carboplatin alone or with bevacizumab for non-small-cell lung cancer. N Engl J Med. 2006;355:2542-2550.

106. Tamiya A, Yamazaki K, Boku N, et al. Safety of bevacizumab treatment in combination with standard chemotherapy for metastatic colorectal cancer: a retrospective review of 65 Japanese patients. Int J Clin Oncol. 2009;14:513-517.

107. Yildiz R, Buyukberber S, Uner A, et al. Bevacizumab Plus Irinotecan-Based Therapy in Metastatic Colorectal Cancer Patients Previously Treated With Oxaliplatin-Based Regimens. Cancer Invest. 2009.

108. Hainsworth JD, Spigel DR, Thompson DS, et al. Paclitaxel/Carboplatin plus Bevacizumab/Erlotinib in the First-Line Treatment of Patients with Carcinoma of Unknown Primary Site. Oncologist. 2009.

109. Lim SH, Beers SA, French RR, Johnson PW, Glennie MJ, Cragg MS. Anti-CD20 monoclonal antibodies - historical and future perspectives. Haematologica. 2009.

110. Cragg MS, Glennie MJ. Antibody specificity controls in vivo effector mechanisms of anti-CD20 reagents. Blood. 2004;103:2738-2743.

111. Glennie MJ, French RR, Cragg MS, Taylor RP. Mechanisms of killing by anti-CD20 monoclonal antibodies. Mol Immunol. 2007;44:3823-3837.

112. Cragg MS, Morgan SM, Chan HT, et al. Complement-mediated lysis by anti-CD20 mAb correlates with segregation into lipid rafts. Blood. 2003;101:1045-1052.

113. Di Gaetano N, Cittera E, Nota R, et al. Complement activation determines the therapeutic activity of rituximab in vivo. J Immunol. 2003;171:1581-1587.

114. Golay J, Cittera E, Di Gaetano N, et al. The role of complement in the therapeutic activity of rituximab in a murine B lymphoma model homing in lymph nodes. Haematologica. 2006;91:176-183.

115. Beers SA, Chan CH, James S, et al. Type II (tositumomab) anti-CD20 monoclonal antibody out performs type I (rituximab-like) reagents in B-cell depletion regardless of complement activation. Blood. 2008;112:4170-4177.

116. Cragg MS, Walshe CA, Ivanov AO, Glennie MJ. The biology of CD20 and its potential as a target for mAb therapy. Curr Dir Autoimmun. 2005;8:140-174.

117. Cartron G, Dacheux L, Salles G, et al. Therapeutic activity of humanized anti-CD20 monoclonal antibody and polymorphism in IgG Fc receptor FcgammaRIIIa gene. Blood. 2002;99:754-758.

118. Weng WK, Levy R. Two immunoglobulin G fragment C receptor polymorphisms independently predict response to rituximab in patients with follicular lymphoma. J Clin Oncol. 2003;21:3940-3947.

119. Polson AG, Ho WY, Ramakrishnan V. Investigational antibody-drug conjugates for hematological malignancies. Expert Opin Investig Drugs;20:75-85.

120. Krop IE, Beeram M, Modi S, et al. Phase I study of trastuzumab-DM1, an HER2 antibody-drug conjugate, given every 3 weeks to patients with HER2-positive metastatic breast cancer. J Clin Oncol;28:2698-2704.

121. Burris HA, 3rd, Rugo HS, Vukelja SJ, et al. Phase II Study of the Antibody Drug Conjugate Trastuzumab-DM1 for the Treatment of Human Epidermal Growth Factor Receptor 2 (HER2) -Positive Breast Cancer After Prior HER2-Directed Therapy. J Clin Oncol;29:398-405.

122. Remillard S, Rebhun LI, Howie GA, Kupchan SM. Antimitotic activity of the potent tumor inhibitor maytansine. Science. 1975;189:1002-1005.

123. Chari RV, Martell BA, Gross JL, et al. Immunoconjugates containing novel maytansinoids: promising anticancer drugs. Cancer Res. 1992;52:127-131.

124. Baselga J, Norton L, Albanell J, Kim YM, Mendelsohn J. Recombinant humanized anti-HER2 antibody (Herceptin) enhances the antitumor activity of paclitaxel and doxorubicin against HER2/neu overexpressing human breast cancer xenografts. Cancer Res. 1998;58:2825-2831.

125. Pegram MD, Slamon DJ. Combination therapy with trastuzumab (Herceptin) and cisplatin for chemoresistant metastatic breast cancer: evidence for receptor-enhanced chemosensitivity. Semin Oncol. 1999;26:89-95.

126. Konecny GE, Thomssen C, Luck HJ, et al. Her-2/neu gene amplification and response to paclitaxel in patients with metastatic breast cancer. J Natl Cancer Inst. 2004;96:1141-1151.

127. Lewis Phillips GD, Li G, Dugger DL, et al. Targeting HER2-positive breast cancer with trastuzumab-DM1, an antibody-cytotoxic drug conjugate. Cancer Res. 2008;68:9280-9290.

128. Lazar GA, Dang W, Karki S, et al. Engineered antibody Fc variants with enhanced effector function. Proc Natl Acad Sci U S A. 2006;103:4005-4010.

129. Stavenhagen JB, Gorlatov S, Tuaillon N, et al. Enhancing the potency of therapeutic monoclonal antibodies via Fc optimization. Adv Enzyme Regul. 2008;48:152-164.

130. Stavenhagen JB, Gorlatov S, Tuaillon N, et al. Fc optimization of therapeutic antibodies enhances their ability to kill tumor cells in vitro and controls tumor expansion in vivo via low-affinity activating Fcgamma receptors. Cancer Res. 2007;67:8882-8890.

131. Kanda Y, Yamada T, Mori K, et al. Comparison of biological activity among nonfucosylated therapeutic IgG1 antibodies with three different N-linked Fc oligosaccharides: the high-mannose, hybrid, and complex types. Glycobiology. 2007;17:104-118.

132. Natsume A, Wakitani M, Yamane-Ohnuki N, et al. Fucose removal from complex-type oligosaccharide enhances the antibody-dependent cellular cytotoxicity of single-gene-encoded antibody comprising a single-chain antibody linked the antibody constant region. J Immunol Methods. 2005;306:93-103.

133. Niwa R, Natsume A, Uehara A, et al. IgG subclass-independent improvement of antibody-dependent cellular cytotoxicity by fucose removal from Asn297-linked oligosaccharides. J Immunol Methods. 2005;306:151-160.

134. Niwa R, Sakurada M, Kobayashi Y, et al. Enhanced natural killer cell binding and activation by low-fucose IgG1 antibody results in potent antibody-dependent cellular cytotoxicity induction at lower antigen density. Clin Cancer Res. 2005;11:2327-2336.

135. Shinkawa T, Nakamura K, Yamane N, et al. The absence of fucose but not the presence of galactose or bisecting N-acetylglucosamine of human IgG1 complex-type oligosaccharides shows the critical role of enhancing antibody-dependent cellular cytotoxicity. J Biol Chem. 2003;278:3466-3473.

136. Suzuki E, Niwa R, Saji S, et al. A nonfucosylated anti-HER2 antibody augments antibody-dependent cellular cytotoxicity in breast cancer patients. Clin Cancer Res. 2007;13:1875-1882.

137. Alduaij W, Ivanov A, Honeychurch J, et al. Novel type II anti-CD20 monoclonal antibody (GA101) evokes homotypic adhesion and actin-dependent, lysosome-mediated cell death in B-cell malignancies. Blood.

138. Robak T. GA-101, a third-generation, humanized and glyco-engineered anti-CD20 mAb for the treatment of B-cell lymphoid malignancies. Curr Opin Investig Drugs. 2009;10:588-596.

139. Ravetch JV, Kinet JP. Fc receptors. Annu Rev Immunol. 1991;9:457-492.

140. Monteiro RC, Van De Winkel JG. IgA Fc receptors. Annu Rev Immunol. 2003;21:177-204.

141. Kim J, Mohanty S, Ganesan LP, et al. FcRn in the yolk sac endoderm of mouse is required for IgG transport to fetus. J Immunol. 2009;182:2583-2589.

142. Lencer WI, Blumberg RS. A passionate kiss, then run: exocytosis and recycling of IgG by FcRn. Trends Cell Biol. 2005;15:5-9.

143. Nimmerjahn F, Ravetch JV. Fcgamma receptors as regulators of immune responses. Nat Rev Immunol. 2008;8:34-47.

144. Nimmerjahn F, Bruhns P, Horiuchi K, Ravetch JV. FcgammaRIV: a novel FcR with distinct IgG subclass specificity. Immunity. 2005;23:41-51.

145. Nimmerjahn F, Ravetch JV. Fcgamma receptors: old friends and new family members. Immunity. 2006;24:19-28.

146. Ravetch JV, Luster AD, Weinshank R, et al. Structural heterogeneity and functional domains of murine immunoglobulin G Fc receptors. Science. 1986;234:718-725.

147. Anderson CL, Grey HM. Receptors for aggregated IgG on mouse lymphocytes: their presence on thymocytes, thymus-derived, and bone marrow-derived lymphocytes. J Exp Med. 1974;139:1175-1188.

148. Leclerc JC, Plater C, Fridman WH. The role of the Fc receptor (FcR) of thymus-derived lymphocytes. I. Presence of FcR on cytotoxic lymphocytes and absence of direct role in cytotoxicity. Eur J Immunol. 1977;7:543-548.

149. Stout RD, Herzenberg LA. The Fc receptor on thymus-derived lymphocytes. I. Detection of a subpopulation of murine T lymphocytes bearing the Fc receptor. J Exp Med. 1975;142:611-621.

150. Ravetch JV, Bolland S. IgG Fc receptors. Annu Rev Immunol. 2001;19:275-290.

151. Schmitt DA, Hanau D, Bieber T, et al. Human epidermal Langerhans cells express only the 40-kilodalton Fc gamma receptor (FcRII). J Immunol. 1990;144:4284-4290.

152. Takai T, Ono M, Hikida M, Ohmori H, Ravetch JV. Augmented humoral and anaphylactic responses in Fc gamma RII-deficient mice. Nature. 1996;379:346-349.

153. Kalergis AM, Ravetch JV. Inducing tumor immunity through the selective engagement of activating Fcgamma receptors on dendritic cells. J Exp Med. 2002;195:1653-1659.

154. Clynes R, Maizes JS, Guinamard R, Ono M, Takai T, Ravetch JV. Modulation of immune complex-induced inflammation in vivo by the coordinate expression of activation and inhibitory Fc receptors. J Exp Med. 1999;189:179-185.

155. Crowell RE, Du Clos TW, Montoya G, Heaphy E, Mold C. C-reactive protein receptors on the human monocytic cell line U-937. Evidence for additional binding to Fc gamma RI. J Immunol. 1991;147:3445-3451.

156. Stanton LW, White RT, Bryant CM, Protter AA, Endemann G. A macrophage Fc receptor for IgG is also a receptor for oxidized low density lipoprotein. J Biol Chem. 1992;267:22446-22451.

157. Galon J, Bouchard C, Fridman WH, Sautes C. Ligands and biological activities of soluble Fc gamma receptors. Immunol Lett. 1995;44:175-181.

158. Bharadwaj D, Stein MP, Volzer M, Mold C, Du Clos TW. The major receptor for C-reactive protein on leukocytes is fcgamma receptor II. J Exp Med. 1999;190:585-590.

159. Mortensen RF, Osmand AP, Lint TF, Gewurz H. Interaction of C-reactive protein with lymphocytes and monocytes: complement-dependent adherence and phagocytosis. J Immunol. 1976;117:774-781.

160. Zahedi K, Mortensen RF. Macrophage tumoricidal activity induced by human C-reactive protein. Cancer Res. 1986;46:5077-5083.

161. Sandor M, Galon J, Takacs L, et al. An alternative Fc gamma-receptor ligand: potential role in T-cell development. Proc Natl Acad Sci U S A. 1994;91:12857-12861.

162. Sandor M, Hagen M, de Andres B, Lynch RG. Developmentally regulated Fc gamma receptor expression in lymphopoiesis Fc gammaR III (CD16) provides an ITAM motif for pro-T and pro-B-cells. Immunol Lett. 1996;54:123-127.

163. Takai T. Roles of Fc receptors in autoimmunity. Nat Rev Immunol. 2002;2:580-592.

164. van Mirre E, Teeling JL, van der Meer JW, Bleeker WK, Hack CE. Monomeric IgG in intravenous Ig preparations is a functional antagonist of FcgammaRII and FcgammaRIIIb. J Immunol. 2004;173:332-339.

165. Hogarth PM, Hulett MD, Osman N. Fc gamma receptors: gene structure and receptor function. Immunol Res. 1992;11:217-225.

166. Nimmerjahn F, Ravetch JV. Divergent immunoglobulin g subclass activity through selective Fc receptor binding. Science. 2005;310:1510-1512.

167. Bruhns P, Iannascoli B, England P, et al. Specificity and affinity of human Fcgamma receptors and their polymorphic variants for human IgG subclasses. Blood. 2009;113:3716-3725.

168. Kaas Q, Ehrenmann F, Lefranc MP. IG, TR and IgSF, MHC and MhcSF: what do we learn from the IMGT Colliers de Perles? Brief Funct Genomic Proteomic. 2007;6:253-264.

169. Zidovetzki R, Rost B, Armstrong DL, Pecht I. Transmembrane domains in the functions of Fc receptors. Biophys Chem. 2003;100:555-575.

170. Unkeless JC, Shen Z, Lin CW, DeBeus E. Function of human Fc gamma RIIA and Fc gamma RIIIB. Semin Immunol. 1995;7:37-44.

171. Sharom FJ, Lehto MT. Glycosylphosphatidylinositol-anchored proteins: structure, function, and cleavage by phosphatidylinositol-specific phospholipase C. Biochem Cell Biol. 2002;80:535-549.

172. Sanchez-Mejorada G, Rosales C. Signal transduction by immunoglobulin Fc receptors. J Leukoc Biol. 1998;63:521-533.

173. Mitchell MA, Huang MM, Chien P, Indik ZK, Pan XQ, Schreiber AD. Substitutions and deletions in the cytoplasmic domain of the phagocytic receptor Fc gamma RIIA: effect on receptor tyrosine phosphorylation and phagocytosis. Blood. 1994;84:1753-1759.

174. Moretta A, Bottino C, Vitale M, et al. Activating receptors and coreceptors involved in human natural killer cell-mediated cytolysis. Annu Rev Immunol. 2001;19:197-223.

175. Cassard L, Cohen-Solal J, Camilleri-Broet S, Fournier E, Fridman WH, Sautes-Fridman C. Fc gamma receptors and cancer. Springer Semin Immunopathol. 2006;28:321-328.

176. Sondermann P, Huber R, Jacob U. Crystal structure of the soluble form of the human fcgamma-receptor IIb: a new member of the immunoglobulin superfamily at 1.7 A resolution. EMBO J. 1999;18:1095-1103.

177. Sondermann P, Jacob U, Kutscher C, Frey J. Characterization and crystallization of soluble human Fc gamma receptor II (CD32) isoforms produced in insect cells. Biochemistry. 1999;38:8469-8477.

178. Maxwell KF, Powell MS, Hulett MD, et al. Crystal structure of the human leukocyte Fc receptor, Fc gammaRIIa. Nat Struct Biol. 1999;6:437-442.

179. Sondermann P, Huber R, Oosthuizen V, Jacob U. The 3.2-A crystal structure of the human IgG1 Fc fragment-Fc gammaRIII complex. Nature. 2000;406:267-273.

180. Radaev S, Motyka S, Fridman WH, Sautes-Fridman C, Sun PD. The structure of a human type III Fcgamma receptor in complex with Fc. J Biol Chem. 2001;276:16469-16477.

181. Sondermann P, Kaiser J, Jacob U. Molecular basis for immune complex recognition: a comparison of Fc-receptor structures. J Mol Biol. 2001;309:737-749.

182. Radaev S, Sun P. Recognition of immunoglobulins by Fcgamma receptors. Mol Immunol. 2002;38:1073-1083.

183. Kato K, Sautes-Fridman C, Yamada W, et al. Structural basis of the interaction between IgG and Fcgamma receptors. J Mol Biol. 2000;295:213-224.

184. Kato K, Fridman WH, Arata Y, Sautes-Fridman C. A conformational change in the Fc precludes the binding of two Fcgamma receptor molecules to one IgG. Immunol Today. 2000;21:310-312.

185. Tamm A, Schmidt RE. IgG binding sites on human Fc gamma receptors. Int Rev Immunol. 1997;16:57-85.

186. Zhang Y, Boesen CC, Radaev S, et al. Crystal structure of the extracellular domain of a human Fc gamma RIII. Immunity. 2000;13:387-395.

187. Guyre PM, Morganelli PM, Miller R. Recombinant immune interferon increases immunoglobulin G Fc receptors on cultured human mononuclear phagocytes. J Clin Invest. 1983;72:393-397.

188. Sivo J, Politis AD, Vogel SN. Differential effects of interferon-gamma and glucocorticoids on Fc gamma R gene expression in murine macrophages. J Leukoc Biol. 1993;54:451-457.

189. Okayama Y, Kirshenbaum AS, Metcalfe DD. Expression of a functional high-affinity IgG receptor, Fc gamma RI, on human mast cells: Up-regulation by IFN-gamma. J Immunol. 2000;164:4332-4339.

190. Yoshie O, Mellman IS, Broeze RJ, Garcia-Blanco M, Lengyel P. Interferon action: effects of mouse alpha and beta interferons on rosette formation, phagocytosis, and surface-antigen expression of cells of the macrophage-type line RAW 309Cr.1. Cell Immunol. 1982;73:128-140.

191. Shushakova N, Skokowa J, Schulman J, et al. C5a anaphylatoxin is a major regulator of activating versus inhibitory FcgammaRs in immune complex-induced lung disease. J Clin Invest. 2002;110:1823-1830.

192. Tridandapani S, Wardrop R, Baran CP, et al. TGF-beta 1 suppresses [correction of supresses] myeloid Fc gamma receptor function by regulating the expression and function of the common gamma-subunit. J Immunol. 2003;170:4572-4577.

193. Pricop L, Redecha P, Teillaud JL, et al. Differential modulation of stimulatory and inhibitory Fc gamma receptors on human monocytes by Th1 and Th2 cytokines. J Immunol. 2001;166:531-537.

194. te Velde AA, Huijbens RJ, de Vries JE, Figdor CG. IL-4 decreases Fc gamma R membrane expression and Fc gamma R-mediated cytotoxic activity of human monocytes. J Immunol. 1990;144:3046-3051.

195. Rudge EU, Cutler AJ, Pritchard NR, Smith KG. Interleukin 4 reduces expression of inhibitory receptors on B cells and abolishes CD22 and Fc gamma RII-mediated B cell suppression. J Exp Med. 2002;195:1079-1085.

196. Joshi T, Ganesan LP, Cao X, Tridandapani S. Molecular analysis of expression and function of hFcgammaRIIbl and b2 isoforms in myeloid cells. Mol Immunol. 2006;43:839-850.

197. Finkelman FD, Holmes J, Katona IM, et al. Lymphokine control of in vivo immunoglobulin isotype selection. Annu Rev Immunol. 1990;8:303-333.

198. Stavnezer J. Regulation of antibody production and class switching by TGF-beta. J Immunol. 1995;155:1647-1651.

199. Mosmann TR, Coffman RL. TH1 and TH2 cells: different patterns of lymphokine secretion lead to different functional properties. Annu Rev Immunol. 1989;7:145-173.

200. Greenberg S, Burridge K, Silverstein SC. Colocalization of F-actin and talin during Fc receptor-mediated phagocytosis in mouse macrophages. J Exp Med. 1990;172:1853-1856.

201. Takai T, Li M, Sylvestre D, Clynes R, Ravetch JV. FcR gamma chain deletion results in pleiotrophic effector cell defects. Cell. 1994;76:519-529.

202. Sylvestre DL, Ravetch JV. Fc receptors initiate the Arthus reaction: redefining the inflammatory cascade. Science. 1994;265:1095-1098.

203. Clynes R, Ravetch JV. Cytotoxic antibodies trigger inflammation through Fc receptors. Immunity. 1995;3:21-26.

204. Hazenbos WL, Gessner JE, Hofhuis FM, et al. Impaired IgG-dependent anaphylaxis and Arthus reaction in Fc gamma RIII (CD16) deficient mice. Immunity. 1996;5:181-188.

205. Meyer D, Schiller C, Westermann J, et al. FcgammaRIII (CD16)-deficient mice show IgG isotype-dependent protection to experimental autoimmune hemolytic anemia. Blood. 1998;92:3997-4002.

206. Ravetch JV, Clynes RA. Divergent roles for Fc receptors and complement in vivo. Annu Rev Immunol. 1998;16:421-432.

207. Korade-Mirnics Z, Corey SJ. Src kinase-mediated signaling in leukocytes. J Leukoc Biol. 2000;68:603-613.

208. Erpel T, Courtneidge SA. Src family protein tyrosine kinases and cellular signal transduction pathways. Curr Opin Cell Biol. 1995;7:176-182.

209. Ghazizadeh S, Bolen JB, Fleit HB. Physical and functional association of Src-related protein tyrosine kinases with Fc gamma RII in monocytic THP-1 cells. J Biol Chem. 1994;269:8878-8884.

210. Durden DL, Kim HM, Calore B, Liu Y. The Fc gamma RI receptor signals through the activation of hck and MAP kinase. J Immunol. 1995;154:4039-4047.

211. Hamada F, Aoki M, Akiyama T, Toyoshima K. Association of immunoglobulin G Fc receptor II with Src-like protein-tyrosine kinase Fgr in neutrophils. Proc Natl Acad Sci U S A. 1993;90:6305-6309.

212. Greenberg S, Chang P, Wang DC, Xavier R, Seed B. Clustered syk tyrosine kinase domains trigger phagocytosis. Proc Natl Acad Sci U S A. 1996;93:1103-1107.

213. Greenberg S, Chang P, Silverstein SC. Tyrosine phosphorylation of the gamma subunit of Fc gamma receptors, p72syk, and paxillin during Fc receptor-mediated phagocytosis in macrophages. J Biol Chem. 1994;269:3897-3902.

214. Indik ZK, Park JG, Pan XQ, Schreiber AD. Induction of phagocytosis by a protein tyrosine kinase. Blood. 1995;85:1175-1180.

215. Kiefer F, Brumell J, Al-Alawi N, et al. The Syk protein tyrosine kinase is essential for Fcgamma receptor signaling in macrophages and neutrophils. Mol Cell Biol. 1998;18:4209-4220.

216. Crowley MT, Costello PS, Fitzer-Attas CJ, et al. A critical role for Syk in signal transduction and phagocytosis mediated by Fcgamma receptors on macrophages. J Exp Med. 1997;186:1027-1039.

217. Raeder EM, Mansfield PJ, Hinkovska-Galcheva V, Shayman JA, Boxer LA. Syk activation initiates downstream signaling events during human polymorphonuclear leukocyte phagocytosis. J Immunol. 1999;163:6785-6793.

218. Stahls A, Liwszyc GE, Couture C, Mustelin T, Andersson LC. Triggering of human natural killer cells through CD16 induces tyrosine phosphorylation of the p72syk kinase. Eur J Immunol. 1994;24:2491-2496.

219. Dai X, Jayapal M, Tay HK, et al. Differential signal transduction, membrane trafficking, and immune effector functions mediated by FcgammaRI versus FcgammaRIIa. Blood. 2009;114:318-327.

220. Garcia-Garcia E, Rosales C. Signal transduction during Fc receptor-mediated phagocytosis. J Leukoc Biol. 2002;72:1092-1108.

221. Atkinson EA, Gerrard JM, Hildes GE, Greenberg AH. Studies of the mechanism of natural killer (NK) degranulation and cytotoxicity. J Leukoc Biol. 1990;47:39-48.

222. Bonnema JD, Karnitz LM, Schoon RA, Abraham RT, Leibson PJ. Fc receptor stimulation of phosphatidylinositol 3-kinase in natural killer cells is associated with protein kinase C-independent granule release and cell-mediated cytotoxicity. J Exp Med. 1994;180:1427-1435.

223. Garcia-Garcia E, Rosales R, Rosales C. Phosphatidylinositol 3-kinase and extracellular signal-regulated kinase are recruited for Fc receptor-mediated phagocytosis during monocyte-to-macrophage differentiation. J Leukoc Biol. 2002;72:107-114.

224. Cooney DS, Phee H, Jacob A, Coggeshall KM. Signal transduction by human-restricted Fc gamma RIIa involves three distinct cytoplasmic kinase families leading to phagocytosis. J Immunol. 2001;167:844-854.

225. Newbrough SA, Mocsai A, Clemens RA, et al. SLP-76 regulates Fcgamma receptor and integrin signaling in neutrophils. Immunity. 2003;19:761-769.

226. Ibata-Ombetta S, Jouault T, Trinel PA, Poulain D. Role of extracellular signal-regulated protein kinase cascade in macrophage killing of Candida albicans. J Leukoc Biol. 2001;70:149-154.

227. Parsa KV, Butchar JP, Rajaram MV, Cremer TJ, Tridandapani S. The tyrosine kinase Syk promotes phagocytosis of Francisella through the activation of Erk. Mol Immunol. 2008;45:3012-3021.

228. Downey GP, Butler JR, Tapper H, et al. Importance of MEK in neutrophil microbicidal responsiveness. J Immunol. 1998;160:434-443.

229. Mansfield PJ, Shayman JA, Boxer LA. Regulation of polymorphonuclear leukocyte phagocytosis by myosin light chain kinase after activation of mitogen-activated protein kinase. Blood. 2000;95:2407-2412.

230. Chimini G, Chavrier P. Function of Rho family proteins in actin dynamics during phagocytosis and engulfment. Nat Cell Biol. 2000;2:E191-196.

231. Hackam DJ, Rotstein OD, Schreiber A, Zhang W, Grinstein S. Rho is required for the initiation of calcium signaling and phagocytosis by Fcgamma receptors in macrophages. J Exp Med. 1997;186:955-966.

232. Caron E, Hall A. Identification of two distinct mechanisms of phagocytosis controlled by different Rho GTPases. Science. 1998;282:1717-1721.

233. Cox D, Chang P, Zhang Q, Reddy PG, Bokoch GM, Greenberg S. Requirements for both Rac1 and Cdc42 in membrane ruffling and phagocytosis in leukocytes. J Exp Med. 1997;186:1487-1494.

234. Gauld SB, Dal Porto JM, Cambier JC. B cell antigen receptor signaling: roles in cell development and disease. Science. 2002;296:1641-1642.

235. Campbell KS, Cambier JC. B lymphocyte antigen receptors (mIg) are non-covalently associated with a disulfide linked, inducibly phosphorylated glycoprotein complex. EMBO J. 1990;9:441-448.

236. Cambier JC, Gauld SB, Merrell KT, Vilen BJ. B-cell anergy: from transgenic models to naturally occurring anergic B cells? Nat Rev Immunol. 2007;7:633-643.

237. Wienands J. Unraveling B cell receptor mechanics. Nat Immunol. 2005;6:1072-1074.

238. Dal Porto JM, Gauld SB, Merrell KT, Mills D, Pugh-Bernard AE, Cambier J. B cell antigen receptor signaling 101. Mol Immunol. 2004;41:599-613.

239. Kulathu Y, Hobeika E, Turchinovich G, Reth M. The kinase Syk as an adaptor controlling sustained calcium signalling and B-cell development. Embo J. 2008;27:1333-1344.

240. Engelke M, Engels N, Dittmann K, Stork B, Wienands J. Ca(2+) signaling in antigen receptor-activated B lymphocytes. Immunol Rev. 2007;218:235-246.

241. Marshall AJ, Niiro H, Yun TJ, Clark EA. Regulation of B-cell activation and differentiation by the phosphatidylinositol 3-kinase and phospholipase Cgamma pathway. Immunol Rev. 2000;176:30-46.

242. Gupta N, DeFranco AL. Lipid rafts and B cell signaling. Semin Cell Dev Biol. 2007;18:616-626.

243. Harnett MM, Katz E, Ford CA. Differential signalling during B-cell maturation. Immunol Lett. 2005;98:33-44.

244. Depoil D, Fleire S, Treanor BL, et al. CD19 is essential for B cell activation by promoting B cell receptor-antigen microcluster formation in response to membrane-bound ligand. Nat Immunol. 2008;9:63-72.

245. Fruman DA, Satterthwaite AB, Witte ON. Xid-like phenotypes: a B cell signalosome takes shape. Immunity. 2000;13:1-3.

246. Jumaa H, Wollscheid B, Mitterer M, Wienands J, Reth M, Nielsen PJ. Abnormal development and function of B lymphocytes in mice deficient for the signaling adaptor protein SLP-65. Immunity. 1999;11:547-554.

247. Okkenhaug K, Ali K, Vanhaesebroeck B. Antigen receptor signalling: a distinctive role for the p110delta isoform of PI3K. Trends Immunol. 2007;28:80-87.

248. D'Ambrosio D, Hippen KL, Cambier JC. Distinct mechanisms mediate SHC association with the activated and resting B cell antigen receptor. Eur J Immunol. 1996;26:1960-1965.

249. Saxton TM, van Oostveen I, Bowtell D, Aebersold R, Gold MR. B cell antigen receptor cross-linking induces phosphorylation of the p21ras oncoprotein activators SHC

and mSOS1 as well as assembly of complexes containing SHC, GRB-2, mSOS1, and a 145-kDa tyrosine-phosphorylated protein. J Immunol. 1994;153:623-636.

250. Tordai A, Franklin RA, Patel H, Gardner AM, Johnson GL, Gelfand EW. Cross-linking of surface IgM stimulates the Ras/Raf-1/MEK/MAPK cascade in human B lymphocytes. J Biol Chem. 1994;269:7538-7543.

251. Cardone MH, Roy N, Stennicke HR, et al. Regulation of cell death protease caspase-9 by phosphorylation. Science. 1998;282:1318-1321.

252. Datta SR, Dudek H, Tao X, et al. Akt phosphorylation of BAD couples survival signals to the cell-intrinsic death machinery. Cell. 1997;91:231-241.

253. Tsuruta F, Masuyama N, Gotoh Y. The phosphatidylinositol 3-kinase (PI3K)-Akt pathway suppresses Bax translocation to mitochondria. J Biol Chem. 2002;277:14040-14047.

254. Khwaja A. Akt is more than just a Bad kinase. Nature. 1999;401:33-34.

255. Cherukuri A, Cheng PC, Pierce SK. The role of the CD19/CD21 complex in B cell processing and presentation of complement-tagged antigens. J Immunol. 2001;167:163-172.

256. Dykstra M, Cherukuri A, Sohn HW, Tzeng SJ, Pierce SK. Location is everything: lipid rafts and immune cell signaling. Annu Rev Immunol. 2003;21:457-481.

257. Filipp D, Moemeni B, Ferzoco A, et al. Lck-dependent Fyn activation requires C terminus-dependent targeting of kinase-active Lck to lipid rafts. J Biol Chem. 2008;283:26409-26422.

258. Rebres RA, Green JM, Reinhold MI, Ticchioni M, Brown EJ. Membrane raft association of CD47 is necessary for actin polymerization and protein kinase C theta translocation in its synergistic activation of T cells. J Biol Chem. 2001;276:7672-7680.

259. Cherukuri A, Dykstra M, Pierce SK. Floating the raft hypothesis: lipid rafts play a role in immune cell activation. Immunity. 2001;14:657-660.

260. Tolar P, Sohn HW, Pierce SK. Viewing the antigen-induced initiation of B-cell activation in living cells. Immunol Rev. 2008;221:64-76.

261. Harwood NE, Batista FD. New insights into the early molecular events underlying B cell activation. Immunity. 2008;28:609-619.

262. Fleire SJ, Goldman JP, Carrasco YR, Weber M, Bray D, Batista FD. B cell ligand discrimination through a spreading and contraction response. Science. 2006;312:738-741.

263. Gupta N, DeFranco AL. Visualizing lipid raft dynamics and early signaling events during antigen receptor-mediated B-lymphocyte activation. Mol Biol Cell. 2003;14:432-444.

264. Sohn HW, Pierce SK, Tzeng SJ. Live cell imaging reveals that the inhibitory FcgammaRIIB destabilizes B cell receptor membrane-lipid interactions and blocks immune synapse formation. J Immunol. 2008;180:793-799.

265. DeFranco AL. Vav and the B cell signalosome. Nat Immunol. 2001;2:482-484.

266. Weber M, Treanor B, Depoil D, et al. Phospholipase C-gamma2 and Vav cooperate within signaling microclusters to propagate B cell spreading in response to membrane-bound antigen. J Exp Med. 2008;205:853-868.

267. Abdel Shakor AB, Kwiatkowska K, Sobota A. Cell surface ceramide generation precedes and controls FcgammaRII clustering and phosphorylation in rafts. J Biol Chem. 2004;279:36778-36787.

268. Strzelecka-Kiliszek A, Korzeniowski M, Kwiatkowska K, Mrozinska K, Sobota A. Activated FcgammaRII and signalling molecules revealed in rafts by ultra-structural observations of plasma-membrane sheets. Mol Membr Biol. 2004;21:101-108.

269. Kwiatkowska K, Sobota A. The clustered Fcgamma receptor II is recruited to Lyn-containing membrane domains and undergoes phosphorylation in a cholesterol-dependent manner. Eur J Immunol. 2001;31:989-998.

270. Katsumata O, Hara-Yokoyama M, Sautes-Fridman C, et al. Association of FcgammaRII with low-density detergent-resistant membranes is important for cross-linking-dependent initiation of the tyrosine phosphorylation pathway and superoxide generation. J Immunol. 2001;167:5814-5823.

271. Marois L, Pare G, Vaillancourt M, Rollet-Labelle E, Naccache PH. Fc gammaRIIIb triggers raft-dependent calcium influx in IgG-mediated responses in human neutrophils. J Biol Chem;286:3509-3519.

272. Xiang Z, Cutler AJ, Brownlie RJ, et al. FcgammaRIIb controls bone marrow plasma cell persistence and apoptosis. Nat Immunol. 2007;8:419-429.

273. Paul E, Nelde A, Verschoor A, Carroll MC. Follicular exclusion of autoreactive B cells requires FcgammaRIIb. Int Immunol. 2007;19:365-373.

274. Clynes R, Dumitru C, Ravetch JV. Uncoupling of immune complex formation and kidney damage in autoimmune glomerulonephritis. Science. 1998;279:1052-1054.

275. Yuasa T, Kubo S, Yoshino T, et al. Deletion of fcgamma receptor IIB renders H-2(b) mice susceptible to collagen-induced arthritis. J Exp Med. 1999;189:187-194.

276. Bolland S, Yim YS, Tus K, Wakeland EK, Ravetch JV. Genetic modifiers of systemic lupus erythematosus in FcgammaRIIB(-/-) mice. J Exp Med. 2002;195:1167-1174.

277. Brownlie RJ, Lawlor KE, Niederer HA, et al. Distinct cell-specific control of autoimmunity and infection by FcgammaRIIb. J Exp Med. 2008;205:883-895.

278. McGaha TL, Karlsson MC, Ravetch JV. FcgammaRIIB deficiency leads to autoimmunity and a defective response to apoptosis in Mrl-MpJ mice. J Immunol. 2008;180:5670-5679.

279. Su K, Yang H, Li X, et al. Expression profile of FcgammaRIIb on leukocytes and its dysregulation in systemic lupus erythematosus. J Immunol. 2007;178:3272-3280.

280. Clatworthy MR, Smith KG. FcgammaRIIb balances efficient pathogen clearance and the cytokine-mediated consequences of sepsis. J Exp Med. 2004;199:717-723.

281. Waisberg M, Tarasenko T, Vickers BK, et al. Genetic susceptibility to systemic lupus erythematosus protects against cerebral malaria in mice. Proc Natl Acad Sci U S A;108:1122-1127.

282. Kyogoku C, Dijstelbloem HM, Tsuchiya N, et al. Fcgamma receptor gene polymorphisms in Japanese patients with systemic lupus erythematosus: contribution of FCGR2B to genetic susceptibility. Arthritis Rheum. 2002;46:1242-1254.

283. Siriboonrit U, Tsuchiya N, Sirikong M, et al. Association of Fcgamma receptor IIb and IIIb polymorphisms with susceptibility to systemic lupus erythematosus in Thais. Tissue Antigens. 2003;61:374-383.

284. Chu ZT, Tsuchiya N, Kyogoku C, et al. Association of Fcgamma receptor IIb polymorphism with susceptibility to systemic lupus erythematosus in Chinese: a common susceptibility gene in the Asian populations. Tissue Antigens. 2004;63:21-27.

285. Floto RA, Clatworthy MR, Heilbronn KR, et al. Loss of function of a lupus-associated FcgammaRIIb polymorphism through exclusion from lipid rafts. Nat Med. 2005;11:1056-1058.

286. Clatworthy MR, Willcocks L, Urban B, et al. Systemic lupus erythematosus-associated defects in the inhibitory receptor FcgammaRIIb reduce susceptibility to malaria. Proc Natl Acad Sci U S A. 2007;104:7169-7174.

287. Willcocks LC, Carr EJ, Niederer HA, et al. A defunctioning polymorphism in FCGR2B is associated with protection against malaria but susceptibility to systemic lupus erythematosus. Proc Natl Acad Sci U S A;107:7881-7885.

288. Sedmak DD, Davis DH, Singh U, van de Winkel JG, Anderson CL. Expression of IgG Fc receptor antigens in placenta and on endothelial cells in humans. An immunohistochemical study. Am J Pathol. 1991;138:175-181.

289. Groger M, Sarmay G, Fiebiger E, Wolff K, Petzelbauer P. Dermal microvascular endothelial cells express CD32 receptors in vivo and in vitro. J Immunol. 1996;156:1549-1556.

290. Lyden TW, Robinson JM, Tridandapani S, et al. The Fc receptor for IgG expressed in the villus endothelium of human placenta is Fc gamma RIIb2. J Immunol. 2001;166:3882-3889.

291. Kim J, Hayton WL, Robinson JM, Anderson CL. Kinetics of FcRn-mediated recycling of IgG and albumin in human: pathophysiology and therapeutic implications using a simplified mechanism-based model. Clin Immunol. 2007;122:146-155.

292. Hogarth PM, Witort E, Hulett MD, et al. Structure of the mouse beta Fc gamma receptor II gene. J Immunol. 1991;146:369-376.

293. Brooks DG, Qiu WQ, Luster AD, Ravetch JV. Structure and expression of human IgG FcRII(CD32). Functional heterogeneity is encoded by the alternatively spliced products of multiple genes. J Exp Med. 1989;170:1369-1385.

294. Budde P, Bewarder N, Weinrich V, Schulzeck O, Frey J. Tyrosine-containing sequence motifs of the human immunoglobulin G receptors FcRIIb1 and FcRIIb2 essential for endocytosis and regulation of calcium flux in B cells. J Biol Chem. 1994;269:30636-30644.

295. Cassel DL, Keller MA, Surrey S, et al. Differential expression of Fc gamma RIIA, Fc gamma RIIB and Fc gamma RIIC in hematopoietic cells: analysis of transcripts. Mol Immunol. 1993;30:451-460.

296. Van Den Herik-Oudijk IE, Westerdaal NA, Henriquez NV, Capel PJ, Van De Winkel JG. Functional analysis of human Fc gamma RII (CD32) isoforms expressed in B lymphocytes. J Immunol. 1994;152:574-585.

297. Takai T. Fc receptors and their role in immune regulation and autoimmunity. J Clin Immunol. 2005;25:1-18.

298. Miettinen HM, Rose JK, Mellman I. Fc receptor isoforms exhibit distinct abilities for coated pit localization as a result of cytoplasmic domain heterogeneity. Cell. 1989;58:317-327.

299. Miettinen HM, Matter K, Hunziker W, Rose JK, Mellman I. Fc receptor endocytosis is controlled by a cytoplasmic domain determinant that actively prevents coated pit localization. J Cell Biol. 1992;116:875-888.

300. Tartour E, de la Salle H, de la Salle C, et al. Identification, in mouse macrophages and in serum, of a soluble receptor for the Fc portion of IgG (Fc gamma R) encoded by an alternatively spliced transcript of the Fc gamma RII gene. Int Immunol. 1993;5:859-868.

301. Minskoff SA, Matter K, Mellman I. Fc gamma RII-B1 regulates the presentation of B cell receptor-bound antigens. J Immunol. 1998;161:2079-2083.

302. Latour S, Fridman WH, Daeron M. Identification, molecular cloning, biologic properties, and tissue distribution of a novel isoform of murine low-affinity IgG receptor homologous to human Fc gamma RIIB1. J Immunol. 1996;157:189-197.

303. Daeron M, Latour S, Malbec O, et al. The same tyrosine-based inhibition motif, in the intracytoplasmic domain of Fc gamma RIIB, regulates negatively BCR-, TCR-, and FcR-dependent cell activation. Immunity. 1995;3:635-646.

304. Maresco DL, Osborne JM, Cooney D, Coggeshall KM, Anderson CL. The SH2-containing 5'-inositol phosphatase (SHIP) is tyrosine phosphorylated after Fc gamma receptor clustering in monocytes. J Immunol. 1999;162:6458-6465.

305. Unkeless JC, Jin J. Inhibitory receptors, ITIM sequences and phosphatases. Curr Opin Immunol. 1997;9:338-343.

306. D'Ambrosio D, Fong DC, Cambier JC. The SHIP phosphatase becomes associated with Fc gammaRIIB1 and is tyrosine phosphorylated during 'negative' signaling. Immunol Lett. 1996;54:77-82.

307. Long EO. Regulation of immune responses through inhibitory receptors. Annu Rev Immunol. 1999;17:875-904.

308. Cox D, Dale BM, Kashiwada M, Helgason CD, Greenberg S. A regulatory role for Src homology 2 domain-containing inositol 5'-phosphatase (SHIP) in phagocytosis mediated by Fc gamma receptors and complement receptor 3 (alpha(M)beta(2); CD11b/CD18). J Exp Med. 2001;193:61-71.

309. Kant AM, De P, Peng X, et al. SHP-1 regulates Fcgamma receptor-mediated phagocytosis and the activation of RAC. Blood. 2002;100:1852-1859.

310. Huber M, Helgason CD, Damen JE, et al. The role of SHIP in growth factor induced signalling. Prog Biophys Mol Biol. 1999;71:423-434.

311. Huang ZY, Hunter S, Kim MK, Indik ZK, Schreiber AD. The effect of phosphatases SHP-1 and SHIP-1 on signaling by the ITIM- and ITAM-containing Fcgamma receptors FcgammaRIIB and FcgammaRIIA. J Leukoc Biol. 2003;73:823-829.

312. Ono M, Bolland S, Tempst P, Ravetch JV. Role of the inositol phosphatase SHIP in negative regulation of the immune system by the receptor Fc(gamma)RIIB. Nature. 1996;383:263-266.

313. Liu Q, Oliveira-Dos-Santos AJ, Mariathasan S, et al. The inositol polyphosphate 5-phosphatase ship is a crucial negative regulator of B cell antigen receptor signaling. J Exp Med. 1998;188:1333-1342.

314. Ravetch JV, Lanier LL. Immune inhibitory receptors. Science. 2000;290:84-89.

315. Chacko GW, Tridandapani S, Damen JE, Liu L, Krystal G, Coggeshall KM. Negative signaling in B lymphocytes induces tyrosine phosphorylation of the 145-kDa inositol polyphosphate 5-phosphatase, SHIP. J Immunol. 1996;157:2234-2238.

316. Joshi T, Butchar JP, Tridandapani S. Fcgamma receptor signaling in phagocytes. Int J Hematol. 2006;84:210-216.

317. Phee H, Jacob A, Coggeshall KM. Enzymatic activity of the Src homology 2 domain-containing inositol phosphatase is regulated by a plasma membrane location. J Biol Chem. 2000;275:19090-19097.

318. Aman MJ, Tosello-Trampont AC, Ravichandran K. Fc gamma RIIB1/SHIP-mediated inhibitory signaling in B cells involves lipid rafts. J Biol Chem. 2001;276:46371-46378.

319. Liu W, Won Sohn H, Tolar P, Meckel T, Pierce SK. Antigen-induced oligomerization of the B cell receptor is an early target of Fc gamma RIIB inhibition. J Immunol;184:1977-1989.

320. Kono H, Kyogoku C, Suzuki T, et al. FcgammaRIIB Ile232Thr transmembrane polymorphism associated with human systemic lupus erythematosus decreases affinity to lipid rafts and attenuates inhibitory effects on B cell receptor signaling. Hum Mol Genet. 2005;14:2881-2892.

321. Isnardi I, Bruhns P, Bismuth G, Fridman WH, Daeron M. The SH2 domain-containing inositol 5-phosphatase SHIP1 is recruited to the intracytoplasmic domain of human FcgammaRIIB and is mandatory for negative regulation of B cell activation. Immunol Lett. 2006;104:156-165.

322. Okada H, Bolland S, Hashimoto A, et al. Role of the inositol phosphatase SHIP in B cell receptor-induced Ca2+ oscillatory response. J Immunol. 1998;161:5129-5132.

323. Diegel ML, Rankin BM, Bolen JB, Dubois PM, Kiener PA. Cross-linking of Fc gamma receptor to surface immunoglobulin on B cells provides an inhibitory signal that closes the plasma membrane calcium channel. J Biol Chem. 1994;269:11409-11416.

324. Bolland S, Pearse RN, Kurosaki T, Ravetch JV. SHIP modulates immune receptor responses by regulating membrane association of Btk. Immunity. 1998;8:509-516.

325. Tamir I, Stolpa JC, Helgason CD, et al. The RasGAP-binding protein p62dok is a mediator of inhibitory FcgammaRIIB signals in B cells. Immunity. 2000;12:347-358.

326. Jacob A, Cooney D, Tridandapani S, Kelley T, Coggeshall KM. FcgammaRIIb modulation of surface immunoglobulin-induced Akt activation in murine B cells. J Biol Chem. 1999;274:13704-13710.

327. Aman MJ, Lamkin TD, Okada H, Kurosaki T, Ravichandran KS. The inositol phosphatase SHIP inhibits Akt/PKB activation in B cells. J Biol Chem. 1998;273:33922-33928.

328. Brown KS, Blair D, Reid SD, Nicholson EK, Harnett MM. FcgammaRIIb-mediated negative regulation of BCR signalling is associated with the recruitment of the MAPkinase-phosphatase, Pac-1, and the 3'-inositol phosphatase, PTEN. Cell Signal. 2004;16:71-80.

329. Sarmay G, Koncz G, Gergely J. Human type II Fcgamma receptors inhibit B cell activation by interacting with the p21(ras)-dependent pathway. J Biol Chem. 1996;271:30499-30504.

330. Neumann K, Oellerich T, Heine I, Urlaub H, Engelke M. Fc gamma receptor IIb modulates the molecular Grb2 interaction network in activated B cells. Cell Signal;23:893-900.

331. Koncz G, Toth GK, Bokonyi G, et al. Co-clustering of Fcgamma and B cell receptors induces dephosphorylation of the Grb2-associated binder 1 docking protein. Eur J Biochem. 2001;268:3898-3906.

332. Yamanashi Y, Tamura T, Kanamori T, et al. Role of the rasGAP-associated docking protein p62(dok) in negative regulation of B cell receptor-mediated signaling. Genes Dev. 2000;14:11-16.

333. Tzeng SJ, Bolland S, Inabe K, Kurosaki T, Pierce SK. The B cell inhibitory Fc receptor triggers apoptosis by a novel c-Abl family kinase-dependent pathway. J Biol Chem. 2005;280:35247-35254.

334. Pearse RN, Kawabe T, Bolland S, Guinamard R, Kurosaki T, Ravetch JV. SHIP recruitment attenuates Fc gamma RIIB-induced B cell apoptosis. Immunity. 1999;10:753-760.

335. Wong S, McLaughlin J, Cheng D, Zhang C, Shokat KM, Witte ON. Sole BCR-ABL inhibition is insufficient to eliminate all myeloproliferative disorder cell populations. Proc Natl Acad Sci U S A. 2004;101:17456-17461.

336. Strasser A. Haematopoietic cell apoptosis. Curr Opin Immunol. 2007;19:485-487.

337. Enders A, Bouillet P, Puthalakath H, Xu Y, Tarlinton DM, Strasser A. Loss of the pro-apoptotic BH3-only Bcl-2 family member Bim inhibits BCR stimulation-induced apoptosis and deletion of autoreactive B cells. J Exp Med. 2003;198:1119-1126.

338. Strasser A. The role of BH3-only proteins in the immune system. Nat Rev Immunol. 2005;5:189-200.

339. Ashman RF, Peckham D, Stunz LL. Fc receptor off-signal in the B cell involves apoptosis. J Immunol. 1996;157:5-11.

340. Bolland S, Ravetch JV. Spontaneous autoimmune disease in Fc(gamma)RIIB-deficient mice results from strain-specific epistasis. Immunity. 2000;13:277-285.

341. Rahman ZS, Manser T. Failed up-regulation of the inhibitory IgG Fc receptor Fc gamma RIIB on germinal center B cells in autoimmune-prone mice is not associated with deletion polymorphisms in the promoter region of the Fc gamma RIIB gene. J Immunol. 2005;175:1440-1449.

342. Benschop RJ, Melamed D, Nemazee D, Cambier JC. Distinct signal thresholds for the unique antigen receptor-linked gene expression programs in mature and immature B cells. J Exp Med. 1999;190:749-756.

343. Brauweiler AM, Cambier JC. Fc gamma RIIB activation leads to inhibition of signalling by independently ligated receptors. Biochem Soc Trans. 2003;31:281-285.

344. Witz IP, Ran M. FcR may function as a progression factor of nonlymphoid tumors. Immunol Res. 1992;11:283-295.

345. Milgrom F, Humphrey LJ, Tonder O, Yasuda J, Witebsky E. Antibody-mediated hemadsorption by tumor tissues. Int Arch Allergy Appl Immunol. 1968;33:478-492.

346. Tonder O, Thunold S. Receptors for immunoglobulin Fc in human malignant tissues. Scand J Immunol. 1973;2:207-215.

347. Ilfeld D, Barzilay J, Dux Z, Ran M. Correlation of Fc gamma receptors on peripheral blood mononuclear cells and survival in patients with metastatic breast cancer. Breast Cancer Res Treat. 1986;7:181-186.

348. Ran M, Teillaud JL, Fridman WH, et al. Increased expression of Fc gamma receptor in cancer patients and tumor bearing mice. Mol Immunol. 1988;25:1159-1167.

349. Svennevig JL, Andersson TR. Cells bearing Fc receptors in human malignant solid tumours. Br J Cancer. 1982;45:201-208.

350. Ran M, Dux Z, Anavi R, Witz IP. Expression of Fc gamma receptors on a subpopulation of nonlymphoid tumor cells and its enrichment. J Natl Cancer Inst. 1984;73:437-446.

351. Berko-Flint Y, Fridman WH, Grossman-Atlas E, et al. Some cellular and molecular characteristics of high and low tumorigenicity variants of polyoma-virus transformed cells. Mol Immunol. 1990;27:1219-1228.

352. Zusman T, Lisansky E, Arons E, et al. Contribution of the intracellular domain of murine Fc-gamma receptor type IIB1 to its tumor-enhancing potential. Int J Cancer. 1996;68:219-227.

353. Zusman T, Gohar O, Eliassi H, et al. The murine Fc-gamma (Fc gamma) receptor type II B1 is a tumorigenicity-enhancing factor in polyoma-virus-transformed 3T3 cells. Int J Cancer. 1996;65:221-229.

354. Langer AB, Emmanuel N, Even J, et al. Phenotypic properties of 3T3 cells transformed in vitro with polyoma virus and passaged once in syngeneic animals. Immunobiology. 1992;185:281-291.

355. Cassard L, Cohen-Solal JF, Fournier EM, et al. Selective expression of inhibitory Fcgamma receptor by metastatic melanoma impairs tumor susceptibility to IgG-dependent cellular response. Int J Cancer. 2008;123:2832-2839.

356. Camilleri-Broet S, Cassard L, Broet P, et al. FcgammaRIIB is differentially expressed during B cell maturation and in B-cell lymphomas. Br J Haematol. 2004;124:55-62.

357. Neauport-Sautes C, Daeron M, Teillaud JL, Blank U, Fridman WH. The occurrence, structural and functional properties of immunoglobulin Fc receptors on murine neoplastic cells. Int Rev Immunol. 1986;1:237-271.

358. Eshel R, Neumark E, Sagi-Assif O, Witz IP. Receptors involved in microenvironment-driven molecular evolution of cancer cells. Semin Cancer Biol. 2002;12:139-147.

359. Cassard L, Cohen-Solal JF, Galinha A, et al. Modulation of tumor growth by inhibitory Fc(gamma) receptor expressed by human melanoma cells. J Clin Invest. 2002;110:1549-1557.

360. Ran M, Langer AB, Eliassi I, et al. Possibilities of interference with the immune system of tumor bearers by non-lymphoid Fc gamma RII expressing tumor cells. Immunobiology. 1992;185:415-425.

361. Clynes R, Takechi Y, Moroi Y, Houghton A, Ravetch JV. Fc receptors are required in passive and active immunity to melanoma. Proc Natl Acad Sci U S A. 1998;95:652-656.

362. Otten MA, van der Bij GJ, Verbeek SJ, et al. Experimental antibody therapy of liver metastases reveals functional redundancy between Fc gammaRI and Fc gammaRIV. J Immunol. 2008;181:6829-6836.

363. Bevaart L, Jansen MJ, van Vugt MJ, Verbeek JS, van de Winkel JG, Leusen JH. The high-affinity IgG receptor, FcgammaRI, plays a central role in antibody therapy of experimental melanoma. Cancer Res. 2006;66:1261-1264.

364. Beers SA, French RR, Chan HT, et al. Antigenic modulation limits the efficacy of anti-CD20 antibodies: implications for antibody selection. Blood;115:5191-5201.

365. Shields RL, Namenuk AK, Hong K, et al. High resolution mapping of the binding site on human IgG1 for Fc gamma RI, Fc gamma RII, Fc gamma RIII, and FcRn and design of IgG1 variants with improved binding to the Fc gamma R. J Biol Chem. 2001;276:6591-6604.

366. Wu J, Edberg JC, Redecha PB, et al. A novel polymorphism of FcgammaRIIIa (CD16) alters receptor function and predisposes to autoimmune disease. J Clin Invest. 1997;100:1059-1070.

367. Musolino A, Naldi N, Bortesi B, et al. Immunoglobulin G fragment C receptor polymorphisms and clinical efficacy of trastuzumab-based therapy in patients with HER-2/neu-positive metastatic breast cancer. J Clin Oncol. 2008;26:1789-1796.

368. Hunter S, Indik ZK, Kim MK, Cauley MD, Park JG, Schreiber AD. Inhibition of Fcgamma receptor-mediated phagocytosis by a nonphagocytic Fcgamma receptor. Blood. 1998;91:1762-1768.

369. Green SK, Karlsson MC, Ravetch JV, Kerbel RS. Disruption of cell-cell adhesion enhances antibody-dependent cellular cytotoxicity: implications for antibody-based therapeutics of cancer. Cancer Res. 2002;62:6891-6900.

370. Dhodapkar KM, Kaufman JL, Ehlers M, et al. Selective blockade of inhibitory Fcgamma receptor enables human dendritic cell maturation with IL-12p70 production and immunity to antibody-coated tumor cells. Proc Natl Acad Sci U S A. 2005;102:2910-2915.

371. Dhodapkar KM, Banerjee D, Connolly J, et al. Selective blockade of the inhibitory Fcgamma receptor (FcgammaRIIB) in human dendritic cells and monocytes induces a type I interferon response program. J Exp Med. 2007;204:1359-1369.

372. Stavenhagen JB, Gorlatov S, Tuaillon N, et al. Fc optimization of therapeutic antibodies enhances their ability to kill tumor cells in vitro and controls tumor expansion in vivo via low-affinity activating Fcgamma receptors. Cancer Res. 2007;67:8882-8890.

373. Veri MC, Gorlatov S, Li H, et al. Monoclonal antibodies capable of discriminating the human inhibitory Fcgamma-receptor IIB (CD32B) from the activating Fcgamma-receptor IIA (CD32A): biochemical, biological and functional characterization. Immunology. 2007;121:392-404.

374. Rankin CT, Veri MC, Gorlatov S, et al. CD32B, the human inhibitory Fc-gamma receptor IIB, as a target for monoclonal antibody therapy of B-cell lymphoma. Blood. 2006;108:2384-2391.

375. Harris AW, Pinkert CA, Crawford M, Langdon WY, Brinster RL, Adams JM. The E mu-myc transgenic mouse. A model for high-incidence spontaneous lymphoma and leukemia of early B cells. J Exp Med. 1988;167:353-371.

376. Elliott TJ, Glennie MJ, McBride HM, Stevenson GT. Analysis of the interaction of antibodies with immunoglobulin idiotypes on neoplastic B lymphocytes: implications for immunotherapy. J Immunol. 1987;138:981-988.

377. Van Rooijen N, Sanders A. Liposome mediated depletion of macrophages: mechanism of action, preparation of liposomes and applications. J Immunol Methods. 1994;174:83-93.

378. Schmidt EV, Pattengale PK, Weir L, Leder P. Transgenic mice bearing the human c-myc gene activated by an immunoglobulin enhancer: a pre-B-cell lymphoma model. Proc Natl Acad Sci U S A. 1988;85:6047-6051.

379. Corcoran LM, Cory S, Adams JM. Transposition of the immunoglobulin heavy chain enhancer to the myc oncogene in a murine plasmacytoma. Cell. 1985;40:71-79.

380. Alexander WS, Schrader JW, Adams JM. Expression of the c-myc oncogene under control of an immunoglobulin enhancer in E mu-myc transgenic mice. Mol Cell Biol. 1987;7:1436-1444.

381. Adams JM, Harris AW, Pinkert CA, et al. The c-myc oncogene driven by immunoglobulin enhancers induces lymphoid malignancy in transgenic mice. Nature. 1985;318:533-538.

382. Taub R, Kirsch I, Morton C, et al. Translocation of the c-myc gene into the immunoglobulin heavy chain locus in human Burkitt lymphoma and murine plasmacytoma cells. Proc Natl Acad Sci U S A. 1982;79:7837-7841.

383. Janz S. Myc translocations in B cell and plasma cell neoplasms. DNA Repair (Amst). 2006;5:1213-1224.

384. Fujita S, Buziba N, Kumatori A, Senba M, Yamaguchi A, Toriyama K. Early stage of Epstein-Barr virus lytic infection leading to the "starry sky" pattern formation in endemic Burkitt lymphoma. Arch Pathol Lab Med. 2004;128:549-552.

385. Langdon WY, Harris AW, Cory S. Growth of E mu-myc transgenic B-lymphoid cells in vitro and their evolution toward autonomy. Oncogene Res. 1988;3:271-279.

386. Sidman CL, Denial TM, Marshall JD, Roths JB. Multiple mechanisms of tumorigenesis in E mu-myc transgenic mice. Cancer Res. 1993;53:1665-1669.

387. Adams JM, Harris AW, Strasser A, Ogilvy S, Cory S. Transgenic models of lymphoid neoplasia and development of a pan-hematopoietic vector. Oncogene. 1999;18:5268-5277.

388. Cory S, Vaux DL, Strasser A, Harris AW, Adams JM. Insights from Bcl-2 and Myc: malignancy involves abrogation of apoptosis as well as sustained proliferation. Cancer Res. 1999;59:1685s-1692s.

389. Kelly PN, Puthalakath H, Adams JM, Strasser A. Endogenous bcl-2 is not required for the development of Emu-myc-induced B-cell lymphoma. Blood. 2007;109:4907-4913.

390. Cory S, Harris AW, Strasser A. Insights from transgenic mice regarding the role of bcl-2 in normal and neoplastic lymphoid cells. Philos Trans R Soc Lond B Biol Sci. 1994;345:289-295.

391. Youle RJ, Strasser A. The BCL-2 protein family: opposing activities that mediate cell death. Nat Rev Mol Cell Biol. 2008;9:47-59.

392. Camilleri-Broet S, Mounier N, Delmer A, et al. FcgammaRIIB expression in diffuse large B-cell lymphomas does not alter the response to CHOP+rituximab (R-CHOP). Leukemia. 2004;18:2038-2040.

393. Drayton DL, Liao S, Mounzer RH, Ruddle NH. Lymphoid organ development: from ontogeny to neogenesis. Nat Immunol. 2006;7:344-353.

394. Lopez-Giral S, Quintana NE, Cabrerizo M, et al. Chemokine receptors that mediate B cell homing to secondary lymphoid tissues are highly expressed in B cell chronic lymphocytic leukemia and non-Hodgkin lymphomas with widespread nodular dissemination. J Leukoc Biol. 2004;76:462-471.

395. Fan S, el-Deiry WS, Bae I, et al. p53 gene mutations are associated with decreased sensitivity of human lymphoma cells to DNA damaging agents. Cancer Res. 1994;54:5824-5830.

396. Ran M, Katz B, Kimchi N, et al. In vivo acquisition of Fc gamma RII expression on polyoma virus-transformed cells derived from tumors of long latency. Cancer Res. 1991;51:612-618.

397. Srinivasan L, Sasaki Y, Calado DP, et al. PI3 kinase signals BCR-dependent mature B cell survival. Cell. 2009;139:573-586.

398. Lam KP, Kuhn R, Rajewsky K. In vivo ablation of surface immunoglobulin on mature B cells by inducible gene targeting results in rapid cell death. Cell. 1997;90:1073-1083.

399. Kraus M, Alimzhanov MB, Rajewsky N, Rajewsky K. Survival of resting mature B lymphocytes depends on BCR signaling via the Igalpha/beta heterodimer. Cell. 2004;117:787-800.

400. Eischen CM, Weber JD, Roussel MF, Sherr CJ, Cleveland JL. Disruption of the ARF-Mdm2-p53 tumor suppressor pathway in Myc-induced lymphomagenesis. Genes Dev. 1999;13:2658-2669.

401. Krug U, Ganser A, Koeffler HP. Tumor suppressor genes in normal and malignant hematopoiesis. Oncogene. 2002;21:3475-3495.

402. Zhang M, Zhang Z, Garmestani K, et al. Activating Fc receptors are required for antitumor efficacy of the antibodies directed toward CD25 in a murine model of adult t-cell leukemia. Cancer Res. 2004;64:5825-5829.

403. Treon SP, Hansen M, Branagan AR, et al. Polymorphisms in FcgammaRIIIA (CD16) receptor expression are associated with clinical response to rituximab in Waldenstrom's macroglobulinemia. J Clin Oncol. 2005;23:474-481.

404. Uchida J, Hamaguchi Y, Oliver JA, et al. The innate mononuclear phagocyte network depletes B lymphocytes through Fc receptor-dependent mechanisms during anti-CD20 antibody immunotherapy. J Exp Med. 2004;199:1659-1669.

405. Unkeless JC. Characterization of a monoclonal antibody directed against mouse macrophage and lymphocyte Fc receptors. J Exp Med. 1979;150:580-596.

406. Malmborg AC, Borrebaeck CA. BIAcore as a tool in antibody engineering. J Immunol Methods. 1995;183:7-13.

407. Cragg MS, Zhang L, French RR, Glennie MJ. Analysis of the interaction of monoclonal antibodies with surface IgM on neoplastic B-cells. Br J Cancer. 1999;79:850-857.

408. Pao LI, Famiglietti SJ, Cambier JC. Asymmetrical phosphorylation and function of immunoreceptor tyrosine-based activation motif tyrosines in B cell antigen receptor signal transduction. J Immunol. 1998;160:3305-3314.

409. Bannish G, Fuentes-Panana EM, Cambier JC, Pear WS, Monroe JG. Ligand-independent signaling functions for the B lymphocyte antigen receptor and their role in positive selection during B lymphopoiesis. J Exp Med. 2001;194:1583-1596.

410. Monroe JG. ITAM-mediated tonic signalling through pre-BCR and BCR complexes. Nat Rev Immunol. 2006;6:283-294.

411. Hamaguchi Y, Xiu Y, Komura K, Nimmerjahn F, Tedder TF. Antibody isotype-specific engagement of Fcgamma receptors regulates B lymphocyte depletion during CD20 immunotherapy. J Exp Med. 2006;203:743-753.

412. Gregoriadis. Liposomes as Drug Carriers. New York: Wiley; 1988.

413. van Rooijen N, van Nieuwmegen R. Elimination of phagocytic cells in the spleen after intravenous injection of liposome-encapsulated dichloromethylene diphosphonate. An enzyme-histochemical study. Cell Tissue Res. 1984;238:355-358.

414. van Rooijen N, Sanders A, van den Berg TK. Apoptosis of macrophages induced by liposome-mediated intracellular delivery of clodronate and propamidine. J Immunol Methods. 1996;193:93-99.

415. van Rooijen N, van Kesteren-Hendrikx E. Clodronate liposomes: perspectives in research and therapeutics. J Liposome Res. 2002;12:81-94.

416. Beum PV, Kennedy AD, Williams ME, Lindorfer MA, Taylor RP. The shaving reaction: rituximab/CD20 complexes are removed from mantle cell lymphoma and chronic lymphocytic leukemia cells by THP-1 monocytes. J Immunol. 2006;176:2600-2609.

417. Beum PV, Lindorfer MA, Taylor RP. Within peripheral blood mononuclear cells, antibody-dependent cellular cytotoxicity of rituximab-opsonized Daudi cells is promoted by NK cells and inhibited by monocytes due to shaving. J Immunol. 2008;181:2916-2924.

418. Lopez-Albaitero A, Lee SC, Morgan S, et al. Role of polymorphic Fc gamma receptor IIIa and EGFR expression level in cetuximab mediated, NK cell dependent in vitro cytotoxicity of head and neck squamous cell carcinoma cells. Cancer Immunol Immunother. 2009;58:1853-1864.

419. Takeda K, Yamaguchi N, Akiba H, et al. Induction of tumor-specific T cell immunity by anti-DR5 antibody therapy. J Exp Med. 2004;199:437-448.

420. Chaudhury C, Mehnaz S, Robinson JM, et al. The major histocompatibility complex-related Fc receptor for IgG (FcRn) binds albumin and prolongs its lifespan. J Exp Med. 2003;197:315-322.

421. Looney RJ, Abraham GN, Anderson CL. Human monocytes and U937 cells bear two distinct Fc receptors for IgG. J Immunol. 1986;136:1641-1647.

422. Pulford K, Ralfkiaer E, MacDonald SM, et al. A new monoclonal antibody (KB61) recognizing a novel antigen which is selectively expressed on a subpopulation of human B lymphocytes. Immunology. 1986;57:71-76.

423. Uchida J, Lee Y, Hasegawa M, et al. Mouse CD20 expression and function. Int Immunol. 2004;16:119-129.

424. DiLillo DJ, Hamaguchi Y, Ueda Y, et al. Maintenance of long-lived plasma cells and serological memory despite mature and memory B cell depletion during CD20 immunotherapy in mice. J Immunol. 2008;180:361-371.

425. Ewings KE, Wiggins CM, Cook SJ. Bim and the pro-survival Bcl-2 proteins: opposites attract, ERK repels. Cell Cycle. 2007;6:2236-2240.

426. Luciano F, Jacquel A, Colosetti P, et al. Phosphorylation of Bim-EL by Erk1/2 on serine 69 promotes its degradation via the proteasome pathway and regulates its proapoptotic function. Oncogene. 2003;22:6785-6793.

427. Ley R, Balmanno K, Hadfield K, Weston C, Cook SJ. Activation of the ERK1/2 signaling pathway promotes phosphorylation and proteasome-dependent degradation of the BH3-only protein, Bim. J Biol Chem. 2003;278:18811-18816.

428. Ley R, Ewings KE, Hadfield K, Howes E, Balmanno K, Cook SJ. Extracellular signal-regulated kinases 1/2 are serum-stimulated "Bim(EL) kinases" that bind to the BH3-only protein Bim(EL) causing its phosphorylation and turnover. J Biol Chem. 2004;279:8837-8847.